INTERPLAY BETWEEN COLLAPSIN RESPONSE MEDIATOR PROTEIN 2 (CRMP2) PHOSPHORYLATION AND SUMOYLATION MODULATES NaV1.7 TRAFFICKING

Erik Thomas Dustrude

Submitted to the faculty of the University Graduate School
in partial fulfillment of the requirements
for the degree
Doctor of Philosophy
in the Program of Medical Neuroscience,
Indiana University

August 2015

Accepted by the Graduate Faculty, of Indiana University, in partial fulfillment of the requirements for the degree of Doctor of Philosophy.

_____
Nickolay Brustovetsky, Ph.D., Chair

_____
Rajesh Khanna, Ph.D.

Doctoral Committee

_____
Theodore Cummins, Ph.D.

_____
Travis Jerde, Ph.D.

July 6, 2015

_____
Alexander Obukhov, Ph.D.

DEDICATION

I dedicate this thesis to my little brother, Matthew Joseph Dustrude, for the love and support and rivalry he has provided me. Without him in my life, I could not have become the person, husband, or scientist that I am today.

ACKNOWLEDGEMENTS

This body of work presented here could not have been possible without the contribution of many people both at Indiana University and The University of Arizona. First, I thank my mentor Dr. Rajesh Khanna for not only guiding my development as a research scientist and enthusiastically opening my eyes to the world of CRMP2, but also for opening his home to me as a colleague and friend. If not for the kindness extended to me from the entire Khanna family, my graduate career, especially my time away from home at The University of Arizona would not have been nearly as wonderful. I thank the members of my thesis committee Drs. Nikolai Broustovetski, Theodore Cummins, Alexander Obukhov, and Travis Jerde for their ideas and insights when designing and guiding this body of work with Dr. Khanna and me. I would also like to thank the people I sought out most when experiments were not working and I was at a loss for how to continue, Dr. Andrei Molosh, James Jackson II, Dr. Xiao-Fang Yang, Dr. Sarah Wilson, Dr. Gerry Oxford, and Dr. Aubin Moutal. I thank the Stark Neuroscience program for offering me a fellowship that supported my second year. For their work in running the programs that saw me through graduate school, I thank Dr. Gerry Oxford, Dr. Grant Nicol, Dr. Cynthia Hingtgen, Dr. Ted Cummins, Dr. Andy Hudmon, and Nastassia Belton of the Stark Neurosciences Research Institute, Monica Henry, formerly of the IU IBMG program, and Terri Vorholzer of the Department of Pharmacology in Arizona.

I have been very lucky to have worked with such amazing people who share a passion for the science we are doing in the Khanna lab. Drs. Joel Brittain and Sarah Wilson relate to me in ways only Dr. Khanna's students can understand. We are all the better versions of ourselves for the experience and I am happy to have shared it with such

genuinely kind and helpful people. Very often Drs. Aubin Moutal, Weina Ju, Xiao-fang Yang, and Yuying Wang shared the experimental burden (and joy) with me. For their expertise and hard work in driving the project forward as well as their friendship I am grateful. I thank Dr. May Khanna, Sophia Khanna, and Gabriel Khanna for their shared relaxation in the pool as well as their insightful conversations about life and science from their expert perspectives of doctor and mother, child, and infant. While in Arizona, Aubin and Liberty Moutal, post-docs in the Khanna lab, offered to let me stay in their home while I traveled to finish my PhD work. They did this when they hardly knew me and it is one of the most generous gifts I have ever received. Through the lavish French meals, the eclectic movies, and the science shared, I have found lifelong friends in the Moutals. I thank my fellow graduate students Aarti Chawla, Cindy Barbosa, Ressha Patel, and Daniel Levey for reminding me every day that I was not earning a PhD alone, and through shared experiences we all grew to be productive members of our labs. Lastly, I thank my entire family for their support. My parents Tom and Joanne and my wife Tara have been constant inspirations to me. The pride they exuded when they speak of my aspirations made it easy to fully dedicate myself to my studies.

Erik Thomas Dustrude

INTERPLAY BETWEEN COLLAPSIN RESPONSE MEDIATOR PROTEIN 2 (CRMP2) PHOSPHORYLATION AND SUMOYLATION MODULATES NaV1.7 TRAFFICKING

The voltage-gated sodium channel Nav1.7 has gained traction as a pain target with recognition that loss-of-function mutations in SCN9A, the gene encoding Nav1.7, are associated with congenital insensitivity to pain, whereas gain-of-function mutations produce distinct pain syndromes due to increased Nav1.7 activity. Selective inhibition of Nav1.7 is fundamental to modulating pain via this channel. Understanding the regulation of Nav1.7 at the cellular and molecular level is critical for advancing better therapeutics for pain.

Although trafficking of Nav1.7 remains poorly understood, recent studies have begun to investigate post-translational modifications of Navs and/or auxiliary subunits as well as protein-protein interactions as Nav-trafficking mechanisms. Here, I tested if post-translational modifications of a novel Nav1.7-interacting protein, the axonal collapsin response mediator protein 2 (CRMP2) by small ubiquitin-like modifier (SUMO) and phosphorylation could affect Nav trafficking and function. Expression of a CRMP2 SUMOylation incompetent mutant (CRMP2-K374A) in neuronal model CAD cells, which express predominantly Nav1.7 currents, led to a significant reduction in huwentoxin-IV-sensitive Nav1.7 currents. Increasing deSUMOylation with sentrin/SUMO-specific protease SENP1 or SENP2 in wildtype CRMP2-expressing CAD cells decreased Nav1.7 currents. Consistent with reduced current density, biotinylation revealed significant reduction in surface Nav1.7 levels of CAD cells expressing CRMP2-

K374A or SENP proteins. Diminution of Nav1.7 sodium current was recapitulated in sensory neurons expressing CRMP2-K374A.

Because CRMP2 functions are regulated by its phosphorylation state, I next investigated possible interplay between phosphorylation and SUMOylation of CRMP2 on Nav1.7. Phosphorylation of CRMP2 by cyclin dependent kinase 5 (Cdk5) was necessary for maintaining Nav1.7 surface expression and current density whereas phosphorylation by Fyn kinase reduced CRMP2 SUMOylation and Nav1.7 current density. Binding to Nav1.7 was decreased following (i) loss of CRMP2 SUMOylation, (ii) loss of CRMP2 phosphorylation by Cdk5, or (iii) gain of CRMP2 phosphorylation by Fyn. Altering CRMP2 modification events simultaneously was not synergistic in reducing Nav1.7 currents, suggesting that Nav1.7 co-opts multiple CRMP2 modifications for regulatory control of this channel. Loss of either CRMP2 SUMOylation or Cdk5 phosphorylation triggered Nav1.7 internalization involving E3 ubiquitin ligase Nedd4-2 as well as endocytosis adaptor proteins Numb and Eps15. Collectively, my findings identify a novel mechanism for regulation of Nav1.7.

Nickolay Brustovetsky, Ph.D., Chair

TABLE OF CONTENTS

LIST OF TABLES

LIST OF FIGURES

FIGURE CONTRIBUTIONS

Figure 1.1. Structure of bacterial VGSC pore and fenestrations to central pore.

This figure was adapted from (Payandeh et al., 2011).

Figure 1.2. Expression of VGSC subtypes and physiology or disease affected by channel dysfunction.

This figure was adapted from (de Lera Ruiz and Kraus, 2015).

Figure 1.3. Requirement of Nav1.7 knockdown from different populations of neurons to affect pain behavior.

This figure was adapted from (Minett et al., 2012).

Figure 2.5. siRNA knockdown of CRMP2.

Western blot performed by Aubin Moutal

Figure 3.5 CRMP2-K374A and increasing deSUMOylation reduces Nav1.7 surface expression.

Biotinylation performed with Weina Ju

Figure 3.9. Blunted SUMOylation of K374A CRMP2 and binding of the mutant to Nav1.7.

Immunprecipitations performed by Aubin Moutal

Figure 3.10. CRMP2 SUMOylation does not alter CRMP2-mediated outgrowth of cortical or DRG neurons.

Outgrowth experiments performed by Sarah Wilson

Figure 4.1. CRMP2 SUMOylation does not affect CRMP2 phosphorylation.

Western blots performed by Aubin Moutal

Figure 4.3. CRMP2-S522A, the Cdk5 site mutant, expression causes a selective reduction in Nav1.7 currents.

Immunprecipitations performed by Aubin Moutal

Figure 4.5. CRMP2 modifications mediate Nav1.7 surface expression.

Western blot performed by Aubin Moutal

Figure 4.7. Fyn site, tyrosine-32, is adjacent to the SUMOylation motif within the crystal structure of CRMP2.

Figure generated by May Khanna

Figure 4.11. Fyn phosphorylation restricts CRMP2 SUMOylation.

Immunprecipitations performed by Aubin Moutal

Figure 4.12. CRMP2 mediated Nav1.7 current reduction requires interaction with the endocytosis proteins Numb and Eps15 and the E3 ubiquitin-protein ligase Nedd4-2.

Western blots performed by Aubin Moutal

Figure 5.2. CRMP2-K374A and CRMP2-S522A reduce DRG excitability.

Patching performed by Xiaofang Yang and Yuying Wang

LIST OF ABBREVIATIONS

Akt	Protein kinase B
AMPA	α-amino-3-hydroxy-5-methyl-4-isoxazolepropionic acid
Arc	Activity-regulated cytoskeleton-associated protein
ATP	Adenosine triphosphate
BACE1	Beta-site amyloid precursor protein cleaving enzyme 1
BDNF	Brain derived neurotrophic factor
BKLF	Basic Kruppel-like factor/Kruppel-like factor
BLAST	Basic local alignment search tool
CAD	Catecholamine A differentiated
CaMKII	Calcium/calmodulin-dependent protein kinase II
Cav	Voltage gated calcium channel subtype
CCI	Chronic constriction injury
Cdk5	Cyclin-dependent kinase 5
CFA	Complete Freund’s adjuvant
CIP	Congenital insensitivity to pain
CRMP	Collapsin Response Mediator Protein
DAXX	Death-domain associated protein

DI-DIV	Domains of voltage-gated sodium channel
DIV	Days *in vitro*
DMEM	Dulbecco's Modified Eagle Medium
DNA	Deoxyribonucleic acid
DRG	Dorsal root ganglia
E1	SUMO activating enzyme
E3	SUMO conjugating enzyme
E3	SUMO ligating enzyme
Elk-1	ETS domain-containing protein
ENaC	Epithelial sodium channel
ENTH	Epsin N-terminal homology
Eps15	epidermal growth factor receptor substrate 15
ERK	Extracellular signal-regulated MAP kinase
ERβ	Estrogen receptor beta
FAK	Focal adhesion kinase
FI	Fast inasctivation
Fyn	proto-oncogene tyrosine-protein kinase
G	Conductance

GAP	GTPase-activating protein
GluK2	Kainate receptor
Grk2	G protein coupled receptor kinase
GSK3β	Glycogen synthase kinase 3 β
HEK293	Human Embryonic Kidney cell line #293
HIC1	Hypermethylated in cancer 1 protein
HSF	Heat-chock factor
HWTX-IV	Huwentoxin 4
IEM	Inherited erythromalegia
IV	Current (I) – Voltage (V)
JNK	c-Jun N-terminal MAP kinase
k	slope value of Boltzmann equation
KAR	Kainate receptor
kDa	Kilo-Dalton
Kv	voltage-gated potassium channel subtype
L1-CAM	L1-cell adhesion molecule
LCM	Lacosamide: [(2R)-2-(acetylamino)-N-benzyl-3-methoxypropanamide
MAP	Mitogen-activated protein

MEF2	Myocyte enhancer factor 2
MICAL-L1	Nedd9-interacting protein with calponin homology and LIM domains – like 1
Nav	Voltage-gated sodium channel subtype
NCX	Sodium/calcium exchanger
NDSM	Negative charge-dependent SUMOylation motif
Nedd4/Nedd4-like	Neural precursor cell expressed developmentally down-regulated protein 4 – E3 ubiquitin ligase
NEM	*N*-Ethylmaleimide
NFκB	Nuclear factor kappa B
NIH	National Institute of Health
NMDA	N-methyl-D-aspartate
NT3	Neurotrophin 3
Numb	Protein numb homolog
OMP	Olfactory marker protein
p38	MAP kinase
pA	Picoamp
PBS	Phosphate buffered saline
Pc2/Cbx4	Polycomb protein 2

PDSM	Phosphorylation-dependent SUMOylation motif
PEI	Polyethylenimine
PEPD	Paroxysmal extreme pain disorder
pF	Picofarad
PI3K	Phosphatidylinositol-4,5-bisphosphate 3-kinase
PIAS1	Protein inhibitor of STAT-1
PKA	Protein kinase A
PKC	Protein kinase C
PML	Promyelotic leukemia protein
PP1	Protein phosphatase 1
PP2A	Protein phosphatase 2A
ProTox-II	Protoxin 2
PS	Presenilin
PVDF	Polyvinylidene difluoride
RhoK	Rho-associated protein kinase
RIPA	Radioimmunoprecipitation assay
RNA	Ribonucleic acid
RT	Room temperature

S1-S6	Transmembrane segments of voltage-gated sodium channel
SAE	SUMO-activating enzyme
SATB1	Special AT-rich sequence binding protein-1
SCN9A	Gene encoding Nav1.7
Sema3A	Semaphorin 3A
SENP	Sentrin/SUMO-specific protease
SFN	Small fiber neuropathy
SGK1	Serum and glucocorticoid-regulated kinase 1
shres	Short hairpin resistant
SI	Slow inactivation
SIM	SUMO-interacting motif
siRNA	Small interfering RNA
SNI	Spared nerve injury
Sra-1	Steroid receptor RNA activator
SUMO	Small Ubiquitin-like Modifier
SVmab1	monoclonal Nav1.7 antibody
TTX	Tetrodotoxin
TTX-R	Tetrodotoxin-resistant

TTX-S	Tetrodotoxin-sensitive
Ubc9	Ubiquitin-conjugating enzyme 9
UBL	Ubiquitin-like protein (SUMO)
UniProt	Universal Protein Resource
$V_{1/2}$	Half-maximal voltage
VGSC	Voltage-gated sodium channel
WAVE	Wiskott-Aldrich syndrome protein-famil verprolin-homologous protein
Wnt	Wingless-type integrated
β subunit	Beta accessory channel subunit

CHAPTER 1.

INTRODUCTION

Pain is a relatable human experience. It developed as an evolutionary survival trait to help animals avoid injuries and dangerous situations. This basic drive for survival holds a great deal of power over our behavior and emotions. In disease and injury, pain can persist beyond what is useful to trigger a beneficial reaction. When this occurs, pain is a detrimental force to society that degrades quality of life and emotional state, decreasing a person's level of function, and creates a financial burden. Conservative estimates from a NIH funded report '*Relieving Pain in America'* warn that ~116 million American adults suffer from chronic pain states that cost the people of the United States between $560-635 billion each year in health care and lost productivity (Institute of Medicine Report from the Committee on Advancing Pain Research and Education, 2011). The report attributes much of this cost to lack of effective therapies. To address this issue, the NIH report challenges researchers to investigate novel pain pathways as targets for future generations of pain-relieving drugs.

This dissertation will describe one such pathway linking modifications of an axonal specification protein, the collapsin response mediator protein 2 (CRMP2) to the regulation of voltage-gated sodium channel Nav1.7, a channel linked inextricably to pain signaling. By identifying mechanisms governing the trafficking of Nav1.7, this work will contribute to enhanced understanding of the biology of Nav1.7 as well as identify possible novel targets for pain relieving therapeutics targeting Nav1.7.

1.1. Voltage-Gated Sodium Channel Nav1.7, a Molecular Target for Pain

1.1.1. Ionic Conductance of Neurons – Historical Perspective

Underlying the transmission of pain is the basic unit of cellular communication between excitable cells – the action potential. This wave of electric potential differences between the inside and outside of the cell was first described during the late 1930s by Sir Alan Hodgkin, Sir Andrew Huxley, Kenneth Cole, and Howard Curtis (Hodgkin, 1937a, b, Curtis and Cole, 1938). The action potential is an electrical wave that travels across the membrane neurons in milliseconds. The shape and duration of the action potential were identified to be choreographed changes in cell membrane permeability to different ionic species (Cole, 1949). Subsequent work identified the ionic species as inwardly flowing sodium ions and outwardly flowing potassium ions (Rothenberg, 1950, Keynes, 1951, Hodgkin and Huxley, 1952b). At its initiation, both the rate and amplitude of the action potential can be experimentally controlled by the concentration of extracellular sodium ions. These early studies concluded then that gain of sodium permeability underlies initiation of neuronal cell-cell communication (Hodgkin and Katz, 1949). Historical papers that outlined initial properties of the action potential laid the foundations for the development of voltage-clamp electrophysiology. Using an amplifier to control the voltage potential across the cell, researchers use this technique to study ionic contributions in neurons. These ionic currents can then be precisely quantified and compared between conditions. This tool has escalated in use over the past 60 years to study fundamental properties of neuronal communication.

Early voltage-clamp experiments resolved that neuronal membranes are selectively permeable to sodium during the rise of an action potential, and that this

permeability is quickly lost as the membrane becomes permeable to potassium during the fall of an action potential (Hodgkin and Huxley, 1952a, c). These shifts in permeability were also determined to be both time and voltage-dependent. Expanding on this work, the existence of moving membrane voltage gates was proposed to control the opening and closing of permeability. Hodgkin and Huxley were able to accurately produce mathematical models of these voltage gates that fit the kinetics of sodium permeability driven activation and inactivation across the cell membrane (Hodgkin and Huxley, 1952d). For their work on the initial descriptions of action potentials and ionic conductance, Sir Alan Hodgkin and Sir Andrew Huxley shared the Nobel Prize in Physiology or Medicine with Sir John C. Eccles in 1963. The channel proteins underlying their work on ionic conductions, however, would remain a mystery for several decades.

1.1.2. Discovery, Structure, and Function of Voltage-Gated Sodium Channels

Identification of the 250kDa voltage-gated sodium channel (VGSC) protein was first achieved by Beneski and Catterall through covalent labeling of channel protein with the agonist, α-scorpion toxin (Beneski and Catterall, 1980). This toxin enhances neuronal activity, thus permitting identification of the proteins underlying this function. By covalent labeling of the channel, the toxin allowed for channel purification from lysate and identification using immunoblotting with antibodies. The discovery and use of this toxin and others greatly advanced the field of biophysics during the 1980s by allowing researchers to discover and characterize interactions with channel proteins. The use of toxins extended beyond their utility as probes to identify and purify channels to their perturbation of channel function, this latter feature was instrumental in early structure-

function analyses to link molecular component of the protein to functional kinetic properties. In 1982, the paralytic shellfish toxin saxitoxin was used to purify an ~250kDa channel protein from rat brain. This protein was reconstituted in phosphatidylcholine vesicles (Talvenheimo et al., 1982) and formed functional channel pores that fluxed sodium and retained sensitivity to channel block by the puffer fish toxin tetrodotoxin (TTX) and stimulated sodium uptake by veratridine, a drug that preferentially binds to activated Na^+ channels causing persistent activation that leads to increased nerve excitability (Sigel, 1987, Barnes and Hille, 1988). Similar studies followed with reconstitution of functional rabbit muscle VGSCs around the same time (Kraner et al., 1985). Using a different method of protein reconstitution, channels from rat brain (Hartshorne et al., 1985) and rabbit T-tubular membranes (Furman et al., 1986) were functionally reconstituted into planar lipid membranes. This allowed for the resolution of single channel currents that displayed voltage-dependent activation. This important finding demonstrated that the voltage-dependence of activation is intrinsic to each channel protein and requires no additional machinery, thus supporting the Hodgkin and Huxley model of activation gates.

Channel identification and purification lead shortly thereafter to breakthroughs in channel cloning and cDNA from *Electrophorus electroplax* was cloned and sequenced in 1984 (Noda et al., 1984). The sequence of this sodium channel provided a stepping-stone to predicting channel structure that aided in identification of key channel features of gating and ion selectivity. Sequence analysis identified the channel as a single 250kDa polypeptide, 1820 amino acid in length. Analysis of secondary and tertiary protein structures predicted four homologous domains (DI-DIV) consisting of six transmembrane

spanning segments (S1-S6) each, and large intracellular N- and C-terminal domains (Guy and Seetharamulu, 1986). Segments S1-S6 are, relatively apolar, transmembrane helical domains, except for S4, which contains several positively charged residues which were hypothesized and later confirmed to function as activation particles (Stuhmer et al., 1989). Between S5 and S6 segments of all four domains a reentrant loop bridges transmembrane regions to form a structure predicted, and later confirmed, to be the outer channel pore (Miller, 1991).

The early model of VGSC protein structure provided a starting point for numerous structure-function relationship studies that followed. As identified by the first sequencing of VGSCs, S4 contains positively charged amino acid side chains that serve as prime candidates for a voltage-sensing mechanism comprising the activation gate. Mutagenesis of these residues and structural comparisons between channels supported this hypothesis. The spacing of positively charged lysine and arginine resides was ideal for uniform orientation towards the center of the channel pore, an organization shared by both calcium (Tanabe et al., 1987) and potassium channels (Tempel et al., 1987). Point mutations that neutralized these positive charges decreased the slope of the voltage-dependence of activation and also shifted the voltage of half maximal activation to more depolarized potentials (Stuhmer et al., 1989). These kinetic shifts reduced channel ability to gate into open confirmations supporting their hypothesized role as the activation gate.

During work with squid giant axons, it was discovered that termination of sodium channel currents by fast-inactivation was disrupted by perfusion of proteases into the cytosolic space (Armstrong, 1981). As such, it was proposed that an intracellular motif is responsible for fast-inactivation. Now armed with predicted protein structural topological

information, researchers identified a curious hydrophobic cluster within the cytoplasmic linker between DIII and DIV. When this cluster was mutated to neutral amino acids, sodium channel fast-inactivation was completely eliminated, identifying this motif as an inactivating particle (West et al., 1992). In another structure-function study, mutagenesis of negatively charged residues within S5-S6 linker that imparted tetrodotoxin and saxitoxin sensitivity introduced permeability of mono and divalent ions to sodium channels (Noda et al., 1989, Schlief et al., 1996). The S5-S6 linker was initially predicted to form an outer pore structure and the loss of selectivity following mutations in this region identify this structure as the selectivity filter. Analogous structures within a variety of ion channels further supported the finding that S5-S6 linker endows ion selectivity to channels (Miller, 1991, Liao et al., 2013).

Recently, the crystal structure of the homotetrameric bacterial voltage-gated sodium channel was solved allowing comparison of sequence predicted models to a sodium channel in closed-pore confirmation with activated voltage sensors (Figure 1.1 from Payandeh et al., 2011) (Payandeh et al., 2011). Confirmation of previously predicted features include arginine derived gating charges, a narrow selectivity filter near the extracellular surface, and voltage sensor mediated shifts of the voltage sensor domains themselves and the S4-S5 linker to dilate the central pore. The structure also prompted discovery of novel features including hydrogen bonding between gating charges and the protein backbone, and fenestrations into the central pore from the sides of the protein structure. These fenestrations are large enough to allow for entry of small, hydrophobic, pore-blocking molecules and confirmation of phenylalanine-203 side chain is hypothesized to alter size of the opening (Figure 1.1 C and D). The resolution of the

crystal structure provides excellent insights into the selectivity of the channel for sodium ions, which we now know requires passage of partially dehydrated sodium ions through a selectivity filter formed by the side chains of glutamate-177. Directly adjacent to this and further into the channel pore, a sodium ion hydrated by a square array of four water molecules can interact with threonine-175 or leucine-176 to pass fully hydrated sodium ions with low energy barriers between positions, a desirable characteristic of a pore that relies on gradient and not energy input to pass ions.

1.1.3. Diversity of Voltage-Gated Sodium Channels and Specific Roles of Nav1.7 in Pain

Nine genes coding for voltage-gated sodium channels alpha pores have been reported to date – Nav1.1-Nav1.9 (Goldin, 1999, Dib-Hajj et al., 2002). These have been broadly classified by their pharmacology and kinetics with members Nav1.1–Nav1.4 and Nav1.6–Nav1.7 being TTX-sensitive, displaying channel block in response to the toxin. In terms of kinetics, these channels are rapidly inactivating. Nav1.5, Nav1.8 and Nav1.9 are TTX-resistant channels and also have slower inactivation kinetics than their TTX-sensitive counterparts (Caffrey et al., 1992). Additionally, Nav1.8, the primary TTX-R contributor to current amplitude displays depolarized voltages of half-maximal activation compared to TTX-S channels, i.e. they require more depolarized voltages to gate open. It is this difference in activation kinetics that allows for electrical separation of TTX-S currents from total currents in voltage-clamp experiments. Using pre-pulse inhibition protocol and post-hoc subtraction of the isolated TTX-R currents, TTX-S currents can be estimated from total currents of cells with heterogeneous expression of sodium channels (Roy and Narahashi, 1992). In neurons, multiple VGSCs are expressed

within the same cell. These channels have variable kinetics, voltage dependencies, sub-cellular localizations, and expression levels that mediate different modalities and code for different electrical properties in the rodent nervous system. Within the nervous system, the nine identified sodium channel isoform display a generalized pattern of expression with Nav1.1, Nav1.2, Nav1.3 and Nav1.6 expression in the central nervous system, Nav1.4 expression in skeletal muscle, Nav1.5 expression in heart tissue, and Nav1.7, Nav1.8 and Nav1.9 expression in the peripheral nervous system (Catterall et al., 2005). These differences code for the diversity of neuronal functions and also make each cell type susceptible to different diseases and pharmacological tools dependent on differences between subtypes. A wide variety of diseases are the result of sodium channel dysfunction throughout the human body (Figure 1.2, adapted from (de Lera Ruiz and Kraus, 2015).

A function ascribed to peripheral Nav channels is pain. Noxious stimuli signal along the axons of dorsal root ganglia (DRG) neurons making their compliment of channels very important to strategies that restrict neuronal signaling of pain. These ganglia of heterogeneous cells, just outside the spinal column, are responsible for nociception, touch and proprioception. Cells of each modality follow a generalized pattern of Nav1.1, Nav1.6, Nav1.7, Nav1.8 and Nav1.9 expression that also correlates to cell body size (Lawson, 2002, Ho and O'Leary, 2011). Large diameter (> 30 μm cell body) DRGs are predominately high conduction velocity, myelinated Aα/β fibers that transmit proprioceptive and touch information utilizing Nav1.1, Nav1.6, and to a lesser extent, Nav1.7 and Nav1.8. This contrasts with smaller diameter (< 30 μm cell body) DRGs that are predominately low condition velocity Aδ and C-fibers transmitting pain

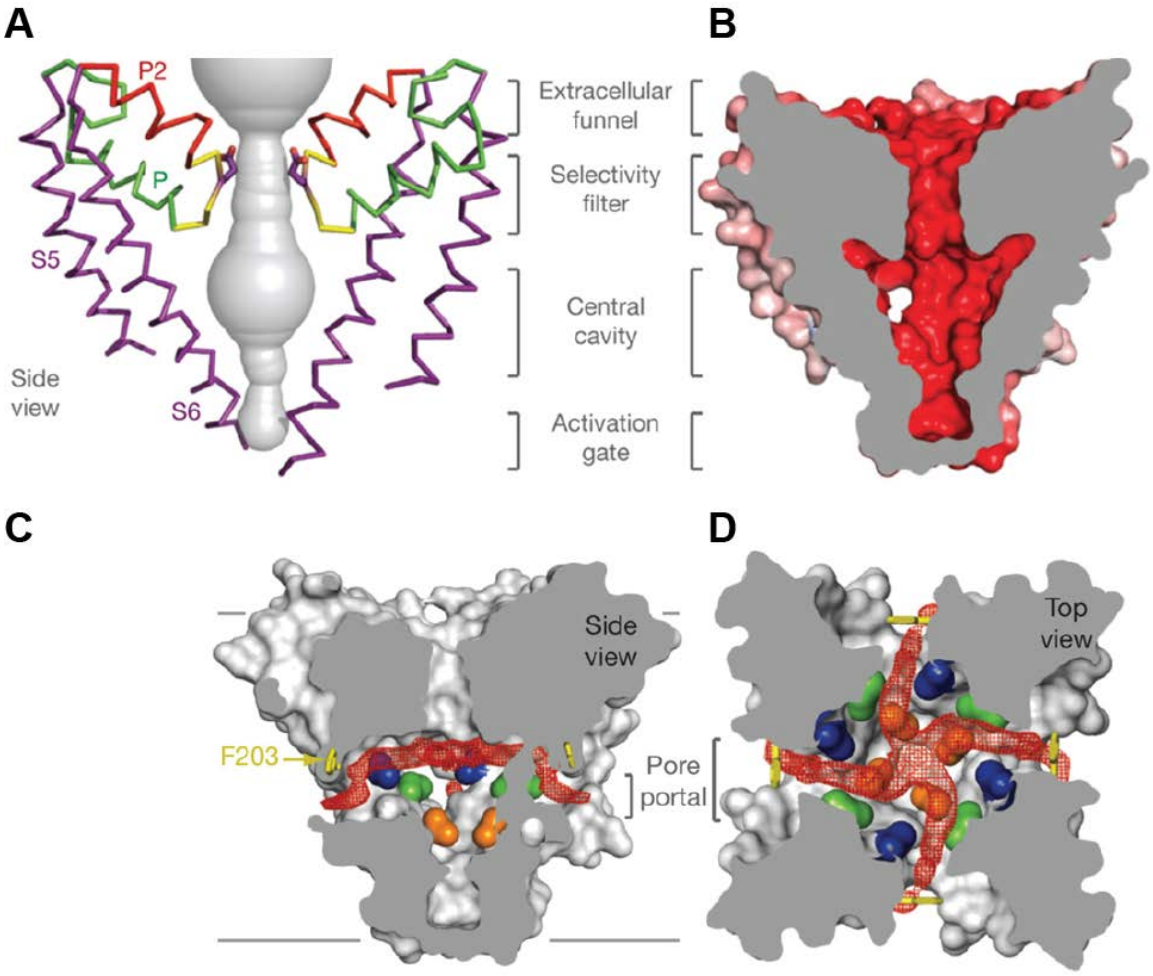

Figure 1.1. Structure of bacterial VGSC pore and fenestrations to central pore. Adapted from (Payandeh et al., 2011). **(A)** Architecture of VGSC pore with Glu-177 selectivity pore in purple, pore structure in yellow, pore helices in green and red, and transmembrane segments in purple. **(B)** Space filling model of channel with negative electrostatic potentials shown by deeper red color. Lighter red color at pore exterior also depicts negative electrostatic potential in a red (-) to blue (+) scale. **(C)** Side view and **(D)** top view of pore with fenestrations highlighted by red wireframe. Confirmation of side Phe203 side chains (yellow) determine aperture of the opening, and different residues implicated in drug block indicated by green, blue and orange ball structures.

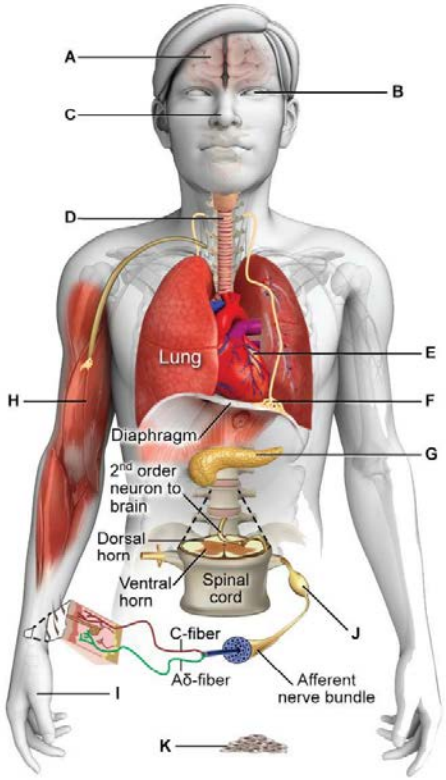

	Tissue	Nav subtype	Effect of dysfunction	References
A	Central Nervous system	1.1, 1.2, 1.3, 1.6	Epilepsy, migraine, autism, ataxia	(Jurkat-Rott et al., 2010, Sanders et al., 2012, Cestele et al., 2013, Djamgoz and Onkal, 2013, Schmunk and Gargus, 2013, Catterall, 2014, Hoeijmakers et al., 2014, Tavassoli et al., 2014)
B	Retnia	1.8, 1.9	Altered visual processing	(O'Brien et al., 2008)
C	Olfactory sensory neurons	1.7	Anosmia	(Cox et al., 2006, Cox et al., 2010, Ahn et al., 2011)
D	Sensory neurons and vagal sensory neurons innervating airways	1.7, 1.8, 1.9	Cough	(Jurkat-Rott et al., 2010, Muroi and Undem, 2011, Sanders et al., 2012, Cestele et al., 2013, Djamgoz and Onkal, 2013, Schmunk and Gargus, 2013, Catterall, 2014, Hoeijmakers et al., 2014, Tavassoli et al., 2014)
E	Heart Muscle	1.5, 1.8	Brugada syndrome, QT syndrome, atrial fibrillation	(Antzelevitch et al., 2014, Hu et al., 2014, van den Boogaard et al., 2014)
F	Nerves, musculature involved in entilation	TTX-S	Respiratory cessation (TTX poisoning)	(Cheng et al., 1968, Muroi and Undem, 2014)
G	Pancreatic β-cells	1.7	Diabetes	(Jurkat-Rott et al., 2010, Sanders et al., 2012, Cestele et al., 2013, Djamgoz and Onkal, 2013, Schmunk and Gargus, 2013, Catterall, 2014, Hoeijmakers et al., 2014, Tavassoli et al., 2014)
H	Skeletal muscle	1.4	Hyperkalaemic periodic paralysis, paramyotonia, congenital, hypokalaemic periodic paralysis	(Jurkat-Rott et al., 2010, Sanders et al., 2012, Cestele et al., 2013, Djamgoz and Onkal, 2013, Schmunk and Gargus, 2013, Catterall, 2014, Hoeijmakers et al., 2014, Tavassoli et al., 2014)
I	Skin	1.7, 1.8, 1.9	Pain disorders, paroxysmal itch	(Dib-Hajj et al., 2013, Bennett and Woods, 2014)
J	DRG neurons	1.6, 1.7, 1.8, 1.9	Pain disorders, paroxysmal itch	(Dib-Hajj et al., 2013, Leipold et al., 2013, Bennett and Woods, 2014)
K	Metastatic cancer cells	1.1-1.9 and beta subunits	Ovarian, cervical, prostate, breast, colon, small cell lung cancer, melanoma, lymphoma	(Brackenbury, 2012, Black and Waxman, 2013, Frede et al., 2013, Fraser et al., 2014, Nelson et al., 2014, Shan et al., 2014)

Figure 1.2. Expression of VGSC subtypes and physiology or disease affected by channel dysfunction

information. Small and medium DRGs have lower expression of Nav1.1 and Nav1.6 and very high levels of Nav1.7, Nav1.8 and Nav1.9 (Ho and O'Leary, 2011). These differences in expression allow VGSCs expressed in small DRGs to be specifically targeted to attenuate pain. A strategy that does not show subtype specificity will produce more side effects due to targeting of all DRGs, other neurons, and heart and muscle tissues.

Extensive studies with sodium channel toxins has recently advanced our understanding of VGSC expression patterns within small DRGs. The μ-conotoxins have differential blocking affinities for Nav1.1, Nav1.6, Nav1.7, Nav1.8, and Nav1.9 and have been utilized to resolve sodium currents in DRGs and to discern the fraction of current carried by each isoform. Using this approach, Nav1.7 has been identified as the dominant TTX-S subtype in small to medium sized DRGs representing nearly 80% of TTX-S current (Zhang et al., 2013) Nav1.7 expression throughout these cells is evident by high signal of Nav1.7 immunolabeling in DRG cell bodies, projections to spinal cord, axons, and peripheral terminals in the dermis (Black et al., 2012). Nav1.7 expression has also been functionally correlated to nociceptive signaling by Nav1.7 immunoreactivity in cells with long duration action potentials, slow conduction velocity, and small cell bodies (C-fibers) (Djouhri et al., 2003).

The Nav1.7 channel, with high expression in nociceptive DRGs, conveys specific properties to dorsal root ganglia cells that are important for the summation of sensory inputs. Compared to other peripheral TTX-S channels, Nav1.7 displays slow closed-state inactivation when driven by a slow voltage ramp. This property is analogous to high responsiveness to inputs over long durations. The channel is able to respond to a broader

range of inputs, which allows it to function as a signal-processing channel for the generation of action potentials (Cummins et al., 1998, Herzog et al., 2003). Though the summation of signals, Nav1.7 generates threshold currents that determine action potential firing. Specific evidence of this property is found in human gain-of-function mutations wherein Nav1.7 becomes more conductive to sodium culminating in hyperexcitable DRGs (Dib-Hajj et al., 2007). Many unique Nav1.7 gain-of-function mutations have been identified as mechanisms for painful human diseases like inherited erythromelalgia (IEM), where a hyperpolarizing shift in channel activation makes Nav1.7 more available in response to voltage changes, and paroxysmal extreme pain disorder (PEPD), where depolarizing shifts in fast-inactivation slows inactivation to reduce the current threshold for subsequent action potentials (Dib-Hajj et al., 2008, Estacion et al., 2008, Estacion et al., 2011, Theile et al., 2011, Estacion et al., 2013). IEM and PEPD as well as Nav1.7 mediated small fiber neuropathy (SFN) (Cannon, 2012, Han et al., 2012, Ahn et al., 2013) present with symptoms such as pain triggered by warmth in the extremities and episodic pain of the face and extremities including burning sensations. The exact *opposite* effect on pain has been observed within patients harboring loss-of-function Nav1.7 mutations. These individuals exhibit congenital insensitivity (CIP) to pain and completely lack thermal and mechanical pain thresholds (Cox et al., 2006, Kurban et al., 2010). The initial observation of CIP is typically made by parents when the child does not respond to injuries and during the first years of life lips, tongue, and finger tips are commonly damaged. In some cases, these self-induced injuries result in amputation if the injury is severe or secondary infection presents without any distress from the child (Bennett and Woods, 2014). In about one third of cases the families of these children are accused of

physical abuse and many children are initially misdiagnosed as mentally handicapped due to lack of painful feedback that allows for appropriate reaction to their environment. The high expression of Nav1.7 in nociceptive DRGs and phenotypes of human patients with Nav1.7 mutations conveys an importance of this channel in pain and has led many researchers to study Nav1.7 in rodent pain models.

One important and powerful approach to examine the role of Nav1.7 in pain is the generation of transgenic mice. Early attempts suffered setbacks due to neonatal lethality of global Nav1.7 knockout (Nassar et al., 2004, Weiss et al., 2011). To overcome this obstacle, researchers cross-bred Nav1.7$^{+/-}$ heterozygote mice with sturdier mouse strains that are resistant to stress. They also employed extreme measures of human-aided postnatal care that allowed for a small fraction (~5%) of global Nav1.7-null mice to survive to adulthood. These mice have overall normal behavior and congenital insensitivity to pain in hot plate, tail clip, formalin, complete Freund's adjuvant, thermal, mechanical, chemical, and inflammatory pain behavioral tests (Gingras et al., 2014). Whereas global Nav1.7 deletion recapitulates congenital insensitivity to pain observed in human loss-of-function SCN9A mutations, mice that lack Nav1.7 and Nav1.8 from their nociceptive neurons undergo normal development of neuropathic pain (Nassar et al., 2005) and mice that lack Nav1.7 in nociceptors versus all DRGs, or all sensory neurons display differential pain behaviors (Minett et al., 2012, Minett et al., 2014a).

Using a Nav1.8-Cre mouse, Nav1.7 was specifically deleted from Nav1.8 positive nociceptors and these Nav1.7-null mice displayed reduced acute pain behavior measured by hind paw withdrawal threshold and reduced mechanical and thermal pain following inflammation induced by formalin or CFA injections (Nassar et al., 2004). In a follow up

study, Nav1.7 and Nav1.8 were both deleted from nociceptive neurons using the same Nav1.8-Cre mice. These Nav1.7/Nav1.8 double-knockout mice displayed normal motor coordination tested by stability on a rotarod, increased thermal and mechanical thresholds for acute pain, and a complete lack of inflammatory pain to formalin injection. These mice, however, underwent normal development of neuropathic pain following ligation of L5 spinal nerve. This pain state therefore is not dependent on Nav1.7 or Nav1.8 expression in nociceptors despite strong evidence that both channels participate in the generation of painful stimuli (Nassar et al., 2005).

Additional Nav1.7 mice in which Nav1.7 was deleted from specific populations of neurons was generated under control of Advillin promoter to knockout Nav1.7 from all DRG neurons and also *Wnt1* promoter to knockout Nav1.7 from both sensory and sympathetic neurons (Minett et al., 2012). Nav1.7-Advillin knockout mice abolished mechanical and inflammatory pain much like other Nav1.7 and Nav1.7/Nav1.8 knockouts. In addition, mice lacking Nav1.7 in all DRGs presented with increased threshold to thermal pain as assessed by Hargreaves' test which was not observed in previous studies when Nav1.7 was knocked out the Nav1.8 promoter (Nassar et al., 2005). Therefore, Nav1.7 activity in all DRG subtypes is required for thermal sensitivity to this test. Within the same study, Nav1.7-Wnt1 knockout mice displayed increased latency of withdrawal in the hotplate test that was not previously observed in Nav1.7 knockout mice under Nav1.8- or Advillin-promoters. Knockout by the Wnt1 promoter removes Nav1.7 expression from all neural crest derived cells that differentiate into sensory and autonomic neurons. Therefore, restriction of Nav1.7 participation within sympathetic neurons is what likely attenuates thermal sensitivity (Minett et al., 2012).

The Nav1.7-Wnt1 knockout mice displayed complete reversal of neuropathic pain suggesting that development of this pain state requires Nav1.7 in sympathetic neurons. One study suggests, however, that some pain states are not dependent on classical nociceptors. In animals treated with the chemotherapeutic agent oxalipatin, complete lack of Nav1.7 was insufficient in preventing onset of pain (Minett et al., 2014b). Release of Substance P, which contributes to NMDA-mediated wind up and sensitization of nociceptive fibers (Herrero et al., 2000) was reduced in Nav1.7-Advillin knockout mice (Minett et al., 2012) as was the response to a small range of noxious cold stimuli (Minett et al., 2014a), suggesting that Nav1.7 in DRG neurons significantly contributes to mechanisms relating to the development of multiple, but not all, pain states.

Due to these differences in Nav1.7 conditional knockouts, the role of Nav1.7 in generation of pain behavior is incompletely understood and appears to involve a variety of neuronal populations (Figure 1.3, adapted from (Minett et al., 2012)). Thus, it is still unclear if Nav1.7 is a necessary and sufficient determinant of pain behavior. Nevertheless, targeting of DRG Nav1.7 channels appears to be a highly pursued strategy to ameliorate several painful conditions as highlighted by research efforts of academic laboratories and pharmaceutical companies investing in Nav1.7-targeted therapies (Table 1.1).

Like mutations that alter channel kinetics, diseases that increase Nav1.7 channel surface expression can enhance current in DRGs and produce numerous pain states. Diabetes mellitus is one such disease frequently associated with hyperalgesic and allodynic pain states that have been correlated with increased TTX-R and TTX-S current density and channel expression (Hong et al., 2004). In animal models of diabetes, Nav1.7

undergoes a ~50% expression increase in small and medium diameter DRG neurons. Similarly, inflammatory pain mediated by 4% carrageenan injected into rat hind paws has also been associated with ~25% increased VGSC expression. In the carrageenan model, DRG expression of Nav1.3, Nav1.7 and Nav1.8 are increased and TTX-S currents undergo ~40% increase in density supporting the hypothesis that VGSC expression underlies inflammatory pain (Black et al., 2004). Nerve damage resulting from treatment with the chemotherapeutic agent paclitaxel results in hyperexcitability of DRGs and associated ~30% increase in Nav1.7 expression (Zhang and Dougherty, 2014). In addition to these examples, mechanical injury to nerves has been shown regulate VGSC expression. Immediately after injury a variety of inflammatory mediators are released, including bradykinin, prostaglandins, neurotransmitters, and neurotrophins. Many of these factors interact with cell surface receptors on neurons to alter signaling pathways, including PKA/PKC pathways known to modulate VGSCs (Julius and Basbaum, 2001). In the specific case of spared nerve injury, where the sural branch of the sciatic nerve is spared while the tibial and common peroneal nerves are ligated, Nav1.7 and Nav1.8 current densities are increased. Additionally, Nav1.7 expression is increased ~100% along the sciatic nerve (Laedermann et al., 2013a). In addition, herpes vector-mediated knockdown of Nav1.7 in DRG sensory neurons significantly prevents the development of hyperalgesia (i.e. an increased response to a painful stimulus) in response to complete Freund's adjuvant (Yeomans et al., 2005).

Spurred, in part, by studies that implicate Nav1.7 in painful human disease and injuries, the channel has become a popular candidate target for therapeutics. Tarantula peptide toxins are selective for Nav1.7 *in vitro* but fail to provide analgesia in pain

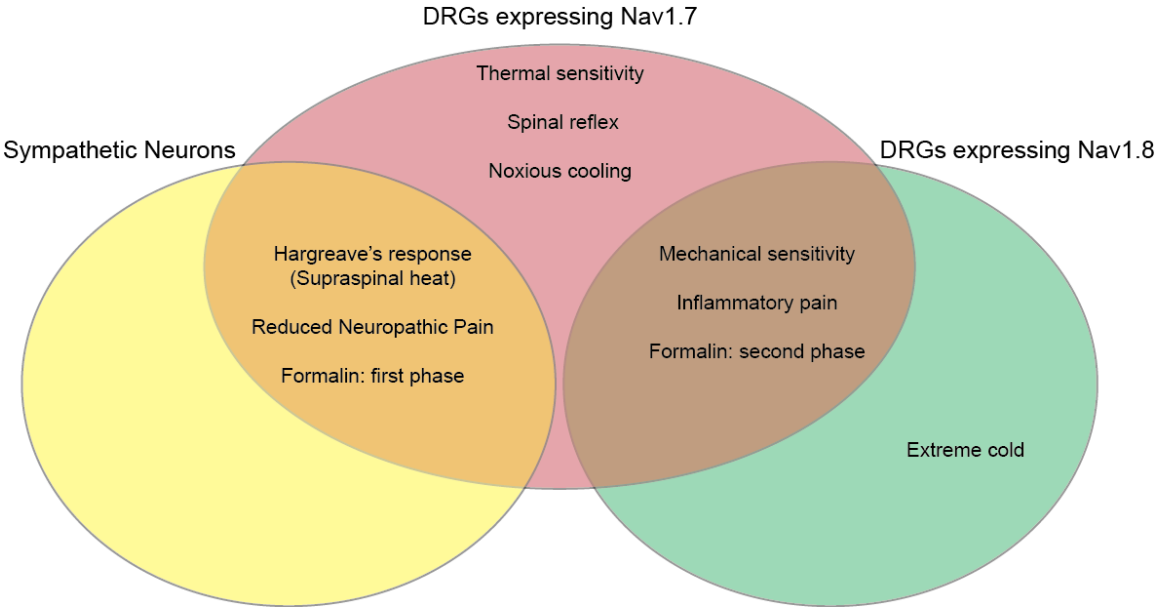

Figure 1.3. Requirement of Nav1.7 knockout from different populations of neurons to affect pain behavior. Figure adapted from (Minett et al., 2012). Nav1.7 expression in Nav1.8-positive DRGs (brown: red/green overlap) is required for mechanical sensitivity, response to the second phase of formalin, and inflammatory pain. Nav1.7 expression in Nav1.8-negative DRGs (red) is required for acute thermal sensitivity, spinal reflex, and noxious cooling, but not extreme cold which is dependent on Nav1.8 (green). Nav1.7 expression in both DRGs and sympathetic neurons (orange: red/yellow overlap) is required for supraspinal heat response, neuropathic pain, and the first phase of formalin response.

Drug	Mechanism	Phase	Indications	Reference(s)
Carbamazepaine	Non-selective Nav block	4	Erythromelalgia	Clinical Trial: NCT02214615
Lacosamide	Non-selective Nav block	3	Painful diabetic neuropathy, fibromyalgia	(Beyreuther et al., 2006, Hao et al., 2006)
Ralfinamide	Non-selective Nav block	2	Evaluation in neuropathic pain	(Veneroni et al., 2003)
TV-45070	Nav1.7/Nav1.8 block	2	Chronic pain conditions	(Bagal et al., 2014)
PF-05089771	Nav1.7/Nav1.8 block	2	Diabetic peripheral Neuropathy	(Bagal et al., 2014) Clinical Trial: NCT02215252
TTX	Non-selective TTX-S block	2	Neuropathic pain	Clinical Trial: NCT01655823
CNV1014802	Nav1.7 block	1/2	Trigeminal neuralgia	(Bagal et al., 2014) Clinical Trial: NCT02359344
DSP-2230	Nav1.7/Nav1.8 block	1/2	Neuropathic pain	(Bagal et al., 2014)
AZD3161	Nav1.7 block	1	Neuropathic and inflammatory pain	Clinical Trial: NCT01240148
CNV-30000223 CNV-3000164	Nav1.7 block	N.A	Undisclosed Patented to target VGSCs	(Shao et al., 2004, de Lera Ruiz and Kraus, 2015)
Benziimidzaole Imidazoryrdine	Nav1.7/Nav1.8 block	N.A.	Patented to target VGSCs	(de Lera Ruiz and Kraus, 2015)
PF-04856264	Nav1.7 block	N.A	Pain	(McCormack et al., 2013, de Lera Ruiz and Kraus, 2015)
HWTX-IV	Nav1.7 block	N.A.	Inflammatory and neuropathic pain in rodents	(Xiao et al., 2008, Xiao et al., 2010, Liu et al., 2014a)
ProTox-II	Nav1.7 block	N.A.	N.A.	(Smith et al., 2007, Schmalhofer et al., 2008, Xiao et al., 2010)
μ-conotoxins	Nav1.7 block and non-selective Nav block	N.A.	N.A.	(Wilson et al., 2011)
Nav1.7 antibody	Nav1.7 block	N.A.	Itch and pain	(Lee et al., 2014)

Table 1.1. Compounds advanced for pain therapy with Nav1.7 mediated mechanisms of action. Compounds not undergoing clinical trials have been demonstrated to reduce Nav1.7 function in heterologous expression systems.

models (Theile and Cummins, 2011b), likely due to lack of penetration past the perineural barrier (Schmalhofer et al., 2008). A Nav1.7-selective centipede-venom peptide was recently reported to elicit analgesia in acute animal pain models, but has not been yet tested in more complex rodent pain models (Yang et al., 2013). A monoclonal antibody (SVmab1) against the voltage-sensor of Nav channels resulted in functional selectivity for Nav1.7, with partial effects on Nav1.6 (Lee et al., 2014). Several small-molecule blockers of hNav1.7 have been described; but they generally lack subtype selectivity (Clare, 2010) (Table 1.1). The work in this thesis will focus on Nav1.7 as an important channel in the regulation of pain, but, importantly, the peripherally expressed Nav1.8 and Nav1.9 channels have also been put forward as important regulators of human pain states (Liu and Wood, 2011). Small-molecule blockers of Nav1.8 and Nav1.9 channels are also of interest to pain researchers.

Nav1.7 expression in the peripheral nervous system endows the channel with modalities other than transmission of pain. One such example is a cough response that is stimulated by the sensation of itch. This Nav1.7-mediated response is transmitted by the vagal nerve and is well-studied in guinea pigs (Muroi and Undem, 2011). Within the guinea pig nodose ganglion of the vagus nerve, Nav1.7 is the dominant TTX-S isoform. As a result of short hairpin interfering RNA (shRNA)-Nav1.7-mediated gene silencing in this ganglion, action potential frequency and cough response in awake guinea pigs were greatly reduced (Muroi and Undem, 2011) Recent work with Nav1.7-specific antibodies that block movement of the voltage-sensor paddle has shown that the channel also has a role in peripheral dermal itch sensations (Lee et al., 2014). Pre-treatment with a Nav1.7-specific antibody provided complete recovery of itch-mediated behavior and synaptic

activity produced by chemically induced itch. The antibody also successfully attenuated pain behavior to directly link Nav1.7 activity to transmission of noxious information.

Nav1.7 has been implicated in anosmia, the loss of olfaction. The channel is expressed highly in olfactory neurons and loss-of-function mutations have provided insight into the role of Nav1.7 in olfaction (Weiss et al., 2011). The University of Pennsylvania Smell Identification Test – a standardized 40-item smell test, assessed patients with congenital insensitivity to pain carrying SCN9A mutations. Compared to wildtype controls, none of these patients were able to detect any of the 40 odors. Several odors such as balsamic vinegar and perfume were described as unpleasant by nine normal ('wildtype control') individuals, and previous to this study none of the test subjects reported any complaints about the lack of smell (Weiss et al., 2011). Based on this result, a Nav1.7 conditional knockout mouse was created using the Cre-*lox*P system to delete the channel from cells that express olfactory marker protein (OMP) present in all classical olfactory sensory neurons. These mice displayed complete loss of synaptic activity in the olfactory glomerulus responsible for transduction of olfactory stimuli and also complete loss of preference for olfactory attractants and repellants including urine, peanut butter, and milk. This study therefore establishes a critical role of Nav1.7 in olfaction.

1.1.4. Regulation of VGSCs: Focus on Nav1.7

Regulation of VGSCs has been reported to be dependent on post-translational modifications and alternative splicing of the channels, expression of accessory channel subunits, modulation of signaling cascades that control transcription, and channel

trafficking (Table 1.2). Phosphorylation by protein kinase A (PKA) and PKC were amongst the first identified modifications to exert modifying control over the channel. Interpretations of results from these studies are difficult, however, due to opposing effects depending on cell background. For example, activation of PKC attenuated Nav1.2 (Cantrell et al., 2002), Nav1.4 (Bendahhou et al., 1995, Murray et al., 1997), Nav1.5 (Schreibmayer et al., 1991), and Nav1.7 (Vijayaragavan et al., 2004) currents when channels are heterogeneously expressed in heterologous cell lines, but the same manipulations positively regulated the channels in primary cells like DRGs (Gold et al., 1998). Heterologous expression systems remain important for identifying regulators of VGSCs because they provide a large amount of consistent experimental material that is sturdy enough to survive harsh experimental manipulations. However, cell-specific effects highlight the importance of studying mechanisms in cell types of interest where the mechanisms are physiologically relevant. In another mode of channel regulation, total DRG sodium current is positively correlated with activation of PKC and negatively correlated with activation of PKA (Vijayaragavan et al., 2004). Additionally, reduction of Nav1.7 by PKA requires prerequisite PKC activity, whereas PKC-mediated enhancement acts independently without any requirement of PKA (Gold et al., 1998).

Nav1.7 is also regulated is by alternative splicing of exon 11. Coding for the L1 cytoplasmic loop (Raymond et al., 2004) domain that is targeted by PKA phosphorylation (Cantrell et al., 2002), expression of different splice variants can alter Nav1.7 channel kinetics. After injury, an ‘11S’ variant that lacks 11 amino acids undergoes disproportionate upregulation compared to other variants. PKA phosphorylation of this particular variant produces a hyperpolarizing shift in activation, which, in addition to

upregulation in response to injury, appears to promote hyperexcitability of DRGs (Chatelier et al., 2008).

Mitogen-activated protein (MAP) kinases can also regulate Nav1.7. These serine/threonine-specific kinases link membrane receptor activation to cytosolic signaling cascades (Seger and Krebs, 1995). In human neuromas, the upregulation of p38 and ERK1/2 MAP kinases has been correlated to upregulation of Nav1.3, Nav1.7, and Nav1.8 (Black et al., 2008). Nerve ligation animal models support MAP kinase regulation of VGSCs in injury and pain models where inhibition of extracellular signal-regulated kinase (ERK), p38 and c-Jun N-terminal kinase (JNK) MAP kinases reversed mechanical allodyinia and p38 inhibition reversed thermal hyperalgesia (Obata et al., 2004). Both Nav1.6 and Nav1.8 are direct targets of p38 phosphorylation that occurs in the L1 cytoplasmic loop of the channels suggesting that these two isoforms may mediate this effect without effect on Nav1.7, which is not phosphorylated by p38. Nav1.6 and Nav1.8 channels are differentially regulated by p38 as Nav1.6 phosphorylation reduces peak current density (Wittmack et al., 2005) while Nav1.8 phosphorylation increases peak current density (Hudmon et al., 2008). Due to preferential expression of Nav1.8 in nociceptive neurons, p38-mediated increases in Nav1.8 link pro-inflammatory mediators to DRG hyperexcitability.

VGSCs are heavily glycosylated proteins with carbohydrates representing up to 30% of protein mass (Schmidt and Catterall, 1986). The cytosolic pool of unprocessed VGSCs are far less glycosylated than fully processed and folded surface VGSCs suggesting a role for this modification in the proper folding and surface trafficking of channels (Schmidt and Catterall, 1986). Heavy glycosylation of Nav1.9 produces a

hyperpolarized shift in channel activation making the channel more available to produce current (Tyrrell et al., 2001). Glycosylation of Nav1.4 can lead to sialylation of glycosylated groups that shifts channel gating to depolarized potentials (Ednie et al., 2015). Nav1.7 glycosylation has some correlation to participation of beta subunits in trafficking as beta1 selectively traffics intermediately glycosylated channel protein (Laedermann et al., 2013b). Finally, glycosylation of Nav1.5 determines channel function in the membrane due to incompletely glycosylated protein displaying lower function than fully glycosylated Nav1.5 (Mercier et al., 2015).

A prominent VGSC regulatory pathway involves modulation by accessory beta (β) channel subunits. Linked by disulfide bonds to the alpha subunit pore, β proteins introduce a variety of regulations and properties to channels, including altered kinetics, biosynthesis and trafficking, sub-cellular localization, and cell adhesion properties (Schmidt and Catterall, 1986, Isom et al., 1992, Srinivasan et al., 1998, Meadows et al., 2002, Yu et al., 2003). Observation of the first identified β proteins, β1 and β2, occurred at the same time as the initial identification of the alpha protein pore (Schmidt and Catterall, 1986). It was noted that these ~35kDa proteins preferentially interacted with functional membrane channel proteins, suggesting a role in biosynthesis and channel membrane expression. This role was further supported by later studies in *Xenopus* oocytes where expression of either β1 (Isom et al., 1992), or β2 (Isom et al., 1995) was demonstrated to increase the trafficking and current density of Nav1.2. Expression of β1 also shifted the curve of channel inactivation towards hyperpolarized potentials. The later identified β3 and β4 proteins can also mediate changes in channel kinetics with data showing hyperpolarized shifts in Nav1.3 activation following expression of β3 (Meadows

et al., 2002) and hyperpolarized shifts in Nav1.2 and Nav1.4 activation following expression of βIV (Yu et al., 2003). The extracellular domain of β subunits, which contain immunoglobulin-like domains that resemble other families of adhesion molecules, can mediate cell-cell interactions and sub-cellular localization. Specifically, the β2 protein interacts with tenascin-C and tenascin-R –extracellular matrix proteins (Srinivasan et al., 1998), and β1-null neurons display a loss of Nav1.6 organization at the axon initial segment (Brackenbury et al., 2010). These proteins can therefore alter cellular distribution and localization of sodium channels, which is important in determining channel function. Channel localization to peripheral terminals would suggest a role in summation of inputs, whereas localization to a Node of Ranvier would suggest a role in propagation of salutatory conduction.

Several studies have suggested that Nav1.7 can be regulated by multiple beta subunits. In HEK293 cells, both β1 and β3 have been shown to upregulate heterologously expressed Nav1.7 channels and display lower levels of glycosylation than Nav1.7 channels alone (Laedermann et al., 2013b). In sensory neurons of β2-null mice, Nav1.7 channel expression and current density is greatly reduced highlighting an important role of βII in Nav1.7 trafficking (Lopez-Santiago et al., 2006). Importantly, β2-null animals display reduced inflammatory and neuropathic pain responses, suggesting the role, albeit indirectly, of Nav1.7 modulation in the development of pain.

Regulation of Nav1.7 in sensory neurons has also been demonstrated by the E3 ubiquitin ligase – neural precursor cell expressed developmentally down-regulated protein 4 (Nedd4-2). Nedd4-2 monoubiquitinates Nav1.7 to mark it for endocytosis (Laedermann et al., 2013a). Following peripheral nerve injury, Nedd4-2 exhibits reduced

expression and therefore has limited activity on Nav1.7, which produces increases to channel expression, current density, and hyperexcitability of neurons. Viral delivery to overexpress Nedd4-2 to recover ligase expression reverses these effects on Nav1.7 in injured animals and alleviates mechanical allodynia.

Surface expression and activity of Nav1.7 can also be altered by transcriptional regulation. Data from two studies suggest that both lithium (Yanagita et al., 2009) and insulin-like growth factor 1 (Yanagita et al., 2011) can inhibit glycogen synthase kinase 3β (GSK3β) in the Phosphatidylinositol-4,5-bisphosphate 3-kinase (PI3K)-Akt-GSK3β signaling pathway to increase Nav1.7 transcriptional rate, mRNA levels, and surface expression.

Despite the above studies, much remains still to be understood in the biology of Nav1.7. In particular, most studies to date have focused on the regulation of the channel directly by post-translational modifications or transcription versus regulation by classically defined accessory subunits or at the transcriptional level. There is very limited information on how other interacting proteins affect Nav1.7 activity and function. The next section provides a background on one such protein that confers a unique regulation on Nav1.7.

1.2. Collapsin Response Mediator Protein 2 (CRMP2)

1.2.1. Background

Collapsin response mediator 2 (CRMP2, also known as DPYSL2/DRP2, Unc-33, Ulip, TUC2) was first identified for its role in mediating axon growth and guidance of

Mediated by	Cell type	Effect	Reference
PKA	DRG	Reduced expression	(Gold et al., 1998)
PKC	DRG	Increased expression	(Gold et al., 1998)
PKC	Oocytes	Decreased expression	(Vijayaragavan et al., 2004)
Splice variant 11S	DRG	Hyperpolarized activation	(Chatelier et al., 2008)
MAP Kinases	DRG	Increased expression	(Black et al., 2008)
GSK3β	Adrenal chromaffin cells	Decreased transcription	(Yanagita et al., 2009)
β1	HEK293	Increased trafficking	(Laedermann et al., 2013b)
β3	HEK293	Increased trafficking	(Laedermann et al., 2013b)
β2	DRG	Increased trafficking	(Lopez-Santiago et al., 2006)
Nedd4-2	DRG	Decreased trafficking	(Laedermann et al., 2013a)
Lithium	Adrenal chromaffin cells	Increased transcription Increased expression	(Yanagita et al., 2009)
Insulin-like growth factor 1	Adrenal chromaffin cells	Increased transcription Increased expression	(Yanagita et al., 2011)

Table 1.2. Modifiers of Nav1.7. Modifiers and effects on Nav1.7 as well as cell types in which these modifications have been observed.

chick dorsal root ganglia neurons (Goshima et al., 1995). Analogs of the protein have been identified in *Caenorhabditis elegans*, *Drosophila melongaster*, rodents, and humans (Hedgecock et al., 1985, Geschwind and Hockfield, 1989, Minturn et al., 1995, Byk et al., 1996, Kitamura et al., 1999, Morris et al., 2012). In mammals, CRMP2 belongs to a family of five structurally similar proteins CRMPs 1–5 that share homology with the liver enzyme dihydropyrimidinase (Wang and Strittmatter, 1997a, Fukada et al., 2000, Schmidt and Strittmatter, 2007). The 'bilobed-lung' configuration of the protein, observed in the solved crystal structure is believed to be shared between all CRMPs (Deo et al., 2004, Stenmark et al., 2007). This shared configuration aids in formation of both homo- and hetero-tetramers between CRMP family proteins. As CRMPs display higher affinity for family proteins than itself, heterotetramers are more common than homotetramers (Wang and Strittmatter, 1997a, Yoneda et al., 2012), but because CRMP2 is the most widely expressed, it is proposed that a high percentage of tetramers contain at least one CRMP2 protein (Wang and Strittmatter, 1996). The effects of oligomerization are not well described and functions of CRMP2 have not been experimentally separated by contribution of CRMP2 within tetramers or contribution of CRMP2 functioning as monomers.

CRMP2 functions during early neurogenesis in axon guidance allow for use of the protein as an early marker of neuronal differentiation (Minturn et al., 1995, Byk et al., 1996, Gaetano et al., 1997). The distal part of the axon is enriched in CRMP2 which influences axonal specification. In hippocampal neurons, over-expression of CRMP2 induced supernumerary axons, axon elongation, and increased axonal branching, while its inhibition with a dominant negative protein suppressed the formation of the primary axon

(Inagaki et al., 2001a, Yoshimura et al., 2005b). Interestingly, CRMP2 can convert established dendrites to axon, is involved in the Sra-1/WAVE/kinesin cargo complex and is required for BDNF/NT3-induced axon outgrowth/branching (Inagaki et al., 2001a, Kawano et al., 2005, Yoshimura et al., 2005b). Axon elongation is ultimately achieved through microtubule assembly and extension, and actin reorganization and membrane genesis at the leading edge of the growth cone. CRMP2 may not only enhance microtubule polymerization but may also modulate membrane tremodeling through interaction with its partners, depending upon specific post-translational modifications (Inagaki et al., 2001b, Nishimura et al., 2003b, Brown et al., 2004, Cole et al., 2004, Yoshimura et al., 2005a, Morinaka et al., 2011) and secreted trophic factors. In hippocampal neurons, NT3 induces axonal growth and branching activity by inhibiting CRMP2 phosphorylation by GSK-3β (Yoshimura et al., 2005b). Conversely, Sema-3A induces axonal retraction by increasing CRMP2 phosphorylation by GSK-3β (Uchida et al., 2005). CRMP2 binds to cytoskeletal proteins tubulin, actin, and vimentin (Fukata et al., 2002a, Vincent et al., 2005, Vuaillat et al., 2008). It has been demonstrated that non-phosphorylated CRMP2 binds strongly to tubulin leading to microtubule formation, while CRMP2, phosphorylated by Rho kinase, suppresses its binding to tubulin and Numb (Arimura et al., 2000a). Two other kinases working in tandem, CDK5 and GSK-3β, also control the interaction of CRMP2 with tubulin.

Emerging literature has demonstrated novel functions of CRMP2, particularly as a trafficking protein via interaction with kinesin and dynein motor proteins (Nishimura et al., 2003b, Kawano et al., 2005, Kimura et al., 2005, Lykissas et al., 2007, Arimura et al., 2009, Rahajeng et al., 2010). In the case of retrograde transport and dynein, CRMP2 has

been proposed to have roles in linking the dynein motor to vesicular cargo through interaction with endocytic vesicle complex protein MICAL-L1 (Rahajeng et al., 2010). Interaction of CRMP2 with endocytosis mediators Numb and α-adaptin proteins also facilitate CRMP2's roles as a trafficking cop (Nishimura et al., 2003a).

Recent work from the Khanna laboratory has expanded the CRMP2 interactome to include, heretofore unknown, partners that include voltage- and ligand-gated ion channels and exchangers. Initial work identified interactions with N-type voltage-gated calcium channels (Cav2.2) (Brittain et al., 2009, Chi et al., 2009a). Enhanced CRMP2 expression mediated increased channel surface expression, enhanced calcium influx, and consequently enhanced neurotransmitter release from presynaptic vesicles (Brittain et al., 2009a, Chi et al., 2009a, Hensley et al., 2011, Khanna et al., 2012). Later work then identified involvement of CRMP2 at the post-synaptic level where interaction with NR2B receptors were demonstrated to interact with NMDA receptors (Al-Hallaq et al., 2007). Other binding partners of CRMP2 include the calcium sensing protein calmodulin (Zhang et al., 2009) and the Ras-GAP neurofibromin protein (Lin and Hsueh, 2008). CRMP2 binding to neurofibromin is proposed to contribute to Neurofibromatosis type 1 disease in which CRMP2 activity on other substrates becomes restricted due to sequestration of cytosolic CRMP2 by neurofibromin (Patrakitkomjorn et al., 2008). The CRMP2 interactome also includes the plasmlemmal sodium/calcium exchanger NCX3 which increases cytosolic calcium by operating in reverse during glutamate toxicity (Brustovetsky et al., 2014). Incubation with Tat-CBD3, a peptide that binds CRMP2 enhances interaction between CRMP2 and NCX3 in rat hippocampal neurons leading to NCX3 internalization and restriction of calcium influx.

1.2.2. CRMP2 Post Translational Modifications and Regulation of Function

As CRMP2 maintains no known enzymatic activity of the related dyhydropyrimidinase protein, its functions are endowed by direct protein interactions with partners in effector pathways (Wang and Strittmatter, 1997a). Post translational modifications, primarily phosphorylation, of CRMP2 allow it to direct interactions with different protein partners and engage in different cellular cascades. While high resolution crystal structures of CRMP2 have been determined, the C-terminal region of CRMP2 wherein the protein is multiply phosphorylated is susceptible to proteolysis (Deo et al., 2004), precluding structure-function analysis.

As a regulatory mechanism, protein phosphorylation involves donation of a phosphate group (PO_4^{3-}) from ATP to a serine, threonine, or tyrosine amino acid residue (Olsen et al., 2006). This transfer is catalyzed by protein kinases that recognize target structural motifs within proteins (Yaffe and Elia, 2001). First observation of this phenomenon was the activation of glycogen phosphorylase b to glycogen phosphorylase a in the rate limiting step of glycogenolysis (Fischer and Krebs, 1955). Sequencing of the human genome has allowed for identification of the human kinome, a full set of protein kinases, which predicts a total of 518 kinase members with a large pool of protein targets (Manning et al., 2002).

Introduction of phosphate groups at physiological pH introduces a double negative charge not found within any of the twenty-one eukaryotic amino acid side chains. This unique side chain charge modification introduces structural and functional

consequences to targeted proteins (Johnson and Lewis, 2001). Hydrogen bonds are largely responsible for these changes as the double negative charge provided by phosphorylation is ideal for hydrogen bond formation between nearby side chains. This acts to stabilize conformational states thus altering secondary and tertiary protein structure (Mandell et al., 2007). Altered protein confirmation can then lead to differential recognition or binding of other proteins (Filippakopoulos et al., 2008) including secondary kinases to provide further effects of phosphorylation (DePaoli-Roach, 1984, Fiol et al., 1988). Protein phosphorylation is made reversible by protein phosphatases that remove phosphate groups from targeted residues (Barford et al., 1998). This on/off regulation of protein phosphorylation acts as a signaling switch to direct protein activity and regulate mature protein function without modifying expression levels.

The canonical function of CRMP2 is regulated by phosphorylated states where CRMP2 is considered ‘active’ in neurite outgrowth when unphosphorylated. Upon phosphorylation CRMP2 becomes ‘inactive’ for outgrowth (Byk et al., 1996). Signaling requirements for CRMP2 function in growth cone collapse have been well described and are initiated by the neurite guidance cue Semaphorin 3A (Sema3A). Sema3A signaling cascade involves activation of multiple kinases and multiple modifications of CRMP2 that culminate in a reduced affinity of CRMP2 for the cytoskeletal protein tubulin and, consequently, a reduced cytoskeleton stability (Fukata et al., 2002a, Kimura et al., 2005). The process is initiated when Sema3A binds neuropilin-1/plexin-A receptors to transduce the signal to the cytosolic space (Takahashi et al., 1999, Sasaki et al., 2002). Intracellularly, the src kinase Fyn becomes active (Sasaki et al., 2002) and hydrogen peroxide is generated through the microtubule associated monooxygenase, calponin and

LIM domain containing 1 (MICAL) protein which then oxidizes CRMP2 (Morinaka et al., 2011). Fyn kinase activates cyclin-dependent kinase 5 (Cdk5) allowing for Cdk5 phosphorylation of CRMP2 at serine-522 (Brown et al., 2004). CRMP2 constructs that harbor serine to alanine mutations at this site, CRMP2-S522A, prevent addition of a phosphate group and restricts Sema3A-CRMP2 mediated growth cone collapse (Brown et al., 2004). Primary phosphorylation by Cdk5, and also disulfide linkage of oxidized CRMP2 to thioredoxin promotes a secondary phosphorylation of CRMP2 by glycogen synthase kinase 3β (GSK3β) (Eickholt et al., 2002, Uchida et al., 2005, Morinaka et al., 2011) at CRMP2 threonine residues threonine-509, threonine-514, and threonine-518 (Brown et al., 2004, Cole et al., 2004, Yoshimura et al., 2005a). In contrast, dephosphorylation of CRMP2-threonine-509/threonine-514 by the phosphatases PP1 and PP2A results in neurite outgrowth (Zhu et al., 2010, Astle et al., 2011). This effect is mediated only by loss of phosphorylation by GSK3β at CRMP2-threonine-509/threonine-514 but not loss of phosphorylation by Cdk5 at CRMP2-Serine-522 because Cdk5 phosphorylation is resistant to phosphatase activity (Cole et al., 2008).

When CRMP2 is unphosphoryalted at threonine-509 and threonine-514 it binds and transports tubulin dimers from cell bodies to the distal, extending, projections (Fukata et al., 2002a, Kimura et al., 2005). In this unphosphorylated state, CRMP2 also stabilizes and promotes the intrinsic GTPase activity of tubulin, further promoting cytoskeleton expansion (Chae et al., 2009). GSK3β phosphorylation of CRMP2 following Sema3A reverses this function by reducing affinity for tubulin to prevent CRMP2 participation in maintenance of the cytoskeleton resulting in neurite retraction (Yoshimura et al., 2005a).

In addition to Cdk5 and GSK3β, CRMP2 is also subject to phosphorylation by Fyn, RhoK, CaMKII, and Yes kinases. Evidence exists that in addition to activation of Cdk5 during Sema3A signaling, Fyn kinase also directly phosphorylates CRMP2 at tyrosine-32 to promote Sema3A mediated growth cone collapse (Uchida et al., 2009). Mutation of this tyrosine to phenylalanine, CRMP2-Y32F, reduces Sema3A CRMP2-mediated effects on neurite retraction by roughly fifty percent. The phosphorylation of CRMP2 at threonine-555 by ras homolog (Rho) associated protein kinase 1 is yet another example of CRMP2 phosphorylation that promotes growth cone collapse by restricting interactions with tubulin (Arimura et al., 2005). This modification is the result of signaling in response to lysophosphatidic acid (Arimura et al., 2000a, Arimura et al., 2005). Some evidence also suggests that this site can be targeted by Ca^{2+}/calmodulin-dependent protein kinase (CaMKII) in a neuroprotective mechanism following glutamate toxicity (Hou et al., 2009).

Other interactions of CRMP2 and cytoskeletal proteins like actin and vimentin allow CRMP2 participation in cytoskeletal regulation outside its canonical function of neurite outgrowth and collapse (Arimura et al., 2005, Vincent et al., 2005). Interaction of CRMP2 and the intermediate filament protein, vimentin, has been described in a non-neuronal function of CRMP2 in CXCL12-induced migration of T-lymphocytes (Varrin-Doyer et al., 2009). This process involves the phosphorylation of CRMP2 by Yes kinase at tyrosine-479, which increases interaction of CRMP2 and vimentin to polarize lymphocytes, a hallmark of a migration in this cell type. Elimination of this modification by CRMP2-Y479F mutant completely prevents this function.

CRMP2 phosphorylation by Cdk5 at serine-522 can guide protein function by governing CRMP2 interactions with N-type voltage gated calcium channels (Brittain et al., 2009a, Chi et al., 2009a, Wang et al., 2010b). This phosphorylation increases CRMP2-Cav2.2 interaction to increase channel trafficking and insertion into the cell membrane. Consequences of this CRMP2 modification in neurons are increased calcium influx and a subsequent increase in neurotransmitter release. In DRG neurons, calcium-dependent neurotransmitter release is responsible for transmission of painful stimuli, therefore targeting Cav2.2 has proved a useful strategy in pain treatments (Staats et al., 2004, Winquist et al., 2005). By extension, targeting CRMP2-Cav2.2 interaction serves this pharmacological goal. A small peptide that mimics a CRMP2 interaction motif with the calcium channels was produced and made cell permeant with the HIV transduction domain 'TAT'. When applied to neurons this peptide reduced Cav2.2 currents and synaptic transmission, and following subcutaneous injection of rats, inflammatory and chronic pain behaviors were attenuated (Brittain et al., 2011b).

In addition to phosphorylation and oxidation, CRMP2 has been identified as a target of O-glycosylation, with a high coincidence of glycosylated CRMP2 found in nerve terminals. CRMP2 localization to this sub-cellular domain could aid in CRMP2 activity in either outgrowth or voltage-gated calcium channel trafficking, but no specific evidence exists to support a functional consequence of this modification (Cole and Hart, 2001). An additional way in which CRMP2 functions can be regulated is via differential expression of CRMP2 splice variants, CRMP2-S or CRMP2-L (Yuasa-Kawada et al., 2003). The short version, CRMP2-S, is missing N-terminal residues 1-36 which can result in differential signaling dependent on CRMP2 phosphorylation at residue Y32.

CRMP2 can also be modified by cleavage. Calpain targeting of CRMP2 in a pathway that feeds back on NMDA receptors reduces receptor expression during bursts of cell hyperexcitability (Bretin et al., 2006). Finally, as shown by me in this thesis, CRMP2 undergoes modification by a small ubiquitin-like modifier (SUMO), which regulates voltage-gated sodium channel membrane expression and will be elaborated in this dissertation in Chapters 3 and 4 (Dustrude et al., 2013).

1.2.3. CRMP2 Involvement in Disease and Injury

Studies of CRMP2 function have been motivated by identification of CRMP2 in a number of neurological diseases. The histological hallmarks of Alzheimer's disease (AD) are neurofibrillary tangles and β-amyloid plaques (Hardy and Selkoe, 2002). Whether these changes have a correlative or causative effect on neuronal death associated with AD has not been investigated. Notwithstanding the link to AD pathophysiology, CRMP2 is found within neurofibrillary tangles of AD brains (Yoshida et al., 1998) where it is phosphorylated at threonine-509, threonine-518, and serine-522 (Gu et al., 2000). These are the *same* sites that become phosphorylated during Sema3A-mediated growth cone collapse to prevent CRMP2's participation in stabilization and elongation of microtubules. Loss of CRMP2 participation in its canonical pathway of cytoskeleton dynamics could therefore contribute to AD pathology of neuronal death. In addition, CRMP2 expression becomes down regulated in AD, which would predictably add to the effect of reduced CRMP2-mediated cytoskeleton outgrowth and stability (Lubec et al., 1999).

The canonical function of CRMP2 in axonogenesis and cytoskeletal regulation is possibly linked to the generation of certain epilepsies. As a multifactorial disease, epilepsy results from a combination of effects including loss of neuronal circuit inhibition, increased excitability, and reorganization of circuitry (Pitkanen and Lukasiuk, 2009). The last of these is observed in the form of mossy fiber sprouting within the epileptic hippocampus (Nadler, 2003). Aberrant innervation of the molecular layer of the hippocampus by mossy fiber projections can produce redundant excitatory circuits that continuously feed-forward upon themselves to contribute to seizures. CRMP2 is reduced in the hippocampus of patients with temporal lobe epilepsies (Czech et al., 2004), and the growth of mossy fiber sprouting is associated with a reduced activity of Sema3A repulsion (Holtmaat et al., 2003). Both of these findings support dysregulation of CRMP2 in these forms of epilepsy. Interestingly, the antiepileptic drug lacosamide, which has primary function on VGSCs to reduce neuronal hyperexcitability, also *directly* interacts with CRMP2 (Wilson and Khanna, 2014, Wilson et al., 2014). Targeting CRMP2 with this functionalized amino acid shows promise in restricting tubulin-binding properties of CRMP2 to restrict activity dependent neurite outgrowth in the development of epilepsy.

Calpain cleavage of CRMP2 has been described following ischemia (Jiang et al., 2007), neurotrauma (Zhang et al., 2007), excitotoxicity (Bretin et al., 2006), as well as nerve growth factor deprivation induced-neurite degeneration (Touma et al., 2007). In cortical neurons challenged with NMDA-stimulated excitotoxicity, the NR2B NMDA receptor subunit underwent a reduction in surface expression. CRMP2 preferentially associates with NR2B-containing NMDA-receptors (Al-Hallaq et al., 2007), and reduction of NR2B surface expression was enhanced by over-expression of CRMP2

(Bretin et al., 2006). Together these data suggest that down regulation of NR2B is a CRMP2 driven neuroprotective mechanism.

A connection between CRMP2 and neurofibromatosis 1 (NF1) has also been uncovered (Lin and Hsueh, 2008). NF1 is an autosomal dominant disorder in which patients are prone to nervous system tumors, or neurofibromas, due to mutations that truncate the NF1 gene encoding for a tumor repressor protein. CRMP2 was shown to interact with the c-terminal of the neurofibromin protein in rat brain (Lin and Hsueh, 2008). Furthermore, knockdown of NF1 in PC12 cell line restricts outgrowth of neurite-like processes and is correlated to increased phosphorylation of CRMP2 protein by Cdk5, GSK3β, and RhoK, each of which blunts CRMP2 participation in outgrowth (Patrakitkomjorn et al., 2008).

1.3. Protein SUMOylation, a novel post-translational modification of CRMP2

1.3.1. Background

The first Small Ubiquitin-like MOdifier (SUMO) protein was identified in 1996 for associating with RAD51 and RAD52 DNA repair pathway proteins in humans. Named ubiquitin-like 1 (UBL1) gene for its moderate homology for both ubiquitin and ubiquitin cross-reacting proteins (Shen et al., 1996), SUMO and ubiquitin are of similar size, 11 kDa and 8 kDa, respectively, and both target lysine residues for covalent modification of target proteins. The forward reaction of protein SUMOylation resembles ubiquitination in its involvement of three enzymes, E1-activating, E2-conjugating and E3-ligase (Takahashi et al., 2001) to form isopeptide bonds between ε-amino group of the

target lysine residue and the carboxyl group of SUMO's C-terminal. Despite these similarities, sequence homology between the SUMO1 and ubiquitin proteins is only ~18% (Muller et al., 2001).

Initial studies of SUMO1 (UBL1, also known as PIC1, sentrin, GMP1, and Smt3c) described the protein as a binding partner of nuclear pore proteins and regulator of cell cycle, transcription, and chromatin organization (Boddy et al., 1996, Matunis et al., 1996, Okura et al., 1996, Lapenta et al., 1997). The first identified target of covalent modification by SUMO was RanGAP1, a nuclear pore protein (Matunis et al., 1996, Mahajan et al., 1997). Discovery of SUMO1 allowed for prediction of other SUMO proteins via chromosome mapping (Lapenta et al., 1997), leading to the identification of SUMO2, SUMO3, and SUMO4. SUMO2 and SUMO3 were identified as additional covalent modifiers within the protein family (Kamitani et al., 1998a, Kamitani et al., 1998b), but because SUMO4 was found to lack introns and is not endogenously expressed, it is considered a pseudogene (Bohren et al., 2004).

Some protein substrates are preferentially modified by one particular SUMO isoform whereas others display overlapping modification by several isoforms (Vertegaal et al., 2006). Evidence to determine how SUMOylation machinery or protein targets display these preferences is lacking. SUMO2 and SUMO3 proteins share 95% sequence homology, but only 50% homology with SUMO1 (Johnson, 2004). Unlike SUMO1, they contain internal, N-terminus, SUMOylation motifs that allow for poly-SUMO2/3 chains (Tatham et al., 2001). The length of unanchored SUMO2/3 polymers can reach eight SUMO proteins when enhanced by overexpression of SUMOylation machinery proteins in cell culture. As SUMO1 lacks internal motifs, it functions as a chain-terminating

addition and expression of SUMO1 drastically reduces the formation of poly-SUMO (Matic et al., 2008). The length and function of poly-SUMO2/3 chains *in vivo* is poorly understood and has hypothesized roles in protein–protein interactions governed by non-covalent interactions with SUMOs by SUMO Interacting Motifs (SIMs) which scaffold interactions involved in SUMO2/3 signaling (Sun and Hunter, 2012).

1.3.2. SUMOylation Machinery

SUMO proteins are formed as inactive pro-SUMOs precursors that become active when the C-terminal is cleaved by sentrin/SUMO-specific protease (SENP) family proteins (Melchior et al., 2003, Mukhopadhyay and Dasso, 2007). Conjugation of SUMO to a target protein is then activated by E1-SUMO-Activating Enzymes (SAEs) 1 and 2, a heterodimer which forms a thioester bond between the SUMO protein and SAE2 (Gong et al., 1999). SUMO is then transferred to the active site of Ubiqutin-conjugating 9 (Ubc9) enzyme to form a highly reactive intermediate that can SUMOylate a target protein (Johnson and Blobel, 1997). Ubc9 is the sole SUMO E2 enzyme in yeast and invertebrates and is predicted to be the only SUMO E2 in vertebrates as well (Desterro et al., 1997, Johnson and Blobel, 1997, Hayashi et al., 2002). Therefore, Ubc9 is responsible for all protein SUMOylation in mammals, and represents the rate limiting step of the forward reaction. For many substrates, Ubc9 is sufficient to recognize and transfer SUMO, and in other cases E3-ligases bind Ubc9 and scaffold the E2 to its targets (Desterro et al., 1999, Okuma et al., 1999).

SUMOylation most commonly occurs on a lysine within a SUMO-consensus motif ψKxD/E, where ψ is a large hydrophobic amino acid (Xu et al., 2008). In some cases, the inverted sequence D/ExKψ also functions to serve as a SUMOylation signal (Matic et al., 2010). Presence of downstream negatively charged residues further classifies a target motif as negative charge-dependent SUMOylation motif (NDSM) which aids Ubc9 interaction (Henley et al., 2014). This negative charge can also be introduced to a motif by protein phosphorylation and allows SUMOylation motifs to be switched on and off in response to kinase and phosphatase activity (Picard et al., 2012). Despite well over 1000 proteins being reportedly SUMOylated, only ~60% of known SUMOylation targets conform to the SUMO-consensus motif. Moreover, not all consensus sequences are SUMOylated (Ulrich, 2009). The consensus motif within CRMP2 at lysine-374 conforms to the more stringent NDSM motif and is conserved throughout all CRMP2 family members CRMPs 1–5 as well as between species (Dustrude et al., 2013). As Ubc9 represents the only E2 enzyme, restricting its function prevents protein SUMOylation globally. In cell lines, knockdown of Ubc9 causes cell death by apoptosis (Hayashi et al., 2002), and Ubc9-knockout mice embryos die at an early post-implantation stage due to deficits in nuclear organization (Nacerddine et al., 2005). Several SUMO1 knockout mice have been produced with between 10% and 100% viability (Alkuraya et al., 2006, Evdokimov et al., 2008, Zhang et al., 2008), with viable mice showing enhancement of SUMO2 and SUMO3 modification, suggesting compensation. Viable mice however, display reduced body weight (Mikkonen et al., 2013), reduced inflammatory responses (Venteclef et al., 2010), and congenital heart disease (Wang et al., 2011a).

Reversing modification of proteins by SUMO requires SENP proteins. This family of proteins, SENP1-3 and SENP5-7 (SENP4 is a paralogue) are responsible for activation of pro-SUMOs and mediate cleavage of SUMO from target proteins by an Ulp domain at their C-terminus (Mukhopadhyay and Dasso, 2007). Of the SENPs, SENP1 and SENP2 have broad specificity for all three SUMO proteins with opposing specificities. SENP1 is more effective at removal of SUMO1, whereas SENP2 is more effective at removal of SUMO2 and SUMO3 (Gong et al., 2000). The remaining SENPs are only able to remove SUMO2 and SUMO3 from targets (Gong and Yeh, 2006), with SENP6 and SENP7 displaying chain editing properties of poly-SUMO chains (Mukhopadhyay et al., 2006, Shen et al., 2009). In many cases, the SUMOylated fraction of a protein amounts to less than 1% (Johnson, 2004). This general feature of SUMOylation turnover puts forward the hypothesis that consequences of protein SUMOylation or deSUMOylation may persist in time after the modification is altered (Hardeland et al., 2002). In this way, only 1% of a substrate might be SUMOylated, but a much greater percentage of protein has undergone SUMOylation recently enough to exert effects of a SUMOylated protein.

1.3.3. Consequences of Protein SUMOylation

As a molecular switch, the SUMOylation of a target protein can have one of three effects. First, SUMOylation may block a binding site of an enzyme or binding partner. The nuclear factor kappa B (NFκB) provides such an example, where SUMOylation and ubiquitination compete for lysine-21. When NFκB is SUMOylated it is then protected from ubiquitin degradation (Desterro et al., 1998). Second, the attached SUMO protein

itself can participate in the binding of new protein partners to change the target's interactome. The first identified target of SUMOylation, RanGAP1, is an example of this case. Interaction of the SUMO protein and RanGAP1, together, recruit RanBP2 for transport to the nuclear pore (Matunis et al., 1996, Mahajan et al., 1997). Third, SUMOylation can alter protein conformation, which can alter activity of the target or change its ability to become modified by additional post-translational modifications. GSK3β is an example of this, where SUMOylation enhances kinase activity and stability (Eun Jeoung et al., 2008) (Figure 1.4).

Turnover of SUMOylation can be regulated by activity of the SUMOylation machinery. The level of Ubc9 expression can govern the rate of SUMOylation and the level of the chain-terminating SUMO1 expression can govern the propensity of SUMO2 and SUMO3 to form poly-SUMO chains (Matic et al., 2008). The SUMO E1 heterodimer SAE1/SAE2 can undergo disulfide binding to E2-Ubc9 following exposure to reactive oxygen species (Bossis and Melchior, 2006). This bond halts further activation and conjugation activities by the SUMOylation machinery to pause further modifications. Additionally, E1 SAE1/SAE2 heterodimer can be inhibited by SUMOylation of the E1-activating enzyme itself (Truong et al., 2012), and Ubc9 can be inhibited from targeting some NDSM targets by acetylation (Hsieh et al., 2013). By these modifications to expression and activity of the SUMOylation machinery, global SUMOylation can become upregulated or inhibited to exert effects on overall cellular SUMOylation. In neurons, compartmentalized cell regulation of sub-cellular SUMOylation has been observed in presynaptic membrane fractions (Feligioni et al., 2009).

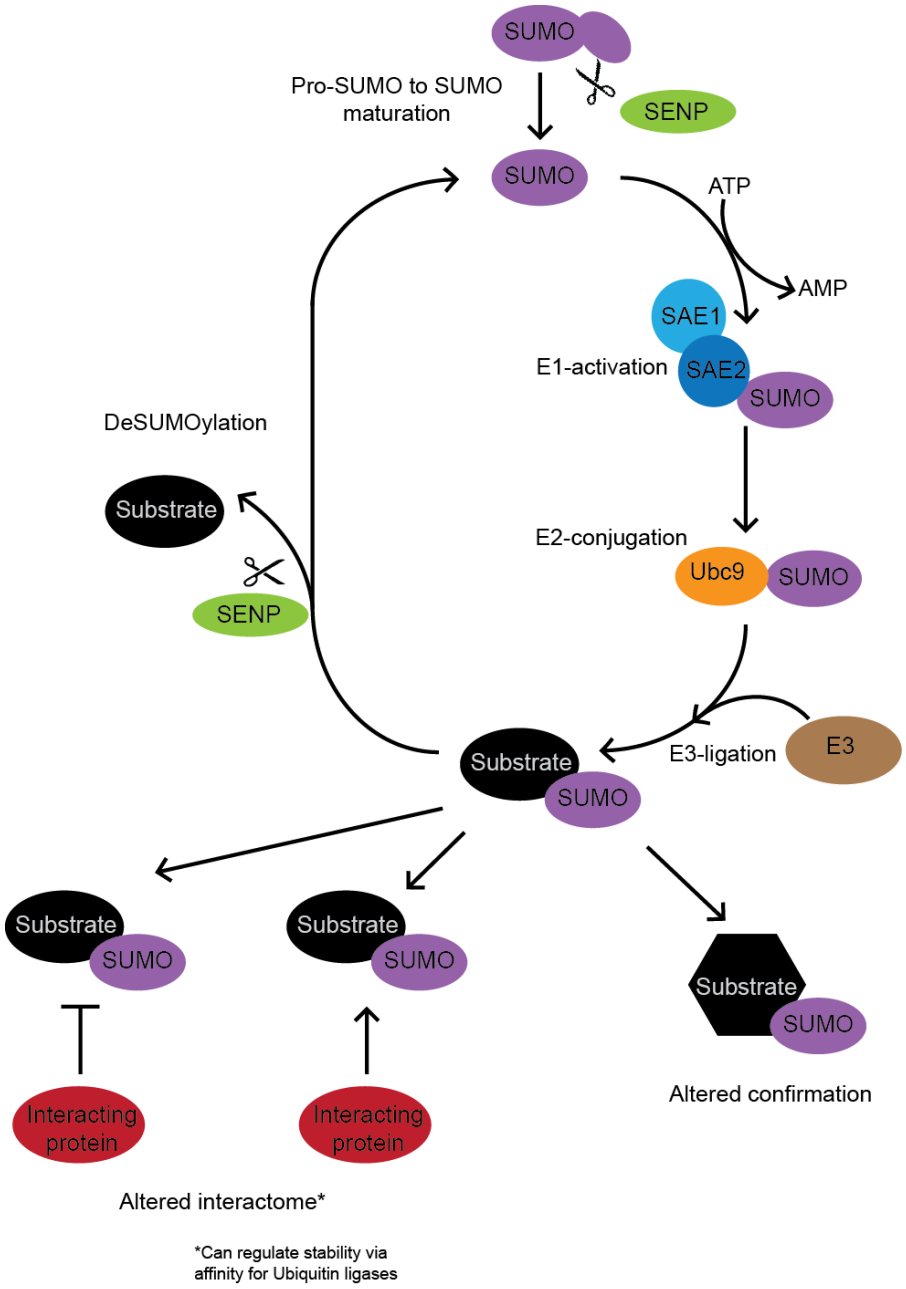

Figure 1.4. SUMOylation cycle and consequences on SUMOylated substrates. SUMOylation is a reversible modification which relies on a cascade of E1-activating, E2-conjugating, and E3-ligating enzymes in the forward reaction. The reverse reaction as well as maturation of Pro-SUMO protein is achieved by cleavage via SENP proteins. Upon SUMOylation, protein function can be altered in one of three major ways. 1) Restriction of interaction and 2) promotion of interaction with different protein partners can alter activity and can also affect protein stability. 3) Altered confirmation may also occur following SUMOylation to mediate secondary modifications or alter substrate activity.

1.3.4. Interplay Between SUMOylation and Other Post Translational Modifications

The best understood regulation of protein SUMOylation is substrate-specific control by post-translational modifications of the substrate itself to change the rate of SUMOylation (Table 1.3). Similar to how CRMP2 post-translational modifications direct the protein's activity, ubiquitination, phosphorylation, and acetylation can all enhance or prevent SUMOylation of certain proteins and have functional consequences on the proteins activity.

There are several examples of membrane proteins that undergo changes in trafficking in response to SUMO signaling. For instance, estrogen receptor β (ERβ) is subject to multiple post-translational modifications (Picard et al., 2012). At lysine-4, ERβ contains a non-consensus SUMOylation motif that is made available for Ubc9 binding following downstream phosphorylation at serine-6 RasV12. This phosphorylation confers a negative charge dependent Ubc9 binding to ERβ that leads to SUMOylation. SUMOylated ERβ is prevented from becoming ubiquitinated thus sparing ERβ from being degraded. Additionally, SUMOylated ERβ prevents the receptor from being transcriptionally regulated by estrogen-responsive element (Picard et al., 2012). In another example, SUMOylation of kainate receptor 2 (GluK2) is both activity- and phosphorylation-dependent and marks the receptor for endocytosis (Martin et al., 2007a, Konopacki et al., 2011).

SUMOylation also plays a role in controlling the endocytosis of α-amino-3-hydroxy-5-methyl-4-isoxazolepropionic acid (AMPA) receptors that respond to the effects of the neurotransmitter glutamate. AMPA receptors themselves are not SUMOylated, but are regulated by interaction with the SUMOylated protein Arc

(Chowdhury et al., 2006, Craig and Henley, 2012, Craig et al., 2012). Activity-regulated cytoskeleton-associated protein (Arc) is an immediate-early gene expressed at excitatory synapses with described interactions with AMPA receptors, endocytic proteins, CaMKII, and stargazin, an AMPA receptor interacting protein (Zhang et al., 2015). Following TTX induced suppression of AMPA currents for 24 hours, AMPA receptors undergo an increase in surface expression that is correlated to reduced SENP1 activity and increased SUMO1 conjugation, both of which increase protein SUMOylation (Craig et al., 2012). By recovering the rate of protein deSUMOylation with SENP1 overexpression, increases to AMPA receptor expression are prevented. TTX-mediated increases to AMPA receptor surface expressions are also prevented when cells express a SUMO-null Arc mutant that prevents Arc SUMOylation and Arc localization to dendrites (Chowdhury et al., 2006, Craig and Henley, 2012, Craig et al., 2012). Increased AMPA receptor surface expression in this case is therefore interpreted as an Arc and Arc SUMOylation dependent process. An interaction between Arc and endocytic proteins is predicted to be an important determinant of this pathway, but has not yet been tested (Craig et al., 2012, Henley et al., 2014). In this thesis, I will describe how SUMOylation of CRMP2 recruits the endocytic machinery, in a manner similar to that proposed in Arc-AMPA receptor regulation, to mediate expression of Nav1.7.

Modified protein	Consequences of modification	Reference
Nuclear factor kappa-light-chain-enhancer of activated B cells (NFκB)	Ubiquitin competes with SUMO to prevent degradation of NFκB	(Desterro et al., 1998)
Promyelotic leukemia protein (PML)	Phosphorylation of PML restricts SUMOylation of PML to prevent PML solubility in nucleus and restrict self-aggregation to preserve activity	(Muller et al., 1998, Kadare et al., 2003)
Wnt/*JNK* signaling protein Axin	deSUMOylation of Axin restricts interaction with MEKK and prevents JNK phosphorylation cascade	(Rui et al., 2002)
E3 SUMO ligase PIAS1	Acetylation competes with SUMOylation on PIAS1 and SUMOylation of the ligase restricts transcription factor SP3 expression	(Sapetschnig et al., 2002)
Focal adhesion kinase (FAK)	SUMOylation of FAK activates FAK autophosphorylation which promotes FAK binding to Src family kinases to activate signaling pathways	(Kadare et al., 2003
Transcription factor Elk-1	Phosphorylation of Elk-1 by MAP kinases triggers activation, but SUMOylation of Elk-1 blocks activation	(Yang et al., 2003)
Heat-shock factors (HSF) 1 and 4b	Phosphorylation of either HSF is required for secondary SUMOylation which suppresses HSF transcriptional activity	(Hietakangas et al., 2003, Hietakangas et al., 2006)
Myocyte enhancer factor 2 (MEF2)	Phosphorylation of MEF2 is required for secondary SUMOylation which then suppresses MEF2 transcriptional activity	(Gregoire et al., 2006)
Tumor suppressor HIC1	Acetylation competes with SUMOylation of HIC1 and HIC1 SUMOylation reduces transcriptional activity	(Stankovic-Valentin et al., 2007)
p53	Ubiquitination of p53 promotes secondary SUMOylation	(Carter et al., 2007)
DNA binding protein SATB1	Phosphorylation of SATB1 restricts secondary SUMOylation	(Tan et al., 2010)
GluK2 Kainite receptor	Phosphorylation of GluK2 is required for secondary SUMOylation which promotes GluK2 endocytosis	(Konopacki et al., 2011)
Estrogen receptor β (ERβ)	Phosphorylation of ERβ is required for secondary SUMOylation which prevents ubiquitination and endocytosis of ERβ	(Picard et al., 2012)
Microtubule stabilizing Tau protein	SUMOylation of Tau promotes Hyperphosphorylation and Hyperphosphorylation of Tau promotes SUMOylation in a feed forward cycle – Both modifications promote Tau protein stability in the cytosol	(Luo et al., 2014)

Table 1.3. Interplay between phosphorylation and SUMOylation status. Examples of proteins that undergo phosphorylation and SUMOylation and the regulation these modifications provide over each other.

1.4. Thesis Aims

A major goal of my work was to identify novel functional interacting partners of the voltage-gated sodium channel Nav1.7. An additional aim of my work was to describe the mechanisms affecting Nav1.7 trafficking. I identified CRMP2 as a novel partner of Nav1.7 and identified its post-translational regulation by the SUMO modification. The studies were hampered by lack of suitable pharmacological tools or genetic models to interrogate these questions. So, my work employed strategies to overexpress or knockdown various proteins in the SUMOylation pathway as well as to overexpress mutant CRMP2 proteins (mimicking loss of SUMOylation, loss of phosphorylation, or constitutive phosphorylation) and then examine the effects of these manipulations on Nav1.7 currents, surface expression, and biochemistry. For these studies, I employed both heterologous and primary cells to interrogate Nav1.7. In particular, I had the following aims:

1. Determine, using biochemical techniques, if CRMP2 is SUMOylated, if CRMP2 interacts with Nav1.7, and if CRMP2 SUMOylation status regulates Nav1.7 currents (in heterologous cells).
2. Determine if CRMP2 SUMOylation-dependent regulation of Nav1.7 currents involves Nav1.7 trafficking (in heterologous cells) using cell surface biotinylation and if CRMP2 SUMOylation-dependent regulation of Nav1.7 currents is specific to Nav1.7 (in heterologous cells and sensory neurons) using whole-cell patch clamp electrophysiology.
3. Determine if CRMP2 SUMOylation and CRMP2 phosphorylation by Fyn, Yes, GSK3β, Cdk5, or RhoK/CaMKII kinases are interdependent or exclusive

in their effects on regulating Nav1.7 currents (in heterologous cells and sensory neurons).

4. Identify trafficking mechanisms by which CRMP2 SUMOylation mediates Nav1.7 current density (in sensory neurons).

CHAPTER 2.

MATERIALS AND METHODS

2.1. CRMP2 sequence analysis and cDNA constructs

2.1.1. Sequence analysis to identify putative motifs of CRMP2 SUMOylation

CRMP2 protein sequences (*Mus musculus* NCBI reference sequence: NP_034085.2, and *Rattus norvegicus* NCBI reference sequence: NP_001099187.1) were analyzed using SUMOplot Analysis Program (Abgent) to identify putative SUMOylation motifs. Five motifs were identified and ranked by likelihood of SUMOylation. Of the predicted SUMOylation motifs, lys-20, lys-374, lys-390, lys-269, and lys-472, the first three met threshold criteria to be considered 'likely SUMOylated' by SUMOplot software. Predicted lysine targets were compared for conservation within the family of CRMP proteins (CRMPs 1–5) (Figure 2.1).

2.1.2. Recombinant proteins

Mouse CRMP-2 cDNA (*Mus musculus* accession # NM_009955.3) was cloned into plasmid pDsRed2-N1 using PCR amplification followed by restriction digest and ligation by Dr. Joel Brittain, a former Khanna laboratory member. A CRMP2-3xFLAG construct was provided by Dr. Akihiro Kurimasa (Tottori University, Tottori, Japan). From these parent CRMP2-dsRed and CRMP2-3xFLAG constructs, recombinant CRMP2 cDNAs were created to study CRMP2 phosphorylation and SUMOyaltion by Dr. Aubin Moutal. CRMP2 mutants were created to harbor SUMO-null mutations, phospho-null mutations, phospho-mimietic mutations, and combinatorial mutations harboring multiple –null or –mimetic residues. CRMP2 mutant constructs were made using QuikChange II XL (Agilent) (Figure 2.2).

A

Position	Sequence	Score
K20	SDRLL IKGG KIVND	0.77
K374	KAVVT GKMD ENQFV	0.67
K390	TSTNA AKVF NLYPR	0.44
K269	VIAQA RKKG TVVYG	0.27
K472	GRYIP RKPF PDFVY	0.09

B

Position	CRMP Family Member				
	1	2	3	4	5
K20	X	✓	✓	✓	✓
K374	✓	✓	✓	✓	✓
K390	✓	✓	✓	X	X
K269	✓	✓	✓	X	X
K472	✓	✓	X	✓	✓

Figure 2.1. CRMP2 putative SUMOylation motifs and conservation. (A) CRMP2 sites that conform to SUMOylation consensus motifs (ranked by Abgent SUMOplot™ Analysis Program). The rat sequence was used for this prediction. **(B)** Conservation of putative SUM-targeted lysines within family of CRMP proteins (*green check marks denote conservation of residues between all CRMPs, black X denotes non-conserved residues*).

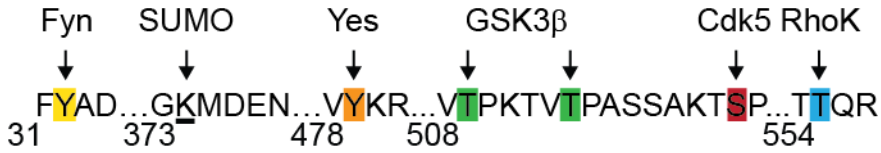

Type of Mutation	**Substitutions**	**Targeted by**	**References**
SUMO-null	K20A K374A K390A	Putative SUMO Putative	This Thesis
Phospho-null	Y32F Y479 T509A/T514A S522A T555A Y32F/S522A	Fyn Yes GSK3β Cdk5 RhoK/ CAMKII	(Uchida et al., 2009) (Varrin-Doyer et al., 2009) (Yoshimura et al., 2005b) (Brittain et al., 2012) (Arimura et al., 2000a) (Hou et al., 2009)
Phospho-mimetic	S522D		This Thesis
SUMO-null/ Phospho-null	Y32F/K374A K374A/Y479F K374A/T509A/T514A K374A/S522A K374A/T555A		This Thesis
SUMO-null/ Phospho-mimetic	K374A/S522D		This Thesis

Figure 2.2. Summary of post-translational modifications of CRMP2 and constructs used in this thesis. *Top*: The kinases that phosphorylate CRMP2 are shown above the linear sequence of mouse CRMP2. The predicted SUMOylation motif in CRMP2 showing lysine-374 (underlined), where SUMO is added the E2 Ubiquitin ligase Ubc9. The two other predicted SUMO sites are not shown. *Bottom***:** Table of constructs used in this thesis including SUMO-null, phospho-null, phospho-mimetic, and combinatorial SUMO/phospho mutants created in a plasmid also encoding the Discosoma red fluorescent protein (DsRed).

Constructs were purified from DH5α *E. coli* using NucloBond Xtra Maxi kit (Macherey-Nagel), and verified by DNA sequencing. HA-SUMO-1, HA-SUMO-2, HA-SUMO-3, and HA-Ubc9 plamids were obtained from Addgene (Cambridge).

2.2. Cell cultures

2.2.1. Primary cortical neuron culture, transfection and neurite outgrowth analysis

Rat cortical neuron cultures were prepared from dissected cortices of day 19 (E19) embryonic rats as described (Goslin and Banker, 1989), with minor modifications. Briefly, cortices were dissociated enzymatically and mechanically (trituration through Pasteur pipette) in a Papain solution (12 U/ml; Worthington) containing Leibovitz's L-15 medium (Invitrogen), 0.42 mg/ml cysteine (Sigma), 250 U/ml DNase 1 (type IV; Sigma), 25 mM NaHCO3, penicillin (50U/ml)/streptomycin (50 μg/ml), 1 mM sodium pyruvate, and 1 mg/ml glucose (Invitrogen). After dissociation, the cells were gently washed by sequential centrifugation in Neurobasal medium containing either 2 mg/ml or 20 mg/ml BSA and Pen/Strep, glucose, pyruvate, and DNase1 (as above) and then plated on poly-D-lysine-coated coverslips or 96-well plates at ~400 cells per mm^2. Growth media (1 ml/well or 100 μl/well for 12- and 96-well plates, respectively) consisted of Neurobasal medium containing 2% NuSerum, 2% NS21 (Chen et al., 2008), supplemented with penicillin/streptomycin (100 U/ml; 50 μg/ml), 0.1 mM L-Glutamine and 0.4 mM/L-glutamax (Invitrogen). 5-fluoro-2′-deoxyuridine (1.5 μg/mL) (Sigma) was added 48 h after plating to reduce the number of nonneuronal cells. After 4 d in culture, half of the growth medium was replaced with medium without 5-fluoro-2'-deoxyuridine.

Neurons were transfected with various cDNA's via Lipofectamine 2000 (Invitrogen) per the manufacturer's instructions at DIV4. Briefly, transfection reagent and cDNA's were separately incubated in a serum-free media base (Neurobasal) (Invitrogen) for 5 min. Mixtures were combined and incubated for 25 min. The combined reagent mixture was added to cells in a drop-wise manner. Cultures were returned to normal culture conditions (37°C, 5% CO_2) for 3-4 h, at which point transfection reagents were washed off with normal media. At DIV6, cells were fixed with 4% paraformaldehyde (Sigma) and imaged using the ImageXpress Micro Widefield High Content Screening System (Molecular Devices). Multiple parameters involved in neurite outgrowth were examined via the neurite outgrowth application module within the MetA Xpress software. This analysis combines the following measurements: number of primary neurites, number of branches, mean process length, and maximum process length to determine a summary of total outgrowth per cell. In some instances, Sholl analysis was used in place of ImageXpress analysis. Sholl analysis was performed with ImageJ software using an automated Sholl analysis plug-in, in which the soma boundary is approximated by an ellipsoid, and neurite intersections are assessed at radial distances (20 µm increments) from the soma. Images were acquired with a Nikon Eclipse 90i microscope by an experimenter blinded to transfection/drug conditions. Images were acquired across 3 separate culture wells.

2.2.2. Primary dorsal root ganglia (DRG) culture and transfection

DRG neurons were isolated from 150 to 174 g female Sprague-Dawley rats. Rats were anesthetized using isoflurane and decapitated. The dorsal side was then cut to

expose the vertebrae and transected in the thoracic region to allow access to the spinal cord. Cutting parallel to the dissection stage, just under the vertebral bone processes, dorsal vertebral bones were removed to expose DRGs just outside the spinal cord. Lumbar dorsal root ganglion were trimmed adjacent to their roots and placed in ice cold bicarbonate free, serum free, sterile Dulbecco's modified Eagle's meadium (bfDMEM). Excised ganglion were then placed in a 15 ml conical with 3.125 mg Neutral Protease (dispase) and 5 mg collagenase, type 1 (Worthington Biochemical Corporation) in 3 ml bfDMEM and gently rocked at 37 ºC for 40 minutes. Following enzymatic digestion, cells were gently titrated with glass polished pipettes to further disassociate cells into a single cell suspension suitable for patch clamp experiments and then gently centrifuged to collect tissue at the bottom. Disassociation media was then removed and cells resuspended in 200 µl supplemented nucleofector solution (Lonza). Cells were then split into two to three groups, 100 µl each, containing 2 µg wildtype or mutant CRMP2 plasmid. Cell suspensions were then transferred to glass cuvettes for electroporation transfection (Amaxa program O-003, Lonza). Following electroporation, cells were diluted in DMEM, plated on 12-mm BD BioCoat poly-D-lysine/lamanin-coated glass coverslips (BD Biosciences, Franklin Lakes, NJ), and maintained at 37 ºC, 5% CO_2 in DMEM supplemented with nerve growth factor (30 ng/ml), 10% fetal bovine serum (FBS), and 1% penicillin/streptomycin (100% stocks, 10 000 U/mL penicillin G sodium and 10 000 µg/mL streptomycin sulfate) (Leclere et al., 2005, Chi et al., 2009a). Under these conditions, transfection efficiencies of ~10–20% were routinely observed along with ~10–20% cell death. Cells were used for patching experiments at 48 to 72 h after

transfection and small cells (< 30 μm) were chosen as in order to target Aδ- and c-fiber nociceptive neurons (Harper and Lawson, 1985, Lawson, 2002).

2.2.3. HEK cell culture and transfection

Human Embryonic Kidney (HEK) cell lines were obtained from Dr. Theodore R. Cummins (Indiana University School of Medicine). cDNA gene encoding Nav1.1 from human was subcloned into the vector pTarget, cDNA genes encoding Nav1.3 from rat and Nav1.7 from human were subcloned into the vector pcDNA3.1-mod, and cDNA encoding Nav1.5 from human was cloned into vector pRcCMVII. Constructs were transfected into HEK293 cells using the calcium phosphate precipitation technique. After 48 h, the cells were passaged into 100 mm dishes and treated with G418 (geneticin, Invitrogen) at 800 μg/ml to select for neomycin-resistant cells. After 2 weeks, colonies were picked and split. The colonies were then tested for functional channel expression using whole cell patch clamp technique. Expression of Nav1.1 (King et al., 2012), Nav1.3 (Cummins et al., 2001), Nav1.5 (Smith et al., 2007), and Nav1.7 (Theile and Cummins, 2011a) was maintained by 500 μg/ml G418 applied at each passage. Stable cell lines were grown under standard tissue culture conditions (5% CO_2 at 37 ºC) in DMEM supplemented with 10% FBS and 1% penicillin/streptomycin (100% stocks, 10 000 U/mL penicillin G sodium and 10 000 μg/mL streptomycin sulfate). For patch clamp experiments cells were transfected with 1 μg/μl of polyethyleneimine (PEI, Sigma), 2 μg of various CRMP2 constructs, and 1 μg/each SUMOylation machinery when applicable to the experiment (SUMO1-3, Ubc9, SENP1-2). Under these conditions efficiencies of ~50% were observed. Cells were plated at 24 h and sodium currents were

recorded at 48 h. For several biochemistry experiments, transfection was achieved with Lipofectamine 2000 (Invitrogen) per manufacturer instructions and experiments performed 48 h after transfection. Under these conditions efficiencies of ~80% were observed.

2.2.4. CAD cell culture

Mouse neuron model catecholamine A differentiated (CAD) cells were grown under standard tissue culture conditions (5% CO_2 at 37 ºC) in DMEM/F12 supplemented with 10% FBS and 1% penicillin/streptomycin (100% stocks, 10 000 U/mL penicillin G sodium and 10 000 μg/mL streptomycin sulfate) as previously described (Wang et al., 2010a, Wang et al., 2011b, Wang et al., 2011c). CAD cells were transfected by polyethyleneimine (Sigma) method for patch clamp experiments as described above for HEK cells with ~50% efficiency. CAD cells were transfected by Lipofectamine 2000 (Invitrogen) for biochemistry experiments with ~80-95% efficiency. All experiments were performed 48 h after transfection.

CAD cells predominantly express Nav1.7 and the channel accounts for ~90% of total Nav mRNA (Wang et al., 2011b). The current-voltage (IV) protocol (Figure 2.3B, top left) was used to survey properties of current-voltage relationship like peak current and activation, and the fast inactivation protocol (Figure 2.3B, bottom left) was used to survey fast inactivation. Representative families of traces for each of these protocols is found in the right half of Figure 2.3B. Highlighted in red in the IV protocol is a voltage pulse to +10 mV which elicits peak sodium current density in Figure 2.3C and is also

near the half-maximal voltage of activation displayed in Figure 2.3D. Highlighted in red in the fast inactivation protocol is a voltage pulse to -70 mV which produces a median current response and is hence near the half-maximal voltage of inactivation displayed in Figure 2.3D. CAD cell currents (Figure 2.3C) typically include a peak current between 0 mV and +10 mV, activation of currents beginning around -40 mV, and reversal potential around +70 mV. The current density of CAD cells undergoes a slight drift between passages, but averages around 60 pA/pF peak currents. Due to drift, controls were repeated within each experiment to normalize data. Importantly, all relationships between conditions were conserved regardless of drift.

CAD cell sodium current densities are between ~50% and ~80% Nav1.7 as resolved by five minute incubation of Nav1.7 specific toxins 125 nM Huwentoxin-IV (Figure 2.3E & F, 80% block, HWTX-IV) (Alomone Laboratories) (Xiao et al., 2008) and 5 nM ProTox-II (Figure 2.3G & H, 50% block; this block typically develops slowly and thus inhibition here is an underestimate of the steady state inhibition observed) (Schmalhofer et al., 2008). The difference of current block resolved by HWTX-IV versus ProTox-II results from differences in development of block as both toxins are highly specific to Nav1.7 at the concentrations used. To accommodate for the slower onset of block by ProTox-II, experiments utilizing ProTox-II involved a 15 minute incubation period and titration of ProTox-II in the extracellular bath that was not possible in paired recording, post-baseline application, studies, like the ones shown in Figure 2.3E-H. CAD cells do not display use-dependent properties of sodium currents at 10 Hz under naïve conditions (Figure 2.3I-K). The protocol used is shown in Figure 2.3I and equivalent currents to each pulse #1 - #30 in Figure 2.3K.

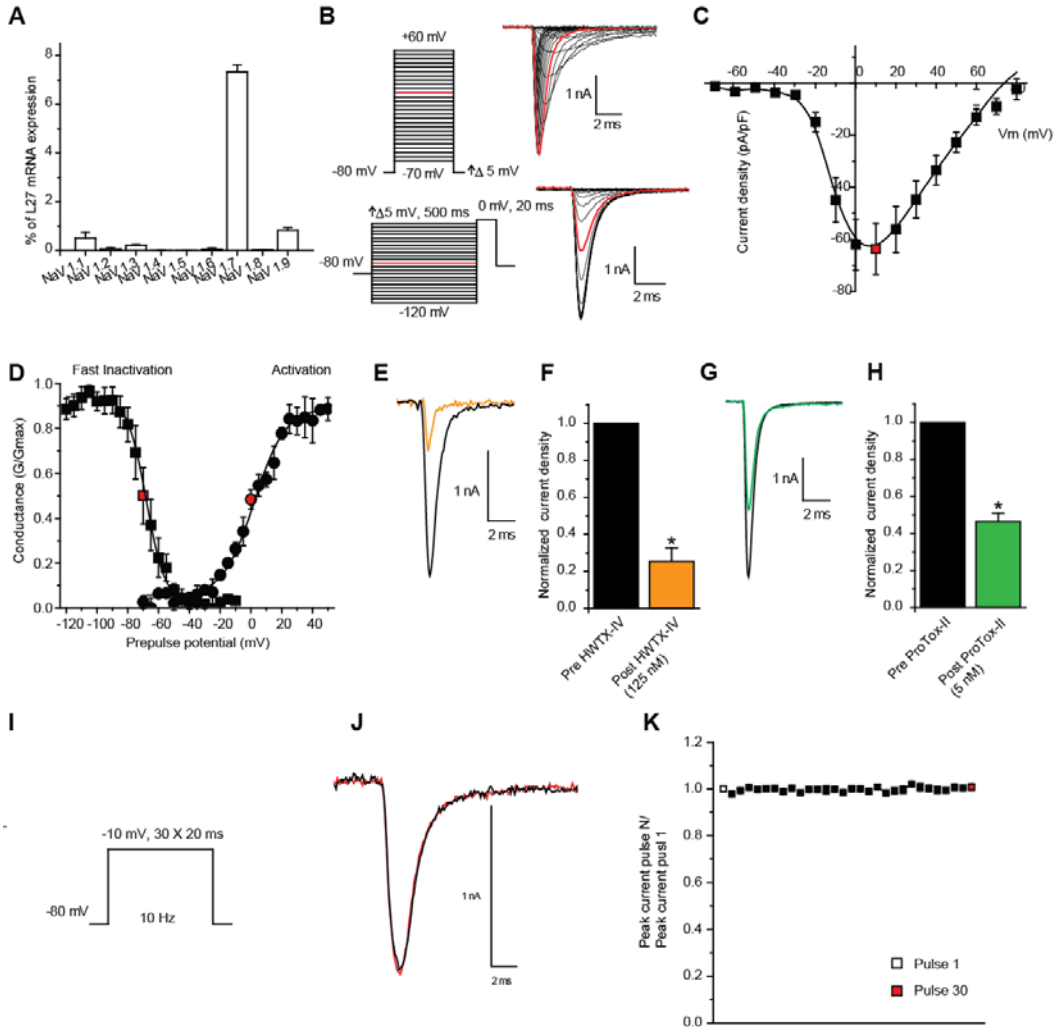
A
% of L27 mRNA expression
Nav 1.1
Nav 1.2
Nav 1.3
Nav 1.4
Nav 1.5
Nav 1.6
Nav 1.7
Nav 1.8
Nav 1.9
B
+60 mV
-80 mV
-70 mV
Δ 5 mV
1 nA
2 ms
Δ5 mV, 500 ms
0 mV, 20 ms
-80 mV
-120 mV
C
Current density (pA/pF)
Vm (mV)
D
Fast Inactivation
Activation
Conductance (Gi/Gmax)
Prepulse potential (mV)
E
F
Normalized current density
Pre HWTX-IV
Post HWTX-IV (125 nM)
G
H
Pre ProTox-II
Post ProTox-II (5 nM)
I
-10 mV, 30 X 20 ms
-80 mV
10 Hz
J
K
Peak current pulse N/ Peak current pusl 1
Pulse 1
Pulse 30

← previous page...Figure 2.3. Properties of CAD cell VGSC currents. **(A)** Quantitative RT-PCR for the indicated *$Na_V1.x$* genes from CAD cells. mRNAs for Na^+ channel isoforms $Na_V1.1$, 1.3, 1.7, and 1.9 were detected from CAD cells. Data are expressed as percent of L27 mRNA (a ribosomal internal control gene) ± SEM (n = 6 for each). Nav1.7 is the dominant transcript. **(B)** Protocols used to generate current-voltage (IV) relationship and activation (*top left*) and fast inactivation (*bottom left*) and families of current traces generated by these protocols (*right*). Description of voltage pulses and durations for these protocols can be found in section 2.3.3. Highlighted by a red voltage step in the IV voltage protocol is a pulse to 0 mV that corresponds to the peak current observed in the representative family of traces (*right*) and summary IV relationship in **C**. This voltage is also typically near the half-maximal voltage of activation shown in **D**. Highlighted by a red voltage step in the fast inactivation protocol is a pulse to -65 mV which corresponds to the median current response observed in the representative family of traces (*right*) and is typically near the half-maximal voltage of inactivation shown in **D**. **(C)** Summary of IV relationship. The sodium current-voltage relationship of CAD cells displays activation of currents starting at around -40 mV, a peak current between 0 mV to +10 mV (0 mV in this experiment), and a reversal potential for sodium around +70 mV. **(D)** Typical fast inactivation (*left curve*, boxes) and activation (*right curve*, circles) observed in CAD cells. Red data points represent half-maximal values of activation and inactivation curves fitted using Boltzmann equation: $y = 1/(1 + \exp(V_{½} - V)/k)$, in which $V_{½}$, V, and k represented midpoint voltage of kinetics, test potential, and slope factor, respectively. **(E)** Representative peak current traces before and 5 minutes after application of 125 nM Huwentoxin-IV or **(G)** 5 nM ProTox-II. **(F)** Summary data of CAD cell peak currents before and after application Huwentoxin-IV or **(H)** 5 nM ProTox-II. **(I)** Protocol used to test use-dependency of CAD cells. A 20 ms pulse to -10 mV was applied at 10 Hz for 30 consecutive pulses. **(J)** Representative traces of CAD cell currents in response to pulse 1 (*black*) and pulse 30 (*red*). **(K)** CAD cells under naïve conditions do not display use-dependent sodium currents as indicated by equivalent currents in pulses 1 through 30. Error bars are hidden by symbols. Asterisks denote statistical significance compared to pre-drug (Student's t-test). Data are means with SEM. n=5-9 cells per condition for each property shown.

2.3. Patch Clamp Electrophysiology

2.3.1. Equipment

Whole cell voltage-clamp recordings were performed at room temperature using HEKA EPC 10 USB amplifier and PatchMaster acquisition software (HEKA Electronics). Electrodes were pulled from standard-walled borosilicate glass capillaries (Warner Instruments) with a P-97 electrode puller (Sutter Instrument). Final electrode resistances were 1-3 MΩ when filled with internal solutions. Whole cell capacitance and series resistance were partially compensated by the amplifier (70%-90%). Linear leak currents were digitally subtracted by P/4. Signals were filtered at 10 kHz and digitized at 10-20 kHz. Analysis was performed using Fitmaster (HEKA Electronics) and Origin 9.1 (OriginLab Corporation).

2.3.2. Patch Clamp Solutions

Na^+ recording solutions for HEK cells and DRG cells were identical. To isolate sodium currents, external solutions contained TEA-Cl (tetraethylammonium chloride) to block voltage-gated potassium channels, and $CdCl_2$ to block voltage-gated calcium channels. All solutions were adjusted for pH with HCl in HEPES buffer and for osmolarity with sucrose, 290-310 mosM/L for internal solutions and 310-315 mosM/L for external solutions (Table 2.1)

2.3.3. Patch Clamp Voltage Protocols

Various voltage protocols were utilized to examine different components of sodium channel activity (*i.e.* current densities and kinetics). For total sodium current from HEK and CAD cells, a standard current-voltage relationship (IV) protocol was used. Cells were depolarized from a holding potential of -80 mV to potentials between -70 mV and +60 mV for 15ms in 5 mV increments. IV protocol allows for analysis of the I-V curve to identify peak sodium currents that are normalized to cell size to determine peak sodium current density (pA/pF). IV protocol also allows for analysis of activation kinetics. HEK and CAD cell fast-inactivation kinetics are analyzed from a protocol designed to elicit fast-inactivation (FI) of sodium channels. Cells are depolarized to various voltage potentials between -120 mV and -10 mV for 500 ms in 5 mV increments to elicit varying degrees of inactivation prior to testing available current with a voltage pulse to 0 mV for 20 ms. Total current was tested at the end of this protocol to verify use-dependence inactivation did not contribute to analysis of fast-inactivation kinetics. CAD cell slow inactivation was examined using a pre-pulse inhibition protocol with hyperpolarized recovery phase. Cells are subjected to voltage pulses between -110 mV and +20 mV in 10 mV increments for 5s to elicit varying degrees of sodium channel fast-inactivation and slow-inactivation. Fast-inactivated channels are then allowed to recover by -120 mV hyperpolarizing pulse for 150 ms such that a 0 mV, 15ms test pulse will resolve changes in available current mediated by slow-inactivation with minimal contribution of fast-inactivation.

Electrophysiology recording solutions [Concentrations in mM]				
Internal Solution		**Cell type**	**External Solution**	
140	CsF	HEK293 /DRG	130	NaCl
15	HEPES		30	TEA-Cl
10	NaCl		10	HEPES
1.1	Cs-EGTA		10	*D*-glucose
			3	KCl
			1	$CaCl_2$
			1	$MgCl_2$
			0.05	$CdCl_2$
110	CsCl	CAD	100	NaCl
25	HEPES		10	HEPES
10	EGTA		10	TEA-Cl
5	$MgSO_4$		10	*D*-glucose
4	Na_2-ATP		4	4-AP
			1	$CaCl_2$
			1	$CdCl_2$
			1	$MgCl_2$
			0.1	$NiCl_2$

Table 2.1. Electrophysiology recording solutions

Recordings from dorsal root ganglia cells utilize separate protocols that aid in separation of current contributions by various sodium channel isoforms. To resolve total sodium current in dorsal root ganglia (DRG) cells, DRG-IV protocol is used. Cells are held at -100 mV to account for hyperpolarized inactivation kinetics of DRG Nav1.X subtypes and then subjected to various depolarizing voltage potentials between -70 mV and +60 mV in 5 mV increments. In the presence of 500 nM tetrodotoxin, tetrodotoxin-resistant (TTX-R, Nav1.8 & Nav1.9) peak current density can be analyzed using the voltage pulse to 0 mV. To isolate tetrodotoxin-sensitive (TTX-S, Nav1.1-Nav1.7) peak current densities, the pre-pulse inactivation protocol H-infinity is used. H-infinity is named for the 'h' constant referring to sodium current inactivation in the Hodgkin and Huxley model for sodium channel kinetics (Hodgkin and Huxley, 1952d) and takes advantage of differential fast-inactivation kinetics of TTX-S and TTX-R channels to electrically isolate and subtract TTX-R/TTX-S current contributions (Roy and Narahashi, 1992). Cells are held at -120 mV and subjected to 1 s voltage pulses between -120 mV and +10 mV in 10 mV increments before available current is tested at 0 mV for 200 ms. These voltage pulses inactivate the compliment of voltage-gated sodium channels to various degrees. TTX-S currents inactivate at more hyperpolarized potentials than TTX-R currents such that the -40 mV pre-pulse reveals only TTX-R current. This TTX-R-only trace can then be digitally subtracted from previous traces that include the entire complement of TTX-R and TTX-S currents to reveal isolated TTX-S currents (Figure 2.4)

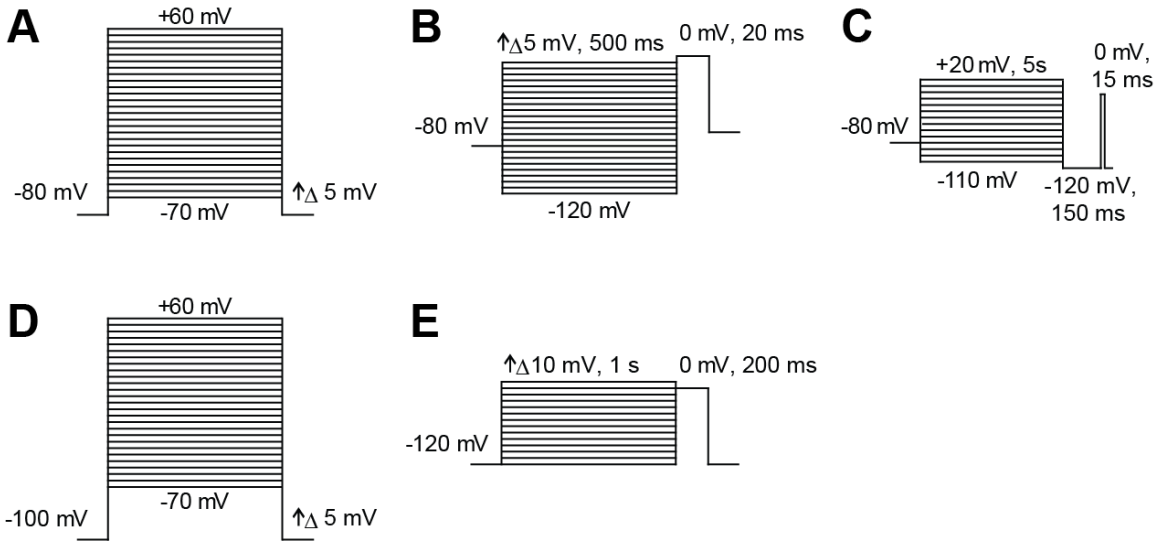

Figure 2.4. Voltage clamp protocols utilized to examine Na^+ currents. (A) Standard current-voltage relationship, IV, (B) Fast-inactivation, FI, (C) Slow-Inactivation, SI, (D) DRG current-voltage for tetrodotoxin-resistant currents, DRG-IV, (E) DRG pre-pulse inhibition for tetrodotoxin-sensitive currents, H-infinity.

2.3.4. Data analysis of current recordings

Sodium channel current recordings were analyzed for peak current density by normalizing the maximum current (Imax, pA, typically found at depolarization between -10 and +10 mV) by cell size (pF) to account for variation in cell size. Outlier cells, defined by greater or less than 2x S.D. for cell size or peak current, were removed from datasets. Averaged pA/pF values were compared between datasets following normalization to controls. Steady-state activation was analyzed using IV protocol data for channel conductance, G, at each voltage step and dividing by maximum conductance (Gmax). G/Gmax, where $G=I/(V_{pulse}-E_{rev})$, I is maximum current in response to V_{pulse} mV, and E_{rev} is the reversal potential of the cell determined by Fitmaster software (HEKA Electronics, Germany). G/Gmax values for each recording were fit to Boltzmann function in Origin 9.1 (OriginLab Corporation, Northampton, MA) then averaged to determine values of half-maximal voltage of activation $V_{1/2}$ and slope factor of activation, k, which were compared between conditions. Boltzmann equation: $y = 1/(1 + \exp(V_{½} - V)/k)$, in which $V_{½}$, V, and k represented midpoint voltage of kinetics, test potential, and slope factor, respectively

Steady-state fast inactivation was analyzed using FI protocol data for channel current, I, at each voltage step and dividing by maximum current (Imax). Normalized I/Imax values were fit to Boltzmann function in Origin 9.1 (OriginLab Corporation, Northampton, MA) and averaged within datasets to determine values of half-maximal voltage of fast inactivation $V_{1/2}$ and slope factor of fast inactivation, k, which were compared between conditions.

Slow inactivation was analyzed by using SI protocol current data, I, for each inhibitory pre-pulse and normalizing to maximum current (Imax). Values of inactivation were averaged and plotted for comparison between datasets.

2.3.5. Compounds used in patching

For patching experiments the following compounds were utilized: Tetrodotoxin (TTX) to block TTX-S Nav1.1—Nav1.7 currents (Alomone Laboratories); Pitstop2 – an inhibitor of pit formation during clathrin-mediated endocytosis (Abcam); and Lactacystin – an inhibitor of the proteasome complex responsible for cellular proteolysis degredation of proteins (Sigma). All compounds were dissolved in DMSO immediately prior to use.

2.4. Biochemistry

2.4.1. Biotinylation to detect cell surface Nav1.7

48 h after transfection, CAD cells were incubated with sulfosuccinimidyl 2-(biotinamido)ethyl-1,3′dithiopropionate (EZ-link Sulfo NHS-SS-biotin; 1 mg/mg protein, Pierce) for 30 min at 4 °C in cold PBS (pH 8.0) to label transmembrane protein fractions. Excess biotin was quenched with PBS containing 100 mM glycine and washed three times with ice-cold PBS. Cells were then transferred from tissue culture dishes to sterile Eppendorf tubes and lysed in RIPA buffer. Following resuspension, samples were triturated 10 times (with a 25-gauge needle) and centrifuged at 100,000 × *g* for 20 min. The biotinylated proteins were separated from clear solubilizate by adsorption onto

streptavidin-agarose beads (Novagen) for 2–4 h at 4 °C. Beads were washed 3–5 times with RIPA buffer, and bound biotinylated proteins were gently eluted off the beads with RIPA buffer containing 2% Triton X-100 and 650 mM NaCl by end-over-end incubation for 1 h at 30 °C. The biotinylated and total fractions were subjected to immunoblotting with β-tubulin and pan-Nav or Nav1.7 antibodies.

2.4.2. Immunocytochemistry

Naïve DRG cells were fixed with 4% paraformaldehyde (diluted in 0.1 mM PBS) for 10 min at room temperature, permeabilized with 0.2% Triton X-100 for 10 min, and then washed three times with 0.01 mM PBS. Cells were then pre-incubated with 10% bovine serum albumin (diluted in 0.1 mM PBS) for 1 h at room temperature to block nonspecific binding with the primary antibody. Nav1.7 (Neuromab) and CRMP2 (Sigma) primary antibodies were diluted (in 0.1 mM PBS) to 1:500 and applied to the cells. After incubation for 2 h at room temperature, the DRG cells were washed again with PBS, and secondary antibodies (anti-mouse Alexa 488, 1:500; Molecular Probes) were incubated in blocking solution for 45 min at RT. Coverslips were mounted in Prolong Gold Antifade mounting media (Molecular Probes). DRG cells were imaged on a Nikon Ti swept-field confocal microscope using a ×60, 1.4 NA lens with a cooled Cascade 512B digital camera (Photometrics). Z stack image pairs were captured through the sample. Images were deblurred off line by an iterative deconvolution protocol (Nikon Elements version 3.0) using a theoretical point-spread function.

2.4.3. siRNA knockdown of CRMP2

Validated small interfering RNAs (siRNAs) against the rat CRMP2 (5′-ACTCCTTCCTCGTGTACAT-3′) sequence (Nishimura et al., 2003) and controls (scrambled sequence with approximately the same percentage of GC but no sequence homology) were used for CRMP2 knockdown (Invitrogen) as previously described (Brittain et al., 2009a, Chi et al., 2009b, Brittain et al., 2011a, Brittain et al., 2011c). DRG and CAD cells were transfected with 250 nM control or CRMP2-specific siRNA along with EGFP or dsRed-CRMP2 constructs to allow visualization. Experiments were performed 48 h following transfection. siRNA knockdown was verified by Western blot in CAD cells, but not DRGs, due to differences in transfection efficiencies that make CAD cells the ideal cell to test siRNA function. As reported previously (Chi et al., 2009b), we observed a loss of CRMP2 immunoreactivity following knockdown of CRMP2 compared to control siRNA (Figure 2.5). Knockdown of CRMP2 with this siRNA has also previously been verified in cultured neurons via immunocytochemistry (Brustovetsky et al., 2014).

2.4.4. Co-Immunoprecipitations

CAD cells were lysed into the immunoprecipitation buffer containing 20 mM Tris-HCl pH=7.4, 50 mM NaCl, 2 mM $MgCl_2$, 10 mM *N*-Ethylmaleimide (NEM), 1% (vol/vol) NP-40, 0.5% (mass/vol) sodium deoxycholate, 0.1% SDS with Protease/phosphatase inhibitors cocktails (Calbiochem) and Benzonase ($50U.mL^{-1}$).

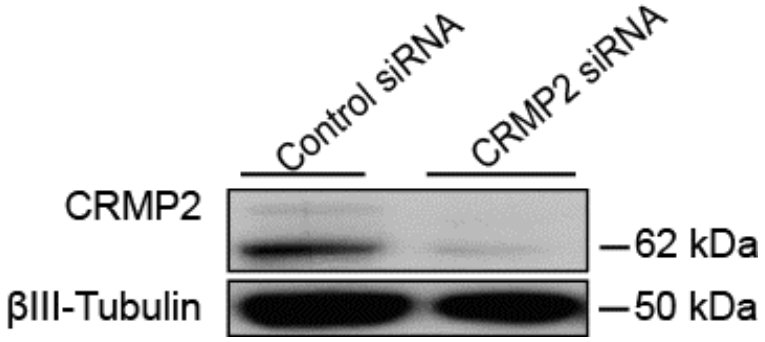

Figure 2.5. siRNA knockdown of CRMP2. Levels of CRMP2 and tubulin in CAD cells following 48 h incubation of control or CRMP2 -siRNA (200 nM).

Total protein concentration was determined by BCA protein assay (Thermo scientific) then 500 μg of total protein was incubated with 2 μg of CRMP2 antibody (Sigma) overnight at 4°C under gentle agitation. Protein G magnetic beads (Life Technologies) pre-equilibrated with the immunoprecipitation buffer, were added to the mixture and allowed to incubate for 1 h at 4°C to recover antibody-captured-complexes. The beads were washed 4 times with the immunoprecipitation buffer before re-suspension in Laemmli buffer and boiling at 95°C for 5 min prior to immunoblotting. For SUMO1 immunoprecipitation, lysates were denatured prior to incubation with SUMO1 antibody in order to identify endogenously SUMOylated protein in accordance with previously described methods (Becker et al., 2013).

2.4.5. Immunoblot analyses

Samples were loaded on 4-20% Novex® gels (Life Technologies). Proteins were transferred for 1h at 100 V using TGS (25mM Tris pH=8.5, 192mM glycine, 0.1% SDS), 20 % methanol as transfer buffer to polyvinylidene difluoride (PVDF) membranes 0.45μm, blocked at room temperature for 1 h with 5% non-fat dry milk then incubated separately in indicated primary antibodies overnight at 4°C. Following incubation in horseradish peroxidase conjugated secondary antibodies (Jackson immunoresearch), blots were revealed by enhanced luminescence (Millipore) before exposure to photographic film. Films were scanned, digitized, and quantified using Un-Scan-It gel version 6.1 scanning software (Silk Scientific Inc).

2.4.6. Plasmids and Antibodies

Antibodies were purchased from commercial vendors: Nav1.7 (NeuroMab, Davis, CA), pan Nav (Alomone Laboratories, Jerusalem, Israel), βIII-Tubulin (Promega, Madison, WI), CRMP2 (Sigma, St. Louis, MO), Numb (Abcam, Cambridge, MA), Eps15 (Abcam, Cambridge, MA), Nedd4-2 (Abcam, Cambridge, MA), Itch (BD biosciences, San Jose, CA). HA-SUMO-1, HA-Ubc9 plasmids were obtained from Addgene (Cambridge, MA). CRMP2 cDNA mutations were introduced by QuikChange II XL (Agilent, Santa Clara, CA) in the pdsRed2-CRMP2 plasmid. Plasmids were purified from DH5α E. coli using the NucleoBond® Xtra Maxi kit (Cat# 740414, Macherey-Nagel, Germany). Introduced mutations were verified by DNA sequencing. Cdk5, Fyn, and DNFyn plasmids were purchased from Addgene (Cambridge, MA).

2.5 Statistical analysis

All data points are shown as mean ± S.E., and *n* is presented as the number of the separate experimental cells. Steady-state activation and inactivation curves were fitted using the Boltzmann equation as follows: $y = 1/(1 + \exp(V_{½} - V)/k)$, in which $V_{½}$, V, and k represented midpoint voltage of kinetics, test potential, and slope factor, respectively. Statistical differences between control and experimental conditions were determined by using Kruskal-Wallis non-parametric one-way ANOVA with a Dunnet's post hoc test or a Student's *t* test when comparing only two conditions. Values of $p < 0.05$ were judged to be statistically significant. Asterisks or pound symbols are used to denote significance and defined in figure legends. All data was compared using OriginPro9.1 or R-project software.

CHAPTER 3.

IDENTIFICATION OF CRMP2 AS A TARGET OF SUMOYLATION AND BINDING PARTNER OF NaV1.7

3.1. Introduction

It is well established that post-translational modifications of CRMP2 direct its activity in neurons (Khanna et al., 2012). Mapping the CRMP2 interactome has unraveled novel targets which enable it to have broad roles in regulation of microtubule dynamics, protein endocytosis, vesicle recycling, and synaptic assembly within neurons (Khanna et al., 2012). Trafficking of ligand- and voltage-gated calcium channels has been recently demonstrated as novel roles for CRMP2 (Bretin et al., 2006, Brittain et al., 2009b, Chi et al., 2009c, Brittain et al., 2011a). In addition to protein targets, CRMP2 is the presumptive secondary target of the anti-epileptic drug (*R*)-lacosamide [(2R)-2-(acetylamino)-N-benzyl-3-methoxypropanamide; LCM], which has its primary action on voltage-gated sodium channels (VGSCs) (Errington et al., 2006, Errington et al., 2008). By stabilizing sodium channels in the slow-inactivated state, LCM is believed to reduce the pathological activity of hyperexcitable neurons typified by prolonged depolarizations, without affecting normal physiological activity (Errington et al., 2008). Work from the Khanna laboratory previously demonstrated that mutations within putative LCM-binding pockets in CRMP2 reduced LCM-induced shifts in slow inactivation of sodium channels compared to channels in the neuronal model CAD cells expressing wild type CRMP2 (Wang et al., 2010a). The data has also demonstrated CRMP2 labeling by fluorescent analogs of LCM could be competitively displaced by excess LCM in rat brain lysates, implying binding of LCM to CRMP2 (Wang et al., 2010a). In contrast to these findings, radiolabeled LCM was not found to bind to lysates from CRMP2-injected oocytes (Wolff et al., 2012). Thus, the exact mechanism by which CRMP2 modulates LCM-induced slow inactivation of sodium channels remains unclear. CRMP2 modulation of voltage-

gated sodium channels may be predicated on involvement of a tertiary protein or modification of either protein.

The Khanna laboratory is interested in delineating the mechanisms by which CRMP2 is directed to its many effectors and how it regulates their functions. Previous studies have implicated post-translational modifications, particularly phosphorylation, in directing CRMP2 interactions and regulating the function of the partner proteins. For instance, phosphorylation by Cdk5 enhances interaction between CRMP2 and voltage-gated calcium channels to modulate calcium influx (Brittain et al., 2012). Phosphorylation by glycogen synthase kinase 3β or Rho-associated protein kinase (ROCK) lowers the capability of CRMP2 to bind to tubulin heterodimers leading to microtubule destabilization, culminating in axon retraction/growth cone collapse (Arimura et al., 2000b, Arimura et al., 2005, Yoshimura et al., 2005b). Oxidation of CRMP2 has been shown to link the redox protein thioredoxin to regulation of CRMP2 phosphorylation and semaphorin 3A-induced growth cone collapse (Morinaka et al., 2011). Proteolysis of CRMP2 by calpains has also been reported and is believed to contribute to neurodegeneration and cell death (Zhang et al., 2007, Brittain et al., 2011a).

Therefore, here I tested how CRMP2 post-translational modifications relate to modulation of voltage-gated sodium channels.

3.2. Knockdown of CRMP2 reduces VGSC current density in CAD cells and DRG neurons

To investigate the relationship between VGSCs and CRMP2, I manipulated endogenous CRMP2 levels in CAD cells using a siRNA against CRMP2 as well as

overexpression of a CRMP2 construct refractory to CRMP2 knockdown, shresCRMP2. CRMP2 siRNA almost completely deleted endogenous CRMP2 from CAD cells (Figure 3.1A, *top blot*: lower band, open arrow) but did not prevent expression of exogenously added shresCRMP2 (Figure 3.1A, *top blot*: top band, closed arrow). For electrophysiology studies, successfully transfected cells were identified by fluorescence of the co-transfected dsRed plasmid and subjected to voltage protocols to assess quantitative measurements of current density, fast inactivation, and activation (see Figure 3.1D). Together these protocols allow for assessment of effects on the channel including shifts in voltage-dependence and changes to overall current production. CAD cells were initially used in these studies as they endogenously express CRMP2 protein (Brittain et al., 2012) and mRNAs for VGSC subtypes Nav1.1, Nav1.3, Nav1.7, and Nav1.9. Notably, in these cells, Nav1.7 is the dominant sodium channel, representing about ~95% of total VGSC gene transcripts and 80% functional channel determined by Nav1.7-selective block with 125nM huwentoxin-IV (Figure 2.3)(Wang et al., 2011b).

Knockdown of CRMP2 resulted in an ~70% reduction of sodium current density (Figure 3.1B, C; *green bar*) without any change in the kinetics of fast inactivation or activation analyzed by Boltzmann properties of half maximal activation ($V_{1/2}$) and slope (*k*) (Figure 3.1E). Addition of shresCRMP2 into CAD cells concomitantly with deletion of endogenous CRMP2 with a CRMP2 siRNA resulted in a recovery of current density to control levels (87.4 ± 11.5% of that observed in CRMP2 control; Figure 3.1E; *brown open symbols*).

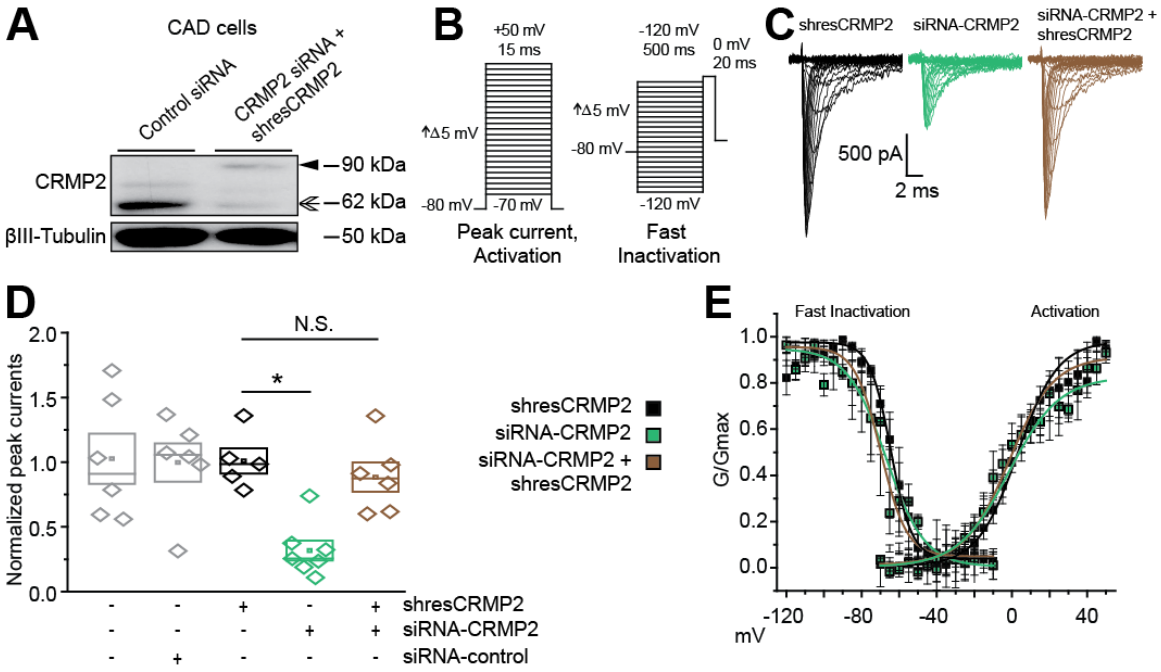

Figure 3.1. CRMP2 controls Nav1.7 current density in CAD cells. (A) Western blot of CAD cells displaying successful knockdown of endogenous CRMP2 by 200 nM siRNA-CRMP2 and 'add-back' of exogenous CRMP2 by overexpression of a wildtype CRMP2 that is resistant to the siRNA (shresCRMP2). **(B)** Voltage protocols used to measure peak current and activation (left) and fast inactivation (right) in CAD cells **(C)** Representative family of traces of sodium currents from CAD cells expressing wildtype shresCRMP2 (*black*), CRMP2 siRNA (*green*), or both (*brown*). **(D)** Box plot of peak current density (pA/pF) measured at 0 mV for shresCRMP2, CRMP2 siRNA, or shresCRMP2 and CRMP2 siRNA transfected CAD cells. Data are normalized to the shresCRMP2 condition. Box plot borders represent SEM and median, square indicates mean, diamonds are individual data points. Asterisk indicates statistically significant differences between siRNACRMP2 and shresCRMP2 expressing cells ($p < 0.05$, one-way ANOVA with Tukey's post-hoc test). **(E)** Representative Boltzmann fits for activation and steady-state inactivation for CAD cells transfected with the indicated constructs are shown. The calculated values for $V_{1/2}$ and k of activation and steady-state inactivation for all conditions tested and the associated statistics are presented in Table 3.1. Sodium current fast inactivation (*left curves*) and activation (*right curves*) were unaffected by knockdown or add-back of CRMP2. 5-7 cells per condition, data is presented as means ± SEM.

The shape of all CAD cell currents tested were equivalent within these experiments (Figure 3.1C) with peak current densities observed in within 1-2 ms of a voltage pulse to 0 mV and decay of current (τ, Tau, by exponential fit) of 550 ± 40 μs regardless of condition, current density, or day of recording. Overexpression of CRMP2 alone did not alter Na^+ current densities compared to CAD cells expressing EGFP (94.3 ± 30.2% of CRMP2 control) or compared to untransfected cells (101.8 ± 19.6% of CRMP2 control). In addition, CAD cells transfected with a control siRNA yielded currents no different from CAD cells expressing shresCRMP2 (98.8 ± 14.9% of CRMP2 control). Based on these data, I can conclude that (*i*) CRMP2 overexpression does not augment Na^+ current density in CAD cells, (*ii*) CRMP2 depletion removes all but 30% of CAD cell Na^+ currents.

The effect of CRMP2 knockdown and add-back on Na^+ currents was examined in acutely isolated primary rat DRG cultures. The sodium currents were electrically (post-hoc subtraction; protocols shown in Figure 3.2A) and pharmacologically (TTX, 500 nM) isolated into tetrodotoxin-sensitive (TTX-S) and tetrodotoxin-resistant (TTX-R) fractions. Small sensory neurons (< 30 μm) were chosen as these are likely Aδ- and c-fiber nociceptive neurons and express high levels of Nav1.7 (Harper and Lawson, 1985, Lawson, 2002, Djouhri et al., 2003, Zhang et al., 2013). The TTX-S sodium current fraction in DRGs electroporated with a CRMP2 siRNA was reduced by ~62% compared to DRGs expressing shresCRMP2 (Figure 3.2D, F). Concomitant electroporation of DRGs with shresCRMP2 and CRMP2 siRNA rescued the reduction in current density to 85.6 ± 12.3% of control (i.e. shresCRMP2 only) levels.

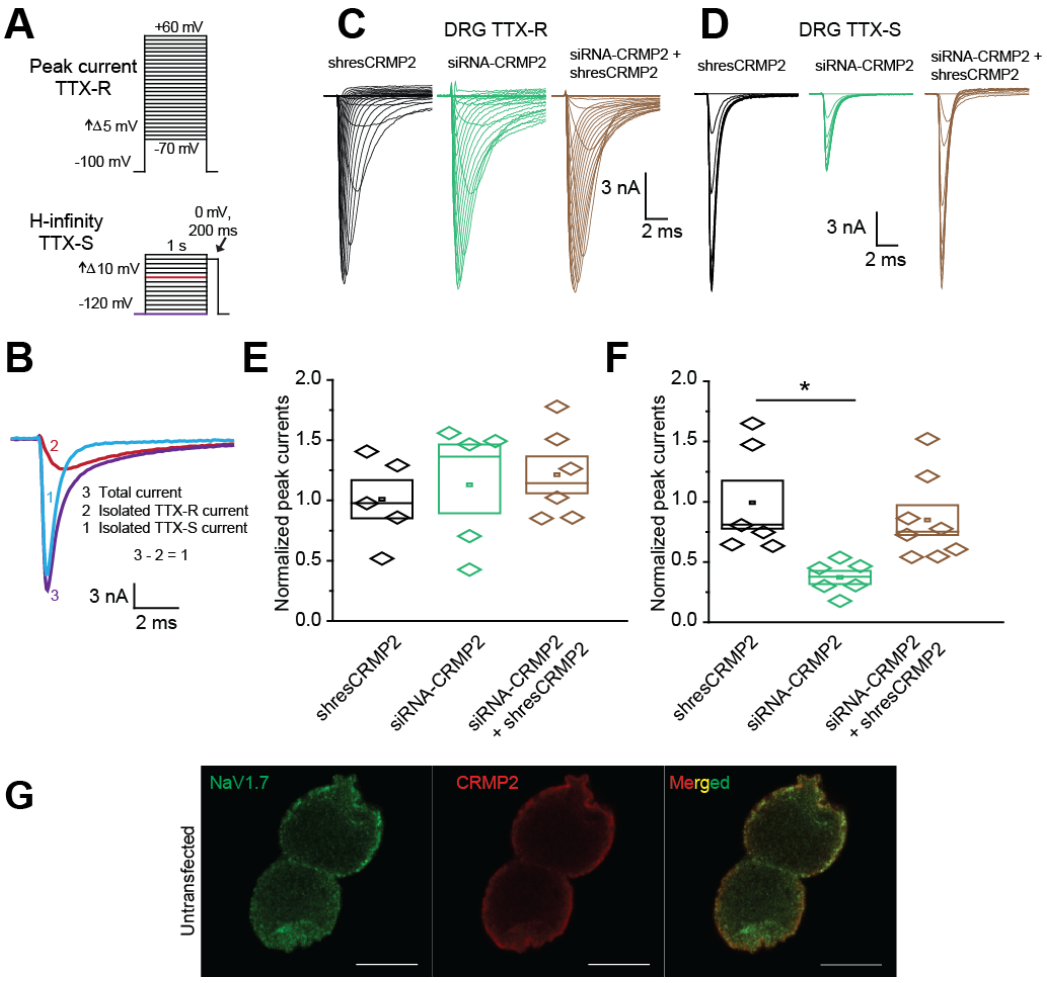

Figure 3.2. CRMP2 controls TTX-S current density in DRG neurons. (A) Voltage protocols used to measure peak TTX-R (*top*) and peak TTX-S (*bottom*) currents from DRG cells. *Purple* and *red* voltage pulses in H-infinity protocol represent the conditioning pulses used to separate TTX-S current by post-hoc subtraction. **(B)** Post-hoc subtraction of TTX-S traces. *Purple* trace (labeled 3) represents total sodium current. *Red* trace (labeled 2) represents current elicited after –40 mV prepulse, a voltage at which the TTX-S current has completely inactivated; this is the TTX-R current. *Blue* trace (labeled 1) is the digital subtraction of 3 from 2 (3-2=1) and represents the TTX-S current. Box plots of normalized peak currents (pA/pF) of TTX-R. Representative family of TTX-R **(C)** or TTX-S **(D)** sodium current traces, in response to the voltage protocol shown in **A**, from DRG neurons transfected with the indicated conditions. Box plots of TTX-R **(E)** and TTX-S **(F)** peak currents measured at 0 mV for shresCRMP2, CRMP2 siRNA, or shresCRMP2 and CRMP2 siRNA transfected DRGs. Data are normalized to shresCRMP2 expressing cells. **(G)** Representative confocal images of untransfected DRG neurons immunolabeled for Nav1.7 (*green*) and CRMP2 (*red*). All cells imaged displayed surface colocalization of CRMP2 and Nav1.7. Scale bar is 10 microns. Data are normalized to the shresCRMP2 condition. Box plot borders represent SEM and median, square indicates mean, diamonds are individual data points. Asterisk indicates statistically significant differences between siRNACRMP2 and the two other conditions tested ($p < 0.05$, one-way ANOVA with Tukey's post-hoc test). n=5-8 cells per condition.

In contrast, the TTX-R current fraction was completely unaffected with current density levels reaching 111.7 ± 23.1% in DRGs electroporated with shresCRMP2 and 120.0 ± 15.1% for DRGs electroporated with both shresCRMP2 and CRMP2 siRNA (Figure 3.2C, E). As TTX-S currents were reduced upon CRMP2 depletion, the data suggests that CRMP2 regulation of sodium currents may be limited to a certain subtype of VGSCs. To observe CRMP2 expression in small diameter DRGs together with Nav1.7, CRMP2 and Nav1.7 were co-stained. (Figure 3.2G).

Given the dominance of Nav1.7 in CAD cell currents (Figure 2.3) and in small DRG neurons (Zhang et al., 2013), I predicted that of TTX-S subtypes, at least Nav1.7 isoform is affected by CRMP2 SUMOylation state, and conclude that total TTX-R currents are not affected. Nav1.9, however, can have very small contribution to total current amplitude and still function to alter neuronal activity. This function is endowed by slow kinetics and a persistent current that lasts several hundred milliseconds longer other VGSC current responses. As a result Nav1.9 currents in DRGs, like Nav1.7, can underlie painful conditions (Lolignier et al., 2015). Nav1.9 currents are not explicitly tested in this thesis; however, results suggest that any potential role for CRMP2 regulation of Nav1.9 does not prevent Nav1.7-mediated reduction of neuronal activity (see Figure 5.2). In a later section I separate the contribution of DRG TTX-S currents using the Nav1.7 specific toxin ProTox-II to verify my Nav1.7-mediated hypothesis (see Figure 3.6).

3.3. Analysis of CRMP2 primary amino acid sequence reveals a stringent and conserved SUMOylation motif that affects VGSC currents in CAD cells and DRG neurons

As discussed in the Introduction (see section 1.2.2), CRMP2 is subject to multiple post-translational modifications that endow CRMP2 with a diversified portfolio of functional outcomes. However, whether all such CRMP2 modifications have been discovered is unknown. An analysis of CRMP2 primary amino acid sequence identified at least 5 sequences that conformed to the SUMO-consensus motif ψKxD/E (see Chapter 1.3) (Figure 3.3A). Notably, these sequences were conserved between most of the other CRMP family members (Figure 3.3B).

Previous investigations of protein SUMOylation have demonstrated that mutating the SUMOylated lysine to either an arginine or alanine eliminates the site of addition of SUMO by Ubc9 (Duprez et al., 1999, Sampson et al., 2001, Perdomo et al., 2005, Merrill et al., 2010). In one study, mutation to arginine lead to false results due to the charge of an arginine residue interfering with voltage-gated potassium channel gating (Feliciangeli et al., 2007). In my thesis I use voltage stimuli to probe ionic currents and therefore choose to mutate putatively targeted lysine residues to uncharged alanine residues. CRMP2-dsRed mutants harboring lysine to alanine (K→A) mutations were produced to eliminate putative SUMOylation motifs that scored as 'likely SUMOylated' by Abgent SUMOplot™ analysis program: K20, K374, and K390 (Figure 3.3B). Of these sites, K374 was particularly interesting due to (*i*) its perfect conservation between CRMPs 1–5, (*ii*) conformity to the SUMO-consensus motif ψKxD/E (see Chapter 1.3), and (*iii*) the presence of downstream aspartic and glutamic acid residues that typify this motif as the more stringent **n**egative charge **d**ependent **S**UMO **m**otif. In a NDSM, interaction with

SUMO-E2 enzyme, Ubc9, can be promoted by the additional negative charges (Henley et al., 2014). Current density and channel kinetics of fast inactivation and activation were analyzed in CAD cells expressing CRMP2-K20A, CRMP2-K374A, and CRMP2-K390A mutants. CAD cell Nav1.7 sodium currents (Figure 3.3C) in cells expressing CRMP2-K20A or CRMP2-K390A, were unchanged compared to those of CAD cells expressing wildtype CRMP2 (Figure 3.3C, D). In contrast, the peak current density observed at 0 mV following CRMP2-K374A expression in CAD cells reduced Nav1.7 current density by ~57% compared to CAD cells expressing wildtype CRMP2 (Figure 3.3C, D). This reduction in Nav1.7 current density was similar in magnitude to that observed in CAD cells in which CRMP2 had been depleted with siRNA-CRMP2 (Figure 3.1D, *green box*). This CRMP2-K374A mediated current reduction was not associated with any changes in fast inactivation or activation kinetics (Figure 3.3E, Table 3.1) compared to CAD cells expressing wildtype CRMP2. CRMP2 SUMO-null mutant had these effects in the presence of endogenous CRMP2 suggesting that it functions as a dominant negative. This could be indicative of the status of CRMP2 SUMOylation in cells, where only a low fraction of unSUMOylated CRMP2 is required for modulation of sodium currents. Alternatively, it could indicate that function of CRMP2 on sodium channels involves CRMP protein tetramerization (Wang and Strittmatter, 1997b) where only one copy of unSUMOylated CRMP2 is required for reduction of currents.

To gain a deeper understanding of the possible importance of this putative SUMOylation site in CRMP2, I compared this SUMOylation motif and the surrounding residues (amino acids 368-381) of human CRMP2 with various species using a Universal Protein Resource (UniProt) database Basic Local Alignment Search Tool (BLAST). A

high rate of conservation within this region would be indicative of negative selection, a process by which important genetic regions are conserved by selection related to an important function or evolutionary advantage (Charlesworth et al., 1993). I found that lysine-374 and 13 flanking residues were perfectly conserved within CRMP2 for mammal species of cat, new world and old world monkeys, mouse, rat, cow, human, panda, pig, treeshrew, ferrets, yak, and bats. These 14 amino acid residues were also perfectly conserved within at least 35 species of Aves and 3 species of Reptiles. Human CRMPs 1, 3, and 4 were 92.9% homologous within this region while CRMP5 was 71.4% homologous. Additionally, 5 fish species had 71.4% conservation of this region. The high rate of conservation within human CRMPs and also CRMP2s of a variety of species indicates that this SUMOylation motif endows important protein function (Figure 3.4). Putative CRMP2 SUMOylation is not conserved, however, in CRMP proteins of *Caenorhabditis elegans* or *Drosophila melanogaster* suggesting that the role of CRMP2 SUMOylation is likely not present, at least within this sequence motif, and thus may not endow protein function in these reductionist model organisms. Furthermore, BLAST analysis suggests that CRMP2 SUMOylation at lysine-374 does not exist outside of phylum Chordata.

To further elucidate the role of CRMP2 SUMOylation on sodium channel currents, I next utilized expression of deSUMOylationg SENP proteins. If SUMOylation is important for determining Nav1.7 currents in CAD cells, then overexpression of SENP1 and SENP2 proteases to enhance deSUMOylation should result in a reduction of Nav1.7 currents similar to that I had observed following overexpression of the SUMO-null CRMP2-K374A mutant. Consistent with this expectation, expression of SENP1 and

SENP2 reduced CAD cell Nav1.7 current density by ~67% compared to CAD cells expressing wildtype CRMP2 without affecting Boltzmann kinetic properties of activation or fast inactivation (Table 3.1). Manipulation of the SUMOylation machinery in CAD cells in the opposite direction by boosting SUMOylation with overexpression of Ubc9 was unable to enhance Nav1.7 currents above those observed in CAD cells expressing wildtype CRMP2 (82.9 ± 14.5% of control) (Table 3.1), suggesting that Nav1.7 regulation is provided by constitutive CRMP2 SUMOylation.

Reduced current densities can result from several modifications to sodium channels including altered channel kinetics, reduced membrane expression, reduced open probability, or reduced single channel conductance. In any of these cases, the complement of channels are less able to pass current because they are less responsive to voltage stimuli or because there are a fewer number of the channels in the plasma membrane. Equivalence of fast inactivation and activation data between conditions contradicts the first possibility of altered kinetics. Therefore, next we performed cell surface biotinylation experiments to test the second possibility of reduced membrane expression. CAD cells expressing either wildtype CRMP2 or the SUMO-null CRMP2-K374A alone or in the additional presence of the deSUMOylating enzymes SENP1 and SENP2 were subjected to cell surface biotinylation as described previously (Brittain et al., 2011a, Brittain et al., 2011b). Immunoblotting with Nav1.7 of streptavidin-enriched complexes from biotinylated CAD cells showed decreased Nav1.7 surface expression in cells expressing CRMP2-K374A versus wild type CRMP2 (Figure 3.5A, *top blot, compare lanes 1 with 3*). Surface Nav1.7 levels, normalized to total tubulin levels, in

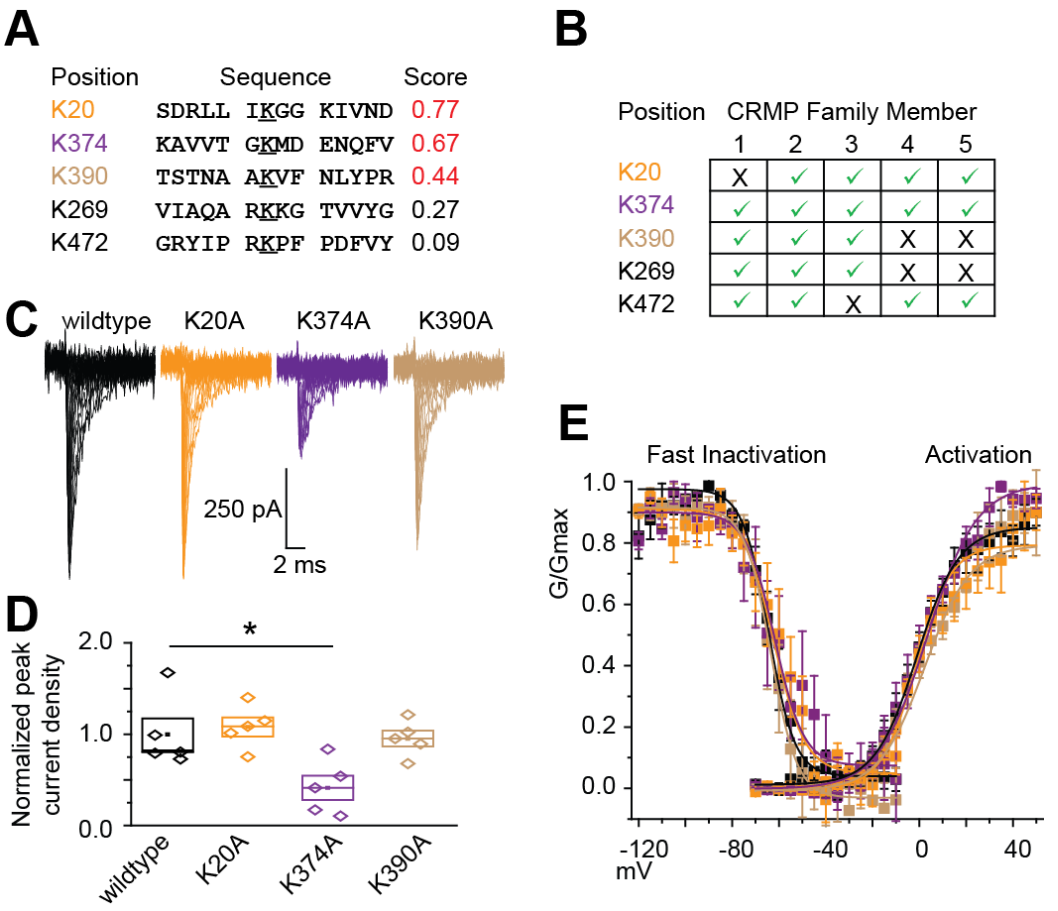

Figure 3.3. CRMP2 lysine-374 controls sodium currents in CAD cells. (A) CRMP2 (*Mus musculus*, GenBankTM accession number NM_009955.3) sequences identified by Abgent SUMOplot™ as potential candidates for SUMOylation. Higher scores denote higher probability of SUMOylation. **(B)** Sequence analysis of identified putative motifs identify strong conservation of all motifs, and perfect conservation of K374A motif throughout all CRMPs. **(C)** Representative family of sodium current traces from CAD cells expressing the indicated CRMP2 alanine mutants. **(D)** Box plot of peak current density (pA/pF) measured at 0 mV from CAD cells transfected for the indicated CRMP2 plasmids. Data are normalized to the CRMP2 condition. Boxes represent quartiles, each data point represents 1 cell. Error bars are behind data symbols in some cases. **(E)** Representative Boltzmann fits for activation and steady-state inactivation for CAD cells transfected with the indicated constructs are shown. The calculated values for $V_{1/2}$ and k of activation and steady-state inactivation for all conditions tested and the associated statistics are presented in Table 3.1. Sodium current fast inactivation (*left curves*) and activation (*right curves*) were unaffected by knockdown expression of CRMP2 mutants. 5 cells per condition, data is presented mean ± SEM. Asterisk indicates statistically significant differences between CRMP2-K374A and all other conditions tested (n=5; $p < 0.05$, one-way ANOVA with Tukey's post-hoc test).

Condition	Peak Current	*n*	Activation			Fast Inactivation		
			$V_{1/2}$	k	n	$V_{1/2}$	k	n
CRMP2	100.0 ± 9.7	*5*	3.0 ± 1.3	10.8 ± 1.0	*5*	-64.4 ± 1.9	5.6 ± 0.7	*5*
Untransfected	101.8 ± 17.9	*6*	2.9 ± 2.8	11.0 ± 1.2	*5*	-68.9 ± 1.1	5.6 ± 0.6	*4*
siRNA-control	98.8 ± 14.9	*6*	3.4 ± 2.0	14.1 ± 1.7	*5*	-68.0 ± 1.3	6.2 ± 0.7	*4*
siRNA-CRMP2	30.2 ± 7.8 *****	*7*	-1.6 ± 3.2	13.4 ± 2.1	*3*	-71.4 ± 2.6	8.0 ± 1.4	*3*
siRNA-CRMP2 + shresCRMP2	87.4 ± 11.5	*6*	-1.4 ± 1.8	11.8 ± 1.2	*5*	-69.8 ± 1.3	6.9 ± 0,6	*4*
shresCRMP2-K374A	42.9 ± 10.0 *****	*5*	3.4 ± 1.4	10.5 ± 0.9	*4*	-63.7 ± 3.1	5.7 ± 0.9	*3*
siRNA-CRMP2 + shresCRMP2-K374A	34.1 ± 2.4 *****	*5*	4.3 ± 1.1	10.8 ± 0.7	*4*	-67.5 ± 0.9	4.7 ± 1.1	*3*
SENP1 + SENP2	36.9 ± 9.0 *****	*5*	3.5 ± 1.6	10.4 ± 0.8	*4*	-65.5 ± 2.2	6.1 ± 1.4	*3*
CRMP2-K20A	109.3 ± 16.5	*5*	2.2 ± 1.9	9.8 ± 0.9	*3*	-63.5 ± 0.6	5.6 ± 0.4	*3*
CRMP2-K390A	93.4 ± 5.0	*5*	-0.1 ± 1.3	9.3 ± 0.9	*3*	-62.2 ± 2.0	6.7 ± 1.3	*3*

Table 3.1. Comparative current densities and Boltzmann–fits of voltage–dependence of channel activation and fast-inactivation for the respective transfection conditions in CAD cells. Values for $V_{1/2}$, the voltage of half–maximal activation and fast inactivation, and slope, were derived from Boltzmann distribution fits to the individual recordings and averaged to determine the mean and standard error of the mean (± S.E.M.). *n* values indicates the number of cells per condition. All transfection conditions contained EGFP or dsRed for identification of construct expression. Asterisks represent statistically significant differences as compared to control (i.e. CRMP2 alone condition) within tested groups ($p<0.05$, ANOVA with Tukey's post–hoc test or Student's t–test).

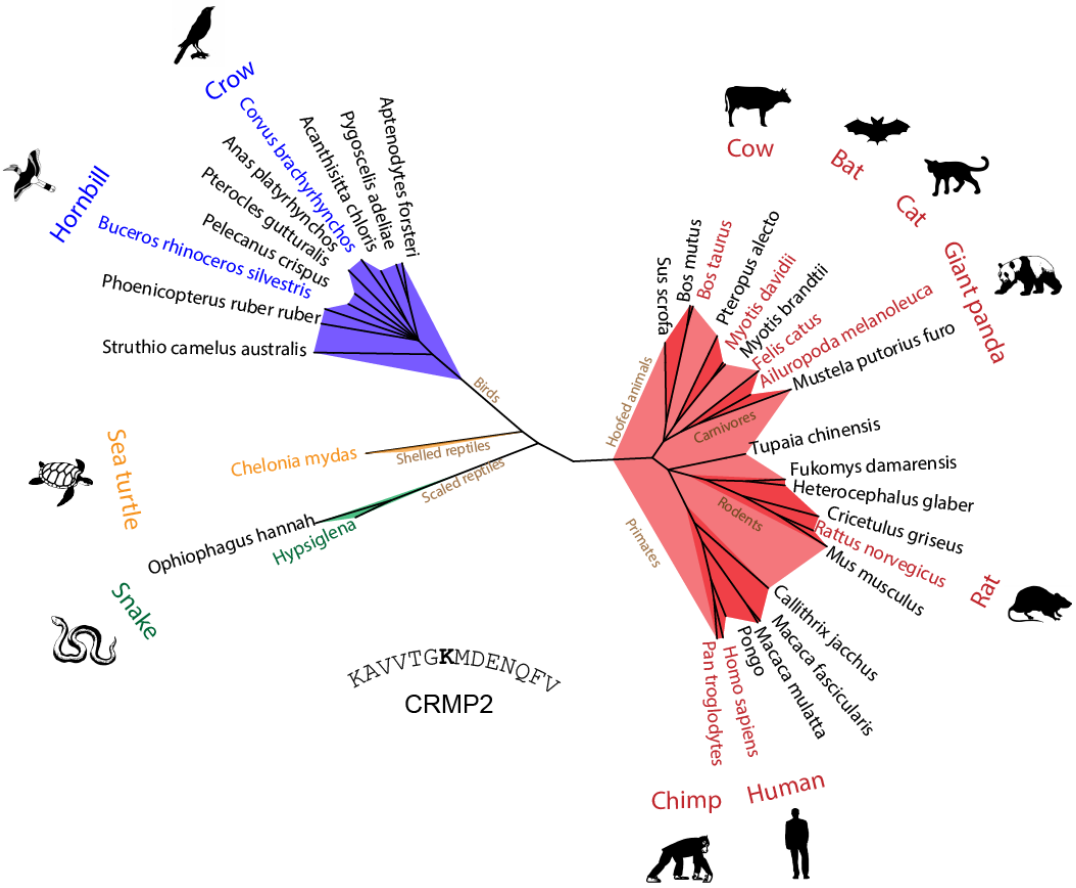

Figure 3.4. Phylogenetic tree of species with perfectly conserved CRMP2 SUMOylation motif and flanking residues. Created using 'Interactive Tree of Life' (iTOL2.0) software (Letunic and Bork, 2007, 2011), this tree lists the genus and species of a sample of organisms with perfectly homology for *Mus musculus*, (GenBankTM accession number NM_009955.3) SUMOylation motif and flanking residues (residues 368-381 shown below tree, which includes the SUMOylated lysine 374 in bold). Species are listed at the end of tree 'branches' and generalized class or order classifications are listed within the lower 'branches' of the tree in brown text. Separation into different branches represents a divergent evolutionary relationship. Surrounding the tree is a sampling of species listed by their common names, matched by color of text. Blue color represents animals of the Class Aves (Birds). Due to the high number of birds identified to have homology within the CRMP2 sequence, only a select number are listed here. Orange represents Order Testudines (shelled reptiles) and green represents Order Squamata (scaled reptiles). Red represents class Mammalia which is subdivided by density of red color into subclasses and orders which are listed by their common names along lower tree 'branches'. No homology exists within the CRMP2 SUMOylation motif and CRMP proteins from *Caenorhabditis elegans* or *Drosophila melanogaster*. Homology appears to be limited to Chordata phylum animals that encompass all listed species.

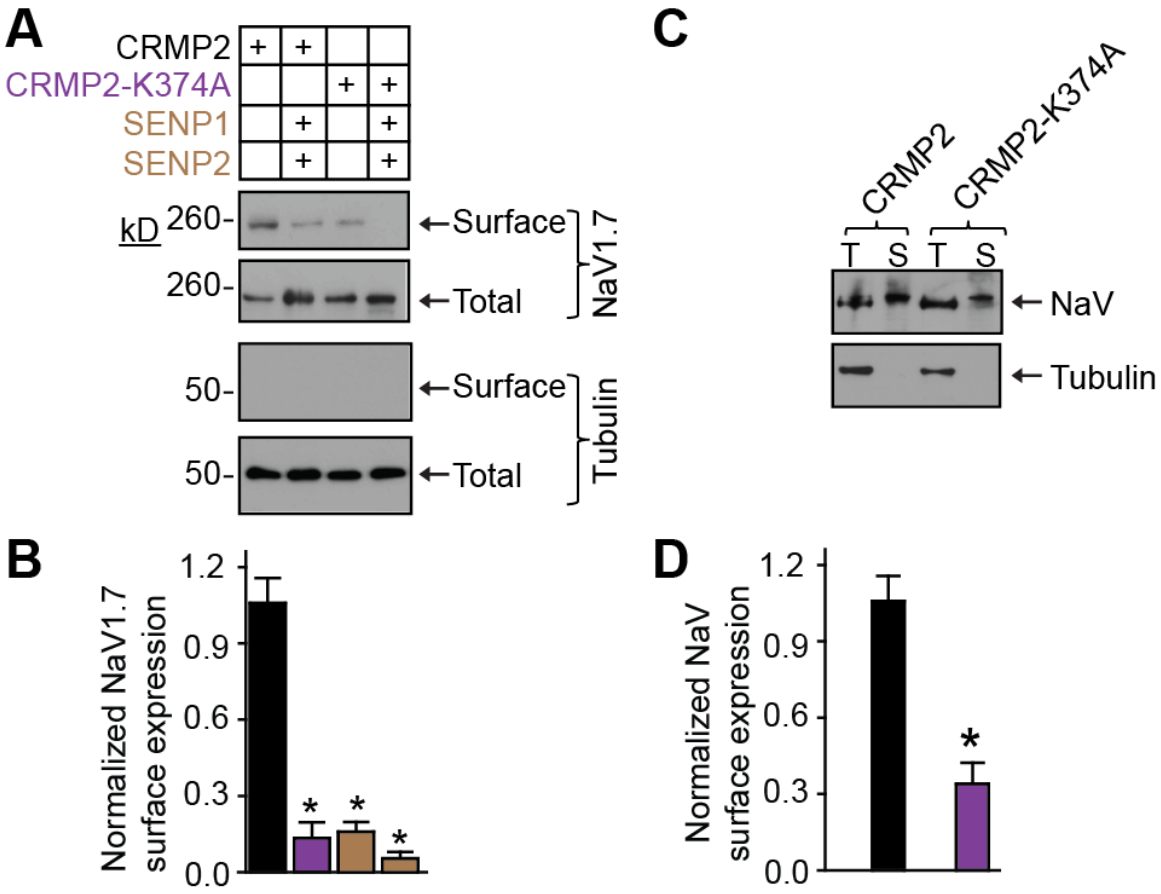

Figure 3.5. CRMP2-K374A and increasing deSUMOylation reduces Nav1.7 surface expression. (**A**) Cell–surface expression of Nav1.7 was monitored using a biotinylation assay. CAD cells expressing wild type CRMP2 or CRMP2-K374A alone or in the presence of deSUMOylating proteases SENP1 and SENP2 were biotinylated, the cell-surface proteins were harvested from the cell lysates, and the precipitates were analyzed by immunoblotting with Nav1.7 (*top 2 blots*) and βIII-tubulin (*bottom 2 blots*) antibodies. Equal amounts of samples were used for the precipitation of biotinylated proteins. Of these samples, the entire biotinylated fraction (surface) and 10% of the non-biotinylated (total) fraction were loaded. CRMP2-K374A overexpression decreased the amount of Nav1.7 at the cell surface compared to CRMP2-transfected cells. No change was observed in the total levels of Nav1.7 or tubulin. (**B**) Averaged Nav1.7 surface expression, normalized to total Nav1.7 and then to total tubulin. **(C)** VGSC surface expression monitored by biotinylation assay described in **A.** panNaV antibody was used to immunoblot lysates. **(D)** Averaged VGSC surface expression, normalized to total VGSC expression and then to total tubulin. Asterisks indicate statistically significant differences between CRMP2 and all other conditions tested ($p < 0.05$, one-way ANOVA with Tukey's post-hoc test). Experiments performed with help of Dr. Weina Ju.

CRMP2-K374A–expressing CAD cells were 15.1 ± 2.5% of those in cells expressing wild type CRMP2 (Figure 3.5A).

Increasing deSUMOylation with the sentrin/SUMO-specific proteases SENP1 and SENP2 (Mukhopadhyay and Dasso, 2007), decreased levels of surface Nav1.7 to 14.2 ± 3.9% of those in cells expressing wild type CRMP2 (Figure 3.5B). Under these conditions, surface Nav1.7 levels in CRMP2-K374A–expressing CAD cells were reduced to 7.9 ± 2.1% of those in cells expressing wild type CRMP2 (Figure 3.5B). Additional experiments with a panNav antibody also demonstrated a substantial reduction in surface expressed Nav channels in CAD cells expressing CRMP2-K374A (Figure 3.5C and D). These results are consistent with the reduction in Nav1.7 current density in CRMP2-K374A–expressing CAD cells observed earlier. Thus, reduced CRMP2 SUMOylation likely accounts for Nav1.7 surface trafficking impairment.

I next examined whether changes in CRMP2 SUMOylation could alter sodium currents in DRGs. Only whole-cell patch clamp electrophysiology experiments were used to test this as the low (~10–20%) transfection efficiencies precluded performing biotinylation experiments in DRGs.

As before, sodium currents were electrically (post-hoc subtraction; protocols as shown in Figure 3.2) and pharmacologically (TTX, 500 nM) isolated into tetrodotoxin-sensitive and tetrodotoxin-resistant fractions. Small sensory neurons (< 30 μm) were chosen for these recordings. The time courses and current delay of estimated TTX-S and TTX-R currents perfectly resemble descriptions of these current types from the first study to electrically isolate these separate components of DRG sodium currents suggesting appropriate patch clamp technique and appropriate separation of currents (Roy and

Narahashi, 1992). As in this paper, TTX-S currents were fast activating and fast inactivating, with less than ~10% current remaining after 5 ms. It was not uncommon for ~50% of TTX-R current to remain after the same duration. The fast activating, fast inactivating TTX-S sodium current fraction (Figure 3.6A) was isolated in DRGs electroporated with a CRMP2-K374A SUMO-null plasmid and currents were reduced by ~74% compared to DRGs expressing wildtype CRMP2 (Figure 3.6A, C). Electroporating the SENP1 + SENP2 proteases to reduce SUMOylation decreased the TTX-S sodium current fraction by ~48% compared to DRGs expressing wildtype CRMP2 (Figure 3.6A, C). The slower activating and inactivating TTX-R sodium current fractions (Figure 3.6B) were not different between the conditions tested (Figure 3.6B, D). Contributions by Nav1.9 to total TTX-R current can be overshadowed by the predominance of Nav1.8 current in these experiments. For this reason, we cannot rule out contribution by possibly altered Nav1.9 though. Nevertheless, effects on TTX-S current are sufficient to result in a net reduction of DRG sodium currens. This hypothesis was confirmed in a later experiment (see Figure 5.2).

3.4. CRMP2 mediated VGSC current reductions are isoform specific

Reduction of TTX-S, but not TTX-R, currents in DRGs following loss of CRMP2 SUMOylation suggests that CRMP2 modulation is Nav isoform specific. To address this possibility, HEK cells stably expressing isoforms hNav1.1 (King et al., 2012), rNav1.3 (Cummins et al., 2001), hNav1.5 (Smith et al., 2007), and hNav1.7 (Theile and Cummins, 2011a) (cells, not expressing additional beta subunits, provided by Dr. Theodore R. Cummins (Department of Pharmacology and Toxicology, Indiana University School of

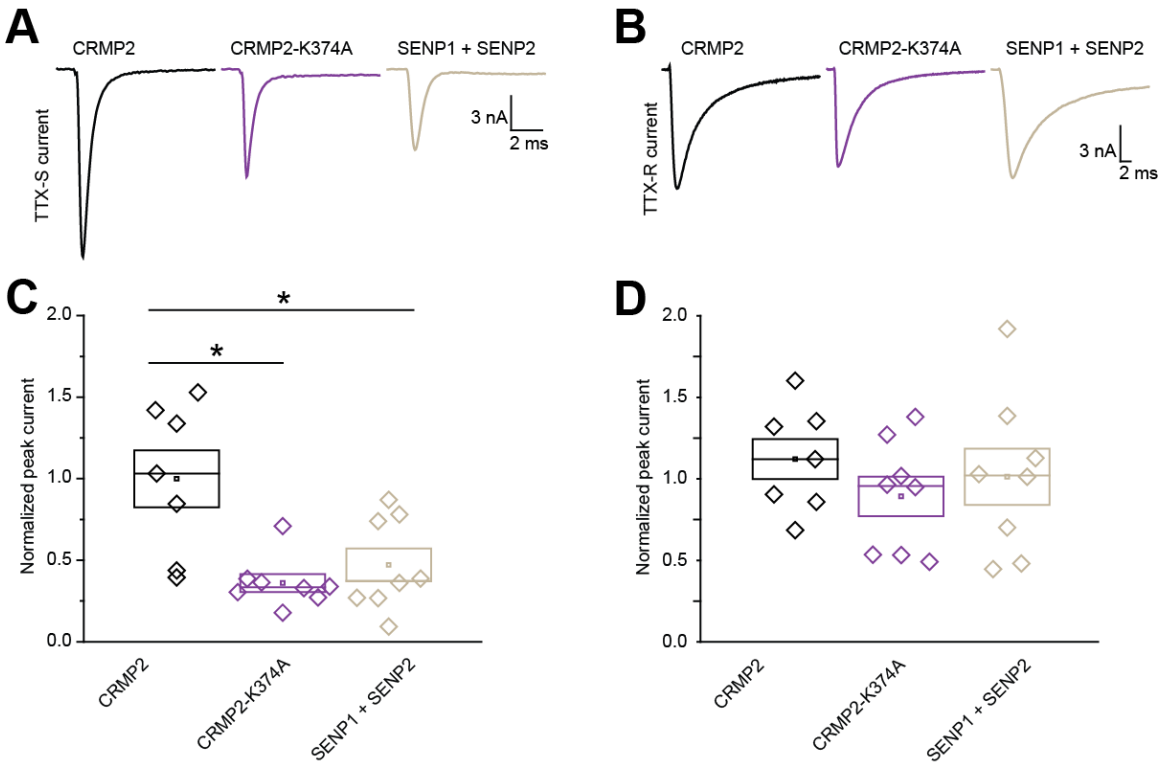

Figure 3.6. CRMP2-K374A and increasing deSUMOylation reduces TTX-S, but not TTX-R, current density in DRG neurons. Representative TTX-S (**A**) and (**B**) TTX-R sodium current traces from small DRGs expressing CRMP2, CRMP2-K374A, or SENP1 + SENP2 proteases. Box plots of peak TTX-S **(C)** and **(D)** TTX-R current density (pA/pF) normalized to CRMP2 condition. Box plot borders represent SEM and median, square indicates mean, diamonds are individual data points. 7-8 cells per condition, error is ± SEM. Asterisks denote statistical significance compared to CRMP2 by one-way ANOVA, * $p < 0.05$.

Medicine)) were transfected with CRMP2 or CRMP2-K374A SUMO-null plasmids and currents were analyzed sodium channel biophysical properties including peak current density, fast inactivation, and activation. Ubc9 and SUMO1 were also cotransfected in these studies due to the low level of expression of these elements of the SUMOylation machinery as determined by quantitative RT-PCR (Dustrude et al., 2013). Of these four HEK-Nav1.X cell lines, only Nav1.7 displayed reduced current density (44.9 ± 10.6% with CRMP2-K374A compared to cells expressing wildtype CRMP2) (Figure 3.7). No changes in channel kinetics were observed for any cell line between the wildtype and SUMO-null CRMP2 conditions (Table 3.2).

TTX-S currents in small DRGs consist of contributions from Nav1.1, Nav1.6, and Nav1.7, with Nav1.7 being the predominant subtype (Zhang et al., 2013). Separation of these TTX-S channels by conopeptides have demonstrated that Nav1.7 produces ~80% of the TTX-S current in the subset of small diameter DRGs (Zhang et al., 2013). To test if CRMP2 regulation is specific to Nav1.7 or if it also can regulate Nav1.1 and Nav1.6, a TTX-S pre-pulse inhibition protocol was repeated in DRGs following block of Nav1.7 with 5 nM ProTox-II. ProTox-II is 100X more selective for Nav1.7 versus other DRG expressed VGSC subtypes allowing for analysis of the cumulative contributions of Nav1.1 and Nav1.6 in the absence of Nav1.7 currents (Schmalhofer et al., 2008). These TTX-S/ProTox-II-R currents were unchanged by expression of CRMP2-K374A demonstrating that currents via Nav1.1 and Nav1.6 are not regulated by changes in putative CRMP2 SUMOylation, and that the observed reduction in total TTX-S current is solely due to Nav1.7 (Figure 3.8A, B).

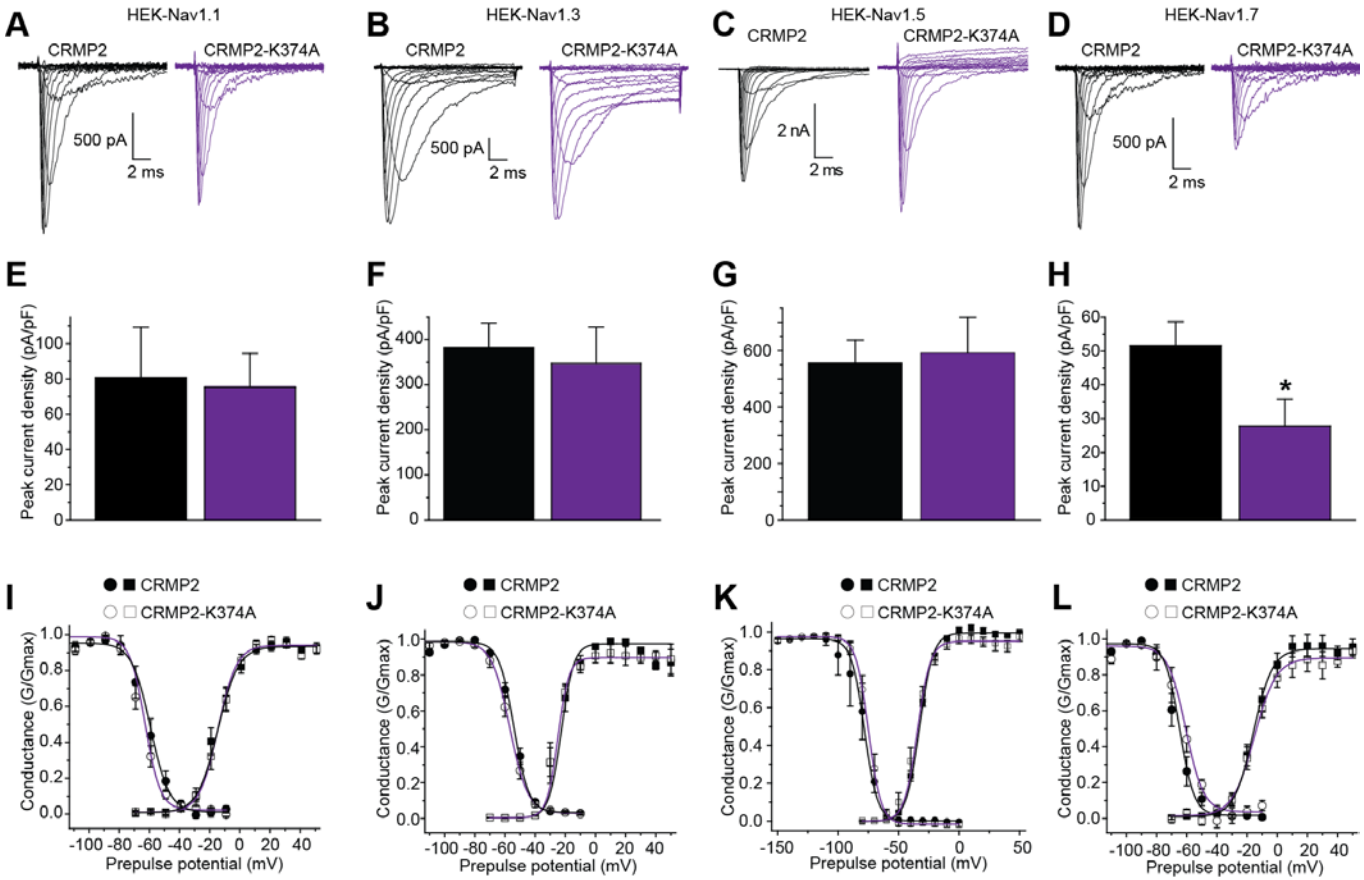

Figure 3.7. Nav1.7, but not Nav1.1, Nav1.3, and Nav1.5, current density is affected by expression of the CRMP2-K374A SUMO-null mutant. (A-D) Exemplar family of current traces from HEK293 cells stably expressing Nav1.1, Nav1.3, Nav1.5, or Nav1.7 transfected with either CRMP2 (*black*) or CRMP2-K374A (*purple*). **(E-H)** Averaged peak current densities (pA/pF). Only Nav1.7-expressing HEK293 cells exhibited a significant current reduction. **(I-L)** Representative Boltzmann fits for activation and steady-state inactivation for all cells transfected with the indicated constructs are shown. The calculated values for $V_{1/2}$ and k of activation and steady-state inactivation for all conditions tested and the associated statistics are presented in Table 3.2. Asterisk denotes statistical significance (n=6-8; Student's t-test, * $p < 0.05$).

Condition	Peak Current		Activation			Inactivation		
		n	$V_{1/2}$	k	n	$V_{1/2}$	k	n
Nav1.1								
CRMP2	100.0 ± 35.1	7	-15.5 ± 0.9	6.8 ± 0.4	7	-60.1 ± 1.9	6.2 ± 1.1	7
CRMP2-K374A	93.2 ± 23.8	7	-15.4 ± 1.8	6.2 ± 1.0	7	-63.7 ± 3.5	5.0 ± 2.1	7
Nav1.3								
CRMP2	100.0 ± 14.2	6	-22.6 ± 3.2	4.1 ± 0.8	6	-54.1 ± 1.8	5.0 ± 0.9	6
CRMP2-K374A	90.7 ± 21.1	6	-25.0 ± 0.6	3.7 ± 0.2	5	-56.9 ± 1.0	6.0 ± 0.6	5
Nav1.5								
CRMP2	100.0 ± 14.2	5	-32.5 ± 0.4	5.5 ± 0.2	5	-76.9 ± 1.6	4.4 ± 0.6	5
CRMP2-K374A	106.3 ± 22.5	6	-34.4 ± 0.6	5.1 ± 0.3	4	-75.1 ± 0.5	5.2 ± 0.3	6
Nav1.7								
CRMP2	100.0 ± 14.1	7	-15.9 ± 0.7	7.7 ± 0.9	7	-64.6 ± 3.5	5.9 ± 1.8	7
CRMP2-K374A	44.9 ± 10.6 *****	5	-15.2 ± 1.1	6.4 ± 0.3	5	-60.6 ± 2.7	4.8 ± 2.0	5

Table 3.2. Comparative current densities and Boltzmann parameters of voltage–dependence of channel activation and fast–inactivation for the respective transfection conditions in HEK293 cells expressing Nav1.1, Nav1.3, Nav1.5, or Nav1.7 channels. Values for $V_{1/2}$, the voltage of half–maximal activation and fast inactivation, and slope, were derived from Boltzmann distribution fits to the individual recordings and averaged to determine the mean and standard error of the mean (± S.E.M.). *n* values are indicated. All transfection conditions had SUMO1 and Ubc9 to boost endogenous SUMOylation. Asterisks represent statistically significant differences as compared to control (i.e. CRMP2 condition) within each tested group ($p<0.05$, ANOVA with Tukey's post–hoc test).

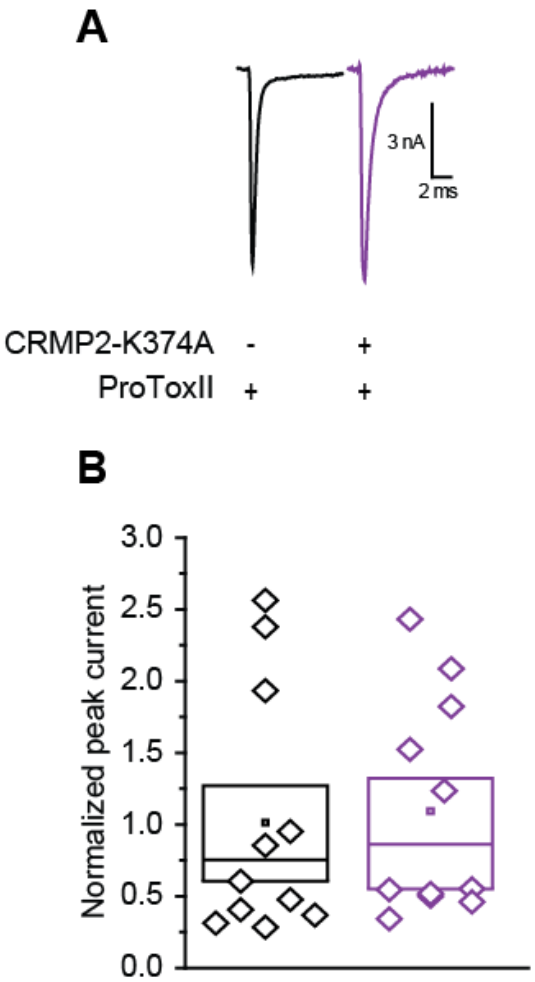

Figure 3.8. CRMP2 regulation of DRG TTX-S currents does not involve Nav1.1 or Nav1.6. (A) Representative peak TTX-S current traces at 0 mV from small DRGs expressing CRMP2 or CRMP2-K374A following 5 nM ProTox-II treatment. **(B)** Summary box plot showing peak sodium current in each condition. There was no difference in peak current density in DRG neurons expressing CRMP2-K374A compared to those expressing wild type CRMP2 ($p < 0.05$, Student's t-test). Boxes represent quartiles, each data point represents 1 cell. Error bars are behind data symbols in some cases. Normalized mean current densities were equivalent meaning remaining current carried by Nav1.1 and Nav1.6 is unaffected by loss of CRMP2 SUMOylation. 11 cells per condition, error is ± SEM. Asterisks denote statistical significance Student's t-test, * $p < 0.05$.

3.5. CRMP2 is SUMOylated and this modification controls its interaction with Nav1.7

To directly test if CRMP2 is endogenously SUMOylated, a protocol for detecting SUMOylated proteins was implemented (Becker et al., 2013). There is no antibody that selectively recognizes SUMOylated CRMP2. Moreover, SUMOylated species are lost upon cell lysis in nondenaturing buffers, owing to highly active SUMO isopeptidases. Therefore, in order to detect SUMOylated CRMP2 but not CRMP2 that may bind to SUMO, the following experiment was performed by Dr. Aubin Moutal, a post-doctoral fellow in the Khanna laboratory. First, CAD cell lysates were prepared in a denaturing lysis buffer containing 1% SDS and 10 mM *N*-ethylmaleimide, then heat denatured to completely unfold and disrupt protein complexes (i.e. non-covalent interactions) and to inactivate SUMO isopeptidases (Xiao et al., 2015), respectively, and then performed an immunoprecipitation (IP; Figure 3.9A) with a SUMO1 antibody followed by immunoblotting with a CRMP2 antibody to detect SUMOylated CRMP2. As shown in Figure 3.9A, SUMOylation of wildtype, but not K374A, CRMP2 was detected (Figure 3.8B; the ~100 kDa representing SUMOylated dsRed-CRMP2). The loss of SUMOylation translated into a reduction in the relative binding between Nav1.7 and CRMP2 (Figure 3.9D, E). CRMP2-Nav1.7 interaction is demonstrated by CRMP2 IP. Altering one protein partner and observing an altered interaction is further evidence that proteins are likely directly interacting as was observed for the CRMP2-Nav1.7 interaction when CRMP2 SUMOylation was prevented by expression of CRMP2-SUMO-null mutant. In addition, these proteins are both available in the same sub-cellular fractions meaning that experimental conditions of cell lysis does not mix separated compartments that individually contain Nav1.7 and CRMP2. Therefore, no artificial interaction is

created to cloud interpretation of the CRMP2 IP results. Lastly, functional data showing regulation of Nav1.7 by alterations of CRMP2 expression and post-translational modifications support my finding of CRMP2-Nav1.7 interaction in protein complex. Thus, these data establish that (*i*) endogenous CRMP2 is SUMOylated,(*ii*) CRMP2 interacts with Nav1.7, and (*iii*) SUMO-null CRMP2 has a reduced propensity for interaction with Nav1.7.

3.6. CRMP2 SUMOylation does not alter CRMP2-mediated enhancement of neurite outgrowth

The Khanna laboratory and others have previously shown that CRMP2 expression specifies axonal ramification and dendritic complexity of neurons (Inagaki et al., 2001a, Wilson et al., 2012). To test whether mutation of a putative SUMOylation motif affects this canonical function of CRMP2, we tested axonal outgrowth in DIV6 cortical neurons or DIV2 DRGs expressing EGFP, CRMP2-K374A or wild type CRMP2. EGFP co-expression was used to identify transfected cells for analyses. Cortical neurons were used due to their extensive past use in studies of CRMP2-mediated outgrowth and DRGs were used for their relevance to my thesis work investigating the role of CRMP2 in trafficking of Nav1.7. Moreover, testing the effect in cortical cells would rule out any cell-specific regulation by SUMO-null CRMP2. Compared to EGFP-expressing neurons, both wild type CRMP2 and CRMP2-K374A increased the number of processes per neuron, the number of branches per neuron, the mean and maximum process lengths, and overall total outgrowth (Figure 3.10A, B).

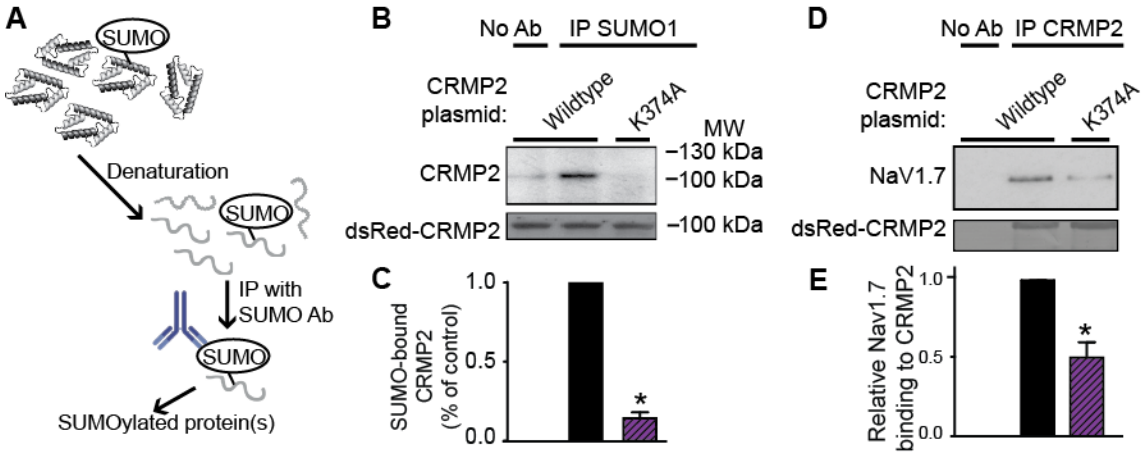

Figure 3.9. Blunted SUMOylation of K374A CRMP2 and binding of the mutant to NaV1.7. (**A**) Schematic of denaturing IP. (**B, C**) Loss of CRMP2 SUMOylation at K374 reduces SUMO-bound CRMP2 compared to control. (**D, E**) Loss of CRMP2 SUMOylation at K374 reduces CRMP2's interaction with Nav1.7. *, $p < 0.05$ vs. wildtype Student's t-test (n=3). Experiment performed by Dr. Aubin Moutal.

On average, the processes per neuron were increased by 21% and 29% for CRMP2 (n=538) and CRMP2-K374A (n=669), respectively, compared to EGFP expressing neurons (4.6 ± 0.1, n=682, $p<0.05$). Branches per neuron were increased by 134% and 90% for CRMP2 and CRMP2-K374A, respectively, compared to EGFP expressing neurons (25.7 ± 1.1, n=682, $p<0.05$). The mean and maximum process lengths per neuron were increased by 75% and 120% for CRMP2 and 18% and 76% for CRMP2-K374A, respectively, compared to EGFP expressing neurons (191.6 ± 7.9, n=682, $p<0.05$ and 613.1 ± 28.8, n=682, $p<0.05$). Finally, overall total outgrowth – a sum of all the above parameters – was 113% and 74% greater in CRMP2 (n=538)- and CRMP2-K374A (n=669)-, respectively, expressing neurons compared to EGFP expressing neurons (Figure 3.10B). Collectively, these results suggest that replacement of CRMP2's lysine (residue 374) or all three residues within the putative SUMO motif (data not shown) maintains CRMP2-mediated axonal specification and dendritic complexity implying that the mutant protein is functional. Similar results were observed in DRGs with total outgrowth being unaffected by the SUMO-null CRMP2 K374A mutant (Figure 3.10C, D). These data support the conclusion that CRMP2-mediated neurite outgrowth is not dependent on its SUMOylation or on the cell type.

3.7. CRMP2 SUMOylation does not alter the pharmacological action of *(R)*-LCM on VGSC slow inactivation

The FDA approved clinical drug Vimpat® (*(R)*-LCM) stabilizes Navs in a slow-inactivated state (Errington et al., 2006, Errington et al., 2008, Sheets et al., 2008).

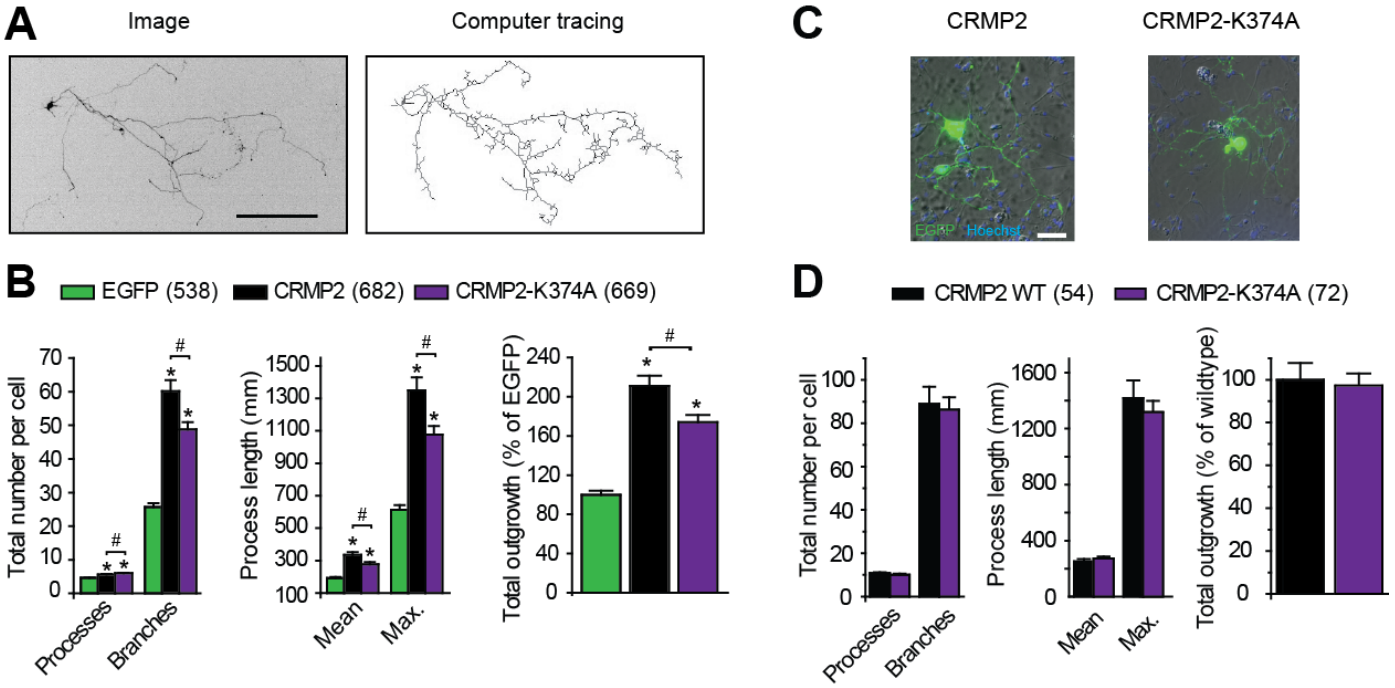

Figure 3.10. CRMP2 SUMOylation does not alter CRMP2-mediated outgrowth of cortical or DRG neurons. (A) Representative inverted black and white image (left) and computer tracing (right) of a cortical neuron at 4X magnification, scale bar is 200 μm. **(B)** Average number of processes, branches, mean and maximum length of processes, and summary outgrowth of cortical cells expressing EGFP, CRMP2, or CRMP2-K374A. **(C)** An example image showing the overlay of EGFP fluorescence (green), nuclear staining with Hoechst (blue) together with the brightfield Hoffman image of transfected DRG neurons. Scale bar equals 50 μm and applies to both panels. Note the similar degree of neurite complexity between the wild type and mutant CRMP2 conditions. * represents statistical significance versus EGFP (ANOVA), # represents statistical significance between CRMP2 plasmids (ANOVA) **(D)** Number of processes and branches, mean and maximum (max.) process length, and normalized total outgrowth for cells co-expressing EGFP and CRMP2 (n=54 from 4 wells), or co-expressing EGFP and CRMP2-K374A (n=72 from 4 wells). There were no statistical differences for any of the parameters between the two conditions ($p > 0.05$, Student's t-test). Experiment performed by Dr. Sarah Wilson, a former member of the Khanna laboratory.

The Khanna laboratory had previously shown that mutating a LCM-coordinating pocket within CRMP2 reduced LCM-dependent enhancement of slow inactivation (Wang et al., 2010a). How this CRMP2 mutation changes LCM's efficacy towards the sodium channel is unknown. Having established SUMOylation of CRMP2 as a novel post-translational modification affecting Nav1.7 channel trafficking and current density, here I tested whether SUMOylation of CRMP2 modifies LCM-induced enhancement of slow inactivation. Using the whole cell patch clamp configuration, I analyzed the effects of LCM on CAD cell VGSCs in the presence of overexpressed wildtype CRMP2 or SUMO-null CRMP2-K374A. The E2-conjugating enzyme Ubc9, which adds SUMOs 1–3 (Wilkinson et al., 2008), and SUMO2 were also expressed; SUMO2 was transfected as preliminary studies revealed no differences between any of the SUMOs on VGSC current densities. Transfected CAD cells were conditioned to potentials ranging from –110 mV to +20 mV (in +10 mV increments) for 5 s, and then fast-inactivated channels were allowed to recover for 150 ms at a hyperpolarized pulse to –120 mV, and the fraction of channels available was tested by a single depolarizing pulse, to 0 mV, for 15 ms (Figure 3.11).

Addition of 100 μM LCM to cells expressing wild type CRMP2 or CRMP2-K374A significantly decreased the fraction of current available compared to those in the absence of LCM. For comparison, representative current traces at –50 mV are highlighted (Figure 3.11B and C). At this potential, the channels are predominantly undergoing slow-inactivation, as it is near the action potential threshold (Wang et al., 2010a, Wang et al., 2011b).

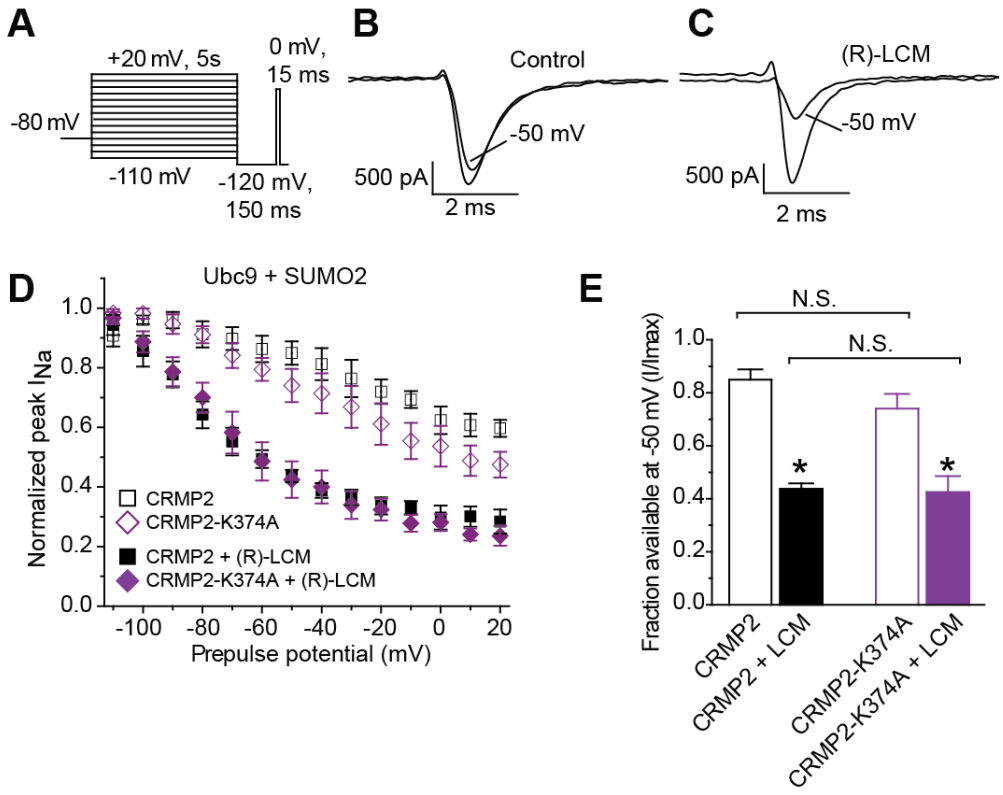

Figure 3.11. CRMP2 SUMOylation does not alter VGSC slow inactivation or response to *(R)*-LCM. (A) Voltage protocol for slow inactivation: currents were evoked by 5-s prepulses between −120 and +20 mV and then allowed to recover from fast inactivation for 150 ms at −120 mV. The fraction of available current was analyzed by a 15-ms test pulse to 0 mV. Cells were treated for 10 min with either 100 μM LCM or vehicle, 0.1% DMSO prior to whole cell patch clamp analysis. **(B)** Representative current traces from CAD cells expressing CRMP2 with Ubc9 and SUMO2 in the absence (*control*, 0.1% DMSO, *left*) or **(C)** presence of 100 μM LCM (*+LCM*, *right*). To highlight the extent of slow inactivation, the maximum elicited current (prepulse to −110 mV) is compared with the trace elicited by a prepulse to −50 mV **(D)** Summary of steady-state slow inactivation curves for CAD cells expressing both Ubc9 and SUMO2 and either CRMP2 (*squares*) or CRMP2-K374A (*diamonds*) in the absence (*open symbols*) or presence (*closed symbols*) of 100 μM LCM. Some error bars are smaller than symbols. All data are represented as means ± SEM. **(e)** Summary of the fraction of available current at −50 mV for the same conditions presented in **B**. Asterisks indicate statistically significant differences in fraction between LCM-treated and untreated CAD cells expressing the indicated constructs ($p < 0.05$, one-way ANOVA with Tukey's post-hoc test) n=5-6 cells per condition.

The slow inactivation versus voltage curves for the transfected cells in the absence and presence of 100 μM LCM are plotted in Figure 3.11D and illustrate a marked reduction in current available (i.e. an enhancement in slow inactivation) in the presence of drug that was not different between the conditions tested ($p>0.05$; ANOVA with Tukey's post-hoc test). At -50 mV, ~48% (n=8) (calculated as 1 minus the normalized I_{Na}) of the Na^+ current was available in LCM-treated CRMP2-expressing cells compared to 43% in CRMP2-K374A-expressing cells (Figure 3.11E; $p>0.05$; ANOVA with Tukey's post-hoc test). These results demonstrate that disruption of the SUMOylation site in CRMP2 does not affect the pharmacological action of LCM-induced enhancement of sodium channel slow inactivation.

3.8. Discussion

Accumulating evidence indicates that the CRMP2 functional proteome is far greater than previously appreciated (Khanna et al., 2012). It is also becoming evident that post-translational modifications, in particular phosphorylation, can influence CRMP2's interactions and in doing so recruit its involvement in different signaling pathways (Ju et al., 2013). In this chapter, I describe a novel modification for CRMP2, SUMOylation, which can alter the trafficking of Nav1.7 (Figure 3.5). The functional regulation of CRMP2 by SUMOylation was studied by *(i)* creating constructs in which the consensus lysine in the SUMOylation motif was mutated to alanine, and *(ii)* by manipulating expression of the SUMOylation machinery with (*a)* overexpression of Ubc9 and SUMOs to boost SUMOylation and (*b*) overexpression of SENP1 and SENP2 to decrease SUMOylation.

Although putative SUMO motifs are typically investigated by mutating the target lysine to arginine (Duprez et al., 1999, Sampson et al., 2001, Perdomo et al., 2005, Feliciangeli et al., 2007, Zhu et al., 2008, Merrill et al., 2010), this is not always the case. For instance, mutation of the SUMO target lysine in the potassium leak channel K2P1 to an arginine had no effect on channel activity, whereas an alanine mutation increased activity consistent with an increase observed in the presence of SENP1 (Rajan et al., 2005). For this reason as well as the fact that alanine residues have been the preferred choice in demonstrating SUMOylation of several proteins including Ran GTPase activating protein 1 (Sampson et al., 2001), acute promyelocytic leukaemia protein (Duprez et al., 1999), the polycomb protein Pc2/Cbx4 (Merrill et al., 2010), and basic Kruppel-like factor/Kruppel-like factor 3 (BKLF) – a zinc finger transcription factor (Perdomo et al., 2005), I chose to mutate the CRMP2 SUMO target lysine residues to alanine to study CRMP2 SUMOylation in this thesis.

While interrogating the potential effects of CRMP2 SUMO mutants on VGSCs, I noticed a clear reduction in macroscopic sodium currents in CAD cells expressing CRMP2-K374A, but not CRMP2-K20A, or CRMP2K390A (Figure 3.3). CAD cells express mRNAs for Nav1.7 (>90% of total Nav mRNA), Nav1.1 and Nav1.3 (Wang et al., 2011b), and treatment with 125 nM huwentoxin-IV confirmed that ~80% of the CAD cell sodium current was carried via Nav1.7. This current was dramatically reduced by expression of CRMP2 SUMO-null mutant in CAD cells as well as expression of deSUMOylating enzymes, SUMO/sentrin-specific peptidases (SENP) 1 or SENP2, suggesting a contribution for SUMOylation of CRMP2 in trafficking of Nav1.7 (Table 3.1). Cell surface biotinylation under the same conditions revealed reduced Nav1.7

surface expression, corroborating the reduction in current density (Figure 3.5), and suggesting that CRMP2 SUMOylation reduces current density likely via reduced trafficking similar to what has been reported for the kainate receptor subunit GluR6 wherein SUMOylation facilitates endocytosis of this receptor (Martin et al., 2007b). Therefore, by genetic or enzymatic manipulation, the removal of CRMP2 SUMOylation leads to reduced Nav1.7 current (Table 3.1). Co-expression of deSUMOylating enzymes SENP1 or SENP2 did not further reduce Nav1.7 current densities in CAD cells expressing CRMP2 SUMO mutants, suggesting that the mutants may serve in a dominant negative manner for Nav1.7 trafficking. Biochemical studies supported the above findings by demonstrating a previously unreported interaction between CRMP2 and Nav1.7 (Figure 3.9D and E) and this novel binding is blunted by prevention of CRMP2 SUMOylation at lysine-374 (Figure 3.9B and C).

The Nav1.7 isoform is preferentially expressed in the peripheral nervous system within ganglia related to nociceptive pain, including dorsal root ganglia, trigeminal ganglia and sympathetic ganglia. In nociceptive neurons responsible for the transduction of pain signals, the channel modulates current threshold required to fire action potentials in response to stimuli (Momin and Wood, 2008, Estacion et al., 2011). Gain-of-function mutations, i.e. those that lower Nav1.7 current threshold for initiation of action potentials, produce allodynia – a lowered stimulus threshold for pain. Such mutations are the cause of pain syndromes including erythromelalgia, paroxysmal extreme pain disorder, and small fiber neuropathy (Estacion et al., 2011). A loss-of-function mutation of Nav1.7 can cause equally detrimental modifications in pain sensation, where stimuli never reach

threshold to propagate pain. Patients with such mutations display a complete loss of pain sensation (Cox et al., 2006).

Of the tetrodotoxin-sensitive voltage-gated sodium channels present in the nervous system, only Nav1.7 lacks a putative SUMOylation motif (Benson et al., 2009). Thus any modification of the channel by SUMOylation may be due to indirect modification of accessory proteins, such as CRMP2 demonstrated in this study. Importantly, only 60% of SUMOylated proteins conform to the SUMOylation consensus sequence meaning that we cannot rule out the possibility of Nav1.7 SUMOylation by sequence analysis alone (Ulrich, 2009). However, by modification of only CRMP2 expression or SUMOylation, this channel is affected in the absence of regulating total cellular SUMOylation. This demonstrates that changes to Nav1.7 current density in my data are due solely to modifications of CRMP2. Mechanisms that specifically or preferentially regulate Nav1.7 are of particular relevance due to the role of Nav1.7 in transduction of peripheral pain. Separation of TTX-S and TTX-R currents in small DRGs revealed that reduction of TTX-S current density, but not TTX-R current density was mediated by expression of CRMP2-K374A or deSUMOylating SENP proteins (Figure 3.6). I therefore conclude that TTX-R channel total current density is not subject to regulation by CRMP2. To test if CRMP2 regulation is specific to Nav1.7 or if it also includes other DRG expressed TTX-S isoforms Nav1.1 and Nav1.6, TTX-S currents were isolated following incubation with 5 nM ProTox-II, a Nav1.7-selective toxin with 100X greater specificity for Nav1.7 than Nav1.1 or Nav1.6 (Schmalhofer et al., 2008) The cumulative contributions by Nav1.1 and Nav1.6 currents were unchanged by expression of CRMP2-K374A demonstrating that currents via Nav1.1 and Nav1.6 are not

regulated by changes in CRMP2 SUMOylation, and that the observed reduction in total TTX-S current is entirely due to Nav1.7 (Figure 3.8A, B).

While Nav1.7 is the predominant voltage-gated sodium channel isoform found in CAD cells, mRNA expression data suggest a secondary contribution by the Nav1.1 isoform (Wang et al., 2011b). Remarkably, in stark contrast to Nav1.7, HEK293 expressed Nav1.1 current density is not affected by expression of CRMP2-K374A, reinforcing that CRMP2 SUMOylation-dependent modulation of sodium current density may be specific to particular sodium channel isoforms (Figure 3.7, Table 3.2). Additional experiments also revealed that Nav1.3 and Nav1.5 currents measured in HEK293 cells display lack of regulation by CRMP2 SUMOylation (Figure 3.7, Table 3.2). Based on this data from HEK293 cells and also data from DRGs, I conclude that CRMP2 SUMOylation preferentially regulates Nav1.7 VGSC subtype trafficking.

In a study of CRMP2 functions not related to Nav1.7 current density, I analyzed both CRMP2-mediated regulation of neurite outgrowth, as well as CRMP2-mediated enhancement of sodium channel slow inactivated state for effects of CRMP2 SUMOylation. Regulation of axonal specification and dendrite complexity is the canonical function of CRMP2 (Arimura et al., 2000a, Inagaki et al., 2001a). In analysis of cortical neuron outgrowth, CRMP2-K374A mutant produced functional proteins as assessed by propensities to increase outgrowth relative to EGFP-transfected neurons.

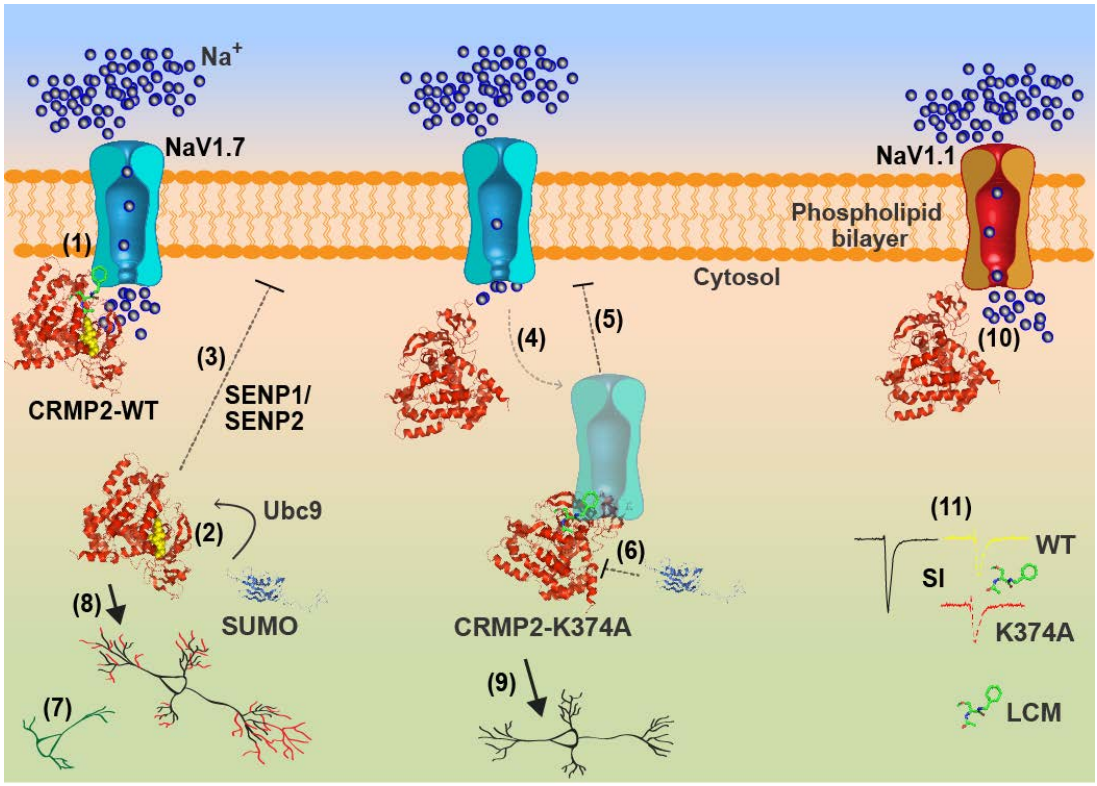

Figure 3.12. Model of CRMP2 SUMOylation and Nav1.7 trafficking. (1) Nav1.7 current density is not affected by co-expression of wild type CRMP2 (PDB code: 2GSE (Deo et al., 2004)), with an intact SUMOylation motif (illustrated in yellow spheres). **(2)** SUMO-1 (PDB code: 1A5R (Bayer et al., 1998), *dark blue*) can be added by the E2-conjugating enzyme Ubc9 to CRMP2 at lysine K374. **(3)** Removal of SUMO by sentrin/SUMO-specific protease (SENP) 1 or SENP2 reduces Nav1.7 current density via a reduction in surface expression. **(4)** Nav1.7 current density is significantly reduced by co-expression of CRMP2-K374A (CRMP2 structure in red without yellow spheres). **(5)** Surface expression of Nav1.7 is reduced in CAD cells expressing CRMP2-K374A mutant. **(6)** Mutant CRMP2 without an intact SUMO motif cannot be SUMOylated. **(7)** When compared to EGFP-transfected neurons, **(8-9)**, neurite outgrowth facilitated by CRMP2 is not affected by disruption of SUMOylation motif. **(10)** Nav1.1 currents, which represent the second largest fraction of sodium currents in CAD cells, are not affected by co-expression of CRMP2-K374A mutant, suggesting selectivity in the mechanism by which SUMO regulates Navs. **(11)** Sodium channel slow inactivation, which is enhanced by the anti-epileptic drug Lacosamide (LCM; green stick model) is not affected by expression of either CRMP2 SUMOylation incompetent mutants. Exemplar traces at -50 mV are shown to illustrate extent of slow inactivation.

That augmented neurite outgrowth was recapitulated to near wild type CRMP2 levels suggested that the mutant CRMP2 proteins are neither misfolded nor unable to oligomerize despite the placement of the SUMO target lysine 374 within the oligomerization domain (amino acids 8-134 and 281-435) of CRMPs (Wang and Strittmatter, 1997c). A regulation of VGSC slow inactivation by CRMP2 was observed when treating CAD cells with the antiepileptic, VGSC blocking, VGSC slow inactivation enhancing drug *(R)*-lacosamide (LCM). LCM has primary action on sodium channels but also binds to CRMP2 (Wilson and Khanna, 2014, Wilson et al., 2014, Moutal et al., 2015). Blocking LCM binding to CRMP2 blunts VGSC slow inactivation by ~80% so I tested whether this function of CRMP2-LCM binding was affected by SUMOylation by probing VGSC slow inactivation (Wang et al., 2010a). Cells expressing CRMP2 and CRMP2-K374A mutant displayed equivalent VGSC slow inactivation in both the absence and presence of LCM (Figure 3.11C). Therefore I concluded that CRMP2 SUMOylation therefore has no effect on VGSC slow inactivation. In other experiments the kinetic properties of fast inactivation and activation were probed, for which CRMP2-K374A also had no effect (Table 3.1). This is in contrast to the fine-tuning of channel function reported for potassium channels Kv1.5 (Benson et al., 2007) and Kv2.1 (Plant et al., 2011): loss of Kv1.5 SUMOylation, by either disruption of the conjugation sites or expression of the SUMO protease SENP2, lead to a selective ~15 mV hyperpolarizing shift in the voltage-dependence of steady-state inactivation (Benson et al., 2007) while SUMOylation of Kv2.1 in hippocampal neurons was shown to regulate firing by shifting the half-maximal activation voltage of channels up to 35 mV (Plant et al., 2011).

The trafficking of VGSCs has not been extensively investigated. Two examples of proteins that alter Nav1.X trafficking are Alzheimer's disease-related secretases beta-site amyloid precursor protein cleaving enzyme 1 BACE1 and presenilin (PS)/γ-secretase which are involved in trafficking on Nav1s via cleavage of auxiliary subunits from the channel complex (Kim et al., 2005, Kim et al., 2007). Other studies have shown that Nav1.1 mutants in familial epilepsy are trafficking defective and their function can be restored by incubation at low temperatures (<30°C), as well as through interactions with modulatory proteins or drugs (Rusconi et al., 2007). There is at least one report linking microtubule dynamics in the trafficking of cardiac Nav1.5 (Casini et al., 2010). For trafficking mechanisms that are specific to Nav1.7 subtype, very little is currently known.

In neurons, Nav1.7 undergoes trafficking guidance by sodium channel beta 2 (β2) subunits, which promote surface expression of Nav1.7 via interactions with cell adhesion molecules and the cytoskeletal protein ankyrin (Malhotra et al., 2000, Lopez-Santiago et al., 2006). The β2 subunit expression is upregulated in sensory neurons in models of neuropathic pain and hypothesized to contribute to pain behavior by enhancing DRG excitability (Pertin et al., 2005). Increased surface expression of Nav1.7 can also be introduced by enhanced channel transcription that has been associated with pain resulting from diabetic neuropathy (Hong et al., 2004), and inflammation (Black et al., 2004). Endocytosis of Nav1.7 also mediates channel surface expression. This regulatory mechanism involves monoubiquitination of the channel by E3 ubiqutin ligase Nedd4-2 to target the channel for endocytosis. This process of Nedd4-2 activity and Nav1.7 endocytosis is interrupted following spared nerve injury model to produce Nav1.7-driven

pain states that result from dysregulated channel surface trafficking (Laedermann et al., 2013a).

The results from this chapter of my thesis advance the field of Nav1.7 trafficking by describing a novel regulatory pathway for Nav1.7 via post-translational modification (SUMOylation) of a cytosolic interacting protein (CRMP2). CRMP2 SUMOylation at lysine-374 was demonstrated by a denaturing SUMO1 immunopreciptation that detected endogenously SUMOylated CRMP2 in CAD cells (Figure 3.9A and B). Cell surface biotinylation data from CAD cells (Figure 3.5) as well as Nav1.7 currents from CAD cells (Figure 3.3) and DRGs (Figure 3.6) revealed a decrease in Nav1.7 function when CRMP2 is unSUMOylated. These relationships between CRMP2 and Nav1.7 along with other results from Chapter 3 are summarized in Figure 3.12. Remarkably, data separating current contributions in DRG neurons as well as from HEK293 cells expressing single VGSC subtypes demonstrated that VGSC modification by CRMP2 is likely *limited* to Nav1.7. This specificity in control of Nav1.7 is an exciting finding that should spur future studies targeting this novel pair of proteins. Given the unequivocal link between pain and Nav1.7, these channels have emerged as an attractive target for drug discovery and this chapter elucidates a novel pathway by which these channels can possibly be regulated.

CHAPTER 4.

INTERPLAY BETWEEN CDK5/FYN PHOSPHORYLATION AND SUMOYLATION OF CRMP2 DETERMINES NaV1.7 CHANNEL TRAFFICKING VIA A NUMB/EPS15 ENDOCYTIC PATHWAY

4.1. Introduction

Although the mechanisms that modulate SUMOylation remain largely unknown, protein phosphorylation has been reported to either enhance or inhibit SUMOylation, depending on the substrate protein. For example, for the kainate receptor (KAR) subunit GluK2, protein kinase C–mediated phosphorylation of GluK2 at serine 868 promotes GluK2 SUMOylation at lysine 886 and both of these events are necessary for the internalization of GluK2-containing KARs that occurs during long-term depression of KAR-mediated synaptic transmission at rat hippocampal mossy fiber synapses (Konopacki et al., 2011). It is now apparent that for many SUMOylated proteins, there is a dynamic crosstalk between protein SUMOylation and phosphorylation (see a limited set of examples in Table 1.3). Either of these modifications can enhance or prevent the other in a substrate-specific manner (reviewed in (Henley et al., 2014)).

Many functions of CRMP2 are subject to modification following phosphorylation of the protein (Khanna et al., 2012); but whether Nav1.7 trafficking and activity are controlled by phosphorylation are unknown and are primary questions of this chapter. In addition, if CRMP2 phosphorylation is determined to be important for Nav1.7 activity, then a secondary question of this Chapter is to determine the nature of the interplay between the modifications in possible control of Nav1.7 activity. Put another way, which modification is dominant over the other? The activity-regulated cytoskeleton-associated (Arc) protein is an example of a SUMOylated protein that can regulate trafficking of a membrane protein, the AMPA receptor, by altering interaction of the receptor with endocytic machinery (Chowdhury et al., 2006, Craig and Henley, 2012, Craig et al., 2012). CRMP2 may resemble the Arc protein as my data so far demonstrates that the

SUMOylation status of CRMP2 allows it to control trafficking of Nav1.7, perhaps via recruitment of proteins that aid in internalization of the channel. Therefore, the relationship between CRMP2 SUMOylation and phosphorylation as well as the relationship between CRMP2 SUMOylation and endocytic machinery will be additional questions addressed in this Chapter.

As stated earlier in the Introductory Chapter of this thesis, CRMP2 is extensively C-terminally phosphorylated at five residues (threonine-509, threonine-514, serine-518, serine-522, and threonine-555) by four different kinases (GSK3β, Cdk5, RhoK, CaMKII). In addition, CRMP2 is also phosphorylated at least two other upstream phosphorylation sites (Y32 by Fyn, Y479 by Yes). The previous Chapter identified CRMP2 as a novel SUMO substrate, however, how CRMP2 SUMOylation is regulated is incompletely understood. One possibility is that CRMP2 phosphorylation affects CRMP2 SUMOylation. To ascertain whether CRMP2 phosphorylation and CRMP2 SUMOylation are interdependent, dsRed-CRMP2 constructs were created wherein phosphorylation and SUMOylation resides were selectively mutated and the effects of these constructs on sodium channels were investigated. Both single phospho-null mutants as well as double phospho-null/SUMO-null mutants were produced to eliminate targeting by each kinase (Figure 4.1A). Additional studies, in some cases, also involved use of overexpression of the kinases themselves or of phospho-mimetic CRMP2 mutations – both manipulations designed to act as a gain of phosphorylation.

Previous reports describe CRMP2 as a trafficking protein that may provide insights as to how CRMP2 regulates Nav1.7. CRMP2 has been reported to function as a membrane trafficking protein for the adhesion molecule L1-CAM (L1-cell adhesion

molecule) in a process that also requires CRMP2 to interact with the endocytic adaptor protein Numb (Nishimura et al., 2003a). Numb protein scaffolds further interactions with endocytic machinery including proteins involved in clathrin-mediated endocytosis (Santolini et al., 2000). Numb's interaction(s) with E3 ubiqutin ligases allow the ligase to monoubiqutinate proteins, which can then become endocytosed. This process involves epidermal growth factor receptor substrate 15 endocytic adapter protein (Eps15) protein binding the monoubiquitylated membrane cargo to induce membrane curvature in the initiating steps of clathrin-mediated endocytosis (Santolini et al., 2000, Woelk et al., 2006, Horvath et al., 2007). A recent study reported that removal of Nav1.7 channel protein from the cell membrane was under control of monoubiqutination of the channel by the E3 ubqiutin ligase Nedd4-2 (Laedermann et al., 2013a). However, other than this publication and one from 2004 on Nav1.7 regulation by Nedd4-2 in oocytes (Fotia et al., 2004), nothing else linking Nav1.7 to the endocytic pathway or CRMP2 has been reported.

4.2. CRMP2 SUMOylation does not alter CRMP2 phosphorylation or total Nav1.7 expression

SUMO1 immunoprecipitation (Figure 3.9) revealed endogenous SUMOylation of CRMP2 at lysine-374. To determine if loss of CRMP2 SUMOylation affected CRMP2 phosphorylation, lysates from CAD cells expressing wildtype CRMP2 and SUMO-null CRMP2-K374A were probed with phospho-specific CRMP2 antibodies and quantified (Figure 4.1 B-D). For all commercially available phospho-specific CRMP2 antibodies – Fyn (pY32), Yes (pY479), GSK3β (pT509/T514), or Cdk5 (pS522) – no changes in

CRMP2 phosphorylation were observed when SUMOylation was blunted (Figure 4.1D). From this data, I conclude that CRMP2 SUMOylation does not regulate CRMP2 phosphorylation. Consistent with previous biotinylation experiments presented in this thesis, total Nav1.7 protein expression was unchanged by loss of lysine-374 SUMOylation. Taken together, these data demonstrate that deSUMOylated CRMP2-dependent loss of Nav1.7 surface expression does not involve reduced translation of the channel (Figure 4.1C).

4.3. CRMP2 phosphorylation mediates effects on Nav1.7

CRMP2 is extensively post-translationally modified by phosphorylation by Fyn, Yes, GSK3β, Cdk5, and RhoK kinases (Figure 4.2A). To test the possibility that CRMP2 phosphorylation, in addition to SUMOylation, may regulate Nav1.7, I asked if loss of phosphorylation alone or in combination with SUMOylation could affect Nav1.7 currents. CAD cells were transfected with CRMP2 phospho-null mutants (i.e. Y32F, Y479F, S509A/514A, S522A, and S555A), CRMP2-K374 SUMO-null mutant, or mutants that combined both phospho- and SUMO-null mutants. Compared to CAD cells expressing wildtype CRMP2, Nav1.7 current density was reduced by ~60% in CAD cells expressing CRMP2-K374A alone or in phospho-mutants also harboring the SUMO-null mutation (Figure 4.2B; hatched bars) with two notable exceptions. First, Nav1.7 currents in CAD cells expressing Y32F (i.e. the Fyn phospho-mutant) alone or in combination with the SUMO-null mutant (Y32F/K374A) were no different from CAD cells expressing wildtype CRMP2 (Figure 4.2B, blue bars).

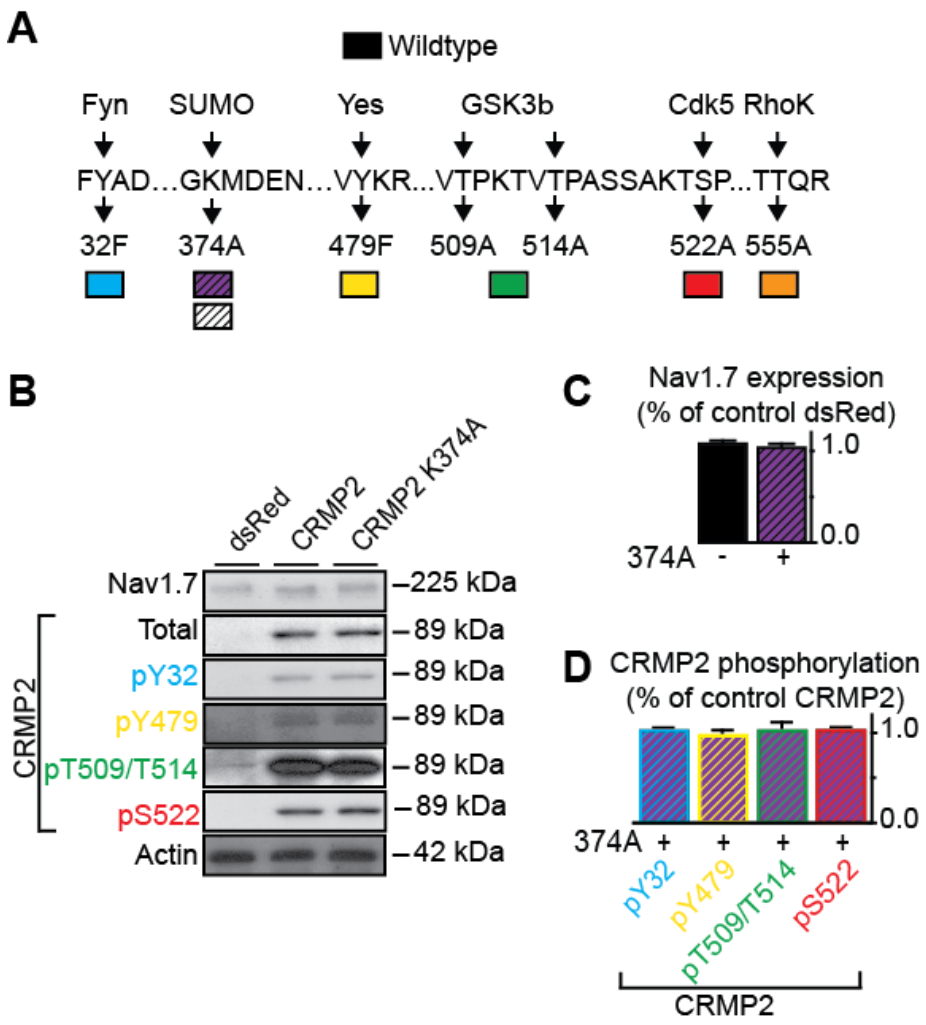

Figure 4.1. CRMP2 SUMOylation does not affect CRMP2 phosphorylation (A) CRMP2 (*Mus musculus*, GenBankTM accession number NM_009955.3) sequence indicating sites of SUMOylation and phosphorylation (kinases identified above the specific residues). The residues were mutated to alanine or phenylalanine to create CRMP2 SUMO-null and CRMP2-phospho null mutants. **(B)** Western blot of lysates from CAD cells expressing dsRed, dsRed-CRMP2 or dsRed-CRMP2-K374A probed for antibodies against Nav1.7, CRMP2, and phospho-specific CRMP2 phosphorylation. **(C)** CRMP2 SUMOylation does not affect total Nav1.7 expression. **(D)** CRMP2 SUMOylation does not affect CRMP2 phosphorylation states. Data is presented as mean ± SEM. Experiment performed by Dr. Aubin Moutal.

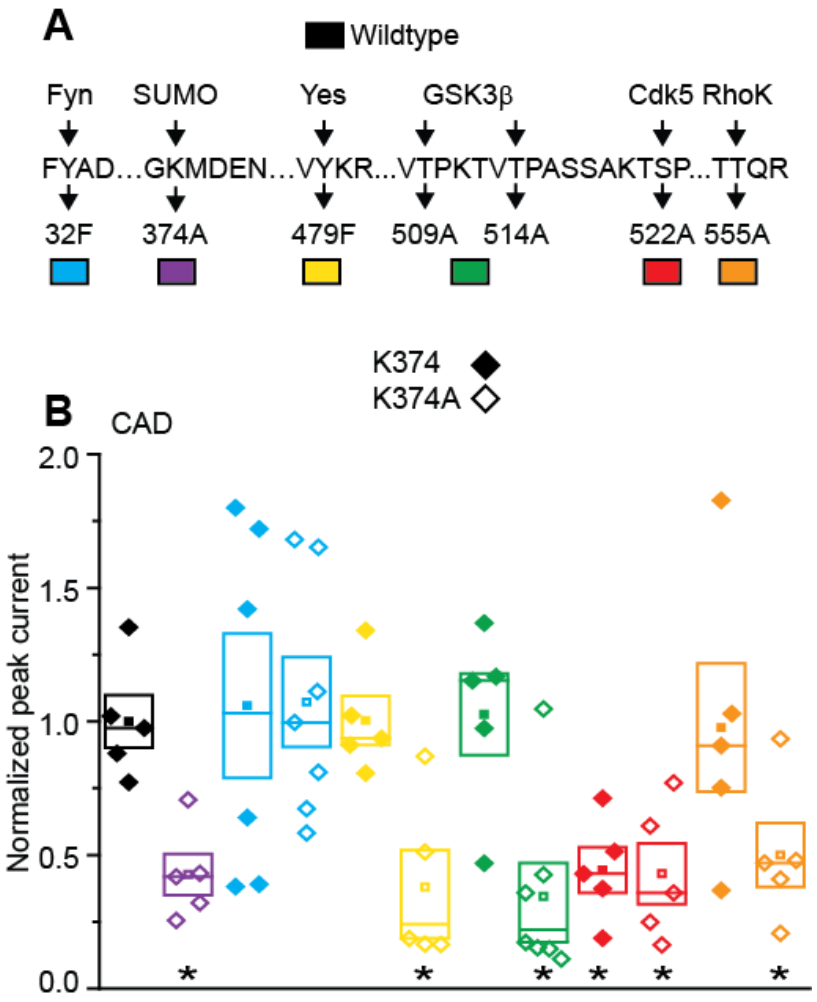

Figure 4.2. CRMP2 modifications regulate Nav1.7 currents. **(A)** CRMP2 sequence and residues mutated for these studies. **(B)** Peak current density (pA/pF) measured at 0 mV for CAD cells transfected with the various constructs as indicated by color code in **A**. Closed symbols contain indicate a lysine at residue 374 and open symbols indicate SUMO-null substitution of lysine 374 for alanine. Data are normalized to the wild type CRMP2 condition. Box plot borders represent SEM and median, square indicates mean, diamonds are individual data points. Asterisks indicate statistically significant differences compared to wildtype CRMP2 expressing control cells ($p < 0.05$, one-way ANOVA with Tukey's post-hoc test; n=5–9).

Second, Nav1.7 currents in CAD cells expressing S522A (i.e. the Cdk5 phospho-mutant) alone, without the additional presence of the SUMO-null mutant (K374A/S522A), were reduced by ~53% compared to those in CAD cells expressing wildtype CRMP2 (Figure 4.2B, red bar). All other single phospho-null mutants had no effect on Nav1.7 current density. These data demonstrate that both Fyn- and Cdk5-mediated phosphorylation of CRMP2 are therefore involved in regulating Nav1.7. As Cdk5 is considered to be a 'priming kinase' (Cole et al., 2006) for CRMP2, I next asked if the loss of Cdk5-mediated phosphorylation of CRMP2 could also affect currents in a native system like DRGs.

Following transfection of CRMP2 mutants, sodium currents were recorded from DRGs and first separated by tetrodotoxin sensitivity into TTX-S Nav1.1, Nav1.6, and Nav1.7 and TTX-R Nav1.8 and Nav1.9 contributions. Both CRMP2-S522A and CRMP2-K374A/S522A mutants reduced TTX-S Na^+ currents in DRGs by ~46% and ~50%, respectively, compared to currents from DRGs transfected with wildtype CRMP2 (Figure 4.3A and B). In contrast, TTX-R currents were not affected by expression of either mutant (Figure 4.3C and D). To further determine the identity of the TTX-S current, I performed additional experiments using the H-infinity protocol in the presence of 5 nM ProTox-II to block Nav1.7 currents and analyze contributions of the remaining Nav1.1 and Nav1.6 currents (Figure 4.3E and F). These experiments demonstrated no differences in TTX-S/ProTox-II-R currents compared to similarly-treated DRGs expressing wildtype CRMP2, demonstrating that loss of CRMP2 phosphorylation at serine-522 results in CRMP2 regulation of *only* the Nav1.7 VGSC isoform in DRGs. Consistent with the specificity of the regulation, the Nav1.7-specific modulation by CRMP2-S522A was

recapitulated in HEK293 cells expressing Nav1.1, Nav1.3, Nav1.5, or Nav1.7 wherein it was observed that co-expression of CRMP2-S522A caused an ~64% reduction in currents *only* in the Nav1.7 cell line (Figure 4.3G).

Since both the CRMP2-K374A and CRMP2-S522A mutants impaired Nav1.7 currents, I next tested whether the biochemical mechanism of regulation of Nav1.7 was similar between these SUMO- and phospho-null CRMP2 states. A denaturing SUMO1 IP was performed from lysates expressing wildtype CRMP2, CRMP2-K374A and CRMP2-S522A, or CRMP2-K374A/S522A. In SUMO- and phospho-null only or combination-null CRMP2 states, the amount of SUMOylated CRMP2 was reduced compared to wildtype CRMP2 (Figure 4.4A, B). Therefore, from these data I can conclude that (*i*) Cdk5-mediated phosphorylation is important for maintaining Nav1.7 current density, and (*ii*) Cdk5 phosphorylation regulates CRMP2 SUMOylation.

To determine if the changes in current density observed in the above experiments translated to changes in surface Nav1.7, a series of biotinylation experiments were performed on wildtype and all phospho-, SUMO- and combination-null CRMP2 mutants. Representative immunoblots of one such experiment is illustrated in Figure 4.5A demonstrating surface (i.e. streptavidin-enriched) and total Nav1.7 as well as dsRed-CRMP2. Immunoblotting for Nav1.7 in streptavidin-enriched complexes from biotinylated CAD cells showed reduced Nav1.7 surface expression in CAD cells expressing CRMP2-K374A (53.8 ± 1.6% of wildtype CRMP2 levels; purple hatched bar) or CRMP2-S522A (19.0 ± 4.8% of wildtype CRMP2 levels; red bars) when normalized to total Nav1.7 expression (Figure 4.5B).

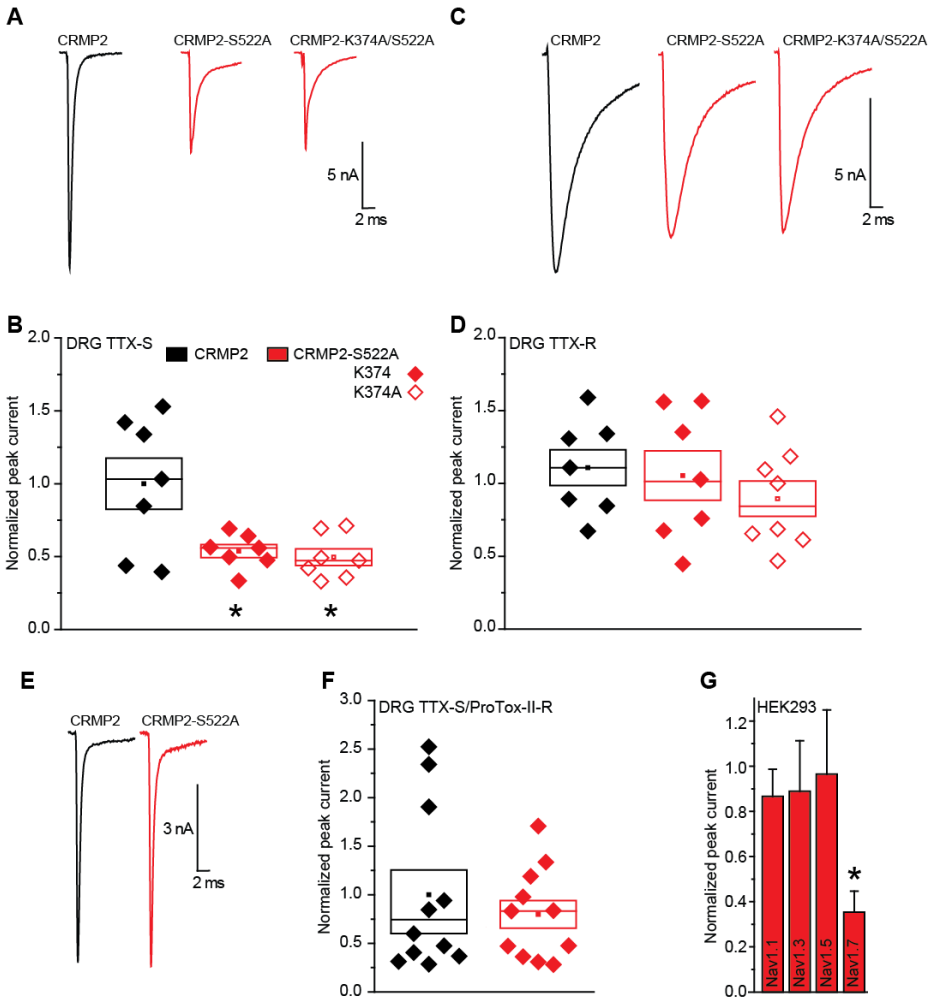

Figure 4.3. CRMP2-S522A, the Cdk5 site mutant, expression causes a selective reduction in Nav1.7 currents. (A) Representative TTX-S current traces from DRGs. **(B)** Box plot of peak TTX-S current density. CRMP2-S522A and CRMP2-K374A/S522A expression reduced TTX-S currents. Box plot borders represent SEM and median, square indicates mean, diamonds are individual data points. Filled symbols indicate presence of lysine (K) 374 in CRMP2 construct, whereas open symbols indicate SUMO-null mutation CRMP2-K374A. Key is shown as inset in **B**. **(C)** Representative TTX-R current traces from DRGs. **(D)** Box plot of peak TTX-R current density. Neither CRMP2 mutant affects TTX-R currents, eliminating possibility of contribution to effect by Nav1.8 and Nav1.9. **(E)** Representative TTX-S/ProTox-II-R current traces from DRGs. **(F)** Box plot of TTX-S/ProTox-II-R current density. CRMP2-S522A does not affect these currents eliminating possibility of contribution to effect by Nav1.1 or Nav1.6. **(G)** Bar graph of normalized current densities from HEK293 cells expressing Nav1.1, Nav1.3, Nav1.5, or Nav1.7 along with CRMP2-S522A. CRMP2-S522A expression decreased only Nav1.7 currents when compared to those expressing wildtype CRMP2. All DRG and HEK293 cell current densities were normalized to cells expressing wildtype CRMP2. Asterisks indicate statistically significant differences compared to wildtype CRMP2 expressing control cells ($p < 0.05$, one-way ANOVA with Tukey's post-hoc test; n=6–11).

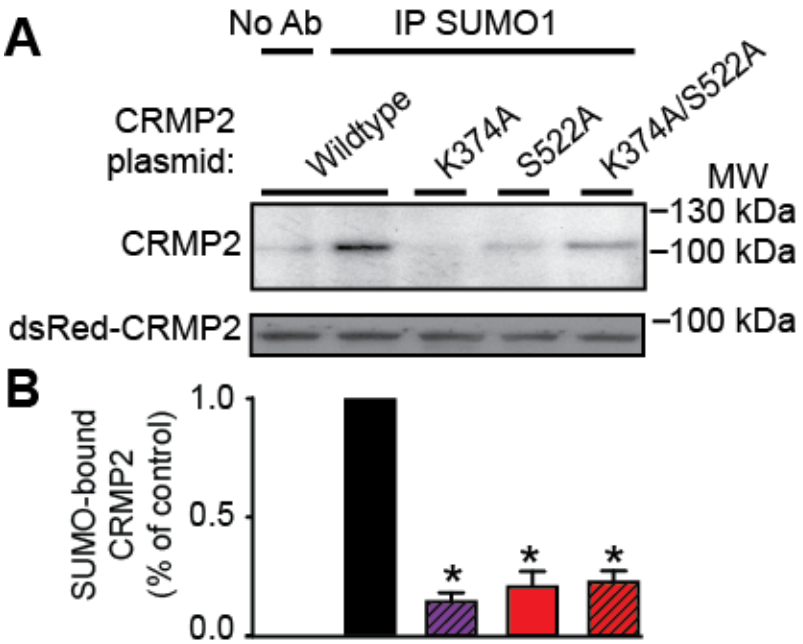

Figure 4.4. CRMP2-S522A, the Cdk5 site mutant, expression causes loss of CRMP2 SUMOylation. (A) Lysates of CAD cells expressing the indicated constructs, following denaturation and immunoprecipitation with a SUMO1 antibody probed with CRMP2 (*top*) or dsRed-CRMP2 (*bottom*). **(B)** Loss of Cdk5-mediated CRMP2 phosphorylation, CRMP2 SUMOylation, or both reduces native CRMP2 SUMOylation. Data are normalized to wildtype CRMP2 condition, error is ± SEM. Asterisks denote statistical significance by one-way ANOVA, * $p < 0.05$.

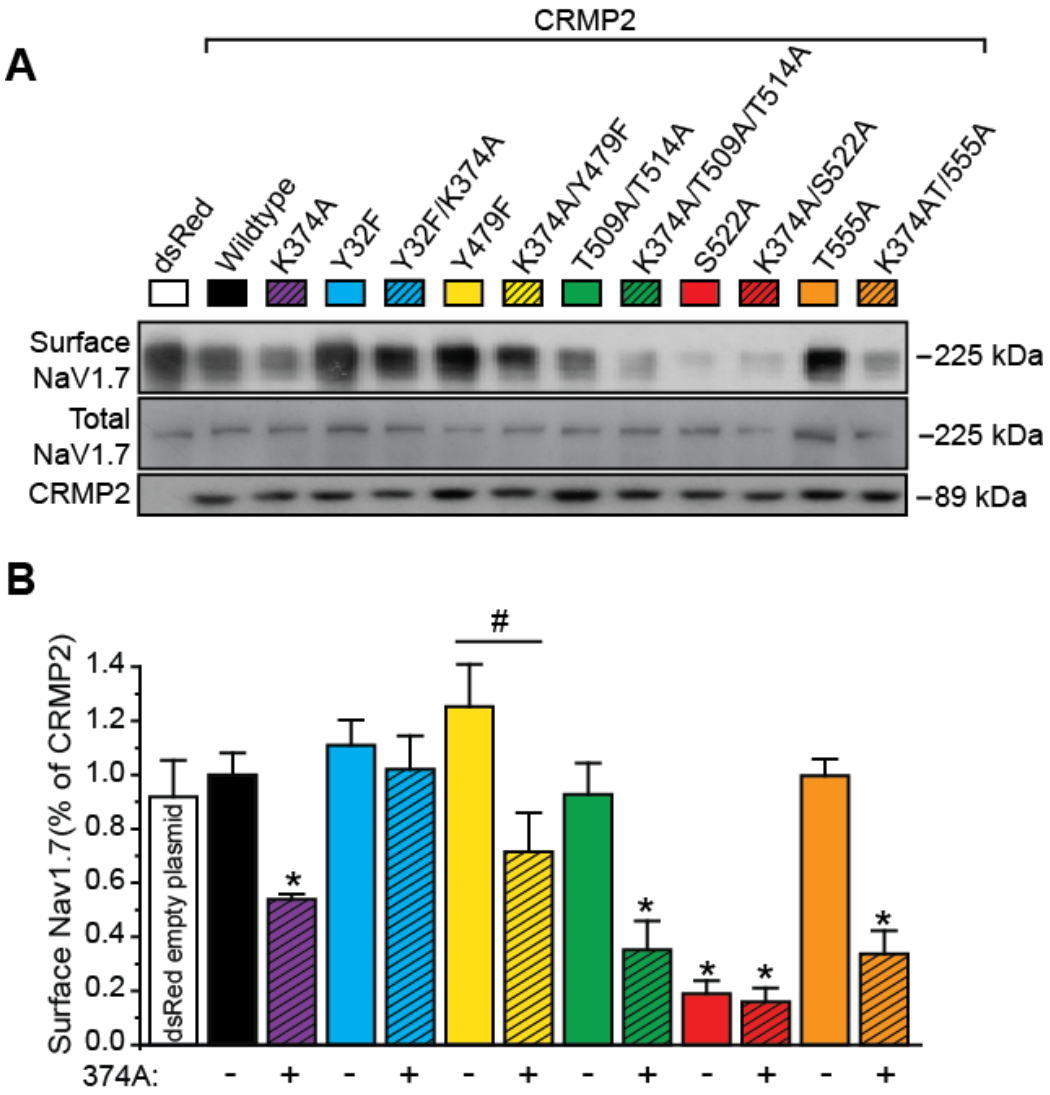

Figure 4.5. CRMP2 modifications mediate Nav1.7 surface expression. **(A)** Representative immunoblots of streptavidin-enriched surface (*top*) and total (*middle*) fractions probed with a Nav1.7 antibody. The bottom blot of lysates was probed with CRMP2 antibody to verify expression of transfected constructs. **(B)** Bar graphs summarizing mean surface Nav1.7 in CAD cells transfected with the indicated plasmids. Data are normalized to total Nav1.7 protein and then to the CRMP2 in each lane and finally plotted as ratio of the wild type CRMP2 condition. Asterisks indicate statistically significant differences compared to wildtype CRMP2 expressing control cells ($p < 0.05$, one-way ANOVA with Tukey's post-hoc test; n=3). Pound symbol denotes statistical significance by Student's t-test, # $p < 0.05$. Experiment performed by Aubin Moutal.

Consistent with earlier electrophysiology experiments, Nav1.7 surface expression was unchanged in cells expressing CRMP2-Y32F/K374A (102.1 ± 11.3%). These data therefore recapitulate the three major findings of CRMP2 regulation of Nav1.7 current density from previous patching experiments; (*i*) reduction of Nav1.7 surface expression by expression of SUMO-null CRMP2-K374A, (*ii*) reduction of Nav1.7 surface expression by expression of phopho-null CRMP2-S522A, and (*iii*) prevention of Nav1.7 surface reduction by SUMO- and phospho–null CRMP2-Y32F/K374A. Reduced channel surface expression without altered channel availability (equivalent kinetics) is also consistent with previous data for the CRMP2-K374A mutant. All biotinylation results for other CRMP2 mutants were consistent with the patching results, with the exception of K374A/Y479. This mutant failed to meet significance by one-way ANOVA, but met significance by a Student's t-test (#) (Figure 4.5B).

4.4. CRMP2 phosphorylation by Cdk5 is dominant in preventing effects of CRMP2 deSUMOylation on Nav1.7 currents

The whole-cell patch clamp electrophysiology and cell surface biotinylation experiments revealed that loss of Cdk5-mediated CRMP2 phosphorylation reduces Nav1.7 current density by reducing surface expression. To further investigate the mechanism by which Cdk5 phosphorylation of CRMP2 controls Nav1.7 current density, I tested if a constitutively active phospho-mimetic CRMP2-S522D mutant or overexpression of Cdk5 kinase to boost Cdk5 levels would be sufficient to overcome the current reduction imposed by loss of CRMP2 phosphorylation at the S522 site or CRMP2 SUMOylation at the K374 site. In patching experiments, both overexpression of Cdk5

and CRMP2-S522D prevented the current reduction imposed by CRMP2 deSUMOylation; Nav1.7 currents in CAD cells expressing Cdk5 and CRMP2-K374A, were 84.3 ± 17.3% of control (i.e. wildtype CRMP2) levels (Figure 4.6A) while those in CAD cells expressing CRMP2-K374A/S522D were 100.8 ± 11.8%, and those in CAD cells expressing the Cdk5-phospho-mimetic and deSUMOylation machinery (i.e. CRMP2-S522D + SENP1 + SENP2) were 112 ± 10.4% (Figure 4.6B). Expression of the Cdk5-phospho-mimetic or the CRMP2-K374A/S522D mutant alone did not affect Nav1.7 current densities compared to cells expressing wildtype CRMP2. These results show that forcing Cdk5-mediated phosphorylation of CRMP2 does not enhance currents, but is sufficient to overcome the reduction in Nav1.7 currents imposed by CRMP2 deSUMOylation. Thus, CRMP2-pS522 phosphorylation is dominant over CRMP2 deSUMOylation in control of Nav1.7 currents.

Expression of a CRMP2-S522A mutant, which is not phosphorylated by Cdk5, along with the Cdk5 kinase provided a positive control and demonstrated a reduction in Nav1.7 currents to 41.3 ± 8.5% compared to cells expressing wildtype CRMP2 (Figure 4.6A), consistent with results obtained with CRMP2-S522A mutant alone (Figure 4.2B). This demonstrates that CRMP2 is the *sole* mediator of Cdk5 regulated changes to Nav1.7 currents. Experiments in DRG neurons verified the dominance of CRMP2-S522D mutant over deSUMOylation of CRMP2 because there was no difference in TTX-S Nav1.7 currents in neurons expressing wildtype, S522D, or K374A/S522D CRMP2 constructs (Figure 4.6C).

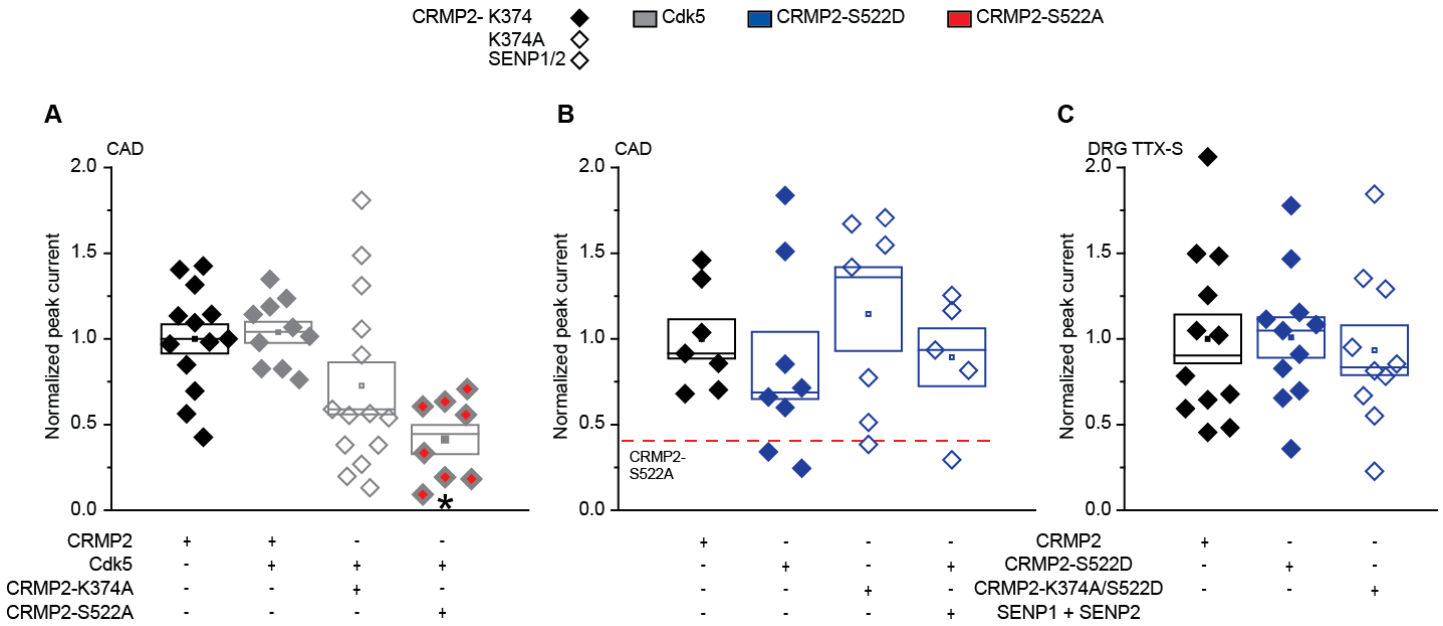

Figure 4.6. Forcing Cdk5 phosphorylation of CRMP2 overrides CRMP2 deSUMOylation loss of Nav1.7 current density. (A, B) Peak current density (pA/pF) measured at 0 mV for CAD cells transfected with the constructs as indicated. Data are normalized to the wildtype CRMP2 condition. Overexpression of Cdk5 kinase prevents loss of current density observed with CRMP2-K374A. Symbol key to data is above the panels. Closed black symbols indicate wildtype CRMP2 expression and open symbols indicate presence of CRMP2-K374A mutant. Grey symbols indicate Cdk5 expression, blue symbols indicate CRMP2-S522D expression, and red symbols indicate CRMP2-S522A expression. Asterisks indicate statistically significant differences compared to wildtype CRMP2 expressing control cells ($p < 0.05$, one-way ANOVA with Tukey's post-hoc test; n=8–14). The phospho-mimetic S522D CRMP2 mutation prevents loss of current density associated with both CRMP2-K374A and SENP expression in CAD cells. Dashed red line indicates mean of peak current density for CAD cells expressing CRMP2-S522A, re-plotted from Figure 4.2. **(C)** Peak TTX-S current densities isolated from small DRGs and normalized to wildtype CRMP2 condition. The phospho-mimetic S522D CRMP2 mutation prevents loss of TTX-S current density associated with the CRMP2-K374A mutation. Box plot borders represent SEM and median, square indicates mean, diamonds are individual data points.

4.5. Loss of Fyn phosphorylation is dominant in preventing effects of CRMP2 deSUMOylation on Nav1.7 currents

Whole-cell patch clamp electrophysiology and cell surface biotinylation experiments on CRMP2 mutants that contained the SUMO-null K374A mutation to prevent SUMOylation all had the general effect of reducing Nav1.7 currents and surface expression. There was one notable *exception*; the double CRMP2-Y32F/K374A mutant, harboring a mutant Fyn phosphorylation site of CRMP2 when combined on the K374A mutation, prevented the current reduction imposed by the CRMP2-K374A mutant. Maintenance of wildtype control level currents and surface expression in CRMP2-Y32F/K374A expressing cells lead to the conclusion that loss of Fyn phosphorylation is dominant over loss of SUMOylation in Nav1.7 regulation.

Within the solved CRMP2 high-resolution crystal structure (Deo et al., 2004, Majava et al., 2008), the site of Fyn phosphorylation, tyrosine-32, lies on the surface of the protein in proximity to the SUMOylation motif at lysine-374 (Figure 4.7). Recent evidence suggests that even different parts of the protein that come together in the folded protein can form consensus recognition motifs for kinases (Duarte et al., 2014). No evidence exists linking secondary, tertiary, or quaternary protein structure to relationship of phosphorylation and SUMOylation. However, there are several examples of phosphorylation-dependent SUMOylation motifs have phosphorylation sites within ~10 amino acids to the SUMOylation (reviewed in (Hietakangas et al., 2006)). This suggests that relationships between phosphorylation and SUMOylation modifications may be proximity-dependent but do not rule out the possibility that “structurally-formed” consensus motifs that are non-proximal may also play a role.

The hypothesis that loss of Fyn phosphorylation is dominant over loss of SUMOylation in Nav1.7 regulation was supported by electrophysiology data in DRG neurons in which data where TTX-S Nav1.7 currents where equivalent between CRMP2-Y32F/K374A and wildtype CRMP2 expressing cells, 91.7 ± 13.4% of wildtype CRMP2 levels (Figure 4.8A), versus the previously reported CRMP2-K374A mutant alone, 36.0 ± 5.5% (see Figure 3.7). Dominance of Y32F was next tested in combination with other conditions that resulted in reduced Nav1.7 current including overexpression of the deSUMOylating machinery or phospho-null CRMP2-S522A mutant (Figure 4.8B). The reduction in Nav1.7 currents imposed by SENP1/SENP2 overexpression or CRMP2-S522A mutant was overcome by the additional presence of the CRMP2-Y32F mutant (Figure 4.8B).

Another tool available to test loss of pY32-CRMP2 phosphorylation is the dominant negative Fyn kinase (DNFyn) that constrains kinase activity. DNFyn contains a point mutation (K299M) within the ATP binding pocket of the kinase that renders it unable to bind and transfer phosphate groups to its substrates, including CRMP2 (Osterhout et al., 1999). This plasmid was coexpressed in CAD cells along with (*i*) CRMP2 mutants that reduced Nav1.7 current density (i.e., CRMP2-K374A, CRMP2-S522A, or CRMP2-K374A/S522A) or (*ii*) CRMP2 mutants that prevented the reduction of Nav1.7 current density (i.e., CRMP2-S522D or CRMP2-K374A/S522D).

In all conditions, sodium currents from CAD cells that co-expressed DNFyn were equivalent to those from CAD cells expressing wildtype CRMP2 (Figure 4.9A). Therefore, loss of Fyn phosphorylation is dominant over all known negative regulations of Nav1.7 currents (purple and red boxes, Figure 4.9A).

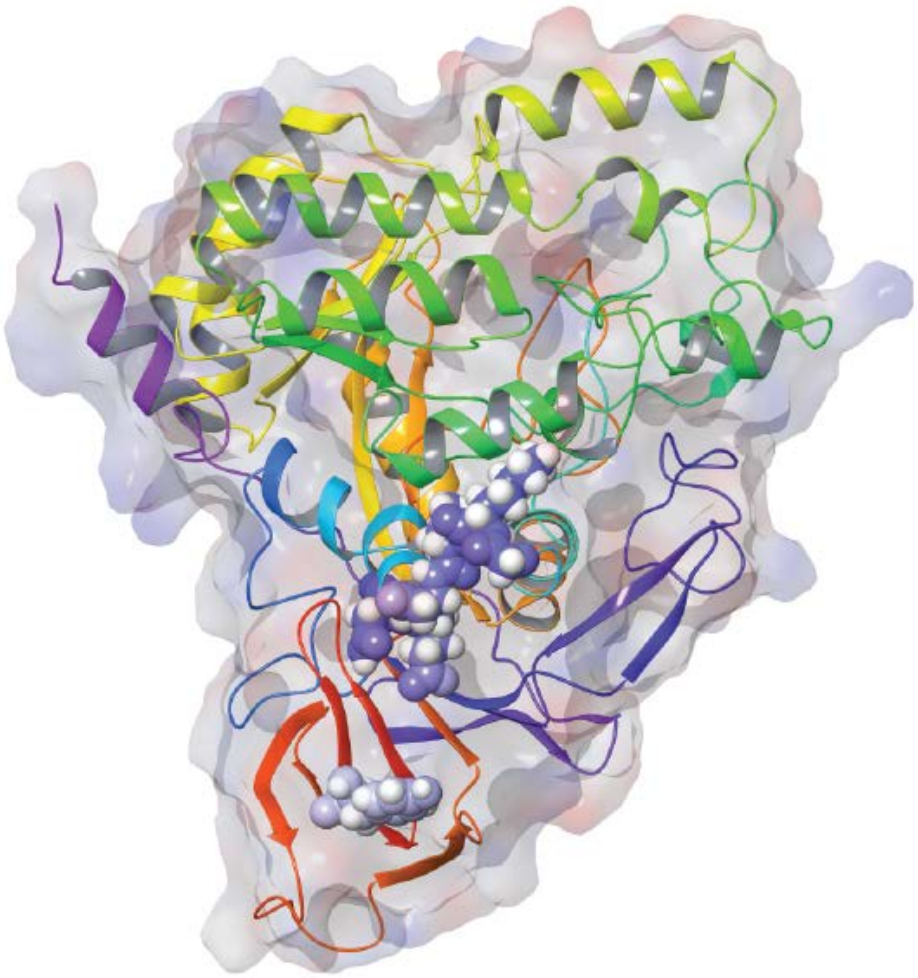

Figure 4.7. Fyn site, tyrosine-32, is adjacent to the SUMOylation motif within the crystal structure of CRMP2. Structural representation of CRMP2 monomer (PDB code: 2GSE (Deo et al., 2004)) with SUMOylation motif (top) and Fyn-targeted tyrosine-32 (bottom) represented by purple and white ball and chain structures. The color of CRMP2 ribbon structure is a gradient from N-terminal (blue) to C-terminal (red). The proximity of the SUMOylation motif and tyrosine-32 on the same surface of CRMP2 is hypothesized to endow interdependence between the modifications. Figure generated using Pymol by Dr. May Khanna (University of Arizona).

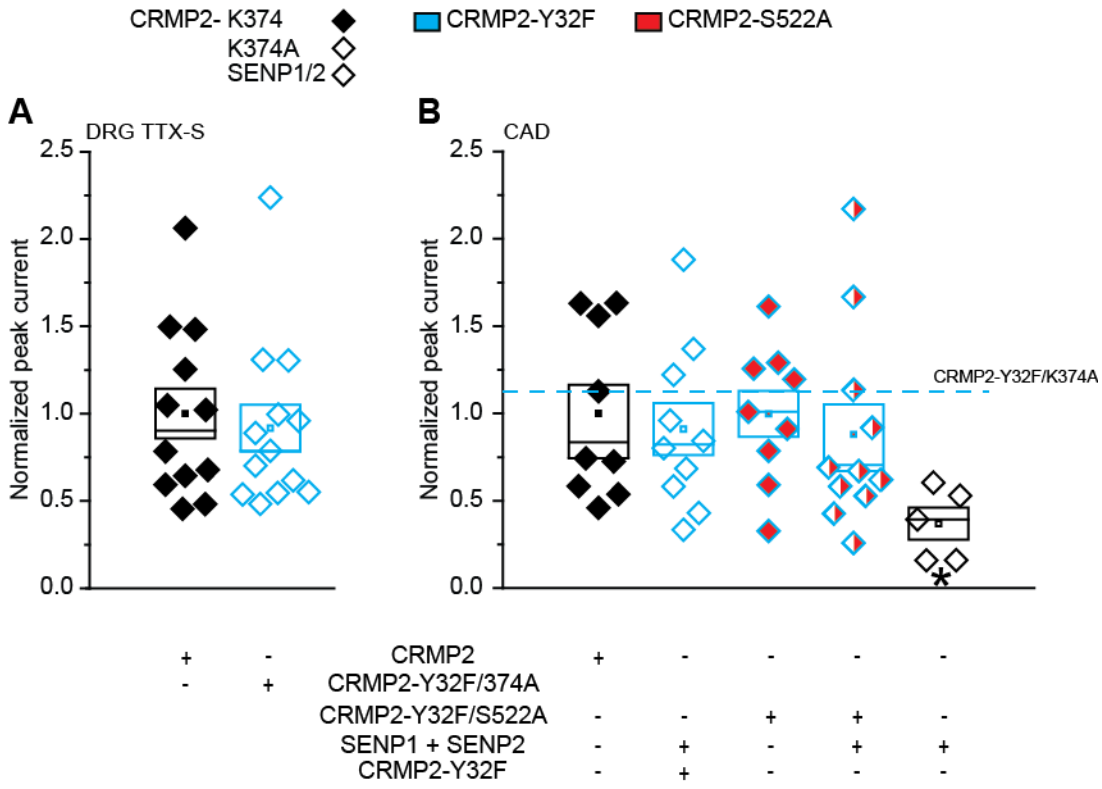

Figure 4.8. The Fyn kinase incompetent CRMP2 mutant, CRMP2-Y32F, overrides the reduction in Nav1.7 current density associated with loss of CRMP2 SUMOylation and loss of CRMP2 phosphorylation by Cdk5. (A) Box plots summarizing peak TTX-S current densities isolated from small DRGs after transfection with the indicated constructs. The CRMP2-Y32F mutation prevents loss of TTX-S current density imposed by the CRMP2-K374A mutation. **(B)** Peak current density (pA/pF) measured at 0 mV for CAD cells transfected with the constructs as indicated. Data are normalized to the wildtype CRMP2 condition. Asterisks indicate statistically significant differences compared to wildtype CRMP2 expressing control cells ($p < 0.05$, one-way ANOVA with Tukey's post-hoc test; n=9–11). The CRMP2-Y32F mutation prevents loss of Nav1.7 current density in CAD cells associated with loss of CRMP2 SUMOylation, loss of CRMP2 phosphorylation by Cdk5, or both combined.

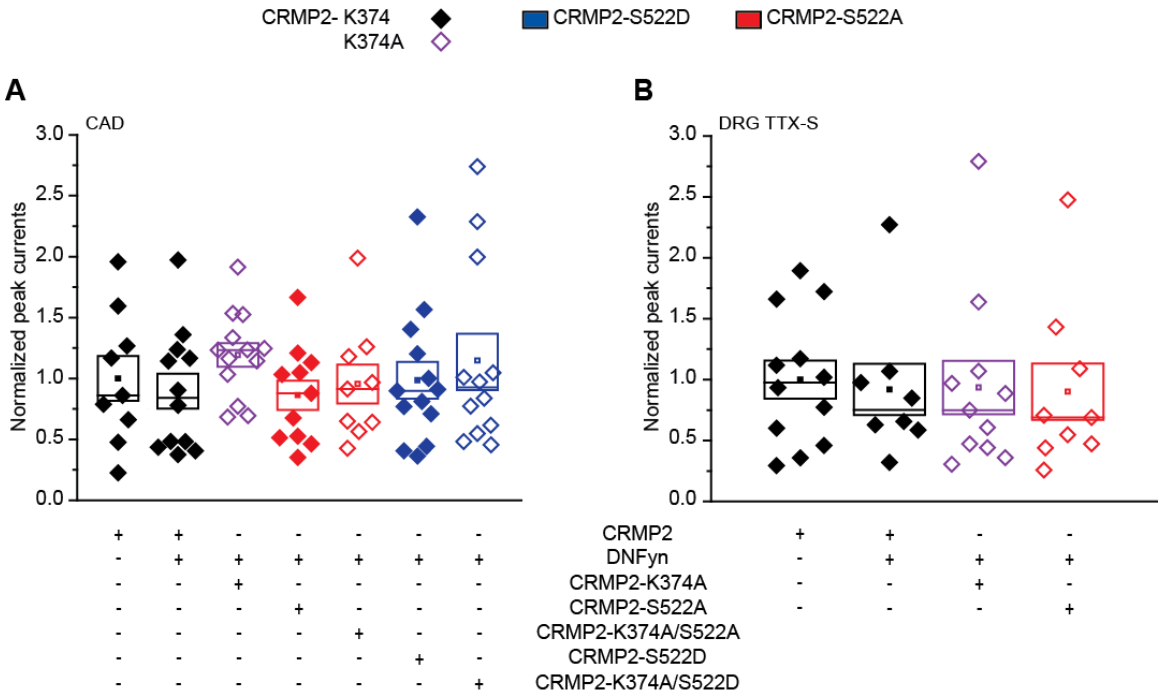

Figure 4.9. Introduction of a kinase-dead mutant of Fyn suppresses loss of Nav1.7 current density imposed by CRMP2-K374A and CRMP2-S522A mutants. (A) Peak current density (pA/pF) measured at 0 mV for CAD cells transfected with the constructs as indicated. Data are presented as normalized to the wildtype CRMP2 plus dominant negative DNFyn condition. Current densities of CAD cells expressing CRMP2 constructs and DNFyn normalized to wildtype control do not produce any changes to Nav1.7 current. **(B)** Peak TTX-S current densities isolated from small DRGs after transfection with the indicated constructs. The reduction in TTX-S currents observed following transfection with CRMP2-K374A or CRMP2-S522A mutants is completely prevented by DNFyn expression. Box plot borders represent SEM and median, square indicates mean, diamonds are individual data points. n=8-13 cells per condition.

To assess any cumulative effects of Cdk5 phosphorylation with loss of Fyn phosphorylation, DNFyn was coexpressed with CRMP2-S522D and CRMP2-K374A/S522D mutants. Expression of the DNFyn kinase mutant or the CRMP2-S522D mutation alone prevented the current density decrement associated the SUMO-null CRMP2-K374A mutant. When expressed together, the lack of increase in observed Nav1.7 currents (Figure 4.9A, blue boxes) suggests that these manipulations have shared mechanism. DNFyn transfection in small DRG neurons was used to evaluate the dominance of DNFyn in regulation of Nav1.7 currents in native neurons. In DRGs, TTX-S Nav1.7 currents were no different between any of the conditions tested, confirming dominance of the DNFyn kinase over CRMP2-K374A– and CRMP2-S522A–mediated Nav1.7 current reductions (Figure 4.9B; purple and red boxes).

4.6. Fyn phosphorylation of CRMP2 reduces Nav1.7 current density by promoting CRMP2 deSUMOylation

To further elucidate the effect of CRMP2 tyrosine-32 modification in regulation of Nav1.7, a competent Fyn kinase was overexpressed to promote CRMP2 Y32 phosphorylation. Although this strategy is less specific than a CRMP2 mutant as it affects global Fyn phosphorylation, there are no phospho-mimetic substitutions possible for tyrosine targeted phosphorylation. The Fyn kinase was overexpressed in CAD cells with CRMP2 mutants that had previously been demonstrated to produce reduced Nav1.7 currents – CRMP2-K374A, CRMP2-Y32F, CRMP2-S522A, CRMP2-K374A/S522A, CRMP2-522D, or CRMP2-K374A/S522D – and Nav1.7 currents were recorded and compared to wildtype control (Figure 4.10A). In electrophysiology experiments with

CAD cells, Fyn expression revealed a new component of CRMP2's regulation of Nav1.7: a significant ~46% reduction in current density was observed in CAD cells co-expressing wildtype CRMP2 and Fyn kinase (Figure 4.10A). With Fyn overexpression, all CRMP2 mutants that previously reduced CAD cell sodium current density (CRMP2-K374A (purple boxes) and CRMP2-S522A (red boxes), Figure 4.10A) still produced currents that were diminished in comparison to cells expressing wildtype CRMP2. Mutants that were previously shown to prevent CRMP2-K374A SUMO-null mediated current reductions, that is, CRMP2-S522D and CRMP2-Y32F, also maintained their effects (blue and cyan; Figure 4.10A). Expression of CRMP2-Y32F mutant with Fyn kinase served as a positive control for Fyn-mediated effects on Nav1.7 current density. Control level Nav1.7 currents in this condition, where Fyn cannot target CRMP2, verify that Fyn-mediated reduction of Nav1.7 CAD cell currents are mediated solely by phosphorylation of CRMP2 and no other Fyn targets. Importantly, the finding that overexpression of Fyn kinase together with wildtype CRMP2 reduced Nav1.7 currents was recapitulated in small DRG currents where the TTX-S, presumptive Nav1.7 current was reduced by ~41% compared to similar currents from DRGs transfected with wildtype CRMP2 (Figure 4.10B). TTX-R current densities were unchanged between the two conditions (Figure 4.10B).

As there was not a synergistic effect of Fyn expression and previous manipulations that reduced Nav1.7 currents (CRMP2–K374A and CRMP2–S522A), it was predicted that this phosphorylation was part of the same regulatory mechanism as Cdk5 phosphorylation and SUMOylation.

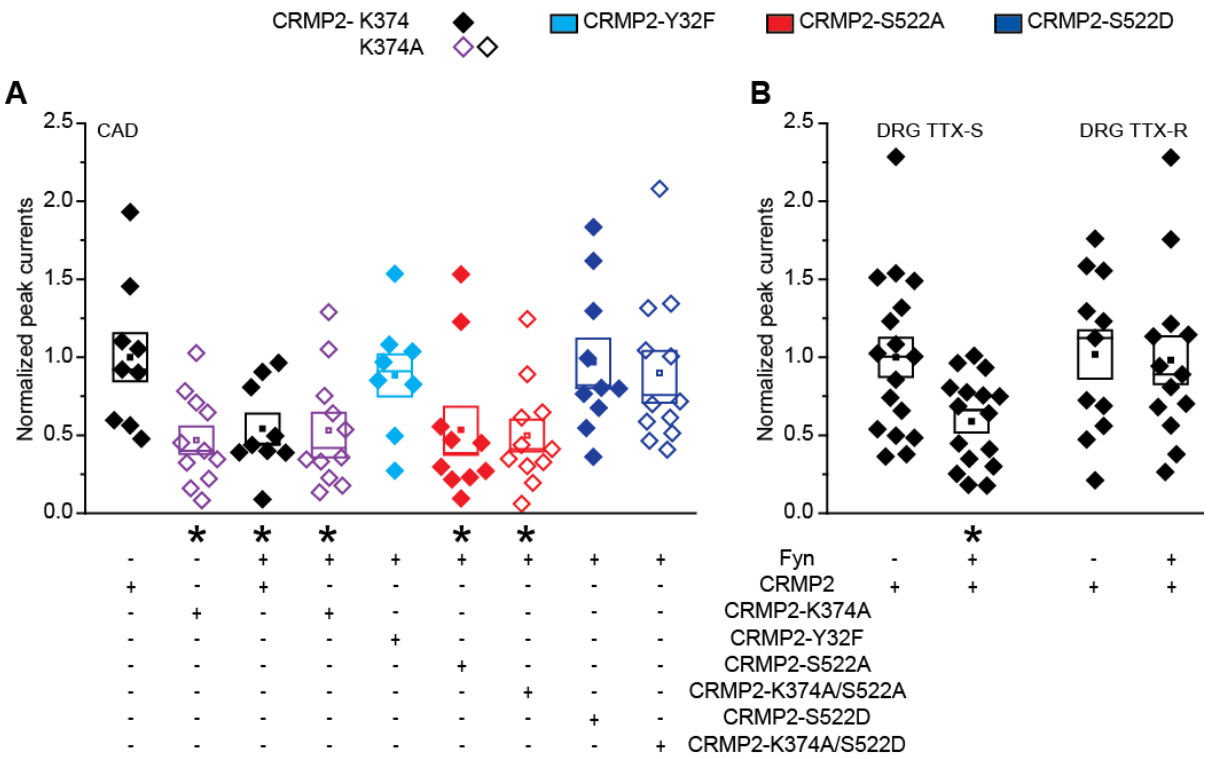

Figure 4.10. Gain of CRMP2 phosphorylation by Fyn restricts Nav1.7 currents. (A) Box plots summarizing peak current densities (pA/pF) measured at 0 mV for CAD cells transfected with the indicated constructs. Data are normalized to the wildtype CRMP2 condition. Asterisks indicate statistically significant differences compared to wildtype CRMP2 expressing control cells ($p < 0.05$, one-way ANOVA with Tukey's post-hoc test; n=8–12). CRMP2 phosphorylation by Fyn reduces Nav1.7 current density (compare second black bar to cyan bar). **(B)** Peak TTX-S and TTX-R current densities isolated from small DRGs after transfection with the indicated constructs. The Fyn kinase reduces the TTX-S current fraction. Asterisk indicates a statistically significant difference from wildtype CRMP2 ($p < 0.05$, one-way ANOVA with Tukey's post-hoc test; n=11-16). Box plot borders represent SEM and median, square indicates mean, diamonds are individual data points.

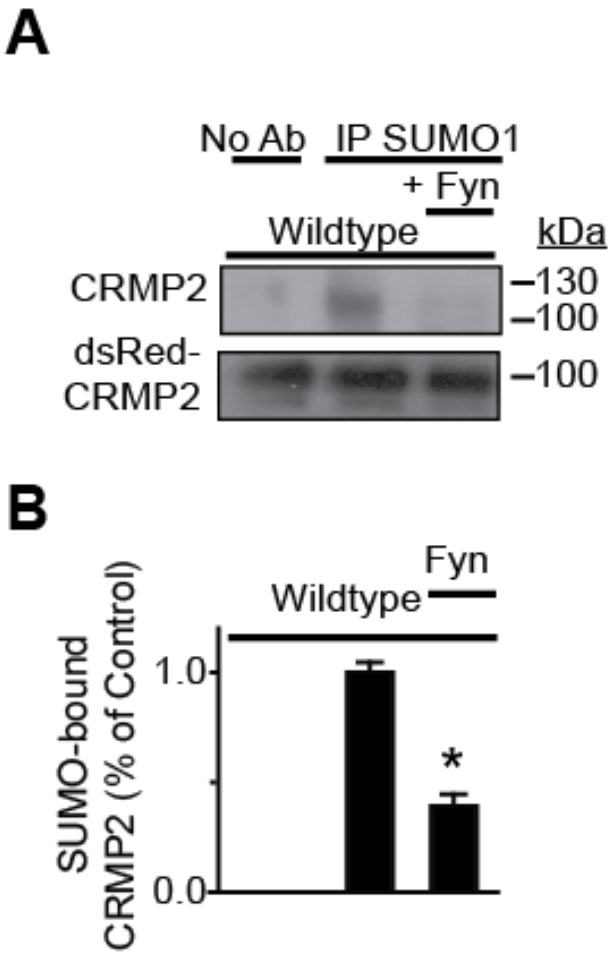

Figure 4.11. Fyn phosphorylation restricts CRMP2 SUMOylation. (A) Lysates of CAD cells expressing the indicated constructs, following denaturation and immunoprecipitation with a SUMO1 antibody probed with CRMP2 (*top*) or dsRed-CRMP2 (*bottom*). **(B)** Summary of amount of SUMOylated CRMP2 Overexpression of Fyn kinase prevents CRMP2 SUMOylation. Asterisk denotes statistical significance compared to wildtype CRMP2 alone ($p < 0.05$, Student's t-test; n=3). Experiment performed by Aubin Moutal, a postdoctoral fellow in the Khanna laboratory.

Consequently, SUMO1 immunoprecipitation from CAD cell lysates wherein wildtype CRMP2 was coexpressed with Fyn kinase led to a significant reduction in the amount of SUMOylated CRMP2 (39.0 ± 5.6% of control wildtype CRMP2 alone, Figure 4.11A, B). I conclude from this data that Fyn phosphorylation of CRMP2, akin to Cdk5 phosphorylation, is a determinant of CRMP2 SUMOylation and regulation of Nav1.7.

4.7. CRMP2 modifications alter its interaction with endocytic proteins and may explain the Nav1.7 current density changes

While the data presented thus far in my thesis demonstrates the importance of CRMP2 modifications in orchestrating Nav1.7 surface trafficking and current density, the mechanism by which this surface loss of Nav1.7 is choreographed is not known. CRMP2 has been previously described as a trafficking protein of the adhesion molecule L1-CAM in which CRMP2 interaction with the endocytic adaptor protein Numb regulated L1-CAM endocytosis (Nishimura et al., 2003a, Jauffred et al., 2013). As an endocytic adapter protein, Numb promotes endocytosis of transmembrane proteins by recruiting components of clathrin-mediated endocytosis machinery including epidermal growth factor receptor substrate 15 (Eps15) endocytic adaptor protein and E3 ubiquitin ligases and relocating cargo to endocytic organelles (Santolini et al., 2000, Tang et al., 2005, Krieger et al., 2013). Numb has been reported to interact with ubiquitin E3 ligase LNX (Dho et al., 1998), Mdm2 (Juven-Gershon et al., 1998), Itch (McGill and McGlade, 2003, McGill et al., 2009), Siah-1 (Susini et al., 2001) – all of which can then monoubiqutinate target proteins to mark them for endocytosis. Numb stabilizes the interaction of Eps15 to monoubiquitinated proteins and induces plasma membrane curvature in the early steps of

clathrin-mediated endocytosis (Santolini et al., 2000, Woelk et al., 2006, Horvath et al., 2007).

There is one report that demonstrates regulation of Nav1.7 surface expression by the Nedd4-2 E3 ubiquitin ligase (Laedermann et al., 2013a). This E3 ubiquitin ligase monoubiquitinates Nav1.7 to signal downregulation of the channel resulting in a decrease in surface expression and current density (Laedermann et al., 2013a). CRMP2 or CRMP2 interaction with Numb endocytic adaptor protein may facilitate interaction with Nedd4-2 ligase. In this case clathrin-mediated endocytosis of Nav1.7 could be dependent on CRMP2 interaction with Numb and Nedd4-2.

In a pilot experiment to further this line of inquiry, CRMP2 and CRMP2-K374A interaction with endocytic proteins Numb, adapter protein Eps15, and ubiquitin ligases Itch and Nedd4-2 were examined (Figure 4.12A). These proteins were selected for analysis because Numb has well described interaction with CRMP2 (Nishimura et al., 2003a), as well as with endocytic adaptor protein Eps15 (Santolini et al., 2000), and Itch (Di Marcotullio et al., 2006). Nedd4-2 was selected due to described interaction with Nav1.7 and similarity to the E3 ubiqutin ligase Itch which interacts with Numb (McGill and McGlade, 2003, McGill et al., 2009, Laedermann et al., 2013a). For each endocytic protein, interaction with CRMP2-K374A was significantly greater than with wildtype CRMP2 (Figure 4.12B). This data indicates that unSUMOylated CRMP2 can facilitate interactions with endocytic machinery.

To determine if these enhanced interactions promote endocytosis of Nav1.7, specific siRNA of each individual endocytic protein were used to knockdown their expression. The siRNAs were validated by Western blots in CAD cells (Figure 4.12C and

D) because the transfection efficiencies in DRGs precluded determination in these native neurons. Between 63.5-86.5% reduction in these proteins was observed (Figure 4.12C). CRMP2 was over-expressed along with the specific siRNAs to ensure that there were no spurious effects on CRMP2 expression.

To determine if the knockdown of these proteins could impact CRMP2 regulation of Nav1.7 currents in DRGs, the siRNAs were then co-transfected with CRMP2 constructs in DRGs and TTX-S currents were analyzed (Figure 4.12E). The previously observed reduction in TTX-S currents by expression of CRMP2-K374A and CRMP2-S522A plasmids was not affected co-transfection of control-scrambled siRNAs with decreases of ~57% and ~50%, respectively (Figure 4.12E). Knockdown of Numb (green), Eps15 (orange), or Nedd4-2 (red) (Figure 4.12E) prevented the reduction in TTX-S currents observed with the CRMP2-K374A and CRMP2-S522A plasmids to control levels. In contrast, knockdown of Itch had no effect on preventing the reduction inTTX-S current density reduction (Figure 4.12E, *blue*). Therefore, modulation of Nav1.7 by CRMP2 SUMOylation and Cdk5 phosphorylation requires the interaction of CRMP2 with Numb, Eps15, and Nedd4-2, but not Itch.

Epidermal growth factor substrate 15 (Eps15) is described to induce membrane curvature to initiate clathrin-mediated endocytosis (Santolini et al., 2000, Woelk et al., 2006, Horvath et al., 2007). This process involves Eps15 interaction with phosphoinositide headgroups of membrane lipids and insertion of Eps15s epsin N-terminal homology helix structure (ENTH domain) between membrane lipid headgroups just shallow of the hydrophobic core (Hurley and Wendland, 2002). This adds mass to the

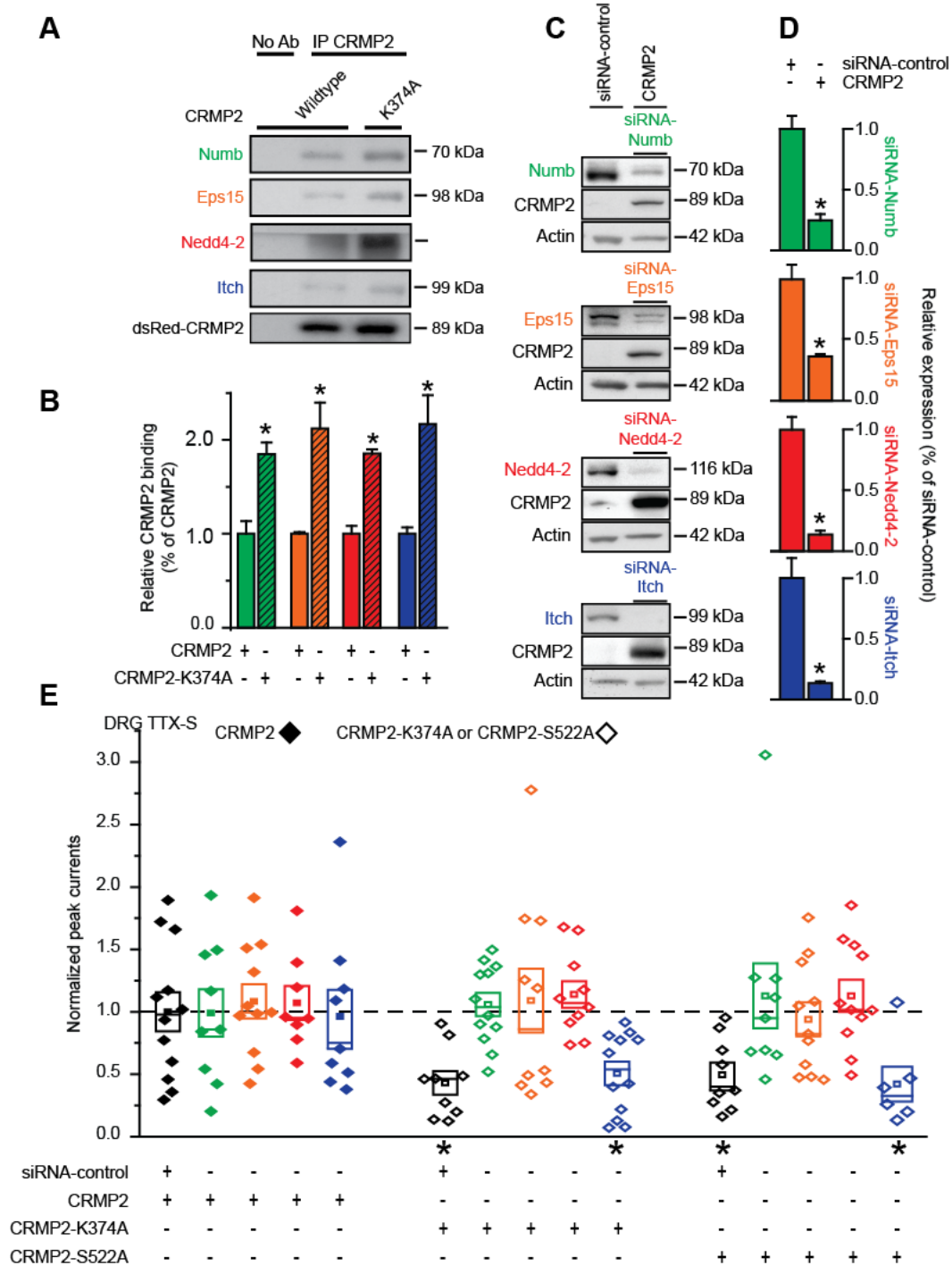
A
No Ab
IP CRMP2
CRMP2
Wildtype
K374A
Numb
Eps15
Nedd4-2
Itch
dsRed-CRMP2
70 kDa
98 kDa
99 kDa
89 kDa
B
Relative CRMP2 binding (% of CRMP2)
2.0
1.0
0.0
CRMP2 + - + - + - + -
CRMP2-K374A - + - + - + - +
C
siRNA-control
CRMP2
siRNA-Numb
Numb
CRMP2
Actin
70 kDa
89 kDa
42 kDa
siRNA-Eps15
Eps15
98 kDa
siRNA-Nedd4-2
Nedd4-2
116 kDa
siRNA-Itch
Itch
99 kDa
D
+ - siRNA-control
- + CRMP2
siRNA-Numb
siRNA-Eps15
siRNA-Nedd4-2
siRNA-Itch
1.0
0.5
0.0
Relative expression (% of siRNA-control)
E
DRG TTX-S
CRMP2
CRMP2-K374A or CRMP2-S522A
Normalized peak currents
3.0
2.5
2.0
1.5
1.0
0.5
0.0
siRNA-control + - - - - + - - - - + - - - -
CRMP2 + + + + + - - - - - - - - - -
CRMP2-K374A - - - - - + + + + + - - - - -
CRMP2-S522A - - - - - - - - - - + + + + +

← **previous page…Figure 4.12. CRMP2 mediated Nav1.7 current reduction requires interaction with the endocytosis proteins Numb and Eps15 and the E3 ubiquitin-protein ligase Nedd4-2. (A)** Representative immunoblots of CRMP2-immunoprecipitates from CAD cells expressing wildtype CRMP2 or CRMP2-K374A and probed with the indicated antibodies. **(B)** Summary of normalized binding of CRMP2 to the indicated proteins. In all cases, binding of Numb, Eps15, Nedd4-2, and Itch was higher for the CRMP2-K374A mutant than wildtype CRMP2. Asterisks denote statistical significance compared to wildtype CRMP2 alone ($p < 0.05$, Student's t-test; n=3). **(C)** Representative blots of lysates from CAD cells transfected with control siRNA or siRNAs against Numb, Eps15, Nedd4-2, and Itch. CRMP2 was over-expressed along with the specific siRNAs to ensure that there were no spurious effects on CRMP2 expression. These blots verify endocytic protein knockdown in CAD cells. Asterisks denote statistical significance compared to siRNA control ($p < 0.05$, Student's t-test; n=3). **(E)** Peak TTX-S current densities isolated from small DRGs after transfection with the indicated plasmids and/or siRNAs. Knockdown of Numb, Eps15, and Nedd4-2, but not Itch, prevents the reduction in TTX-S Nav1.7 currents observed following expression of CRMP2-K374A and CRMP2-S522A mutants. Box plot borders represent SEM and median, square indicates mean, diamonds are individual data points. Asterisks indicate statistically significant differences compared to wildtype CRMP2 expressing control cells ($p < 0.05$, one-way ANOVA with Tukey's post-hoc test; n=6–11). Biochemistry experiment illustrated in A-D performed by Aubin Moutal.

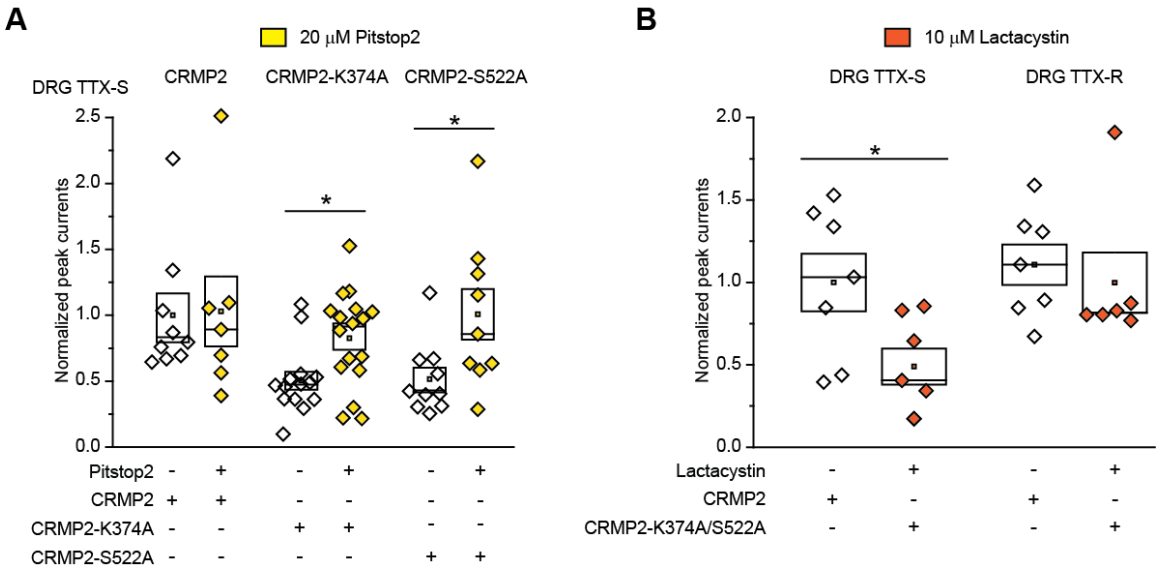

Figure 4.13. CRMP2 mediated endocytosis of Nav1.7 is clathrin-dependent and proteasome-independent (A) Box plots of peak TTX-S current densities isolated from small DRGs after transfection with the indicated plasmids and indicated treatment of 20 μM Pitstop2 or 0.1% DMSO control. Pitstop2 application for 30 minutes rescued the decrease of TTX-S currents in cells expressing CRMP2-K374A and CRMP2-S522A. **(B)** Box plots of peak TTX-S (*left*) and peak TTX-R (*right*) currents expressing the indicated plasmids and indicated treatment of 10 μM Pitstop2 or 0.1% DMSO control. Lactacystin treatment did not prevent TTX-S current density reduction by CRMP2-K374A/S522A. Box plot borders represent SEM and median, square indicates mean, diamonds are individual data points. Asterisks indicate statistically significant differences compared to cells without Pitstop2 treatment ($p < 0.05$, Student's t-test; n=7–13).

intracellular leaflet and bulges the membrane outward in relation to Eps15 and the intracellular cargo to produce membrane curvature (Hurley and Wendland, 2002). To resolve whether clathrin-mediated endocytosis is responsible for CRMP2 regulation of Nav1.7, I used the clathrin assembly inhibitor Pitstop2 on DRGs transfected with CRMP2, CRMP2-K374A, or CRMP2-S522A. Application of 20μM of Pitstop2 to DRGs for 30 min rescued the decrease of Nav1.7 currents imposed by CRMP2-K374A and CRMP2-S522A expressing DRGs and did not affect currents of cells expressing wildtype CRMP2 (Figure 4.13A). In another experiment to test determine if Nav1.7 trafficking by CRMP2 requires degradation of the channel, I treated DRGs expressing CRMP2-K374A/S522A DRGs with 10μM Lactacystin for 24 hours to inhibit proteasome function (Fenteany et al., 1995). Lactacystin had no effect on preventing reduction of TTX-S currents in these cells (Figure 4.13B). Based on these DRG data following knockdown of Numb, Eps15, and Nedd4-2, inhibition of clathrin-mediated endocytosis, and inhibition of proteasome, I conclude that endocytosis, but not degradation, of the Nav1.7 channel brings about the observed reduction in Nav1.7 current density and surface expression seen with the CRMP2-K374A SUMO null plasmid.

4.8. Discussion

In this Chapter I built upon evidence from Chapter 3 that CRMP2 SUMOylation regulates Nav1.7 current density and surface expression. Here, I provide evidence that CRMP2 phosphorylation regulates CRMP2 SUMOylation to exert downstream effects on Nav1.7 trafficking. Of the multiple kinases that target CRMP2 (see section 1.2.2), I demonstrated that phosphorylation by Cdk5 and Fyn regulates CRMP2 SUMOylation.

Cdk5 phosphorylation is mandatory for CRMP2 SUMOylation and maintenance of Nav1.7 currents. Loss of phosphorylation by Cdk5 decreased the level of SUMOylated CRMP2 in CAD cells, which, in turn, resulted in decreased Nav1.7 current densities. Phosphorylation of CRMP2 by Fyn kinase blunted CRMP2 SUMOylation to decrease Nav1.7 current densities. Loss of Fyn phosphorylation prevented loss of Nav1.7 current densities associated with expression of the unSUMOylated CRMP2. The mechanism by which SUMO-null CRMP2 exerts effect on Nav1.7 was determined to be clathrin-mediated endocytosis. This occurs by CRMP2-mediated recruitment of three proteins that initiate endocytosis – Numb, Eps15, and E3 ubiqutin ligase Nedd4-2.

Phosphorylation introduces a double negative charge to amino acids that is not present in any amino acids incorporated into proteins. As a result, phosphorylation can introduce hydrogen binding between amino acid side chains that alters protein conformation (Johnson and Lewis, 2001). Therefore, the regulations of SUMOylation by phosphorylation could likely be due to altered protein conformation. SUMOylation of some proteins is reportedly altered by their phosphorylation state (some examples can be found in Table 1.3). In some cases, phosphorylation N-terminal (e.g., Heat-shock factors 1 and 4b, and Estrogen receptor β) (Hietakangas et al., 2006, Picard et al., 2012) or C-terminal (GluK2 receptor) (Konopacki et al., 2011) to the SUMOylation motif can trigger protein SUMOylation. In other cases, phosphorylation of immediately N-terminal residues prevents subsequent SUMOylation (e.g., for the transcription factor SATB1) (Tan et al., 2010). There are also cases where the primary amino acid sequence alone does not mediate the relationship between phosphorylation and SUMOylation. This is the case for the transcription factor Elk-1 where phosphorylation of a residue over 100 amino

acids C-terminal of the SUMOylation motif triggers the secondary modification (Yang et al., 2003). In the latter case it seems possible that the protein's tertiary structure may change following phosphorylation allowing for a conformational change in the protein that facilitates subsequent SUMOylation, but this possibility has not been investigated. The relationship between CRMP2 SUMOylation and phosphorylation may also fall into this category as the SUMOylated residue lysine-374 is 341 residues away from the target of Fyn (tyrosine-32) and 147 residues away from the target of Cdk5 phosphorylation (serine-522).

The solved crystal structure of rat CRMP2 (Deo et al., 2004) allows for atomic localization of the SUMOylation motif centered at CRMP2 lysine-374. The crystal structure also allows mapping of the phosphorylation site of Fyn, tyrosine-32. Because the existing CRMP2 structures are all C-terminally truncated, the exact location of the Cdk5 serine 522 is not known. The C-terminal domain is not present in the structure because the region is likely (*i*) susceptible to proteolysis and *(ii*) unfolded (Figure 4.7). The Fyn targeted tyrosine-32 and SUMO targeted lysine-374 lie within direct proximity to each other on the surface of CRMP2 monomers. This allows the possibility of a physical or hydrophobic block of the SUMOylation motif following Fyn phosphorylation. Such a relationship could explain the reduced SUMOylation of Fyn-phosphorylated CRMP2 (Figure 4.11). Additionally, the CRMP2 SUMOylation motif lies on an accessible surface of the protein in monomeric (Figure 4.11) and tetrameric forms (data not shown). This is important because surface positioning of a SUMOylation consensus sequence is a requirement of SUMOylation. The majority of predicted SUMOylation consensus sequences are *not* SUMOylated and this is likely due to

presence of the motif in internal or buried parts of the protein (Pichler et al., 2005, Henley et al., 2014). For these predicted motifs, the simultaneous occurrence of another post-translational modification, e.g., phosphorylation, may modify the SUMOylation process. The structural context of the SUMOylation process is not yet fully understood, but it is safe to assume that lysine residues that are not surface-exposed will not qualify for SUMOylation Thus, a SUMOylation site is necessary, but not sufficient, for SUMOylation to take place. It is possible that CRMP2 phosphorylation by Fyn at tyrosine-32 modifies the SUMOylation process to bury SUMOylation motif within CRMP2 or that phosphorylation by Cdk5 at serine-522 modifies the SUMOylation process by exposing the motif during CRMP2 phosphorylation-dependent regulation of SUMOylation. An underdeveloped area of SUMOylation research is the participation of SUMOylation E3 ligases and their role in substrate recognition during Ubc9 binding. E3 ligases bind to SUMO-conjugated Ubc9 and function to target SUMOylation to specific substrates. (Flotho and Melchior, 2013). The regulation of CRMP2 SUMOylation by phosphorylation may be facilitated by changes of access to lysine-374 by an, as of yet undescribed, E3 SUMO ligase. SUMOylation of CRMP2 by specific E3 proteins, and not others, would provide yet another layer of regulation to the growing model of CRMP2-mediated Nav1.7 regulation.

UnSUMOylated CRMP2 displays a reduced Nav1.7 binding in CAD cells (Figure 3.9), which I first hypothesized to be the cause of reduced Nav1.7 surface expression. This would be the case if stability of Nav1.7 at the membrane was provided by interaction with CRMP2 and altered interaction shifted Nav1.7 membrane turnover. The data in Chapter 4 demonstrates that recruitment of endocytic machinery by

unSUMOylated CRMP2 aids in CRMP2-mediated Nav1.7 regulation (Figure 4.12). This data now supports an alternate hypothesis in which CRMP2 SUMOylation does not alter CRMP2 affinity for Nav1.7 and the reduced interaction of CRMP2 and Nav1.7 is instead the result of reduced Nav1.7 membrane expression where the interaction between CRMP2 and Nav1.7 occurs. In addition, the requirement of endocytic machinery may explain the dominant positive nature of CRMP2-S522D or CRMP2-Y32F where these CRMP2s do not display enhanced interaction with endocytic machinery regardless of SUMOylation status. This hypothesis should be tested in future works.

CRMP2 phosphorylation by Cdk5 to prevent Nav1.7 endocytosis is an interesting mechanism that may connect CRMP2 regulation of Nav1.7 to painful conditions. In several studies, animals suffering from inflammatory (Yang et al., 2007, Zhang et al., 2014) or neuropathic (Li et al., 2014, Yang et al., 2014) pain displayed increased levels of Cdk5 activity. Intrathecal injection roscovitine, a Cdk5-inhibiting compound, proved effective in alleviating neuropathic pain after chronic compression injury of DRGs (Yang et al., 2014). My work demonstrates the Cdk5 phosphorylation of CRMP2 prevents Nav1.7 internalization. Consequently, Cdk5 activity may bolster Nav1.7 currents in these painful conditions which is prevented by action of roscovitine. Akin to prevention of Nav1.7 currents by expression of CRMP2-S522A plasmid (Figure 4.2 and 4.3), the CRMP2-mediated function of reducing Nav1.7 currents could contribute to the roscovitine mechanism-of-action to provide pain relief.

Fyn activity has been reported to be instrumental in the development of α-amino-3-hydroxy-5-methyl-4-isoxazolepropionic acid (AMPA) and N-methyl-D-aspartate (NMDA) receptor-mediated sensitization to pain (Liu et al., 2014b). In this single study,

expression of a constitutively active Fyn produced mechanical allodynia and thermal hyperalgesia via enhanced expression of these receptors. AMPA and NMDA receptors are located at the post-synaptic membranes of second order neurons within the spinal dorsal horn (Liu et al., 2014b). This study indicates that increased Fyn activity in these cells promotes pain sensitization, whereas my data indicates that increased Fyn activity in DRG cells would restrict pain sensitization. The outcome of Fyn activity on pain is therefore incongruent in these two different cell types. As a result, targeting global Fyn activity could have inconsistent effects on pain behavior.

Interestingly, Fyn activity can activate Cdk5 activity (Uchida et al., 2009). As CRMP2 phosphorylation by either kinase mediates Nav1.7 current densities in opposite directions, this could allow for variable levels of Fyn activity to have opposing effects on Nav1.7. Direct Fyn phosphorylation of CRMP2 reduces Nav1.7 currents, yet Fyn activation of Cdk5, and subsequent activity of Cdk5 on CRMP2, would prevent reduction of Nav1.7 currents (Figure 4.10, *compare Fyn + CRMP2 condition to Fyn + CRMP2-S522D Cdk5-phospho-mimetic*). This relationship, however, is contradicted by data that shows CRMP2 SUMOylation is reduced when Fyn kinase is overexpressed (Figure 4.11). One possible explanation is that when CRMP2 is unSUMOylated and unphosphoryalted by Cdk5, the protein is primed for Fyn phosphorylation. Following Fyn phosphorylation, CRMP2 could become resistant to SUMOylation by presence of the phosphate group on Fyn-targeted tyrosine-32. Then, pY32 must first be removed in order to achieve SUMOylation. By this explanation, in spite of increased cellular Cdk5 activity, CRMP2 could remain unSUMOylated. My data (Figure 4.11) supports this conclusion and could

be further supported by detection of increased Cdk5 activity, but not increased CRMP2 SUMOylation in Fyn overexpressing CAD cells.

Endocytosis of voltage-gated channels is an incompletely described mechanism for sodium channel regulation. It has been demonstrated that Nav1.1, Nav1.2, Nav1.5, Nav1.6, Nav1.7, Nav1.8 and the α, β, and γ epithelial sodium channels (ENaC) all contain PY domains that are targeted by E3 ubiquitin ligases (Staub et al., 2000, Fotia et al., 2004, van Bemmelen et al., 2004, Rougier et al., 2005, Cachemaille et al., 2012, Laedermann et al., 2013a). The same family of nine Nedd4/Nedd4-like E3 ubiquitin ligases targets all of these channels and the interaction occurs between the PY motifs of the channels to the WW protein-interacting domain of the ubiquitin ligases (Fotia et al., 2004). The overexpression of Nedd4/Nedd4-like E3 ubiquitin ligases promotes an internalization of these channels to undefined endocytic compartments (Fotia et al., 2004, van Bemmelen et al., 2004, Rougier et al., 2005). A lack of diversity among E3 ligase-sodium channel interactions is surprising despite the differential expression patterns of sodium channels required for diversity of neuron cell types (Catterall et al., 2005). It is also surprising because Nedd4/Nedd4-like E3 ubiquitin ligases are widely expressed throughout populations of excitable cells (Fotia et al., 2004, Rougier et al., 2005). Therefore, channel endocytosis by Nedd4/Nedd4-like E3 ligases is not the result of affinity between specific combinations of E3 ligases and channels, but instead the result of E3 ligase post translational modification or channel interactions that prevent the channel-E3 ligase interaction.

Examples of blunted endocytosis following E3 modification include phosphorylation of Nedd4/Nedd4-like proteins by serum and glucocorticoid-regulated

kinase 1 (SGK1) and protein kinase B (Akt) to inhibit the endocytosis of ENaCs (Debonneville et al., 2001, Lee et al., 2007) or voltage-dependent potassium channel Kv7.1 (Andersen et al., 2013). Examples where channel endocytosis is prevented include association of ENaCs α–β subunit that has undergone phosphorylation by the G protein-coupled receptor kinase, Grk2 (Dinudom et al., 2004). Through interaction with the modified accessory protein, ENaCs become resistant to ubiquitination and endocytosis. A similar case exists for L-type voltage-gated calcium channels which are resistant to ubiquitination, and therefore endocytosis, when interacting with their β subunit (Altier et al., 2011). As an accessory protein of Nav1.7, SUMOylated CRMP2 may function in a similar capacity to prevent Nav1.7 endocytosis. Studies addressing regulation of VGSC endocytosis are currently lacking.

I demonstrated that inhibition of the proteasome, with the small molecule lactacystin, does not prevent nor enhance CRMP2-mediated Nav1.7 internalization. Therefore, it seems that CRMP2-mediate endocytosis of Nav1.7 does not require protein degradation and that internalized Nav1.7 may eventually be recycled to the cell surface. To further elucidate the process by which Nav1.7 endocytosis is regulated, a time course imaging study could be undertaken using extracellular epitope recognizing Nav1.7 antibodies or a tagged Nav1.7 channel that could track cellular Nav1.7. Co-labeling for Nav1.7 channel protein and various markers of specific endocytic organelles could determine what happens to Nav1.7 during CRMP2-K374A mediated internalization and also provide substantial evidence that the channel is either recycled or degraded.

My studies in this Chapter focused on regulation of Nav1.7 expressed in small diameter DRGs in part because of the high relevance of this cell type to a variety of

painful conditions (Dib-Hajj et al., 2013) but also due to the high fraction of TTX-S currents of the Nav1.7 subtype (Zhang et al., 2013) and endogenous expression of CRMP2 in these cells (Quach et al., 2004, Brittain et al., 2011b). In future studies SUMOylation of CRMP2 and regulation of Nav1.7 should be extended to different neuron types and paired with studies of injured animals. This would help to elucidate the role, if any, of CRMP2-mediated Nav1.7 regulation in pain and would validate targeting of the mechanisms described in Chapter 4 for the treatment of painful conditions.

CHAPTER 5.

CONCLUSION AND DISCUSSION

5.1. Summary and consolidation of a working model of CRMP2-mediated Nav1.7 trafficking

In this thesis I report several novel findings. *First*, I identified a novel interaction partner of Nav1.7, CRMP2. *Second*, I identified a novel modification of CRMP2, the addition of the small ubiquitin like modifier (SUMO). *Third*, I found that SUMOylation, which I showed to occur at lysine 374 of CRMP2, is a molecular switch for CRMP2 regulation of Nav1.7; preventing CRMP2 from being SUMOylated at this residue blunts Nav1.7 surface expression and current densities without affecting kinetic properties of slow inactivation, fast inactivation, or activation. *Fourth*, I reported that CRMP2 expression is necessary for constitutive Nav1.7 currents in CAD cells and in DRG sensory neurons. *Fifth*, I demonstrated that blocking CRMP2 SUMOylation has no effect on a classical function of CRMP2, that of CRMP2-mediated neurite outgrowth. *Sixth*, the reduction in Nav1.7 surface expression and current densities due to interference with CRMP2 modification was not because of increased Nav1.7 translation. *Seventh*, using pharmacological and electrical isolation of VGSC subtypes, I determined that CRMP2 regulates *only* Nav1.7, while sparing other DRG expressed channel subtypes including Nav1.1, Nav1.3, Nav1.6, and Nav1.8 as well as the cardiac Nav1.5 channel. *Eighth*, I determined that CRMP2 SUMOylation was regulated positively by Cdk5 phosphorylation and negatively by Fyn phosphorylation allowing for the interplay between multiple modifications of CRMP2 to choreograph Nav1.7 function. *Finally*, the molecular mechanism by which SUMO-null CRMP2 reduces surface Nav1.7 was discovered to require clathrin-dependent endocytosis involving activity of Numb, Eps15

and Nedd4-2 proteins which, scaffold interactions of endocytosis machinery, initiate endocytosis, and target Nav1.7 for internalization, respectively.

Collectively, my thesis has described CRMP2 as a novel modulator of Nav1.7 endocytosis (Figure 5.1) and has laid deep and broad foundations for the CRMP2 and Nav1.7 trafficking fields. Given the unequivocal link between Nav1.7 activity and human pain, inhibiting CRMP2 SUMOylation represents an attractive therapeutic target for drug discovery, thus spurring translational studies based on my work.

5.2. Discussion of CRMP2-Nav1.7 signaling model and future studies

This thesis work has identified and described many features of CRMP2s regulation of Nav1.7. Like many rewarding projects, new trajectories of experimentation have been uncovered by this work. Given adequate funding and time, the following projects could be considered to further advance the understanding of CRMP2-Nav1.7 signaling. In the next section of potential future studies, I will place my findings on CRMP2 and Nav1.7 trafficking and function in the context of published reports. My thesis and these future studies serve to expand the field of Nav1.7 trafficking and provide novel targets to modulate this channels function in pain.

5.2.1. Role of general cellular SUMOylation and CRMP2 SUMOylation in pain

There are no reports linking SUMOylation to pain. The limited evidence that exists is very circumstantial. For example, some evidence exists linking global SUMOylation rate to the inflammatory disorder rheumatoid arthritis (Meinecke et al., 2007). In rheumatoid

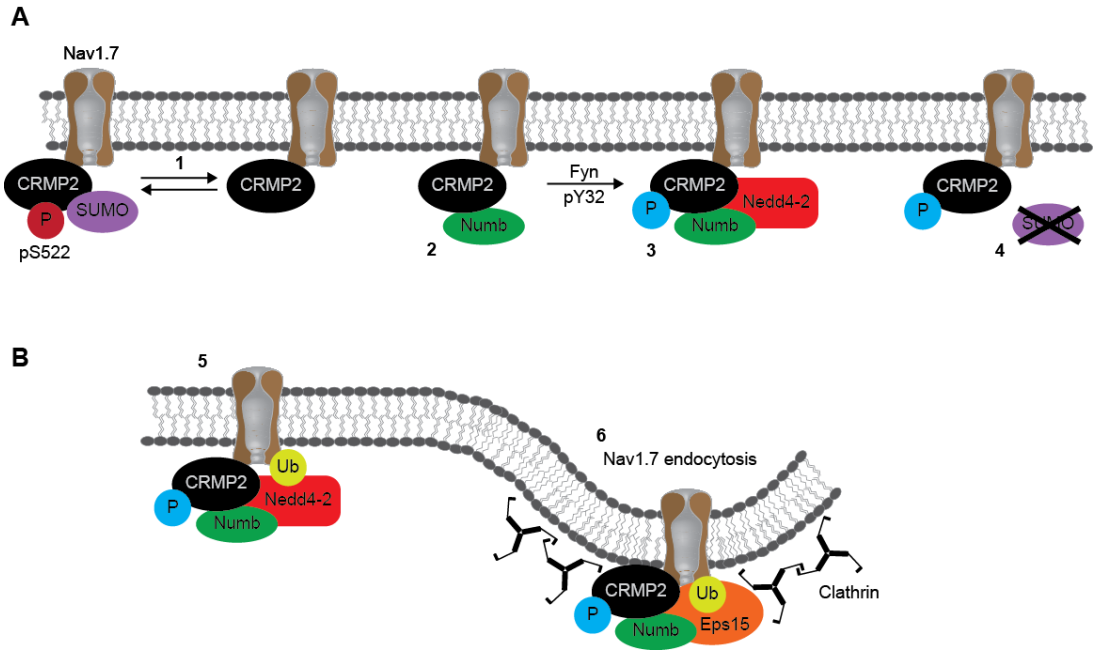

Figure 5.1. Model describing how CRMP2 SUMOylation and phosphorylation co-opt to direct Nav1.7 endocytosis and trafficking. (A) CRMP2 SUMOylation **(1)** is prevented when CRMP2 phosphorylation by Cdk5 at S522 is prevented. UnSUMOylated CRMP2 **(2)** has an enhanced interaction with Numb, and subsequent phosphorylation by Fyn kinase **(3)** allows further recruitment of E3 ubiquitin ligase Nedd4-2. When phosphorylated by Fyn **(4)**, CRMP2 SUMOylation is prevented and when unphosphoryalted by Fyn, effects of loss of CRMP2 SUMOylation are prevented **(B)** Nedd4-2 monoubiquitinates Nav1.7 **(5)** to trigger endocytosis which requires the endocytosis adapter protein Eps15 **(6)**. Incubation of 20 µM Pitstop2 with unSUMOylted CRMP2-K374A expressing DRGs recovers TTX-S currents suggesting that CRMP2-mediated endocytosis of Nav1.7 is clathrin-dependent.

arthritis, SUMO1 expression and increased cellular SUMOylation results in nuclear sequestration of the proapoptotic adaptor molecule death-domain associated protein (DAXX) in synovial fibroblasts of patients.

The mechanism of DAXX sequestration is unknown but it is known to prevent DAXX activity in promoting apoptosis. A resistance of fibroblasts to apoptosis is an underlying cause of chronic inflammation and pain in rheumatoid arthritis. Sequestration of DAXX is relieved by overexpression of the deSUMOylating protein SENP1, following which cell death is restored (Meinecke et al., 2007). Cellular SUMOylation, therefore, could possibly be targeted as a therapy for rheumatoid arthritis relief. A tenuous link to Nav1.7 and rheumatoid arthritis can be surmised from a report describing an enhanced susceptibility to symptomatic knee osteoarthritis and multiple regional pain in patients expressing the Nav1.7 R1150W (Valdes et al., 2011). My findings, along with this limited circumstantial evidence identify a plausible new link between this modification and pain. My data suggests that increased levels of DRG cellular SUMOylation could result in increased CRMP2 SUMOylation, prevent internalization of Nav1.7 to dysregulate channel trafficking, and ultimately cause Nav1.7-mediated pain. It is possible then that increased global SUMOylation serves as a general signal to trigger pain. However, not enough data exists to conclusively support this hypothesis.

One possible link between global SUMOylation and pain involves activation of protein kinase B (or Akt). Following injury, Akt activation is increased where the kinase contributes to cell survival pathways including inactivation of apoptogenic factors (Noshita et al., 2001). Akt activity has recently been implicated in a feed forward process that promotes Akt SUMOylation that further enhances Akt activity. Targets of Akt

include the SUMOylation machinery proteins Ubc9 and SUMO1 and when either is phosphorylated by Akt, total cellular SUMOylation is increased (Lin et al., 2015). As an inactivator of apoptogenic factors (Noshita et al., 2001), this feed forward pathway to enhance global SUMOyaltion is in agreement with the previous example of SUMOylation in rheumatoid arthritis, in which pain is also linked to loss of apoptosis (Meinecke et al., 2007). The data from these publications supports the general idea that increases in Akt phosphorylation and SUMOylation due to enhancement of Akt expression following ischemia and injury (Li et al., 2015) may be linked to general pain pathways. Many examples of injury are also associated with increased Nav1.7 expression including lumbar 5 spinal nerve ligation (Fukuoka et al., 2015), intervertebral disc injury (Sadamasu et al., 2014), sciatic nerve compression (Mukai et al., 2014), and spared nerve injury (ligation of two of three sciatic nerve branches) (Laedermann et al., 2013a). In theory, Akt activation could facilitate global cellular SUMOylation, including that of CRMP2, to prevent endocytosis of Nav1.7 to increase channel surface expression leading to increased sodium currents, hyperexcitability and ultimately, pain.

From my data, I know that CRMP2 SUMOylation can be blocked to reduce Nav1.7 trafficking, but it is not yet known if this reduction can be linked to analgesia or whether dysregulation of CRMP2 SUMOylation may underlie the development of pain behavior. Studies of tissue(s) from injured animals (DRGs, spinal cord etc.) could link Akt activity, global SUMOylation, CRMP2 SUMOylation and CRMP2 regulation of Nav1.7 to pain behaviors. Participation of CRMP2 SUMOylation in the physiological development of pain would also validate the mechanism of CRMP2 SUMOylation as a target for drug development. In my thesis the Nav1.7 currents in isolated DRG cells are

likely at a maximum within my assay for CRMP2 SUMOylation because CRMP2 overexpression did not increase currents above levels seen in cells without exogenous CRMP2. However, given the role of CRMP2 SUMOylation in trafficking Nav1.7, I cannot rule out the possibility that Nav1.7 in other sub-cellular locations including nerve terminals or axons may be increased upon enhancement of CRMP2 SUMOylation. Future studies in the Khanna laboratory will probe these putative relationships by performing a full biochemical workup of tissues between injured and uninjured animals in a model of neuropathic pain in which Nav1.7 had been implicated (Table 5.1). Through probing of dorsal spinal cord (where nociceptive DRG neurons innervate (Black et al., 2012)) and DRGs lysates for levels p-threonine-35 Ubc9 (Lin et al., 2015), phosphorylation of SUMOylation machinery by Akt could be compared. These tissues could be further analyzed for levels of SUMOylated and phosphorylated (particularly by Cdk5 and Fyn) CRMP2 to determine whether CRMP2 is participating in generation of pain by dysregulation of Nav1.7. Any combination of increased CRMP2 SUMOylation, increased Cdk5 phosphorylation, or decreased Fyn phosphorylation would support this link.

This biochemical data of injured tissues could also be paired with DRG whole-cell recordings and transfection of CRMP2-K374A. If an increased Nav1.7 current density in DRGs of injured animals could be prevented by expression of CRMP2-K374A, then this study would serve as a proof-of-principle for targeting CRMP2 SUMOylation to treat pain. For greatest likelihood of success in initial studies, animal models of pain that include Nav1.7-dependent mechanisms should be utilized (Table 5.1).

Type of Model	Induction paradigm	Induction & Onset of pain	Pain Behaviors	Effects on VGSCs	Additional Nav1.7-related functions	References
Early painful diabetic neuropathy	Streptozocin injection	45mg/kg single dose Pain-like behaviors develop within 4 weeks	Mechanical allodynia Thermal hyperalgesia	Nav1.3 + Nav1.6 - Nav1.7 + Nav1.8 -	Increased slow ramp currents (property of Nav1.7)	(Calcutt et al., 1996, Ahlgren et al., 1997, Malcangio and Tomlinson, 1998, Hong et al., 2004)
Chemotherapy induced peripheral neuropathy	Paclitaxel injection	4 alternate day injections of 2mg/kg Pain like behaviors develop within 7-14 days	Mechanical allodynia	Nav1.1 + Nav1.6 + Nav1.7 +	Increased spontaneous DRG activity	(Cavaletti et al., 2000, Dougherty et al., 2004, Reeves et al., 2012, Zhang and Dougherty, 2014)
Inflammatory pain	Carageenan injection	4% in 150ul sterile saline (right plantar hind paw) Pain-like behaviors develop within 4 days	Edema Mechanical allodynia Thermal hyperalgesia	Nav1.3 + Nav1.7 + Nav1.8 +	40% increase in DRG total sodium current	(Iadarola et al., 1988, Black et al., 2004)
Neuropathic	Spared nerve injury	Ligation of common peroneal and tibial branches of the sciatic nerve, sparing of sural nerve Pain-like behaviors develop within 7 days	Mechanical allodynia Increased duration of heat withdrawal	Nav1.7 + Nav1.8 +	Increased 1.7 expression along sciatic nerve but not DRG cell body	(Decosterd and Woolf, 2000, Cachemaille et al., 2012, Laedermann et al., 2013a)

Table 5.1. Animal models of pain behavior affecting Nav1.7.

Another possible link to pain comes from my data on Cdk5. I determined that blocking Cdk5 phosphorylation of CRMP2 enhances Nav1.7 endocytosis and reduces current density. Increased Cdk5 activity has been linked to thermal hyperalgesia following CFA injection and mechanical neuropathic pain following chronic constriction injury (CCI) (Yang et al., 2007, Li et al., 2014, Zhang et al., 2014, Fang et al., 2015). Intrathecal administration of the Cdk5 inhibitor roscovitine prevents mechanical neuropathic by processes attributed to downregulation of NMDA receptors (Yang et al., 2014) and also prevents inflammation-induced thermal hyperalgesia by blocking Cdk5 activation of tumor necrosis factor-α (Fang et al., 2015). As stated earlier, the CRMP2 phospho-null CRMP2-S522A mutant for the CRMP2 site in Cdk5 significantly reduces Nav1.7 currents (see Figure 4.2) while the CRMP2 phospho-mimetic CRMP2-S522D mutant does not exhibit changes in Nav1.7 current (Figure 4.6). Taken together, my data could support a scenario in which Cdk5 sensitized pain states involve a dysregulation of Nav1.7 trafficking brought about by CRMP2. It would be interesting to probe tissues from injured animals both before and after roscovitine treatment to determine if changes to CRMP2 SUMOylation correlate with animal pain behaviors.

In my thesis I did not test how phosphorylation by Cdk5 or loss of phosphorylation by Fyn is dominant over CRMP2 SUMOylation. These phosphorylation statuses effectively block the phenotype of reduced Nav1.7 current associated with non-SUMOylated CRMP2. Therefore, these modifications could be responsible for regulating onset of rodent or human pain behavior. I hypothesize that dominance of these phosphorylation events is endowed by requirement of CRMP2 interaction with endocytic proteins Numb, Eps15, and Nedd4-2 for endocytosis of Nav1.7. Should dominant

modifications prevent CRMP2 interactions with endocytic proteins, it would sufficiently explain the lack of effect by non-SUMOylated CRMP2.

5.2.2. Targeting CRMP2 SUMOylation for possible therapeutic relief of pain

To develop my data on the importance of CRMP2 SUMOylation to Nav1.7 and then to link it possibly to animal pain behavior, I propose a series of experiments designed to mimic CRMP2 deSUMOylation to achieve a reduction in Nav1.7. This can be done by overexpression of the SUMO-null CRMP2-K374A in the DRGs of injured animals. While viral strategies may be advantageous here, using a non-viral transfection, CRMP2-K374A expression could be introduced to the DRGs of injured animals likely via a lumbar puncture or via an intrathecal route to the dorsal spinal cord or direct injection into DRGs. If successful, this strategy would permit expression in the superficial lamina layer I of the dorsal spinal cord where DRGs project to (Black et al., 2012). This may be achievable using either lipid– (for example, Turbofect, Life Technologies) or polyethylenimine–complexed DNA transfection techniques which have shown efficacy when transfecting spinal cord tissue *in vivo* (Yao et al., 2012). By forcing expression of CRMP2-K374A after injury, a potential reversal of pain in response to CRMP2-K374A expression may be possible. Success of this strategy would provide proof-of-concept for further studies investigating CRMP2 SUMOylation as a novel pharmacological target for pain and could be paired with biochemistry and patch clamp methods to correlate behavior with alterations in level of CRMP2 SUMOylation and Nav1.7 currents. Failure of this experiment to correlate pain behavior and loss of CRMP2 SUMOylation could occur if dominant positive CRMP2 phosphorylation by Fyn or Cdk5

is present. In this case it may be required to modulate both SUMOylation and phosphorylation for desired therapeutic benefit. Repeating behavior experiments with *in vivo* administration of CRMP2-K374A *prior* to the injury could help assess if CRMP2 SUMOylation mediated Nav1.7 activity is important in the development of pain states.

I have shown in this thesis that CRMP2 modulation of neurite outgrowth is not affected by CRMP2 SUMOylation. However, CRMP2 is a promiscuous protein with many functions in neurons (Khanna et al., 2012). Some of these functions regulate other ion channels that, like Nav1.7, can alter neuronal activity, i.e. NR2B subunit (Bretin et al., 2006), and Cav2.2 (Brittain et al., 2012). A role, if any, for CRMP2 SUMOylation in regulating these proteins has not yet been described. To validate CRMP2 SUMOylation as a *druggable target* for regulation of Nav1.7 with minimal off-target effects, the role of CRMP2 SUMOylation in these and other functions of CRMP2 will need to be analyzed. One important consideration in targeting CRMP2 SUMOylation is that the CRMP2 SUMOylation motif, centered at lysine-374, conforms to the typical SUMOylation consensus motif. Therefore, pharmacological targeting of CRMP2 SUMOylation will need to only interfere with CRMP2 SUMOylation and no other targets of SUMOylation to avoid disrupting turnover of total cellular SUMOylation.

5.2.3. Addressing specificity in regulation of Nav.x by CRMP2 and possibly other CRMPs

A major finding of my thesis is that CRMP2 SUMOylation is a specific regulator of Nav1.7. By pharmacological and electrical isolation of current from endogenous

VGSC subtypes in DRGs, I determined that only Nav1.7 channels are affected (see Figures 3.6 and 3.8). Nav1.7 is a high-value target for the development of pain therapeutics. Thus, this remarkable specificity for Nav1.7 is a highly desirable characteristic of a drug target due to the established role of Nav1.7 in human painful conditions (Dib-Hajj et al., 2013) and also to avoid effects of targeting central nervous system, skeletal muscle, or cardiac expressed VGSC subtypes (Catterall et al., 2005). The molecular determinants of CRMP2 specificity for Nav1.7 were not determined in my thesis.

Due to shared relationship between the majority of VGSCs (Nav1.1, Nav1.2, Nav1.5, Nav1.6, Nav1.7, Nav1.8) and the Nedd4/Nedd4-like E3 ubiquitin ligase family responsible for their endocytosis (Fotia et al., 2004, van Bemmelen et al., 2004, Abriel and Staub, 2005, Rougier et al., 2005), I predict that specificity of CRMP2 regulation for Nav1.7 is not determined by regulation of the endocytic machinery. Instead, I propose that specific regulation of Nav1.7 by CRMP2 is due to the specific affinity of CRMP2 for this Nav1.7 subtype. CRMP2 modulation of Nav1.7 currents was dependent on both CRMP2 expression, CRMP2 SUMOylation, and CRMP2 phosphorylation. Enhanced interaction of CRMP2 with endocytic machinery upon loss of SUMOylation readily explains the dependence on SUMOylation, but this was not further interrogated in this thesis. A possible scenario to explain dependence of Nav1.7 endocytosis on CRMP2 expression is CRMP2 antagonism of Nav1.7 interaction with Nedd4-2 when CRMP2 is SUMOylated. When CRMP2 is not present at the membrane, Nedd4-2 may interact with Nav1.7 by a CRMP2-independent mechanism and recovery of CRMP2 expression would render the channel resistant to ubiquitination and endocytosis. Interactions of L-type

voltage-gated calcium channels and Kv7.1 voltage-gated potassium channels with their respective β subunits are examples where accessory proteins antagonize ubiqutination of channels (Altier et al., 2011, Andersen et al., 2013).

Identification of domains involved in the CRMP2-Nav1.7 interaction could be used as a basis of comparison to advance the mechanistic understanding of CRMP2 regulation of Nav1.7 and also investigate potential regulation of other VGSCs by other CRMP family member proteins. CRMP2 binding to Nav1.7 but lack of binding (or weak binding) to other VGSC subtypes may explain the specificity of action observed in my work. Alternatively, another protein that preferentially binds Nav1.7 maybe involved, which, in concert with CRMP2 SUMOylation, regulates Nav1.7. These possibilities were not studied in my thesis but should form the basis of future studies, as identifying the nature of how specificity of targeting Nav1.7 is achieved is very exciting and potentially highly translationally relevant.

CRMPs are a family of five proteins (Khanna et al., 2012). In DRGs, expression of CRMP4 is very low in naïve conditions, but significantly increases following sciatic nerve axotomy (Jang et al., 2010). As my data places CRMP2 as a determinant of Nav1.7 trafficking in DRGs (Figure 3.2), it would be interesting if CRMP4 could participate similarly following axotomy. An analysis of CRMP4 SUMOylation status and its effect on Nav1.7 trafficking in DRGs using a CRMP4-K374A mutant would allow for such a determination. If CRMP4 does not interact with Nav1.7 then a comparison of the homology between CRMP2 and CRMP4 could serve as a starting point to determine what sequences of CRMP2 are involved in interaction with Nav1.7.

CRMP2 likely interacts with intracellular domains of Nav1.7 as CRMP2 is a cytosolic protein (Khanna et al., 2012). To identify Nav1.7 domains responsible for CRMP2-Nav1.7 interaction, tagged intracellular domains of Nav1.7 could be expressed in a heterologous cell line and probed for interaction with CRMP2. A CRMP2 immunopreciptation followed by immunoblotting with an antibody versus the tag motif would determine which domains of Nav1.7 interact with CRMP2. The five major intracellular domains of Nav1.7, the N-terminus, L1, L2, and L3 loops, and C-terminus, have been made available to the Khanna lab as part of a collaboration to perform such a study (Stamboulian et al., 2010). Other shorter pieces of the intracellular loops could also be tested. An alternative strategy would require identification of a VGSC subtype that does not interact with CRMP2. For example, assume Nav1.2 does not bind CRMP2. Then, a Nav1.7-Nav1.2 chimeric channel could be produced by substituting domains of Nav1.7 for domains of Nav1.2. Following expression in empty HEK293 cells, interaction of the chimera with CRMP2 and effect of CRMP2-K374A on current density could be probed with biochemical and electrophysiological techniques, respectively. Following identification of specific domain chimeras that prevent CRMP2-Nav1.7 regulation or interaction, smaller and smaller regions, i.e. 50 or 10 amino acid segments could be substituted until the specific channel regions required for CRMP2 binding are identified.

CRMP2-Nav1.7 interaction could also be studied using a peptide spot blot of the Nav1.7 intracellular domains or CRMP2. The spot blot could then be probed with the opposite protein, purified CRMP2 protein, or channel fragments. Such a strategy was previously used in the Khanna laboratory to define interacting domains between CRMP2 and the voltage-gated calcium channel Cav2.2 (Brittain et al., 2011b). By producing

overlapping 15 amino acid segments of Nav1.7 intracellular domains, the residues of Nav1.7 involved in CRMP2 binding could be identified. By flipping the spots blot to probe CRMP2 peptides against Nav1.7 domains, interacting residues on the surface of CRMP2 could be identified. The CRMP2 SUMOylation motif (4 residues) centered on lysine-374 is perfectly homologous to other CRMPs and the flanking sequences (14 residues) is between 71.4% and 92.9% homologous to other CRMPs (as elaborated in Chapter 3.3). Additionally, the C-terminal domains of Nav1.1, Nav1.2, Nav1.3, Nav1.5, Nav1.6 Nav1.7, and Nav1.8 all contain an ubiquitin E3 ligase targeted PY domain (Fotia et al., 2004, Rougier et al., 2005). This suggests that if other CRMPs can bind VGSCs, SUMOylation of these CRMPs and endocytosis of these VGSCs may occur in a mechanism similar to CRMP2 and Nav1.7. Study of CRMP family proteins and VGSCs could progress as in this thesis and aim to identify endogenous SUMOylation of the other CRMPs which can then be combined with co-expression studies with SUMO-null CRMP.x variants with VGSC subtypes in heterologous cell lines. The most promising of these that exhibit Nav current reductions could then be recapitulated in primary cell culture based on the overlapping expression patterns of CRMPs and VGSCs in the nervous system (Quach et al., 2000, Bretin et al., 2005, Catterall et al., 2005, Jang et al., 2010, Tsutiya and Ohtani-Kaneko, 2012).

In addition to voltage-gated sodium channels, similarly structured voltage-gated calcium channels are candidates for regulation by CRMP2 SUMOylation. Cav2.2 is demonstrated to interact with CRMP2 (Brittain et al., 2012). This means that if regulation of Nav1.7 by CRMP2 is governed strictly by CRMP2 interaction with the channel, there is no obstacle for similar regulation of Cav2.2. If CRMP2 regulation of Nav1.7 is instead

derived from a CRMP2-Numb interaction, it is possible that CRMP2-Numb interaction is dependent on participation of Nav1.7 but does not occur for Cav2.2. This scenario could explain subtype specificity observed within the large family of similarly structured ion channels.

5.2.4. Role of CRMP2 SUMOylation on DRG excitability and Nav1.7 in non-nociceptive neurons

As a functional readout of neuron activity, DRG excitability is intimately linked to Nav1.7 activity and increases of activity correlate to pain-like behavior in animal models. The Nav1.7-I739V mutation causes a doubling of action potentials and represents a case where altered Nav1.7 is the sole determinant of neuropathic pain condition, small fiber neuropathy, in human patients with the mutation (Han et al., 2012). Examples of Nav1.7 mediated enhancement of DRG excitability and pain are numerous and involve channel mutations underlying paroxysmal extreme pain disorder and inherited erythromelalgia in addition to small fiber neuropathy (overview of mutations in (Dib-Hajj et al., 2013)). Chronic inflammatory pain can also produce increases to nociceptive C-fiber excitability (Weng et al., 2012).

In addition to excitability driven by Nav1.7 in DRGs, recent evidence from John Woods' group supports a role of non-nociceptor Nav1.7 currents in pain behavior. Nav1.7 knockout mice require deletion from sympathetic neurons, in addition to DRGs, to prevent neuropathic pain behavior (Minett et al., 2012). A different animal behavior study recapitulated this finding in wildtype mice by showing that blocking sympathetic

nerve activity after injury recovers baseline pain behavior (Iwase et al., 2012). Blocking of sympathetic nerve activity also produced reduced DRG excitability indicating that communication between neuronal subpopulations is involved during development of neuropathic pain. Therefore, electrophysiological analysis of CRMP2-mediated Nav1.7 regulation is warranted in sympathetic neurons. A common regulation of Nav1.7 by CRMP2 in both DRGs and sympathetic neurons would extend the efficacy of CRMP2-targted pain therapies to non-nociceptor mediated pain states, including neuropathic pain.

In a continuation of my thesis work by the Khanna laboratory, Dr. Yuying Wang and Dr. Xiaofang Yang have collected excitability data from DRG neurons expressing wildtype CRMP2, CRMP2-K374A, and CRMP2-S522A (Figure 5.2). Compared to wildtype CRMP2 expressing DRGs, a significant decrease in the number of action potentials was observed in cells expressing CRMP2-K374A and CRMP2-S522A (Figure 5.2B) as well as an increased rheobase value for CRMP2-S522A expressing cells (Figure 5.2C). This change to rheobase for CRMP2-S522A expressing cells but not CRMP2-K374A expressing cells may indicate that CRMP2-S522A affects additional VGSC subtypes or gating properties compared to CRMP2-K374A. This will be elucidated in future studies and may reveal that CRMP2 SUMOylation is a better *druggable target* than CRMP2 phosphorylation by Cdk5 due to greater specificity for effect on only Nav1.7 current density. The resting membrane potential was not different between any conditions (Figure 5.2D). These data suggest that CRMP2 mutants, that reduce Nav1.7 currents, also reduce DRG excitability. This exciting result allows prediction that CRMP2 mediated reduction of Nav1.7 surface expression would be beneficial in treating painful conditions where Nav1.7 induced DRG hyperexcitability is the underlying cause of pain.

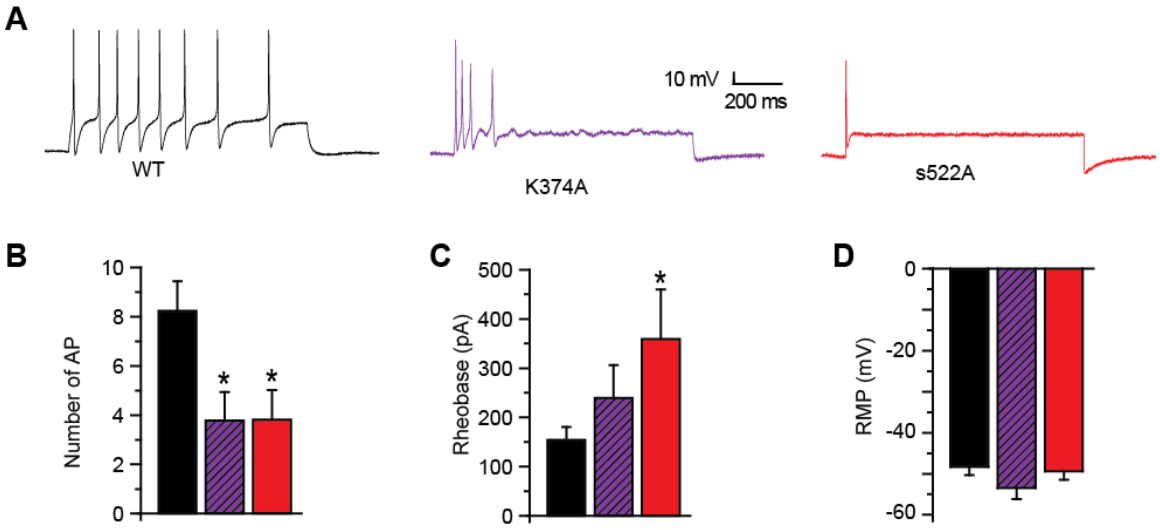

Figure 5.2. CRMP2-K374A and CRMP2-S522A reduce DRG excitability. **(A)** Representative voltage responses to current injection of CRMP2, CRMP2-K374A, and CRMP2-S522A expressing small DRGs. **(B)** The average number of action potentials in response to 1 second of current injection was reduced by CRMP2-K374A (*purple*) or CRMP2-S522A (*red*) expression. **(C)** Rheobase, the amplitude of current required to provoke an action potential, was significantly increased in CRMP2-S522A (*red*), but not CRMP2-K374A (*purple*) expressing DRGs. **(D)** The resting membrane potential, which when depolarized can induce hyperexcitability of DRGs, was unchanged between conditions. Errors are SEM. Asterisks indicate statistically significant differences compared to all other conditions ($p < 0.05$, one-way ANOVA with Tukey's post-hoc; n=11–17). Experiment performed by Drs. Xiaofang Yang and Yuying Wang, postdoctoral associates in the Khanna laboratory.

The regulation of Nav1.7 via CRMP2-regulated trafficking may provide benefits compared to the more common strategy of channel antagonism. In a case where Nav1.7 turnover is regulated by channel activity, a typical agonist may lead to upregulation of Nav1.7 surface expression due to prevention of activity. Then upon termination of treatment neurons may be sensitized or continued treatment may require higher doses. An example of this is morphine treatment for pain where sodium currents are potentiated by morphine-3-glucuronide, a morphine metabolite (Due et al., 2014). Targeting Nav1.7 trafficking would prevent this complication by controlling the neurons potential for activity, not only the neurons current ability to produce activity. By the same logic, CRMP2-regualted trafficking of Nav1.7 could be paired with conventional Nav1.7 channel antagonism to dramatically enhance efficacy of these strategies.

5.2.5. Does CRMP oligomerization affect Nav1.7 trafficking and current density?

CRMP family proteins form tetramers with self and non-self CRMP monomers (Wang and Strittmatter, 1997b). Formation of tetramers occurs *in vivo* as evident by 250 kDa CRMP immunoreactivity following size exclusion chromatography. This value is exactly 4x greater than the 62kDa mass of CRMP monomers. In solution, individual CRMP proteins display different dispositions to form homotetramers as a function of protein concentration (Ponnusamy and Lohkamp, 2013). As concentration increases, CRMP propensity to form tetramers also increases. These *in vitro* experiments showed that CRMP1 is found in roughly equal fractions of monomer and homotetramers, CRMP2 is found primarily in homotetramers, and CRMP5 is found exclusively in monomers (Ponnusamy and Lohkamp, 2013). CRMP2 displayed the greatest increase of

tetramerization as a function of protein concentration. The formation of heterotetramers was described to occur between non-conserved residues, and as a result heterotetramers are more favorable conformations than homotetramers *in vivo* (Ponnusamy and Lohkamp, 2013). However, functions of CRMP2 monomers versus CRMP2 in homo or heterotetramers remain largely understudied.

An example of how oligomerization may affect CRMP-mediated functions is illustrated by studies on CRMP5, the most distantly related CRMP member. The CRMP family member protein, CRMP5, has been shown to antagonize the effects of CRMP2 on neurite outgrowth. Following GSK3β-mediated threonine-516 phosphorylation of CRMP5 (Brot et al., 2014), CRMP5 competes with CRMP2 for tubulin binding which results in block of CRMP2-mediated outgrowth (Brot et al., 2010). The overexpression of CRMP2 is unable to recover outgrowth of hippocampal neurons when CRMP5 is expressed suggesting that CRMP5 is dominant over the effects of CRMP2 in this function (Brot et al., 2010). Based on this relationship between CRMPs, it seems possible that expression of CRMP family proteins, or CRMP heterotetramerization with CRMP2 might modulate CRMP2s regulation of Nav1.7. To test these possibilities, CRMP proteins (e.g., CRMP5) could be co-expressed in CAD cells with wildtype CRMP2 or CRMP2-K374A. This would uncover any changes to CRMP2-mediated Nav1.7 regulation induced by the presence of other CRMPs. Intriguingly, because CRMP5 antagonizes CRMP2 function, it is tempting to speculate that its assembly within a CRMP heteromer might by itself be sufficient to regulate Nav1.7. Moreover, if CRMP5 associates with the SUMO-null CRMP2-K374A, then perhaps the Nav1.7 current

reduction imposed by the homomeric CRMP2-K374A may be nullified by a heteromeric CRMP5-CRMP2-K374A protein.

There is only a single report of a CRMP2 function being ascribed to a specific oligomeric form of CRMP2, the facilitation of tubulin heterodimerization by CRMP2 monomers, and no studies have ascribed a specific role for CRMP2 tetramers (Fukata et al., 2002b). The authors used sucrose density gradient centrifugation to demonstrate that the purified CRMP2 and tubulin was 162.2 kDa in molecular weight which corresponded to a tubulin heterodimer (α tubulin = 52.2 kDa plus β tubulin = 49.9 kDa) plus a CRMP2 monomer of ~60 kDa (Fukata et al., 2002b). In early studies of VGSCs, channel-binding toxins were used to purify channels from brain (Talvenheimo et al., 1982). If a Nav1.7 specific toxin like Huwentoxin-IV (Xiao et al., 2010) or Protox-II (Schmalhofer et al., 2008) were used to purify Nav1.7 from DRG or peripheral nerves, a similar sucrose density gradient centrifugation experiment could be performed to identify the weight of the CRMP2-Nav1.7 complex. A weight of ~310 kDa would indicate Nav1.7 interacts with a single CRMP2 monomer, whereas a weight of ~500 kDa would indicate Nav1.7 interaction with a CRMP2 tetramer. A control for this study would be identification of CRMP2 tetramerization in the absence of Nav1.7 which can be induced by divalent cations calcium or magnesium (Ponnusamy and Lohkamp, 2013).

Another experiment to test the effects of CRMP2 tetramerization on Nav1.7 hinges on development of a small molecule inhibitor of CRMP2 SUMOylation as well as identification of a CRMP protein that does not interact with Nav1.7. In these cases, CRMP2 could be co-expressed in CAD cells with varying levels of a second CRMP family protein to identify effects of CRMP tetramerization on CRMP2 mediated Nav1.7

endocytosis. As an example, one could compare transfection of 1 µg CRMP2 and 1 µg CRMP1 versus 1 µg CRMP2 and 4 µg CRMP1 under the assumption that CRMP1 does not display affinity for Nav1.7. Then at higher levels of CRMP1 expression, CRMP2 will have tendency to associate into tetramers that contain less CRMP2. Application of a small molecule inhibitor of CRMP2 SUMOylation to these cells could then reveal alterations in Nav1.7 trafficking. A concentration within the linear range of effects versus concentration near the IC50 would best allow for identification of altered efficacy. If the CRMP2 ratio in tetramers is not important for regulation of Nav1.7 then each condition will display equivalent current densities. However, if presence of multiple CRMP2 copies within a tetramer is required for Nav1.7 internalization, then higher expression of CRMP1 will blunt the effect of the small molecule inhibitor.

5.2.6. Identification of additional regulators/partners of CRMP2-Nav1.7 signaling

My studies identified Numb, Eps15 and Nedd4-2 as proteins required for Nav1.7 internalization through interactions by CRMP2. The link between these proteins and the mechanism of endocytosis was supported by previous literature that established an interaction of Numb with CRMP2 (Nishimura et al., 2003a, Arimura et al., 2005) and dysregulation of Nav1.7 surface expression to reduced Nedd4-2 expression (Laedermann et al., 2013a). CRMP2 regulation of Nav1.7 is determinant on both CRMP2 expression and CRMP2 SUMOylation. CRMP2 SUMOylation status readily explains the facilitation of Nav1.7 endocytosis by the identified binding partners Numb, Eps15, and Nedd4-2. In the section 5.2.3 I hypothesize that CRMP2 expression may determine Nav1.7 expression

by antagonism of channel ubiquitination. Such a mechanism could involve channel interaction with SUMOylated CRMP2 or non-Fyn-phosphorylated CRMP2. The mechanism(s) by which CRMP2 SUMOylation and phosphorylation co-opt recruitment of endocytic proteins and by which CRMP2 expression maintains Nav1.7 surface expression may rely on participation of additional protein partners.

Identification of additional protein partners of CRMP2 and/or Nav1.7 could kick-start a search for proteins and mechanisms that serve this function. This could be accomplished by quantitative mass spectrometry of CRMP2 from empty HEK293 cells versus HEK293 cells expressing Nav1.7 with CRMP2. Then, any changes to CRMP2-interacting proteins would be dependent on CRMP2 interaction with the channel. A reciprocal experiment would involve quantitative mass spectrometry of Nav1.7 from cells where CRMP2 expression was depleted by siRNA or enhanced by overexpression plasmids.

The VGSC accessory protein β2 is an identified binding partner of Nav1.7 and plays an important role in channel forward trafficking. This has been shown in β2-null mice that display reduced Nav1.7 protein expression, decreased TTX-S current densities, and decreased thermal and inflammatory pain thresholds (Lopez-Santiago et al., 2006). Whether this subunit is synergistic or competitive in CRMP2 regulation of the channel is unknown. The first identification of beta subunits noted that they interacted only with mature membrane expressed channels positing a role for these auxiliary subunits in biogenesis and trafficking (Schmidt and Catterall, 1986). If CRMP2 interaction with immature Nav1.7 enhances Nav1.7 interaction with β2 subunits, it could explain the Nav1.7 forward trafficking properties observed in response to changing CRMP2

expression. Additionally, β2 interaction with surface expressed Nav1.7 could alter channel ubiquitination either by CRMP2-dependent or -independent mechanisms. In addition to new CRMP2-interacting proteins, CRMP2 SUMOylation may also be regulated by other modifications of CRMP2. I have described interplay between CRMP2 SUMOylation and phosphorylation, but CRMP2 also undergoes glycosylation and oxidation which have not yet been studied in combination with CRMP2 SUMOylation (Morinaka et al., 2011, Khanna et al., 2012).

Elaboration of these mechanisms, and completion of other studies listed in Chapter 5, will build upon the data presented in this thesis to expand the molecular mechanism(s) by which CRMP2 regulates Nav1.7. It is my fervent hope that these studies will also spur the translation of CRMP2-mediated Nav1.7 regulation for the eventual treatment of human pain. Given animal behavior data demonstrating complete lack of inflammatory and chronic pain following Nav1.7 knockout under *Wnt1* promotor (Minett et al., 2012, Minett et al., 2014a), I propose that CRMP2-medaited trafficking of Nav1.7 could be targeted to treat a wide variety of human pain conditions, including those where efficacy of currently available drugs is limited.

CHAPTER 6.

REFERENCES

Abriel H, Staub O (2005) Ubiquitylation of ion channels. Physiology 20:398-407.

Ahlgren SC, Wang JF, Levine JD (1997) C-fiber mechanical stimulus-response functions are different in inflammatory versus neuropathic hyperalgesia in the rat. Neuroscience 76:285-290.

Ahn HS, Black JA, Zhao P, Tyrrell L, Waxman SG, Dib-Hajj SD (2011) Nav1.7 is the predominant sodium channel in rodent olfactory sensory neurons. Molecular pain 7:32.

Ahn HS, Vasylyev DV, Estacion M, Macala LJ, Shah P, Faber CG, Merkies IS, Dib-Hajj SD, Waxman SG (2013) Differential effect of D623N variant and wild-type Na(v)1.7 sodium channels on resting potential and interspike membrane potential of dorsal root ganglion neurons. Brain research 1529:165-177.

Al-Hallaq RA, Conrads TP, Veenstra TD, Wenthold RJ (2007) NMDA di-heteromeric receptor populations and associated proteins in rat hippocampus. J Neurosci 27:8334-8343.

Alkuraya FS, Saadi I, Lund JJ, Turbe-Doan A, Morton CC, Maas RL (2006) SUMO1 haploinsufficiency leads to cleft lip and palate. Science 313:1751.

Altier C, Garcia-Caballero A, Simms B, You H, Chen L, Walcher J, Tedford HW, Hermosilla T, Zamponi GW (2011) The Cavbeta subunit prevents RFP2-mediated ubiquitination and proteasomal degradation of L-type channels. Nature neuroscience 14:173-180.

Andersen MN, Krzystanek K, Petersen F, Bomholtz SH, Olesen SP, Abriel H, Jespersen T, Rasmussen HB (2013) A phosphoinositide 3-kinase (PI3K)-serum- and glucocorticoid-inducible kinase 1 (SGK1) pathway promotes Kv7.1 channel surface expression by inhibiting Nedd4-2 protein. The Journal of biological chemistry 288:36841-36854.

Antzelevitch C, Nesterenko V, Shryock JC, Rajamani S, Song Y, Belardinelli L (2014) The role of late I Na in development of cardiac arrhythmias. Handbook of experimental pharmacology 221:137-168.

Arimura N, Inagaki N, Chihara K, Menager C, Nakamura N, Amano M, Iwamatsu A, Goshima Y, Kaibuchi K (2000a) Phosphorylation of collapsin response mediator protein-2 by Rho-kinase. Evidence for two separate signaling pathways for growth cone collapse. The Journal of biological chemistry 275:23973-23980.

Arimura N, Inagaki N, Chihara K, Menager C, Nakamura N, Amano M, Iwamatsu A, Goshima Y, Kaibuchi K (2000b) Phosphorylation of collapsin response mediator protein-2 by Rho-kinase. Evidence for two separate signaling pathways for growth cone collapse. JBiolChem 275:23973-23980.

Arimura N, Kimura T, Nakamuta S, Taya S, Funahashi Y, Hattori A, Shimada A, Ménager C, Kawabata S, Fujii K, Iwamatsu A, Segal RA, Fukuda M, Kaibuchi K (2009) Anterograde Transport of TrkB in Axons Is Mediated by Direct Interaction with Slp1 and Rab27. Developmental Cell 16:675-686.

Arimura N, Menager C, Kawano Y, Yoshimura T, Kawabata S, Hattori A, Fukata Y, Amano M, Goshima Y, Inagaki M, Morone N, Usukura J, Kaibuchi K (2005) Phosphorylation by Rho kinase regulates CRMP-2 activity in growth cones. Molecular and cellular biology 25:9973-9984.

Armstrong CM (1981) Sodium channels and gating currents. Physiological reviews 61:644-683.

Astle MV, Ooms LM, Cole AR, Binge LC, Dyson JM, Layton MJ, Petratos S, Sutherland C, Mitchell CA (2011) Identification of a proline-rich inositol polyphosphate 5-phosphatase (PIPP)*collapsin response mediator protein 2 (CRMP2) complex that regulates neurite elongation. J Biol Chem 286:23407-23418.

Bagal SK, Chapman ML, Marron BE, Prime R, Storer RI, Swain NA (2014) Recent progress in sodium channel modulators for pain. Bioorganic & medicinal chemistry letters 24:3690-3699.

Barford D, Das AK, Egloff MP (1998) The structure and mechanism of protein phosphatases: insights into catalysis and regulation. Annual review of biophysics and biomolecular structure 27:133-164.

Barnes S, Hille B (1988) Veratridine modifies open sodium channels. The Journal of general physiology 91:421-443.

Bayer P, Arndt A, Metzger S, Mahajan R, Melchior F, Jaenicke R, Becker J (1998) Structure determination of the small ubiquitin-related modifier SUMO-1. Journal of molecular biology 280:275-286.

Becker J, Barysch SV, Karaca S, Dittner C, Hsiao HH, Berriel Diaz M, Herzig S, Urlaub H, Melchior F (2013) Detecting endogenous SUMO targets in mammalian cells and tissues. Nature structural & molecular biology 20:525-531.

Bendahhou S, Cummins TR, Potts JF, Tong J, Agnew WS (1995) Serine-1321-independent regulation of the mu 1 adult skeletal muscle Na+ channel by protein kinase C. Proceedings of the National Academy of Sciences of the United States of America 92:12003-12007.

Beneski DA, Catterall WA (1980) Covalent labeling of protein components of the sodium channel with a photoactivable derivative of scorpion toxin. Proceedings of the National Academy of Sciences of the United States of America 77:639-643.

Bennett DL, Woods CG (2014) Painful and painless channelopathies. The Lancet Neurology 13:587-599.

Benson M, Iniguez-Lluhi JA, Martens J (2009) SUMO Modification of Ion Channels. In: SUMO Regulation of Cellular Processes (Wilson, V. G., ed), pp 117-136: Springer Science+Business Media.

Benson MD, Li QJ, Kieckhafer K, Dudek D, Whorton MR, Sunahara RK, Iniguez-Lluhi JA, Martens JR (2007) SUMO modification regulates inactivation of the voltage-gated potassium channel Kv1.5. ProcNatlAcadSciUSA 104:1805-1810.

Beyreuther B, Callizot N, Stohr T (2006) Antinociceptive efficacy of lacosamide in a rat model for painful diabetic neuropathy. European journal of pharmacology 539:64-70.

Black JA, Frezel N, Dib-Hajj SD, Waxman SG (2012) Expression of Nav1.7 in DRG neurons extends from peripheral terminals in the skin to central preterminal branches and terminals in the dorsal horn. Molecular pain 8:82.

Black JA, Liu S, Tanaka M, Cummins TR, Waxman SG (2004) Changes in the expression of tetrodotoxin-sensitive sodium channels within dorsal root ganglia neurons in inflammatory pain. Pain 108:237-247.

Black JA, Nikolajsen L, Kroner K, Jensen TS, Waxman SG (2008) Multiple sodium channel isoforms and mitogen-activated protein kinases are present in painful human neuromas. Annals of neurology 64:644-653.

Black JA, Waxman SG (2013) Noncanonical roles of voltage-gated sodium channels. Neuron 80:280-291.

Boddy MN, Howe K, Etkin LD, Solomon E, Freemont PS (1996) PIC 1, a novel ubiquitin-like protein which interacts with the PML component of a multiprotein complex that is disrupted in acute promyelocytic leukaemia. Oncogene 13:971-982.

Bohren KM, Nadkarni V, Song JH, Gabbay KH, Owerbach D (2004) A M55V polymorphism in a novel SUMO gene (SUMO-4) differentially activates heat shock transcription factors and is associated with susceptibility to type I diabetes mellitus. The Journal of biological chemistry 279:27233-27238.

Bossis G, Melchior F (2006) Regulation of SUMOylation by reversible oxidation of SUMO conjugating enzymes. Molecular cell 21:349-357.

Brackenbury WJ (2012) Voltage-gated sodium channels and metastatic disease. Channels 6:352-361.

Brackenbury WJ, Calhoun JD, Chen C, Miyazaki H, Nukina N, Oyama F, Ranscht B, Isom LL (2010) Functional reciprocity between Na+ channel Nav1.6 and beta1 subunits in the coordinated regulation of excitability and neurite outgrowth. Proceedings of the National Academy of Sciences of the United States of America 107:2283-2288.

Bretin S, Reibel S, Charrier E, Maus-Moatti M, Auvergnon N, Thevenoux A, Glowinski J, Rogemond V, Premont J, Honnorat J, Gauchy C (2005) Differential expression of CRMP1, CRMP2A, CRMP2B, and CRMP5 in axons or dendrites of distinct neurons in the mouse brain. The Journal of comparative neurology 486:1-17.

Bretin S, Rogemond V, Marin P, Maus M, Torrens Y, Honnorat J, Glowinski J, Premont J, Gauchy C (2006) Calpain product of WT-CRMP2 reduces the amount of surface NR2B NMDA receptor subunit. J Neurochem 98:1252-1265.

Brittain JM, Chen L, Wilson SM, Brustovetsky T, Gao X, Ashpole NM, Molosh AI, You H, Hudmon A, Shekhar A, White FA, Zamponi GW, Brustovetsky N, Chen J, Khanna R (2011a) Neuroprotection against traumatic brain injury by a peptide derived from the collapsin response mediator protein 2 (CRMP2). The Journal of biological chemistry 286:37778-37792.

Brittain JM, Duarte DB, Wilson SM, Zhu W, Ballard C, Johnson PL, Liu N, Xiong W, Ripsch MS, Wang Y, Fehrenbacher JC, Fitz SD, Khanna M, Park CK, Schmutzler BS, Cheon BM, Due MR, Brustovetsky T, Ashpole NM, Hudmon A, Meroueh SO, Hingtgen CM, Brustovetsky N, Ji RR, Hurley JH, Jin X, Shekhar A, Xu XM, Oxford GS, Vasko MR, White FA, Khanna R (2011b) Suppression of inflammatory and neuropathic pain by uncoupling CRMP-2 from the presynaptic Ca(2)(+) channel complex. Nature medicine 17:822-829.

Brittain JM, Duarte DB, Wilson SM, Zhu W, Ballard C, Johnson PL, Liu N, Xiong W, Ripsch MS, Wang Y, Fehrenbacher JC, Fitz SD, Khanna M, Park CK, Schmutzler BS, Cheon BM, Due MR, Brustovetsky T, Ashpole NM, Hudmon A, Meroueh SO, Hingtgen CM, Brustovetsky N, Ji RR, Hurley JH, Jin X, Shekhar A, Xu XM,

Oxford GS, Vasko MR, White FA, Khanna R (2011c) Suppression of inflammatory and neuropathic pain by uncoupling CRMP-2 from the presynaptic Ca(2+) channel complex. Nature Medicine.

Brittain JM, Piekarz AD, Wang Y, Kondo T, Cummins TR, Khanna R (2009a) An atypical role for collapsin response mediator protein 2 (CRMP-2) in neurotransmitter release via interaction with presynaptic voltage-gated calcium channels. Journal of Biological Chemistry 284:31375-31390.

Brittain JM, Piekarz AD, Wang Y, Kondo T, Cummins TR, Khanna R (2009b) An atypical role for collapsin response mediator protein 2 (CRMP-2) in neurotransmitter release via interaction with presynaptic voltage-gated calcium channels. The Journal of biological chemistry 284:31375-31390.

Brittain JM, Wang Y, Eruvwetere O, Khanna R (2012) Cdk5-mediated phosphorylation of CRMP-2 enhances its interaction with CaV2.2. FEBS letters 586:3813-3818.

Brot S, Rogemond V, Perrot V, Chounlamountri N, Auger C, Honnorat J, Moradi-Ameli M (2010) CRMP5 interacts with tubulin to inhibit neurite outgrowth, thereby modulating the function of CRMP2. The Journal of neuroscience : the official journal of the Society for Neuroscience 30:10639-10654.

Brot S, Smaoune H, Youssef-Issa M, Malleval C, Benetollo C, Besancon R, Auger C, Moradi-Ameli M, Honnorat J (2014) Collapsin response-mediator protein 5 (CRMP5) phosphorylation at threonine 516 regulates neurite outgrowth inhibition. The European journal of neuroscience 40:3010-3020.

Brown M, Jacobs T, Eickholt B, Ferrari G, Teo M, Monfries C, Qi RZ, Leung T, Lim L, Hall C (2004) Alpha2-chimaerin, cyclin-dependent Kinase 5/p35, and its target collapsin response mediator protein-2 are essential components in semaphorin 3A-induced growth-cone collapse. J Neurosci 24:8994-9004.

Brustovetsky T, Pellman JJ, Yang XF, Khanna R, Brustovetsky N (2014) Collapsin response mediator protein 2 (CRMP2) interacts with N-methyl-D-aspartate (NMDA) receptor and Na+/Ca2+ exchanger and regulates their functional activity. The Journal of biological chemistry 289:7470-7482.

Byk T, Dobransky T, Cifuentes-Diaz C, Sobel A (1996) Identification and molecular characterization of Unc-33-like phosphoprotein (Ulip), a putative mammalian homolog of the axonal guidance-associated unc-33 gene product. J Neurosci 16:688-701.

Cachemaille M, Laedermann CJ, Pertin M, Abriel H, Gosselin RD, Decosterd I (2012) Neuronal expression of the ubiquitin ligase Nedd4-2 in rat dorsal root ganglia:

modulation in the spared nerve injury model of neuropathic pain. Neuroscience 227:370-380.

Caffrey JM, Eng DL, Black JA, Waxman SG, Kocsis JD (1992) Three types of sodium channels in adult rat dorsal root ganglion neurons. Brain research 592:283-297.

Calcutt NA, Jorge MC, Yaksh TL, Chaplan SR (1996) Tactile allodynia and formalin hyperalgesia in streptozotocin-diabetic rats: effects of insulin, aldose reductase inhibition and lidocaine. Pain 68:293-299.

Cannon SC (2012) Small fiber neuropathy: a bit less idiopathic? Neurology 78:1626-1627.

Cantrell AR, Tibbs VC, Yu FH, Murphy BJ, Sharp EM, Qu Y, Catterall WA, Scheuer T (2002) Molecular mechanism of convergent regulation of brain Na(+) channels by protein kinase C and protein kinase A anchored to AKAP-15. Molecular and cellular neurosciences 21:63-80.

Carter S, Bischof O, Dejean A, Vousden KH (2007) C-terminal modifications regulate MDM2 dissociation and nuclear export of p53. Nature cell biology 9:428-435.

Casini S, Tan HL, Demirayak I, Remme CA, Amin AS, Scicluna BP, Chatyan H, Ruijter JM, Bezzina CR, van Ginneken AC, Veldkamp MW (2010) Tubulin polymerization modifies cardiac sodium channel expression and gating. CardiovascRes 85:691-700.

Catterall WA (2014) Sodium channels, inherited epilepsy, and antiepileptic drugs. Annual review of pharmacology and toxicology 54:317-338.

Catterall WA, Goldin AL, Waxman SG (2005) International Union of Pharmacology. XLVII. Nomenclature and structure-function relationships of voltage-gated sodium channels. Pharmacological reviews 57:397-409.

Cavaletti G, Cavalletti E, Oggioni N, Sottani C, Minoia C, D'Incalci M, Zucchetti M, Marmiroli P, Tredici G (2000) Distribution of paclitaxel within the nervous system of the rat after repeated intravenous administration. Neurotoxicology 21:389-393.

Cestele S, Schiavon E, Rusconi R, Franceschetti S, Mantegazza M (2013) Nonfunctional NaV1.1 familial hemiplegic migraine mutant transformed into gain of function by partial rescue of folding defects. Proceedings of the National Academy of Sciences of the United States of America 110:17546-17551.

Chae YC, Lee S, Heo K, Ha SH, Jung Y, Kim JH, Ihara Y, Suh PG, Ryu SH (2009) Collapsin response mediator protein-2 regulates neurite formation by modulating tubulin GTPase activity. Cellular Signalling 21:1818-1826.

Charlesworth B, Morgan MT, Charlesworth D (1993) The effect of deleterious mutations on neutral molecular variation. Genetics 134:1289-1303.

Chatelier A, Dahllund L, Eriksson A, Krupp J, Chahine M (2008) Biophysical properties of human Na v1.7 splice variants and their regulation by protein kinase A. Journal of neurophysiology 99:2241-2250.

Chen Y, Stevens B, Chang J, Milbrandt J, Barres BA, Hell JW (2008) NS21: re-defined and modified supplement B27 for neuronal cultures. J Neurosci Methods 171:239-247.

Cheng KK, Ling YL, Wang JC (1968) The failure of respiration in death by tetrodotoxin posioning. Quarterly journal of experimental physiology and cognate medical sciences 53:119-128.

Chi XX, Schmutzler BS, Brittain JM, Hingtgen CM, Nicol GD, Khanna R (2009a) Regulation of N-type voltage-gated calcium (CaV2.2) channels and transmitter release by collapsin response mediator protein-2 (CRMP-2) in sensory neurons. JCell Sci 23:4351-4362.

Chi XX, Schmutzler BS, Brittain JM, Wang Y, Hingtgen CM, Nicol GD, Khanna R (2009b) Regulation of N-type voltage-gated calcium channels (Cav2.2) and transmitter release by collapsin response mediator protein-2 (CRMP-2) in sensory neurons. Journal of Cell Science 122:4351-4362.

Chi XX, Schmutzler BS, Brittain JM, Wang Y, Hingtgen CM, Nicol GD, Khanna R (2009c) Regulation of N-type voltage-gated calcium channels (Cav2.2) and transmitter release by collapsin response mediator protein-2 (CRMP-2) in sensory neurons. Journal of cell science 122:4351-4362.

Chowdhury S, Shepherd JD, Okuno H, Lyford G, Petralia RS, Plath N, Kuhl D, Huganir RL, Worley PF (2006) Arc/Arg3.1 interacts with the endocytic machinery to regulate AMPA receptor trafficking. Neuron 52:445-459.

Clare JJ (2010) Targeting voltage-gated sodium channels for pain therapy. Expert opinion on investigational drugs 19:45-62.

Cole AR, Causeret F, Yadirgi G, Hastie CJ, McLauchlan H, McManus EJ, Hernandez F, Eickholt BJ, Nikolic M, Sutherland C (2006) Distinct priming kinases contribute

to differential regulation of collapsin response mediator proteins by glycogen synthase kinase-3 in vivo. The Journal of biological chemistry 281:16591-16598.

Cole AR, Knebel A, Morrice NA, Robertson LA, Irving AJ, Connolly CN, Sutherland C (2004) GSK-3 phosphorylation of the Alzheimer epitope within collapsin response mediator proteins regulates axon elongation in primary neurons. J Biol Chem 279:50176-50180.

Cole AR, Soutar MP, Rembutsu M, Van Aalten L, Hastie CJ, McLauchlan H, Peggie M, Balastik M, Lu KP, Sutherland C (2008) Relative resistance of Cdk5-phosphorylated CRMP2 to dephosphorylation. J Biol Chem.

Cole KS (1949) Some physical aspects of bioelectric phenomena. Proceedings of the National Academy of Sciences of the United States of America 35:558-566.

Cole RN, Hart GW (2001) Cytosolic O-glycosylation is abundant in nerve terminals. Journal of neurochemistry 79:1080-1089.

Cox JJ, Reimann F, Nicholas AK, Thornton G, Roberts E, Springell K, Karbani G, Jafri H, Mannan J, Raashid Y, Al-Gazali L, Hamamy H, Valente EM, Gorman S, Williams R, McHale DP, Wood JN, Gribble FM, Woods CG (2006) An SCN9A channelopathy causes congenital inability to experience pain. Nature 444:894-898.

Cox JJ, Sheynin J, Shorer Z, Reimann F, Nicholas AK, Zubovic L, Baralle M, Wraige E, Manor E, Levy J, Woods CG, Parvari R (2010) Congenital insensitivity to pain: novel SCN9A missense and in-frame deletion mutations. Human mutation 31:E1670-1686.

Craig TJ, Henley JM (2012) SUMOylation, Arc and the regulation homeostatic synaptic scaling: Implications in health and disease. Communicative & integrative biology 5:634-636.

Craig TJ, Jaafari N, Petrovic MM, Jacobs SC, Rubin PP, Mellor JR, Henley JM (2012) Homeostatic synaptic scaling is regulated by protein SUMOylation. The Journal of biological chemistry 287:22781-22788.

Cummins TR, Aglieco F, Renganathan M, Herzog RI, Dib-Hajj SD, Waxman SG (2001) Nav1.3 sodium channels: rapid repriming and slow closed-state inactivation display quantitative differences after expression in a mammalian cell line and in spinal sensory neurons. The Journal of neuroscience : the official journal of the Society for Neuroscience 21:5952-5961.

Cummins TR, Howe JR, Waxman SG (1998) Slow closed-state inactivation: a novel mechanism underlying ramp currents in cells expressing the hNE/PN1 sodium channel. The Journal of neuroscience : the official journal of the Society for Neuroscience 18:9607-9619.

Curtis HJ, Cole KS (1938) Transverse Electric Impedance of the Squid Giant Axon. The Journal of general physiology 21:757-765.

Czech T, Yang JW, Csaszar E, Kappler J, Baumgartner C, Lubec G (2004) Reduction of hippocampal collapsin response mediated protein-2 in patients with mesial temporal lobe epilepsy. Neurochem Res 29:2189-2196.

de Lera Ruiz M, Kraus RL (2015) Voltage-Gated Sodium Channels: Structure, Function, Pharmacology and Clinical Indications. Journal of medicinal chemistry.

Debonneville C, Flores SY, Kamynina E, Plant PJ, Tauxe C, Thomas MA, Munster C, Chraibi A, Pratt JH, Horisberger JD, Pearce D, Loffing J, Staub O (2001) Phosphorylation of Nedd4-2 by Sgk1 regulates epithelial Na(+) channel cell surface expression. The EMBO journal 20:7052-7059.

Decosterd I, Woolf CJ (2000) Spared nerve injury: an animal model of persistent peripheral neuropathic pain. Pain 87:149-158.

Deo RC, Schmidt EF, Elhabazi A, Togashi H, Burley SK, Strittmatter SM (2004) Structural bases for CRMP function in plexin-dependent semaphorin3A signaling. The EMBO journal 23:9-22.

DePaoli-Roach AA (1984) Synergistic phosphorylation and activation of ATP-Mg-dependent phosphoprotein phosphatase by F A/GSK-3 and casein kinase II (PC0.7). J Biol Chem 259:12144-12152.

Desterro JM, Rodriguez MS, Hay RT (1998) SUMO-1 modification of IkappaBalpha inhibits NF-kappaB activation. Molecular cell 2:233-239.

Desterro JM, Rodriguez MS, Kemp GD, Hay RT (1999) Identification of the enzyme required for activation of the small ubiquitin-like protein SUMO-1. The Journal of biological chemistry 274:10618-10624.

Desterro JM, Thomson J, Hay RT (1997) Ubch9 conjugates SUMO but not ubiquitin. FEBS letters 417:297-300.

Dho SE, Jacob S, Wolting CD, French MB, Rohrschneider LR, McGlade CJ (1998) The mammalian numb phosphotyrosine-binding domain. Characterization of binding

specificity and identification of a novel PDZ domain-containing numb binding protein, LNX. The Journal of biological chemistry 273:9179-9187.

Di Marcotullio L, Ferretti E, Greco A, De Smaele E, Po A, Sico MA, Alimandi M, Giannini G, Maroder M, Screpanti I, Gulino A (2006) Numb is a suppressor of Hedgehog signalling and targets Gli1 for Itch-dependent ubiquitination. Nature cell biology 8:1415-1423.

Dib-Hajj S, Black JA, Cummins TR, Waxman SG (2002) NaN/Nav1.9: a sodium channel with unique properties. Trends in neurosciences 25:253-259.

Dib-Hajj SD, Cummins TR, Black JA, Waxman SG (2007) From genes to pain: Na v 1.7 and human pain disorders. Trends in neurosciences 30:555-563.

Dib-Hajj SD, Estacion M, Jarecki BW, Tyrrell L, Fischer TZ, Lawden M, Cummins TR, Waxman SG (2008) Paroxysmal extreme pain disorder M1627K mutation in human Nav1.7 renders DRG neurons hyperexcitable. Molecular pain 4:37.

Dib-Hajj SD, Yang Y, Black JA, Waxman SG (2013) The Na(V)1.7 sodium channel: from molecule to man. Nature reviews Neuroscience 14:49-62.

Dinudom A, Fotia AB, Lefkowitz RJ, Young JA, Kumar S, Cook DI (2004) The kinase Grk2 regulates Nedd4/Nedd4-2-dependent control of epithelial Na+ channels. Proceedings of the National Academy of Sciences of the United States of America 101:11886-11890.

Djamgoz MB, Onkal R (2013) Persistent current blockers of voltage-gated sodium channels: a clinical opportunity for controlling metastatic disease. Recent patents on anti-cancer drug discovery 8:66-84.

Djouhri L, Newton R, Levinson SR, Berry CM, Carruthers B, Lawson SN (2003) Sensory and electrophysiological properties of guinea-pig sensory neurones expressing Nav 1.7 (PN1) Na+ channel alpha subunit protein. The Journal of physiology 546:565-576.

Dougherty PM, Cata JP, Cordella JV, Burton A, Weng HR (2004) Taxol-induced sensory disturbance is characterized by preferential impairment of myelinated fiber function in cancer patients. Pain 109:132-142.

Duarte ML, Pena DA, Nunes Ferraz FA, Berti DA, Paschoal Sobreira TJ, Costa-Junior HM, Abdel Baqui MM, Disatnik MH, Xavier-Neto J, Lopes de Oliveira PS, Schechtman D (2014) Protein folding creates structure-based, noncontiguous

consensus phosphorylation motifs recognized by kinases. Science signaling 7:ra105.

Due MR, Yang XF, Allette YM, Randolph AL, Ripsch MS, Wilson SM, Dustrude ET, Khanna R, White FA (2014) Carbamazepine potentiates the effectiveness of morphine in a rodent model of neuropathic pain. PloS one 9:e107399.

Duprez E, Saurin AJ, Desterro JM, Lallemand-Breitenbach V, Howe K, Boddy MN, Solomon E, de The H, Hay RT, Freemont PS (1999) SUMO-1 modification of the acute promyelocytic leukaemia protein PML: implications for nuclear localisation. Journal of cell science 112 (Pt 3):381-393.

Dustrude ET, Wilson SM, Ju W, Xiao Y, Khanna R (2013) CRMP2 protein SUMOylation modulates NaV1.7 channel trafficking. The Journal of biological chemistry 288:24316-24331.

Ednie AR, Harper JM, Bennett ES (2015) Sialic acids attached to N- and O-glycans within the Nav1.4 D1S5-S6 linker contribute to channel gating. Biochimica et biophysica acta 1850:307-317.

Eickholt BJ, Walsh FS, Doherty P (2002) An inactive pool of GSK-3 at the leading edge of growth cones is implicated in Semaphorin 3A signaling. J Cell Biol 157:211-217.

Errington AC, Coyne L, Stohr T, Selve N, Lees G (2006) Seeking a mechanism of action for the novel anticonvulsant lacosamide. Neuropharmacology 50:1016-1029.

Errington AC, Stohr T, Heers C, Lees G (2008) The investigational anticonvulsant lacosamide selectively enhances slow inactivation of voltage-gated sodium channels. Molecular pharmacology 73:157-169.

Estacion M, Dib-Hajj SD, Benke PJ, Te Morsche RH, Eastman EM, Macala LJ, Drenth JP, Waxman SG (2008) NaV1.7 gain-of-function mutations as a continuum: A1632E displays physiological changes associated with erythromelalgia and paroxysmal extreme pain disorder mutations and produces symptoms of both disorders. The Journal of neuroscience : the official journal of the Society for Neuroscience 28:11079-11088.

Estacion M, Han C, Choi JS, Hoeijmakers JG, Lauria G, Drenth JP, Gerrits MM, Dib-Hajj SD, Faber CG, Merkies IS, Waxman SG (2011) Intra- and interfamily phenotypic diversity in pain syndromes associated with a gain-of-function variant of NaV1.7. Molecular pain 7:92.

Estacion M, Yang Y, Dib-Hajj SD, Tyrrell L, Lin Z, Yang Y, Waxman SG (2013) A new Nav1.7 mutation in an erythromelalgia patient. Biochemical and biophysical research communications 432:99-104.

Eun Jeoung L, Sung Hee H, Jaesun C, Sung Hwa S, Kwang Hum Y, Min Kyoung K, Tae Yoon P, Sang Sun K (2008) Regulation of glycogen synthase kinase 3beta functions by modification of the small ubiquitin-like modifier. The open biochemistry journal 2:67-76.

Evdokimov E, Sharma P, Lockett SJ, Lualdi M, Kuehn MR (2008) Loss of SUMO1 in mice affects RanGAP1 localization and formation of PML nuclear bodies, but is not lethal as it can be compensated by SUMO2 or SUMO3. Journal of cell science 121:4106-4113.

Fang H, Zhang HH, Yang BX, Huang JL, Shun JL, Kong FJ, Peng X, Chen ZG, Lu JM (2015) Cdk5 contributes to inflammation-induced thermal hyperalgesia mediated by the p38 MAPK pathway in microglia. Brain research.

Feliciangeli S, Bendahhou S, Sandoz G, Gounon P, Reichold M, Warth R, Lazdunski M, Barhanin J, Lesage F (2007) Does sumoylation control K2P1/TWIK1 background K+ channels? Cell 130:563-569.

Feligioni M, Nishimune A, Henley JM (2009) Protein SUMOylation modulates calcium influx and glutamate release from presynaptic terminals. The European journal of neuroscience 29:1348-1356.

Fenteany G, Standaert RF, Lane WS, Choi S, Corey EJ, Schreiber SL (1995) Inhibition of proteasome activities and subunit-specific amino-terminal threonine modification by lactacystin. Science 268:726-731.

Filippakopoulos P, Kofler M, Hantschel O, Gish GD, Grebien F, Salah E, Neudecker P, Kay LE, Turk BE, Superti-Furga G, Pawson T, Knapp S (2008) Structural coupling of SH2-kinase domains links Fes and Abl substrate recognition and kinase activation. Cell 134:793-803.

Fiol CJ, Haseman JH, Wang YH, Roach PJ, Roeske RW, Kowalczuk M, DePaoli-Roach AA (1988) Phosphoserine as a recognition determinant for glycogen synthase kinase-3: phosphorylation of a synthetic peptide based on the G-component of protein phosphatase-1. Archives of biochemistry and biophysics 267:797-802.

Fischer EH, Krebs EG (1955) Conversion of phosphorylase b to phosphorylase a in muscle extracts. The Journal of biological chemistry 216:121-132.

Flotho A, Melchior F (2013) Sumoylation: a regulatory protein modification in health and disease. Annual review of biochemistry 82:357-385.

Fotia AB, Ekberg J, Adams DJ, Cook DI, Poronnik P, Kumar S (2004) Regulation of neuronal voltage-gated sodium channels by the ubiquitin-protein ligases Nedd4 and Nedd4-2. The Journal of biological chemistry 279:28930-28935.

Fraser SP, Ozerlat-Gunduz I, Brackenbury WJ, Fitzgerald EM, Campbell TM, Coombes RC, Djamgoz MB (2014) Regulation of voltage-gated sodium channel expression in cancer: hormones, growth factors and auto-regulation. Philosophical transactions of the Royal Society of London Series B, Biological sciences 369:20130105.

Frede J, Fraser SP, Oskay-Ozcelik G, Hong Y, Ioana Braicu E, Sehouli J, Gabra H, Djamgoz MB (2013) Ovarian cancer: Ion channel and aquaporin expression as novel targets of clinical potential. European journal of cancer 49:2331-2344.

Fukada M, Watakabe I, Yuasa-Kawada J, Kawachi H, Kuroiwa A, Matsuda Y, Noda M (2000) Molecular characterization of CRMP5, a novel member of the collapsin response mediator protein family. J Biol Chem 275:37957-37965.

Fukata Y, Itoh TJ, Kimura T, Menager C, Nishimura T, Shiromizu T, Watanabe H, Inagaki N, Iwamatsu A, Hotani H, Kaibuchi K (2002a) CRMP-2 binds to tubulin heterodimers to promote microtubule assembly. NatCell Biol 4:583-591.

Fukata Y, Itoh TJ, Kimura T, Menager C, Nishimura T, Shiromizu T, Watanabe H, Inagaki N, Iwamatsu A, Hotani H, Kaibuchi K (2002b) CRMP-2 binds to tubulin heterodimers to promote microtubule assembly. Nature cell biology 4:583-591.

Fukuoka T, Miyoshi K, Noguchi K (2015) De novo expression of Nav1.7 in injured putative proprioceptive afferents: Multiple tetrodotoxin-sensitive sodium channels are retained in the rat dorsal root after spinal nerve ligation. Neuroscience 284:693-706.

Furman RE, Tanaka JC, Mueller P, Barchi RL (1986) Voltage-dependent activation in purified reconstituted sodium channels from rabbit T-tubular membranes. Proceedings of the National Academy of Sciences of the United States of America 83:488-492.

Gaetano C, Matsuo T, Thiele CJ (1997) Identification and characterization of a retinoic acid-regulated human homologue of the unc-33-like phosphoprotein gene (hUlip) from neuroblastoma cells. J Biol Chem 272:12195-12201.

Geschwind DH, Hockfield S (1989) Identification of proteins that are developmentally regulated during early cerebral corticogenesis in the rat. The Journal of neuroscience : the official journal of the Society for Neuroscience 9:4303-4317.

Gingras J, Smith S, Matson DJ, Johnson D, Nye K, Couture L, Feric E, Yin R, Moyer BD, Peterson ML, Rottman JB, Beiler RJ, Malmberg AB, McDonough SI (2014) Global Nav1.7 knockout mice recapitulate the phenotype of human congenital indifference to pain. PloS one 9:e105895.

Gold MS, Levine JD, Correa AM (1998) Modulation of TTX-R INa by PKC and PKA and their role in PGE2-induced sensitization of rat sensory neurons in vitro. The Journal of neuroscience : the official journal of the Society for Neuroscience 18:10345-10355.

Goldin AL (1999) Diversity of mammalian voltage-gated sodium channels. Annals of the New York Academy of Sciences 868:38-50.

Gong L, Li B, Millas S, Yeh ET (1999) Molecular cloning and characterization of human AOS1 and UBA2, components of the sentrin-activating enzyme complex. FEBS letters 448:185-189.

Gong L, Millas S, Maul GG, Yeh ET (2000) Differential regulation of sentrinized proteins by a novel sentrin-specific protease. The Journal of biological chemistry 275:3355-3359.

Gong L, Yeh ET (2006) Characterization of a family of nucleolar SUMO-specific proteases with preference for SUMO-2 or SUMO-3. The Journal of biological chemistry 281:15869-15877.

Goshima Y, Nakamura F, Strittmatter P, Strittmatter SM (1995) Collapsin-induced growth cone collapse mediated by an intracellular protein related to UNC-33. Nature 376:509-514.

Goslin K, Banker G (1989) Experimental observations on the development of polarity by hippocampal neurons in culture. The Journal of cell biology 108:1507-1516.

Gregoire S, Tremblay AM, Xiao L, Yang Q, Ma K, Nie J, Mao Z, Wu Z, Giguere V, Yang XJ (2006) Control of MEF2 transcriptional activity by coordinated phosphorylation and sumoylation. The Journal of biological chemistry 281:4423-4433.

Gu Y, Hamajima N, Ihara Y (2000) Neurofibrillary tangle-associated collapsin response mediator protein-2 (CRMP-2) is highly phosphorylated on Thr-509, Ser-518, and Ser-522. Biochemistry (Mosc) 39:4267-4275.

Guy HR, Seetharamulu P (1986) Molecular model of the action potential sodium channel. Proceedings of the National Academy of Sciences of the United States of America 83:508-512.

Han C, Hoeijmakers JG, Ahn HS, Zhao P, Shah P, Lauria G, Gerrits MM, te Morsche RH, Dib-Hajj SD, Drenth JP, Faber CG, Merkies IS, Waxman SG (2012) Nav1.7-related small fiber neuropathy: impaired slow-inactivation and DRG neuron hyperexcitability. Neurology 78:1635-1643.

Hao JX, Stohr T, Selve N, Wiesenfeld-Hallin Z, Xu XJ (2006) Lacosamide, a new anti-epileptic, alleviates neuropathic pain-like behaviors in rat models of spinal cord or trigeminal nerve injury. European journal of pharmacology 553:135-140.

Hardeland U, Steinacher R, Jiricny J, Schar P (2002) Modification of the human thymine-DNA glycosylase by ubiquitin-like proteins facilitates enzymatic turnover. The EMBO journal 21:1456-1464.

Hardy J, Selkoe DJ (2002) The amyloid hypothesis of Alzheimer's disease: progress and problems on the road to therapeutics. Science 297:353-356.

Harper AA, Lawson SN (1985) Conduction velocity is related to morphological cell type in rat dorsal root ganglion neurones. The Journal of physiology 359:31-46.

Hartshorne RP, Keller BU, Talvenheimo JA, Catterall WA, Montal M (1985) Functional reconstitution of the purified brain sodium channel in planar lipid bilayers. Proceedings of the National Academy of Sciences of the United States of America 82:240-244.

Hayashi T, Seki M, Maeda D, Wang W, Kawabe Y, Seki T, Saitoh H, Fukagawa T, Yagi H, Enomoto T (2002) Ubc9 is essential for viability of higher eukaryotic cells. Experimental cell research 280:212-221.

Hedgecock EM, Culotti JG, Thomson JN, Perkins LA (1985) Axonal guidance mutants of Caenorhabditis elegans identified by filling sensory neurons with fluorescein dyes. Dev Biol 111:158-170.

Henley JM, Craig TJ, Wilkinson KA (2014) Neuronal SUMOylation: mechanisms, physiology, and roles in neuronal dysfunction. Physiological reviews 94:1249-1285.

Hensley K, Venkova K, Christov A, Gunning W, Park J (2011) Collapsin Response Mediator Protein-2: An Emerging Pathologic Feature and Therapeutic Target for Neurodisease Indications. Molecular Neurobiology.

Herrero JF, Laird JM, Lopez-Garcia JA (2000) Wind-up of spinal cord neurones and pain sensation: much ado about something? Progress in neurobiology 61:169-203.

Herzog RI, Cummins TR, Ghassemi F, Dib-Hajj SD, Waxman SG (2003) Distinct repriming and closed-state inactivation kinetics of Nav1.6 and Nav1.7 sodium channels in mouse spinal sensory neurons. The Journal of physiology 551:741-750.

Hietakangas V, Ahlskog JK, Jakobsson AM, Hellesuo M, Sahlberg NM, Holmberg CI, Mikhailov A, Palvimo JJ, Pirkkala L, Sistonen L (2003) Phosphorylation of serine 303 is a prerequisite for the stress-inducible SUMO modification of heat shock factor 1. Molecular and cellular biology 23:2953-2968.

Hietakangas V, Anckar J, Blomster HA, Fujimoto M, Palvimo JJ, Nakai A, Sistonen L (2006) PDSM, a motif for phosphorylation-dependent SUMO modification. Proceedings of the National Academy of Sciences of the United States of America 103:45-50.

Ho C, O'Leary ME (2011) Single-cell analysis of sodium channel expression in dorsal root ganglion neurons. Molecular and cellular neurosciences 46:159-166.

Hodgkin AL (1937a) Evidence for electrical transmission in nerve: Part I. The Journal of physiology 90:183-210.

Hodgkin AL (1937b) Evidence for electrical transmission in nerve: Part II. The Journal of physiology 90:211-232.

Hodgkin AL, Huxley AF (1952a) The components of membrane conductance in the giant axon of Loligo. J Physiol 116:473-496.

Hodgkin AL, Huxley AF (1952b) Currents carried by sodium and potassium ions through the membrane of the giant axon of Loligo. J Physiol 116:449-472.

Hodgkin AL, Huxley AF (1952c) The dual effect of membrane potential on sodium conductance in the giant axon of Loligo. J Physiol 116:497-506.

Hodgkin AL, Huxley AF (1952d) A quantitative description of membrane current and its application to conduction and excitation in nerve. The Journal of physiology 117:500-544.

Hodgkin AL, Katz B (1949) The effect of sodium ions on the electrical activity of giant axon of the squid. The Journal of physiology 108:37-77.

Hoeijmakers JG, Faber CG, Merkies IS, Waxman SG (2014) Channelopathies, painful neuropathy, and diabetes: which way does the causal arrow point? Trends in molecular medicine 20:544-550.

Holtmaat AJ, Gorter JA, De Wit J, Tolner EA, Spijker S, Giger RJ, Lopes da Silva FH, Verhaagen J (2003) Transient downregulation of Sema3A mRNA in a rat model for temporal lobe epilepsy. A novel molecular event potentially contributing to mossy fiber sprouting. Experimental neurology 182:142-150.

Hong S, Morrow TJ, Paulson PE, Isom LL, Wiley JW (2004) Early painful diabetic neuropathy is associated with differential changes in tetrodotoxin-sensitive and -resistant sodium channels in dorsal root ganglion neurons in the rat. The Journal of biological chemistry 279:29341-29350.

Horvath CA, Vanden Broeck D, Boulet GA, Bogers J, De Wolf MJ (2007) Epsin: inducing membrane curvature. Int J Biochem Cell Biol 39:1765-1770.

Hou ST, Jiang SX, Aylsworth A, Ferguson G, Slinn J, Hu H, Leung T, Kappler J, Kaibuchi K (2009) CaMKII phosphorylates collapsin response mediator protein 2 and modulates axonal damage during glutamate excitotoxicity. Journal of neurochemistry 111:870-881.

Hsieh YL, Kuo HY, Chang CC, Naik MT, Liao PH, Ho CC, Huang TC, Jeng JC, Hsu PH, Tsai MD, Huang TH, Shih HM (2013) Ubc9 acetylation modulates distinct SUMO target modification and hypoxia response. The EMBO journal 32:791-804.

Hu D, Barajas-Martinez H, Pfeiffer R, Dezi F, Pfeiffer J, Buch T, Betzenhauser MJ, Belardinelli L, Kahlig KM, Rajamani S, DeAntonio HJ, Myerburg RJ, Ito H, Deshmukh P, Marieb M, Nam GB, Bhatia A, Hasdemir C, Haissaguerre M, Veltmann C, Schimpf R, Borggrefe M, Viskin S, Antzelevitch C (2014) Mutations in SCN10A are responsible for a large fraction of cases of Brugada syndrome. Journal of the American College of Cardiology 64:66-79.

Hudmon A, Choi JS, Tyrrell L, Black JA, Rush AM, Waxman SG, Dib-Hajj SD (2008) Phosphorylation of sodium channel Na(v)1.8 by p38 mitogen-activated protein kinase increases current density in dorsal root ganglion neurons. The Journal of neuroscience : the official journal of the Society for Neuroscience 28:3190-3201.

Hurley JH, Wendland B (2002) Endocytosis: driving membranes around the bend. Cell 111:143-146.

Iadarola MJ, Brady LS, Draisci G, Dubner R (1988) Enhancement of dynorphin gene expression in spinal cord following experimental inflammation: stimulus specificity, behavioral parameters and opioid receptor binding. Pain 35:313-326.

Inagaki N, Chihara K, Arimura N, Menager C, Kawano Y, Matsuo N, Nishimura T, Amano M, Kaibuchi K (2001a) CRMP-2 induces axons in cultured hippocampal neurons. Nature neuroscience 4:781-782.

Inagaki N, Chihara K, Arimura N, Menager C, Kawano Y, Matsuo N, Nishimura T, Amano M, Kaibuchi K (2001b) CRMP-2 induces axons in cultured hippocampal neurons. Nature neuroscience 4:781-782.

Institute of Medicine Report from the Committee on Advancing Pain Research C, Education (2011) Relieving Pain in America, A Blueprint for Transforming Prevention, Care, Education and Research: The National Academies Press.

Isom LL, De Jongh KS, Patton DE, Reber BF, Offord J, Charbonneau H, Walsh K, Goldin AL, Catterall WA (1992) Primary structure and functional expression of the beta 1 subunit of the rat brain sodium channel. Science 256:839-842.

Isom LL, Ragsdale DS, De Jongh KS, Westenbroek RE, Reber BF, Scheuer T, Catterall WA (1995) Structure and function of the beta 2 subunit of brain sodium channels, a transmembrane glycoprotein with a CAM motif. Cell 83:433-442.

Iwase T, Takebayashi T, Tanimoto K, Terashima Y, Miyakawa T, Kobayashi T, Tohse N, Yamashita T (2012) Sympathectomy attenuates excitability of dorsal root ganglion neurons and pain behaviour in a lumbar radiculopathy model. Bone & joint research 1:198-204.

Jang SY, Shin YK, Jung J, Lee SH, Seo SY, Suh DJ, Park HT (2010) Injury-induced CRMP4 expression in adult sensory neurons; a possible target gene for ciliary neurotrophic factor. Neuroscience letters 485:37-42.

Jauffred B, Llense F, Sommer B, Wang Z, Martin C, Bellaiche Y (2013) Regulation of centrosome movements by numb and the collapsin response mediator protein during Drosophila sensory progenitor asymmetric division. Development 140:2657-2668.

Jiang SX, Kappler J, Zurakowski B, Desbois A, Aylsworth A, Hou ST (2007) Calpain cleavage of collapsin response mediator proteins in ischemic mouse brain. Eur J Neurosci 26:801-809.

Johnson ES (2004) Protein modification by SUMO. Annual review of biochemistry 73:355-382.

Johnson ES, Blobel G (1997) Ubc9p is the conjugating enzyme for the ubiquitin-like protein Smt3p. The Journal of biological chemistry 272:26799-26802.

Johnson LN, Lewis RJ (2001) Structural basis for control by phosphorylation. Chemical reviews 101:2209-2242.

Ju W, Li Q, Wilson SM, Brittain JM, Meroueh L, Khanna R (2013) SUMOylation alters CRMP2 regulation of calcium influx in sensory neurons. Channels 7.

Julius D, Basbaum AI (2001) Molecular mechanisms of nociception. Nature 413:203-210.

Jurkat-Rott K, Holzherr B, Fauler M, Lehmann-Horn F (2010) Sodium channelopathies of skeletal muscle result from gain or loss of function. Pflugers Archiv : European journal of physiology 460:239-248.

Juven-Gershon T, Shifman O, Unger T, Elkeles A, Haupt Y, Oren M (1998) The Mdm2 oncoprotein interacts with the cell fate regulator Numb. Molecular and cellular biology 18:3974-3982.

Kadare G, Toutant M, Formstecher E, Corvol JC, Carnaud M, Boutterin MC, Girault JA (2003) PIAS1-mediated sumoylation of focal adhesion kinase activates its autophosphorylation. The Journal of biological chemistry 278:47434-47440.

Kamitani T, Kito K, Nguyen HP, Fukuda-Kamitani T, Yeh ET (1998a) Characterization of a second member of the sentrin family of ubiquitin-like proteins. The Journal of biological chemistry 273:11349-11353.

Kamitani T, Nguyen HP, Kito K, Fukuda-Kamitani T, Yeh ET (1998b) Covalent modification of PML by the sentrin family of ubiquitin-like proteins. The Journal of biological chemistry 273:3117-3120.

Kawano Y, Yoshimura T, Tsuboi D, Kawabata S, Kaneko-Kawano T, Shirataki H, Takenawa T, Kaibuchi K (2005) CRMP-2 is involved in kinesin-1-dependent transport of the Sra-1/WAVE1 complex and axon formation. Molecular and cellular biology 25:9920-9935.

Keynes RD (1951) The ionic movements during nervous activity. J Physiol 114:119-150.

Khanna R, Wilson SM, Brittain JM, Weimer J, Sultana R, Butterfield A, Hensley K (2012) Opening Pandora's jar: a primer on the putative roles of CRMP2 in a panoply of neurodegenerative, sensory and motor neuron, and central disorders. Future neurology 7:749-771.

Kim DY, Carey BW, Wang H, Ingano LA, Binshtok AM, Wertz MH, Pettingell WH, He P, Lee VM, Woolf CJ, Kovacs DM (2007) BACE1 regulates voltage-gated sodium channels and neuronal activity. Nature cell biology 9:755-764.

Kim DY, Ingano LA, Carey BW, Pettingell WH, Kovacs DM (2005) Presenilin/gamma-secretase-mediated cleavage of the voltage-gated sodium channel beta2-subunit regulates cell adhesion and migration. The Journal of biological chemistry 280:23251-23261.

Kimura T, Watanabe H, Iwamatsu A, Kaibuchi K (2005) Tubulin and CRMP-2 complex is transported via Kinesin-1. J Neurochem 93:1371-1382.

King AM, Yang XF, Wang Y, Dustrude ET, Barbosa C, Due MR, Piekarz AD, Wilson SM, White FA, Salome C, Cummins TR, Khanna R, Kohn H (2012) Identification of the benzyloxyphenyl pharmacophore: a structural unit that promotes sodium channel slow inactivation. ACS chemical neuroscience 3:1037-1049.

Kitamura K, Takayama M, Hamajima N, Nakanishi M, Sasaki M, Endo Y, Takemoto T, Kimura H, Iwaki M, Nonaka M (1999) Characterization of the human dihydropyrimidinase-related protein 2 (DRP-2) gene. DNA research : an international journal for rapid publication of reports on genes and genomes 6:291-297.

Konopacki FA, Jaafari N, Rocca DL, Wilkinson KA, Chamberlain S, Rubin P, Kantamneni S, Mellor JR, Henley JM (2011) Agonist-induced PKC phosphorylation regulates GluK2 SUMOylation and kainate receptor endocytosis. Proceedings of the National Academy of Sciences of the United States of America 108:19772-19777.

Kraner SD, Tanaka JC, Barchi RL (1985) Purification and functional reconstitution of the voltage-sensitive sodium channel from rabbit T-tubular membranes. The Journal of biological chemistry 260:6341-6347.

Krieger JR, Taylor P, Gajadhar AS, Guha A, Moran MF, McGlade CJ (2013) Identification and selected reaction monitoring (SRM) quantification of endocytosis factors associated with Numb. Molecular & cellular proteomics : MCP 12:499-514.

Kurban M, Wajid M, Shimomura Y, Christiano AM (2010) A nonsense mutation in the SCN9A gene in congenital insensitivity to pain. Dermatology 221:179-183.

Laedermann CJ, Cachemaille M, Kirschmann G, Pertin M, Gosselin RD, Chang I, Albesa M, Towne C, Schneider BL, Kellenberger S, Abriel H, Decosterd I (2013a) Dysregulation of voltage-gated sodium channels by ubiquitin ligase NEDD4-2 in neuropathic pain. The Journal of clinical investigation 123:3002-3013.

Laedermann CJ, Syam N, Pertin M, Decosterd I, Abriel H (2013b) beta1- and beta3-voltage-gated sodium channel subunits modulate cell surface expression and glycosylation of Nav1.7 in HEK293 cells. Frontiers in cellular neuroscience 7:137.

Lapenta V, Chiurazzi P, van der Spek P, Pizzuti A, Hanaoka F, Brahe C (1997) SMT3A, a human homologue of the S. cerevisiae SMT3 gene, maps to chromosome 21qter and defines a novel gene family. Genomics 40:362-366.

Lawson SN (2002) Phenotype and function of somatic primary afferent nociceptive neurones with C-, Adelta- or Aalpha/beta-fibres. Experimental physiology 87:239-244.

Leclere PG, Panjwani A, Docherty R, Berry M, Pizzey J, Tonge DA (2005) Effective gene delivery to adult neurons by a modified form of electroporation. JNeurosciMethods 142:137-143.

Lee IH, Dinudom A, Sanchez-Perez A, Kumar S, Cook DI (2007) Akt mediates the effect of insulin on epithelial sodium channels by inhibiting Nedd4-2. The Journal of biological chemistry 282:29866-29873.

Lee JH, Park CK, Chen G, Han Q, Xie RG, Liu T, Ji RR, Lee SY (2014) A monoclonal antibody that targets a NaV1.7 channel voltage sensor for pain and itch relief. Cell 157:1393-1404.

Leipold E, Liebmann L, Korenke GC, Heinrich T, Giesselmann S, Baets J, Ebbinghaus M, Goral RO, Stodberg T, Hennings JC, Bergmann M, Altmuller J, Thiele H, Wetzel A, Nurnberg P, Timmerman V, De Jonghe P, Blum R, Schaible HG, Weis J, Heinemann SH, Hubner CA, Kurth I (2013) A de novo gain-of-function mutation in SCN11A causes loss of pain perception. Nature genetics 45:1399-1404.

Li K, Zhao GQ, Li LY, Wu GZ, Cui SS (2014) Epigenetic upregulation of Cdk5 in the dorsal horn contributes to neuropathic pain in rats. Neuroreport 25:1116-1121.

Li W, Yang Y, Hu Z, Ling S, Fang M (2015) Neuroprotective effects of DAHP and Triptolide in focal cerebral ischemia via apoptosis inhibition and PI3K/Akt/mTOR pathway activation. Frontiers in neuroanatomy 9:48.

Liao M, Cao E, Julius D, Cheng Y (2013) Structure of the TRPV1 ion channel determined by electron cryo-microscopy. Nature 504:107-112.

Lin CH, Liu SY, Lee EH (2015) SUMO modification of Akt regulates global SUMOylation and substrate SUMOylation specificity through Akt phosphorylation of Ubc9 and SUMO1. Oncogene.

Lin YL, Hsueh YP (2008) Neurofibromin interacts with CRMP-2 and CRMP-4 in rat brain. Biochem Biophys Res Commun 369:747-752.

Liu M, Wood JN (2011) The roles of sodium channels in nociception: implications for mechanisms of neuropathic pain. Pain medicine 12 Suppl 3:S93-99.

Liu Y, Wu Z, Tang D, Xun X, Liu L, Li X, Nie D, Xiang Y, Yi J, Yi J (2014a) Analgesic effects of Huwentoxin-IV on animal models of inflammatory and neuropathic pain. Protein and peptide letters 21:153-158.

Liu YN, Yang X, Suo ZW, Xu YM, Hu XD (2014b) Fyn kinase-regulated NMDA receptor- and AMPA receptor-dependent pain sensitization in spinal dorsal horn of mice. European journal of pain 18:1120-1128.

Lolignier S, Bonnet C, Gaudioso C, Noel J, Ruel J, Amsalem M, Ferrier J, Rodat-Despoix L, Bouvier V, Aissouni Y, Prival L, Chapuy E, Padilla F, Eschalier A, Delmas P, Busserolles J (2015) The nav1.9 channel is a key determinant of cold pain sensation and cold allodynia. Cell reports 11:1067-1078.

Lopez-Santiago LF, Pertin M, Morisod X, Chen C, Hong S, Wiley J, Decosterd I, Isom LL (2006) Sodium channel beta2 subunits regulate tetrodotoxin-sensitive sodium channels in small dorsal root ganglion neurons and modulate the response to pain. The Journal of neuroscience : the official journal of the Society for Neuroscience 26:7984-7994.

Lubec G, Nonaka M, Krapfenbauer K, Gratzer M, Cairns N, Fountoulakis M (1999) Expression of the dihydropyrimidinase related protein 2 (DRP-2) in Down syndrome and Alzheimer's disease brain is downregulated at the mRNA and dysregulated at the protein level. J Neural Transm Suppl 57:161-177.

Luo HB, Xia YY, Shu XJ, Liu ZC, Feng Y, Liu XH, Yu G, Yin G, Xiong YS, Zeng K, Jiang J, Ye K, Wang XC, Wang JZ (2014) SUMOylation at K340 inhibits tau

degradation through deregulating its phosphorylation and ubiquitination. Proceedings of the National Academy of Sciences of the United States of America 111:16586-16591.

Lykissas MG, Batistatou AK, Charalabopoulos KA, Beris AE (2007) The role of neurotrophins in axonal growth, guidance, and regeneration. Current neurovascular research 4:143-151.

Mahajan R, Delphin C, Guan T, Gerace L, Melchior F (1997) A small ubiquitin-related polypeptide involved in targeting RanGAP1 to nuclear pore complex protein RanBP2. Cell 88:97-107.

Majava V, Loytynoja N, Chen WQ, Lubec G, Kursula P (2008) Crystal and solution structure, stability and post-translational modifications of collapsin response mediator protein 2. The FEBS journal 275:4583-4596.

Malcangio M, Tomlinson DR (1998) A pharmacologic analysis of mechanical hyperalgesia in streptozotocin/diabetic rats. Pain 76:151-157.

Malhotra JD, Kazen-Gillespie K, Hortsch M, Isom LL (2000) Sodium channel beta subunits mediate homophilic cell adhesion and recruit ankyrin to points of cell-cell contact. The Journal of biological chemistry 275:11383-11388.

Mandell DJ, Chorny I, Groban ES, Wong SE, Levine E, Rapp CS, Jacobson MP (2007) Strengths of hydrogen bonds involving phosphorylated amino acid side chains. Journal of the American Chemical Society 129:820-827.

Manning G, Whyte DB, Martinez R, Hunter T, Sudarsanam S (2002) The protein kinase complement of the human genome. Science 298:1912-1934.

Martin S, Nishimune A, Mellor JR, Henley JM (2007a) SUMOylation regulates kainate-receptor-mediated synaptic transmission. Nature 447:321-325.

Martin S, Wilkinson KA, Nishimune A, Henley JM (2007b) Emerging extranuclear roles of protein SUMOylation in neuronal function and dysfunction. Nature reviews Neuroscience 8:948-959.

Matic I, Schimmel J, Hendriks IA, van Santen MA, van de Rijke F, van Dam H, Gnad F, Mann M, Vertegaal AC (2010) Site-specific identification of SUMO-2 targets in cells reveals an inverted SUMOylation motif and a hydrophobic cluster SUMOylation motif. Molecular cell 39:641-652.

Matic I, van Hagen M, Schimmel J, Macek B, Ogg SC, Tatham MH, Hay RT, Lamond AI, Mann M, Vertegaal AC (2008) In vivo identification of human small ubiquitin-like modifier polymerization sites by high accuracy mass spectrometry and an in vitro to in vivo strategy. Molecular & cellular proteomics : MCP 7:132-144.

Matunis MJ, Coutavas E, Blobel G (1996) A novel ubiquitin-like modification modulates the partitioning of the Ran-GTPase-activating protein RanGAP1 between the cytosol and the nuclear pore complex. The Journal of cell biology 135:1457-1470.

McCormack K, Santos S, Chapman ML, Krafte DS, Marron BE, West CW, Krambis MJ, Antonio BM, Zellmer SG, Printzenhoff D, Padilla KM, Lin Z, Wagoner PK, Swain NA, Stupple PA, de Groot M, Butt RP, Castle NA (2013) Voltage sensor interaction site for selective small molecule inhibitors of voltage-gated sodium channels. Proceedings of the National Academy of Sciences of the United States of America 110:E2724-2732.

McGill MA, Dho SE, Weinmaster G, McGlade CJ (2009) Numb regulates post-endocytic trafficking and degradation of Notch1. The Journal of biological chemistry 284:26427-26438.

McGill MA, McGlade CJ (2003) Mammalian numb proteins promote Notch1 receptor ubiquitination and degradation of the Notch1 intracellular domain. The Journal of biological chemistry 278:23196-23203.

Meadows LS, Chen YH, Powell AJ, Clare JJ, Ragsdale DS (2002) Functional modulation of human brain Nav1.3 sodium channels, expressed in mammalian cells, by auxiliary beta 1, beta 2 and beta 3 subunits. Neuroscience 114:745-753.

Meinecke I, Cinski A, Baier A, Peters MA, Dankbar B, Wille A, Drynda A, Mendoza H, Gay RE, Hay RT, Ink B, Gay S, Pap T (2007) Modification of nuclear PML protein by SUMO-1 regulates Fas-induced apoptosis in rheumatoid arthritis synovial fibroblasts. Proceedings of the National Academy of Sciences of the United States of America 104:5073-5078.

Melchior F, Schergaut M, Pichler A (2003) SUMO: ligases, isopeptidases and nuclear pores. Trends in biochemical sciences 28:612-618.

Mercier A, Clement R, Harnois T, Bourmeyster N, Bois P, Chatelier A (2015) Nav1.5 channels can reach the plasma membrane through distinct N-glycosylation states. Biochimica et biophysica acta 1850:1215-1223.

Merrill JC, Melhuish TA, Kagey MH, Yang SH, Sharrocks AD, Wotton D (2010) A role for non-covalent SUMO interaction motifs in Pc2/CBX4 E3 activity. PloS one 5:e8794.

Mikkonen L, Hirvonen J, Janne OA (2013) SUMO-1 regulates body weight and adipogenesis via PPARgamma in male and female mice. Endocrinology 154:698-708.

Miller C (1991) 1990: annus mirabilis of potassium channels. Science 252:1092-1096.

Minett MS, Eijkelkamp N, Wood JN (2014a) Significant determinants of mouse pain behaviour. PloS one 9:e104458.

Minett MS, Falk S, Santana-Varela S, Bogdanov YD, Nassar MA, Heegaard AM, Wood JN (2014b) Pain without nociceptors? Nav1.7-independent pain mechanisms. Cell reports 6:301-312.

Minett MS, Nassar MA, Clark AK, Passmore G, Dickenson AH, Wang F, Malcangio M, Wood JN (2012) Distinct Nav1.7-dependent pain sensations require different sets of sensory and sympathetic neurons. Nature communications 3:791.

Minturn JE, Fryer HJ, Geschwind DH, Hockfield S (1995) TOAD-64, a gene expressed early in neuronal differentiation in the rat, is related to unc-33, a C. elegans gene involved in axon outgrowth. The Journal of neuroscience : the official journal of the Society for Neuroscience 15:6757-6766.

Momin A, Wood JN (2008) Sensory neuron voltage-gated sodium channels as analgesic drug targets. Current opinion in neurobiology 18:383-388.

Morinaka A, Yamada M, Itofusa R, Funato Y, Yoshimura Y, Nakamura F, Yoshimura T, Kaibuchi K, Goshima Y, Hoshino M, Kamiguchi H, Miki H (2011) Thioredoxin mediates oxidation-dependent phosphorylation of CRMP2 and growth cone collapse. Science signaling 4:ra26.

Morris DH, Dubnau J, Park JH, Rawls JM, Jr. (2012) Divergent functions through alternative splicing: the Drosophila CRMP gene in pyrimidine metabolism, brain, and behavior. Genetics 191:1227-1238.

Moutal A, Francois-Moutal L, Perez-Miller S, Cottier K, Chew LA, Yeon SK, Dai J, Park KD, Khanna M, Khanna R (2015) (S)-Lacosamide Binding to Collapsin Response Mediator Protein 2 (CRMP2) Regulates CaV2.2 Activity by Subverting Its Phosphorylation by Cdk5. Molecular neurobiology.

Mukai M, Sakuma Y, Suzuki M, Orita S, Yamauchi K, Inoue G, Aoki Y, Ishikawa T, Miyagi M, Kamoda H, Kubota G, Oikawa Y, Inage K, Sainoh T, Sato J, Nakamura J, Takaso M, Toyone T, Takahashi K, Ohtori S (2014) Evaluation of behavior and expression of NaV1.7 in dorsal root ganglia after sciatic nerve compression and application of nucleus pulposus in rats. European spine journal : official publication of the European Spine Society, the European Spinal Deformity Society, and the European Section of the Cervical Spine Research Society 23:463-468.

Mukhopadhyay D, Ayaydin F, Kolli N, Tan SH, Anan T, Kametaka A, Azuma Y, Wilkinson KD, Dasso M (2006) SUSP1 antagonizes formation of highly SUMO2/3-conjugated species. The Journal of cell biology 174:939-949.

Mukhopadhyay D, Dasso M (2007) Modification in reverse: the SUMO proteases. Trends in biochemical sciences 32:286-295.

Muller S, Hoege C, Pyrowolakis G, Jentsch S (2001) SUMO, ubiquitin's mysterious cousin. Nature reviews Molecular cell biology 2:202-210.

Muller S, Matunis MJ, Dejean A (1998) Conjugation with the ubiquitin-related modifier SUMO-1 regulates the partitioning of PML within the nucleus. The EMBO journal 17:61-70.

Muroi Y, Undem BJ (2011) Targeting peripheral afferent nerve terminals for cough and dyspnea. Current opinion in pharmacology 11:254-264.

Muroi Y, Undem BJ (2014) Targeting voltage gated sodium channels NaV1.7, Na V1.8, and Na V1.9 for treatment of pathological cough. Lung 192:15-20.

Murray KT, Hu NN, Daw JR, Shin HG, Watson MT, Mashburn AB, George AL, Jr. (1997) Functional effects of protein kinase C activation on the human cardiac Na+ channel. Circulation research 80:370-376.

Nacerddine K, Lehembre F, Bhaumik M, Artus J, Cohen-Tannoudji M, Babinet C, Pandolfi PP, Dejean A (2005) The SUMO pathway is essential for nuclear integrity and chromosome segregation in mice. Developmental cell 9:769-779.

Nadler JV (2003) The recurrent mossy fiber pathway of the epileptic brain. Neurochemical research 28:1649-1658.

Nassar MA, Levato A, Stirling LC, Wood JN (2005) Neuropathic pain develops normally in mice lacking both Na(v)1.7 and Na(v)1.8. Molecular pain 1:24.

Nassar MA, Stirling LC, Forlani G, Baker MD, Matthews EA, Dickenson AH, Wood JN (2004) Nociceptor-specific gene deletion reveals a major role for Nav1.7 (PN1) in acute and inflammatory pain. Proceedings of the National Academy of Sciences of the United States of America 101:12706-12711.

Nelson M, Millican-Slater R, Forrest LC, Brackenbury WJ (2014) The sodium channel beta1 subunit mediates outgrowth of neurite-like processes on breast cancer cells and promotes tumour growth and metastasis. International journal of cancer Journal international du cancer 135:2338-2351.

Nishimura T, Fukata Y, Kato K, Yamaguchi T, Matsuura Y, Kamiguchi H, Kaibuchi K (2003a) CRMP-2 regulates polarized Numb-mediated endocytosis for axon growth. Nature cell biology 5:819-826.

Nishimura T, Fukata Y, Kato K, Yamaguchi T, Matsuura Y, Kamiguchi H, Kaibuchi K (2003b) CRMP-2 regulates polarized Numb-mediated endocytosis for axon growth. NatCell Biol 5:819-826.

Noda M, Shimizu S, Tanabe T, Takai T, Kayano T, Ikeda T, Takahashi H, Nakayama H, Kanaoka Y, Minamino N, et al. (1984) Primary structure of Electrophorus electricus sodium channel deduced from cDNA sequence. Nature 312:121-127.

Noda M, Suzuki H, Numa S, Stuhmer W (1989) A single point mutation confers tetrodotoxin and saxitoxin insensitivity on the sodium channel II. FEBS letters 259:213-216.

Noshita N, Lewen A, Sugawara T, Chan PH (2001) Evidence of phosphorylation of Akt and neuronal survival after transient focal cerebral ischemia in mice. Journal of cerebral blood flow and metabolism : official journal of the International Society of Cerebral Blood Flow and Metabolism 21:1442-1450.

O'Brien BJ, Caldwell JH, Ehring GR, Bumsted O'Brien KM, Luo S, Levinson SR (2008) Tetrodotoxin-resistant voltage-gated sodium channels Na(v)1.8 and Na(v)1.9 are expressed in the retina. The Journal of comparative neurology 508:940-951.

Obata K, Yamanaka H, Kobayashi K, Dai Y, Mizushima T, Katsura H, Fukuoka T, Tokunaga A, Noguchi K (2004) Role of mitogen-activated protein kinase activation in injured and intact primary afferent neurons for mechanical and heat hypersensitivity after spinal nerve ligation. The Journal of neuroscience : the official journal of the Society for Neuroscience 24:10211-10222.

Okuma T, Honda R, Ichikawa G, Tsumagari N, Yasuda H (1999) In vitro SUMO-1 modification requires two enzymatic steps, E1 and E2. Biochemical and biophysical research communications 254:693-698.

Okura T, Gong L, Kamitani T, Wada T, Okura I, Wei CF, Chang HM, Yeh ET (1996) Protection against Fas/APO-1- and tumor necrosis factor-mediated cell death by a novel protein, sentrin. Journal of immunology 157:4277-4281.

Olsen JV, Blagoev B, Gnad F, Macek B, Kumar C, Mortensen P, Mann M (2006) Global, in vivo, and site-specific phosphorylation dynamics in signaling networks. Cell 127:635-648.

Osterhout DJ, Wolven A, Wolf RM, Resh MD, Chao MV (1999) Morphological differentiation of oligodendrocytes requires activation of Fyn tyrosine kinase. The Journal of cell biology 145:1209-1218.

Patrakitkomjorn S, Kobayashi D, Morikawa T, Wilson MM, Tsubota N, Irie A, Ozawa T, Aoki M, Arimura N, Kaibuchi K, Saya H, Araki N (2008) Neurofibromatosis type 1 (NF1) tumor suppressor, neurofibromin, regulates the neuronal differentiation of PC12 cells via its associating protein, CRMP-2. J Biol Chem 283:9399-9413.

Payandeh J, Scheuer T, Zheng N, Catterall WA (2011) The crystal structure of a voltage-gated sodium channel. Nature 475:353-358.

Perdomo J, Verger A, Turner J, Crossley M (2005) Role for SUMO modification in facilitating transcriptional repression by BKLF. Molecular and cellular biology 25:1549-1559.

Pertin M, Ji RR, Berta T, Powell AJ, Karchewski L, Tate SN, Isom LL, Woolf CJ, Gilliard N, Spahn DR, Decosterd I (2005) Upregulation of the voltage-gated sodium channel beta2 subunit in neuropathic pain models: characterization of expression in injured and non-injured primary sensory neurons. The Journal of neuroscience : the official journal of the Society for Neuroscience 25:10970-10980.

Picard N, Caron V, Bilodeau S, Sanchez M, Mascle X, Aubry M, Tremblay A (2012) Identification of estrogen receptor beta as a SUMO-1 target reveals a novel phosphorylated sumoylation motif and regulation by glycogen synthase kinase 3beta. Molecular and cellular biology 32:2709-2721.

Pichler A, Knipscheer P, Oberhofer E, van Dijk WJ, Korner R, Olsen JV, Jentsch S, Melchior F, Sixma TK (2005) SUMO modification of the ubiquitin-conjugating enzyme E2-25K. Nature structural & molecular biology 12:264-269.

Pitkanen A, Lukasiuk K (2009) Molecular and cellular basis of epileptogenesis in symptomatic epilepsy. Epilepsy & behavior : E&B 14 Suppl 1:16-25.

Plant LD, Dowdell EJ, Dementieva IS, Marks JD, Goldstein SA (2011) SUMO modification of cell surface Kv2.1 potassium channels regulates the activity of rat hippocampal neurons. The Journal of general physiology 137:441-454.

Ponnusamy R, Lohkamp B (2013) Insights into the oligomerization of CRMPs: crystal structure of human collapsin response mediator protein 5. Journal of neurochemistry 125:855-868.

Quach TT, Duchemin AM, Rogemond V, Aguera M, Honnorat J, Belin MF, Kolattukudy PE (2004) Involvement of collapsin response mediator proteins in the neurite extension induced by neurotrophins in dorsal root ganglion neurons. Molecular and cellular neurosciences 25:433-443.

Quach TT, Mosinger B, Jr., Ricard D, Copeland NG, Gilbert DJ, Jenkins NA, Stankoff B, Honnorat J, Belin MF, Kolattukudy P (2000) Collapsin response mediator protein-3/unc-33-like protein-4 gene: organization, chromosomal mapping and expression in the developing mouse brain. Gene 242:175-182.

Rahajeng J, Giridharan SS, Naslavsky N, Caplan S (2010) Collapsin response mediator protein-2 (Crmp2) regulates trafficking by linking endocytic regulatory proteins to dynein motors. Journal of Biological Chemistry.

Rajan S, Plant LD, Rabin ML, Butler MH, Goldstein SA (2005) Sumoylation silences the plasma membrane leak K+ channel K2P1. Cell 121:37-47.

Raymond CK, Castle J, Garrett-Engele P, Armour CD, Kan Z, Tsinoremas N, Johnson JM (2004) Expression of alternatively spliced sodium channel alpha-subunit genes. Unique splicing patterns are observed in dorsal root ganglia. The Journal of biological chemistry 279:46234-46241.

Reeves BN, Dakhil SR, Sloan JA, Wolf SL, Burger KN, Kamal A, Le-Lindqwister NA, Soori GS, Jaslowski AJ, Kelaghan J, Novotny PJ, Lachance DH, Loprinzi CL (2012) Further data supporting that paclitaxel-associated acute pain syndrome is associated with development of peripheral neuropathy: North Central Cancer Treatment Group trial N08C1. Cancer 118:5171-5178.

Rothenberg MA (1950) Studies on permeability in relation to nerve function, ionic movements across exonal membranes. Biochim Biophys Acta 4:96-114.

Rougier JS, van Bemmelen MX, Bruce MC, Jespersen T, Gavillet B, Apotheloz F, Cordonier S, Staub O, Rotin D, Abriel H (2005) Molecular determinants of voltage-gated sodium channel regulation by the Nedd4/Nedd4-like proteins. American journal of physiology Cell physiology 288:C692-701.

Roy ML, Narahashi T (1992) Differential properties of tetrodotoxin-sensitive and tetrodotoxin-resistant sodium channels in rat dorsal root ganglion neurons. The Journal of neuroscience : the official journal of the Society for Neuroscience 12:2104-2111.

Rui HL, Fan E, Zhou HM, Xu Z, Zhang Y, Lin SC (2002) SUMO-1 modification of the C-terminal KVEKVD of Axin is required for JNK activation but has no effect on Wnt signaling. The Journal of biological chemistry 277:42981-42986.

Rusconi R, Scalmani P, Cassulini RR, Giunti G, Gambardella A, Franceschetti S, Annesi G, Wanke E, Mantegazza M (2007) Modulatory proteins can rescue a trafficking defective epileptogenic Nav1.1 Na+ channel mutant. The Journal of neuroscience : the official journal of the Society for Neuroscience 27:11037-11046.

Sadamasu A, Sakuma Y, Suzuki M, Orita S, Yamauchi K, Inoue G, Aoki Y, Ishikawa T, Miyagi M, Kamoda H, Kubota G, Oikawa Y, Inage K, Sainoh T, Sato J, Nakamura J, Toyone T, Takahashi K, Ohtori S (2014) Upregulation of NaV1.7 in dorsal root ganglia after intervertebral disc injury in rats. Spine 39:E421-426.

Sampson DA, Wang M, Matunis MJ (2001) The small ubiquitin-like modifier-1 (SUMO-1) consensus sequence mediates Ubc9 binding and is essential for SUMO-1 modification. The Journal of biological chemistry 276:21664-21669.

Sanders SJ, Murtha MT, Gupta AR, Murdoch JD, Raubeson MJ, Willsey AJ, Ercan-Sencicek AG, DiLullo NM, Parikshak NN, Stein JL, Walker MF, Ober GT, Teran NA, Song Y, El-Fishawy P, Murtha RC, Choi M, Overton JD, Bjornson RD, Carriero NJ, Meyer KA, Bilguvar K, Mane SM, Sestan N, Lifton RP, Gunel M, Roeder K, Geschwind DH, Devlin B, State MW (2012) De novo mutations revealed by whole-exome sequencing are strongly associated with autism. Nature 485:237-241.

Santolini E, Puri C, Salcini AE, Gagliani MC, Pelicci PG, Tacchetti C, Di Fiore PP (2000) Numb is an endocytic protein. The Journal of cell biology 151:1345-1352.

Sapetschnig A, Rischitor G, Braun H, Doll A, Schergaut M, Melchior F, Suske G (2002) Transcription factor Sp3 is silenced through SUMO modification by PIAS1. The EMBO journal 21:5206-5215.

Sasaki Y, Cheng C, Uchida Y, Nakajima O, Ohshima T, Yagi T, Taniguchi M, Nakayama T, Kishida R, Kudo Y, Ohno S, Nakamura F, Goshima Y (2002) Fyn and Cdk5 mediate semaphorin-3A signaling, which is involved in regulation of dendrite orientation in cerebral cortex. Neuron 35:907-920.

Schlief T, Schonherr R, Imoto K, Heinemann SH (1996) Pore properties of rat brain II sodium channels mutated in the selectivity filter domain. European biophysics journal : EBJ 25:75-91.

Schmalhofer WA, Calhoun J, Burrows R, Bailey T, Kohler MG, Weinglass AB, Kaczorowski GJ, Garcia ML, Koltzenburg M, Priest BT (2008) ProTx-II, a selective inhibitor of NaV1.7 sodium channels, blocks action potential propagation in nociceptors. Molecular pharmacology 74:1476-1484.

Schmidt EF, Strittmatter SM (2007) The CRMP family of proteins and their role in Sema3A signaling. Advances in Experimental Medicine and Biology 600:1-11.

Schmidt JW, Catterall WA (1986) Biosynthesis and processing of the alpha subunit of the voltage-sensitive sodium channel in rat brain neurons. Cell 46:437-444.

Schmunk G, Gargus JJ (2013) Channelopathy pathogenesis in autism spectrum disorders. Frontiers in genetics 4:222.

Schreibmayer W, Dascal N, Lotan I, Wallner M, Weigl L (1991) Molecular mechanism of protein kinase C modulation of sodium channel alpha-subunits expressed in Xenopus oocytes. FEBS letters 291:341-344.

Seger R, Krebs EG (1995) The MAPK signaling cascade. FASEB journal : official publication of the Federation of American Societies for Experimental Biology 9:726-735.

Shan B, Dong M, Tang H, Wang N, Zhang J, Yan C, Jiao X, Zhang H, Wang C (2014) Voltage-gated sodium channels were differentially expressed in human normal prostate, benign prostatic hyperplasia and prostate cancer cells. Oncology letters 8:345-350.

Shao B, Victory S, Ilyin VI, Goehring RR, Sun Q, Hogenkamp D, Hodges DD, Islam K, Sha D, Zhang C, Nguyen P, Robledo S, Sakellaropoulos G, Carter RB (2004) Phenoxyphenyl pyridines as novel state-dependent, high-potency sodium channel inhibitors. Journal of medicinal chemistry 47:4277-4285.

Sheets PL, Heers C, Stoehr T, Cummins TR (2008) Differential block of sensory neuronal voltage-gated sodium channels by lacosamide [(2R)-2-(acetylamino)-N-benzyl-3-methoxypropanamide], lidocaine, and carbamazepine. The Journal of pharmacology and experimental therapeutics 326:89-99.

Shen LN, Geoffroy MC, Jaffray EG, Hay RT (2009) Characterization of SENP7, a SUMO-2/3-specific isopeptidase. The Biochemical journal 421:223-230.

Shen Z, Pardington-Purtymun PE, Comeaux JC, Moyzis RK, Chen DJ (1996) UBL1, a human ubiquitin-like protein associating with human RAD51/RAD52 proteins. Genomics 36:271-279.

Sigel E (1987) Effects of veratridine on single neuronal sodium channels expressed in Xenopus oocytes. Pflugers Archiv : European journal of physiology 410:112-120.

Smith JJ, Cummins TR, Alphy S, Blumenthal KM (2007) Molecular interactions of the gating modifier toxin ProTx-II with NaV 1.5: implied existence of a novel toxin binding site coupled to activation. The Journal of biological chemistry 282:12687-12697.

Srinivasan J, Schachner M, Catterall WA (1998) Interaction of voltage-gated sodium channels with the extracellular matrix molecules tenascin-C and tenascin-R. Proceedings of the National Academy of Sciences of the United States of America 95:15753-15757.

Staats PS, Yearwood T, Charapata SG, Presley RW, Wallace MS, Byas-Smith M, Fisher R, Bryce DA, Mangieri EA, Luther RR, Mayo M, McGuire D, Ellis D (2004) Intrathecal ziconotide in the treatment of refractory pain in patients with cancer or AIDS: a randomized controlled trial. Jama 291:63-70.

Stamboulian S, Choi JS, Ahn HS, Chang YW, Tyrrell L, Black JA, Waxman SG, Dib-Hajj SD (2010) ERK1/2 mitogen-activated protein kinase phosphorylates sodium channel Na(v)1.7 and alters its gating properties. The Journal of neuroscience : the official journal of the Society for Neuroscience 30:1637-1647.

Stankovic-Valentin N, Deltour S, Seeler J, Pinte S, Vergoten G, Guerardel C, Dejean A, Leprince D (2007) An acetylation/deacetylation-SUMOylation switch through a phylogenetically conserved psiKXEP motif in the tumor suppressor HIC1 regulates transcriptional repression activity. Molecular and cellular biology 27:2661-2675.

Staub O, Abriel H, Plant P, Ishikawa T, Kanelis V, Saleki R, Horisberger JD, Schild L, Rotin D (2000) Regulation of the epithelial Na+ channel by Nedd4 and ubiquitination. Kidney international 57:809-815.

Stenmark P, Ogg D, Flodin S, Flores A, Kotenyova T, Nyman T, Nordlund P, Kursula P (2007) The structure of human collapsin response mediator protein 2, a regulator of axonal growth. Journal of Neurochemistry 101:906-917.

Stuhmer W, Conti F, Suzuki H, Wang XD, Noda M, Yahagi N, Kubo H, Numa S (1989) Structural parts involved in activation and inactivation of the sodium channel. Nature 339:597-603.

Sun H, Hunter T (2012) Poly-small ubiquitin-like modifier (PolySUMO)-binding proteins identified through a string search. The Journal of biological chemistry 287:42071-42083.

Susini L, Passer BJ, Amzallag-Elbaz N, Juven-Gershon T, Prieur S, Privat N, Tuynder M, Gendron MC, Israel A, Amson R, Oren M, Telerman A (2001) Siah-1 binds and regulates the function of Numb. Proceedings of the National Academy of Sciences of the United States of America 98:15067-15072.

Takahashi T, Fournier A, Nakamura F, Wang LH, Murakami Y, Kalb RG, Fujisawa H, Strittmatter SM (1999) Plexin-neuropilin-1 complexes form functional semaphorin-3A receptors. Cell 99:59-69.

Takahashi Y, Toh-e A, Kikuchi Y (2001) A novel factor required for the SUMO1/Smt3 conjugation of yeast septins. Gene 275:223-231.

Talvenheimo JA, Tamkun MM, Catterall WA (1982) Reconstitution of neurotoxin-stimulated sodium transport by the voltage-sensitive sodium channel purified from rat brain. The Journal of biological chemistry 257:11868-11871.

Tan JA, Song J, Chen Y, Durrin LK (2010) Phosphorylation-dependent interaction of SATB1 and PIAS1 directs SUMO-regulated caspase cleavage of SATB1. Molecular and cellular biology 30:2823-2836.

Tanabe T, Takeshima H, Mikami A, Flockerzi V, Takahashi H, Kangawa K, Kojima M, Matsuo H, Hirose T, Numa S (1987) Primary structure of the receptor for calcium channel blockers from skeletal muscle. Nature 328:313-318.

Tang H, Rompani SB, Atkins JB, Zhou Y, Osterwalder T, Zhong W (2005) Numb proteins specify asymmetric cell fates via an endocytosis- and proteasome-independent pathway. Molecular and cellular biology 25:2899-2909.

Tatham MH, Jaffray E, Vaughan OA, Desterro JM, Botting CH, Naismith JH, Hay RT (2001) Polymeric chains of SUMO-2 and SUMO-3 are conjugated to protein substrates by SAE1/SAE2 and Ubc9. The Journal of biological chemistry 276:35368-35374.

Tavassoli T, Kolevzon A, Wang AT, Curchack-Lichtin J, Halpern D, Schwartz L, Soffes S, Bush L, Grodberg D, Cai G, Buxbaum JD (2014) De novo SCN2A splice site mutation in a boy with Autism spectrum disorder. BMC medical genetics 15:35.

Tempel BL, Papazian DM, Schwarz TL, Jan YN, Jan LY (1987) Sequence of a probable potassium channel component encoded at Shaker locus of Drosophila. Science 237:770-775.

Theile JW, Cummins TR (2011a) Inhibition of Navbeta4 peptide-mediated resurgent sodium currents in Nav1.7 channels by carbamazepine, riluzole, and anandamide. Molecular pharmacology 80:724-734.

Theile JW, Cummins TR (2011b) Recent developments regarding voltage-gated sodium channel blockers for the treatment of inherited and acquired neuropathic pain syndromes. Frontiers in pharmacology 2:54.

Theile JW, Jarecki BW, Piekarz AD, Cummins TR (2011) Nav1.7 mutations associated with paroxysmal extreme pain disorder, but not erythromelalgia, enhance Navbeta4 peptide-mediated resurgent sodium currents. The Journal of physiology 589:597-608.

Touma E, Kato S, Fukui K, Koike T (2007) Calpain-mediated cleavage of collapsin response mediator protein(CRMP)-2 during neurite degeneration in mice. Eur J Neurosci 26:3368-3381.

Truong K, Lee TD, Chen Y (2012) Small ubiquitin-like modifier (SUMO) modification of E1 Cys domain inhibits E1 Cys domain enzymatic activity. The Journal of biological chemistry 287:15154-15163.

Tsutiya A, Ohtani-Kaneko R (2012) Postnatal alteration of collapsin response mediator protein 4 mRNA expression in the mouse brain. Journal of anatomy 221:341-351.

Tyrrell L, Renganathan M, Dib-Hajj SD, Waxman SG (2001) Glycosylation alters steady-state inactivation of sodium channel Nav1.9/NaN in dorsal root ganglion neurons and is developmentally regulated. The Journal of neuroscience : the official journal of the Society for Neuroscience 21:9629-9637.

Uchida Y, Ohshima T, Sasaki Y, Suzuki H, Yanai S, Yamashita N, Nakamura F, Takei K, Ihara Y, Mikoshiba K, Kolattukudy P, Honnorat J, Goshima Y (2005) Semaphorin3A signalling is mediated via sequential Cdk5 and GSK3beta phosphorylation of CRMP2: implication of common phosphorylating mechanism underlying axon guidance and Alzheimer's disease. Genes to cells : devoted to molecular & cellular mechanisms 10:165-179.

Uchida Y, Ohshima T, Yamashita N, Ogawara M, Sasaki Y, Nakamura F, Goshima Y (2009) Semaphorin3A signaling mediated by Fyn-dependent tyrosine phosphorylation of collapsin response mediator protein 2 at tyrosine 32. The Journal of biological chemistry 284:27393-27401.

Ulrich HD (2009) The SUMO system: an overview. Methods in molecular biology 497:3-16.

Valdes AM, Arden NK, Vaughn FL, Doherty SA, Leaverton PE, Zhang W, Muir KR, Rampersaud E, Dennison EM, Edwards MH, Jameson KA, Javaid MK, Spector TD, Cooper C, Maciewicz RA, Doherty M (2011) Role of the Nav1.7 R1150W amino acid change in susceptibility to symptomatic knee osteoarthritis and multiple regional pain. Arthritis care & research 63:440-444.

van Bemmelen MX, Rougier JS, Gavillet B, Apotheloz F, Daidie D, Tateyama M, Rivolta I, Thomas MA, Kass RS, Staub O, Abriel H (2004) Cardiac voltage-gated sodium channel Nav1.5 is regulated by Nedd4-2 mediated ubiquitination. Circulation research 95:284-291.

van den Boogaard M, Smemo S, Burnicka-Turek O, Arnolds DE, van de Werken HJ, Klous P, McKean D, Muehlschlegel JD, Moosmann J, Toka O, Yang XH, Koopmann TT, Adriaens ME, Bezzina CR, de Laat W, Seidman C, Seidman JG, Christoffels VM, Nobrega MA, Barnett P, Moskowitz IP (2014) A common genetic variant within SCN10A modulates cardiac SCN5A expression. The Journal of clinical investigation 124:1844-1852.

Varrin-Doyer M, Vincent P, Cavagna S, Auvergnon N, Noraz N, Rogemond V, Honnorat J, Moradi-Ameli M, Giraudon P (2009) Phosphorylation of collapsin response mediator protein 2 on Tyr-479 regulates CXCL12-induced T lymphocyte migration. The Journal of biological chemistry 284:13265-13276.

Veneroni O, Maj R, Calabresi M, Faravelli L, Fariello RG, Salvati P (2003) Anti-allodynic effect of NW-1029, a novel Na(+) channel blocker, in experimental animal models of inflammatory and neuropathic pain. Pain 102:17-25.

Venteclef N, Jakobsson T, Ehrlund A, Damdimopoulos A, Mikkonen L, Ellis E, Nilsson LM, Parini P, Janne OA, Gustafsson JA, Steffensen KR, Treuter E (2010) GPS2-dependent corepressor/SUMO pathways govern anti-inflammatory actions of LRH-1 and LXRbeta in the hepatic acute phase response. Genes & development 24:381-395.

Vertegaal AC, Andersen JS, Ogg SC, Hay RT, Mann M, Lamond AI (2006) Distinct and overlapping sets of SUMO-1 and SUMO-2 target proteins revealed by quantitative proteomics. Molecular & cellular proteomics : MCP 5:2298-2310.

Vijayaragavan K, Boutjdir M, Chahine M (2004) Modulation of Nav1.7 and Nav1.8 peripheral nerve sodium channels by protein kinase A and protein kinase C. Journal of neurophysiology 91:1556-1569.

Vincent P, Collette Y, Marignier R, Vuaillat C, Rogemond V, Davoust N, Malcus C, Cavagna S, Gessain A, Machuca-Gayet I, Belin MF, Quach T, Giraudon P (2005) A role for the neuronal protein collapsin response mediator protein 2 in T lymphocyte polarization and migration. J Immunol 175:7650-7660.

Vuaillat C, Varrin-Doyer M, Bernard A, Sagardoy I, Cavagna S, Chounlamountri I, Lafon M, Giraudon P (2008) High CRMP2 expression in peripheral T lymphocytes is associated with recruitment to the brain during virus-induced neuroinflammation. Journal of neuroimmunology 193:38-51.

Wang J, Chen L, Wen S, Zhu H, Yu W, Moskowitz IP, Shaw GM, Finnell RH, Schwartz RJ (2011a) Defective sumoylation pathway directs congenital heart disease. Birth defects research Part A, Clinical and molecular teratology 91:468-476.

Wang LH, Strittmatter SM (1996) A family of rat CRMP genes is differentially expressed in the nervous system. J Neurosci 16:6197-6207.

Wang LH, Strittmatter SM (1997a) Brain CRMP forms heterotetramers similar to liver dihydropyrimidinase. J Neurochem 69:2261-2269.

Wang LH, Strittmatter SM (1997b) Brain CRMP forms heterotetramers similar to liver dihydropyrimidinase. Journal of neurochemistry 69:2261-2269.

Wang LH, Strittmatter SM (1997c) Brain CRMP forms heterotetramers similar to liver dihydropyrimidinase. JNeurochem 69:2261-2269.

Wang Y, Brittain JM, Jarecki BW, Park KD, Wilson SM, Wang B, Hale R, Meroueh SO, Cummins TR, Khanna R (2010a) In silico docking and electrophysiological characterization of lacosamide binding sites on collapsin response mediator protein-2 identifies a pocket important in modulating sodium channel slow inactivation. The Journal of biological chemistry 285:25296-25307.

Wang Y, Brittain JM, Wilson SM, Khanna R (2010b) Emerging roles of collapsin response mediator proteins (CRMPs) as regulators of voltage-gated calcium channels and synaptic transmission. Communicative & integrative biology 3:172-175.

Wang Y, Park KD, Salome C, Wilson SM, Stables JP, Liu R, Khanna R, Kohn H (2011b) Development and characterization of novel derivatives of the antiepileptic drug lacosamide that exhibit far greater enhancement in slow inactivation of voltage-gated sodium channels. ACS chemical neuroscience 2:90-106.

Wang Y, Wilson SM, Brittain JM, Ripsch MS, Salome C, Park KD, White FA, Khanna R, Kohn H (2011c) Merging Structural Motifs of Functionalized Amino Acids and alpha-Aminoamides Results in Novel Anticonvulsant Compounds with Significant Effects on Slow and Fast Inactivation of Voltage-gated Sodium Channels and in the Treatment of Neuropathic Pain. ACS chemical neuroscience 2:317-322.

Weiss J, Pyrski M, Jacobi E, Bufe B, Willnecker V, Schick B, Zizzari P, Gossage SJ, Greer CA, Leinders-Zufall T, Woods CG, Wood JN, Zufall F (2011) Loss-of-function mutations in sodium channel Nav1.7 cause anosmia. Nature 472:186-190.

Weng X, Smith T, Sathish J, Djouhri L (2012) Chronic inflammatory pain is associated with increased excitability and hyperpolarization-activated current (Ih) in C- but not Adelta-nociceptors. Pain 153:900-914.

West JW, Patton DE, Scheuer T, Wang Y, Goldin AL, Catterall WA (1992) A cluster of hydrophobic amino acid residues required for fast Na(+)-channel inactivation. Proceedings of the National Academy of Sciences of the United States of America 89:10910-10914.

Wilkinson KA, Nishimune A, Henley JM (2008) Analysis of SUMO-1 modification of neuronal proteins containing consensus SUMOylation motifs. Neuroscience letters 436:239-244.

Wilson MJ, Yoshikami D, Azam L, Gajewiak J, Olivera BM, Bulaj G, Zhang MM (2011) mu-Conotoxins that differentially block sodium channels NaV1.1 through 1.8 identify those responsible for action potentials in sciatic nerve. Proceedings of the National Academy of Sciences of the United States of America 108:10302-10307.

Wilson SM, Khanna R (2014) Specific Binding of Lacosamide to Collapsin Response Mediator Protein 2 (CRMP2) and Direct Impairment of its Canonical Function: Implications for the Therapeutic Potential of Lacosamide. Molecular neurobiology.

Wilson SM, Moutal A, Melemedjian OK, Wang Y, Ju W, Francois-Moutal L, Khanna M, Khanna R (2014) The functionalized amino acid (S)-Lacosamide subverts CRMP2-mediated tubulin polymerization to prevent constitutive and activity-dependent increase in neurite outgrowth. Frontiers in cellular neuroscience 8:196.

Wilson SM, Xiong W, Wang Y, Ping X, Head JD, Brittain JM, Gagare PD, Ramachandran PV, Jin X, Khanna R (2012) Prevention of posttraumatic axon sprouting by blocking collapsin response mediator protein 2-mediated neurite outgrowth and tubulin polymerization. Neuroscience 210:451-466.

Winquist RJ, Pan JQ, Gribkoff VK (2005) Use-dependent blockade of Cav2.2 voltage-gated calcium channels for neuropathic pain. Biochemical pharmacology 70:489-499.

Wittmack EK, Rush AM, Hudmon A, Waxman SG, Dib-Hajj SD (2005) Voltage-gated sodium channel Nav1.6 is modulated by p38 mitogen-activated protein kinase. The Journal of neuroscience : the official journal of the Society for Neuroscience 25:6621-6630.

Woelk T, Oldrini B, Maspero E, Confalonieri S, Cavallaro E, Di Fiore PP, Polo S (2006) Molecular mechanisms of coupled monoubiquitination. Nat Cell Biol 8:1246-1254.

Wolff C, Carrington B, Varrin-Doyer M, Vandendriessche A, Van der Perren C, Famelart M, Gillard M, Foerch P, Rogemond V, Honnorat J, Lawson A, Miller K (2012) Drug binding assays do not reveal specific binding of lacosamide to collapsin response mediator protein 2 (CRMP-2). CNS neuroscience & therapeutics 18:493-500.

Xiao Y, Bingham JP, Zhu W, Moczydlowski E, Liang S, Cummins TR (2008) Tarantula huwentoxin-IV inhibits neuronal sodium channels by binding to receptor site 4 and trapping the domain ii voltage sensor in the closed configuration. The Journal of biological chemistry 283:27300-27313.

Xiao Y, Blumenthal K, Jackson JO, 2nd, Liang S, Cummins TR (2010) The tarantula toxins ProTx-II and huwentoxin-IV differentially interact with human Nav1.7 voltage sensors to inhibit channel activation and inactivation. Molecular pharmacology 78:1124-1134.

Xiao Y, Pollack D, Nieves E, Winchell A, Callaway M, Vigodner M (2015) Can your protein be sumoylated? A quick summary and important tips to study SUMO-modified proteins. Analytical biochemistry 477:95-97.

Xu J, He Y, Qiang B, Yuan J, Peng X, Pan XM (2008) A novel method for high accuracy sumoylation site prediction from protein sequences. BMC bioinformatics 9:8.

Yaffe MB, Elia AE (2001) Phosphoserine/threonine-binding domains. Current opinion in cell biology 13:131-138.

Yanagita T, Maruta T, Nemoto T, Uezono Y, Matsuo K, Satoh S, Yoshikawa N, Kanai T, Kobayashi H, Wada A (2009) Chronic lithium treatment up-regulates cell surface Na(V)1.7 sodium channels via inhibition of glycogen synthase kinase-3 in adrenal chromaffin cells: enhancement of Na(+) influx, Ca(2+) influx and catecholamine secretion after lithium withdrawal. Neuropharmacology 57:311-321.

Yanagita T, Satoh S, Uezono Y, Matsuo K, Nemoto T, Maruta T, Yoshikawa N, Iwakiri T, Minami K, Murakami M (2011) Transcriptional up-regulation of cell surface Na V 1.7 sodium channels by insulin-like growth factor-1 via inhibition of glycogen synthase kinase-3beta in adrenal chromaffin cells: enhancement of 22Na+ influx, 45Ca2+ influx and catecholamine secretion. Neuropharmacology 61:1265-1274.

Yang L, Gu X, Zhang W, Zhang J, Ma Z (2014) Cdk5 inhibitor roscovitine alleviates neuropathic pain in the dorsal root ganglia by downregulating N-methyl-D-aspartate receptor subunit 2A. Neurological sciences : official journal of the Italian Neurological Society and of the Italian Society of Clinical Neurophysiology 35:1365-1371.

Yang S, Xiao Y, Kang D, Liu J, Li Y, Undheim EA, Klint JK, Rong M, Lai R, King GF (2013) Discovery of a selective NaV1.7 inhibitor from centipede venom with analgesic efficacy exceeding morphine in rodent pain models. Proceedings of the National Academy of Sciences of the United States of America 110:17534-17539.

Yang SH, Jaffray E, Hay RT, Sharrocks AD (2003) Dynamic interplay of the SUMO and ERK pathways in regulating Elk-1 transcriptional activity. Molecular cell 12:63-74.

Yang YR, He Y, Zhang Y, Li Y, Li Y, Han Y, Zhu H, Wang Y (2007) Activation of cyclin-dependent kinase 5 (Cdk5) in primary sensory and dorsal horn neurons by peripheral inflammation contributes to heat hyperalgesia. Pain 127:109-120.

Yao L, Yao S, Daly W, Hendry W, Windebank A, Pandit A (2012) Non-viral gene therapy for spinal cord regeneration. Drug discovery today 17:998-1005.

Yeomans DC, Levinson SR, Peters MC, Koszowski AG, Tzabazis AZ, Gilly WF, Wilson SP (2005) Decrease in inflammatory hyperalgesia by herpes vector-mediated knockdown of Nav1.7 sodium channels in primary afferents. Human gene therapy 16:271-277.

Yoneda A, Morgan-Fisher M, Wait R, Couchman JR, Wewer UM (2012) A collapsin response mediator protein 2 isoform controls myosin II-mediated cell migration and matrix assembly by trapping ROCK II. Molecular and cellular biology 32:1788-1804.

Yoshida H, Watanabe A, Ihara Y (1998) Collapsin response mediator protein-2 is associated with neurofibrillary tangles in Alzheimer's disease. J Biol Chem 273:9761-9768.

Yoshimura T, Kawano Y, Arimura N, Kawabata S, Kikuchi A, Kaibuchi K (2005a) GSK-3[beta] Regulates Phosphorylation of CRMP-2 and Neuronal Polarity. Cell 120:137-149.

Yoshimura T, Kawano Y, Arimura N, Kawabata S, Kikuchi A, Kaibuchi K (2005b) GSK-3beta regulates phosphorylation of CRMP-2 and neuronal polarity. Cell 120:137-149.

Yu FH, Westenbroek RE, Silos-Santiago I, McCormick KA, Lawson D, Ge P, Ferriera H, Lilly J, DiStefano PS, Catterall WA, Scheuer T, Curtis R (2003) Sodium channel beta4, a new disulfide-linked auxiliary subunit with similarity to beta2. The Journal of neuroscience : the official journal of the Society for Neuroscience 23:7577-7585.

Yuasa-Kawada J, Suzuki R, Kano F, Ohkawara T, Murata M, Noda M (2003) Axonal morphogenesis controlled by antagonistic roles of two CRMP subtypes in microtubule organization. The European journal of neuroscience 17:2329-2343.

Zhang FP, Mikkonen L, Toppari J, Palvimo JJ, Thesleff I, Janne OA (2008) Sumo-1 function is dispensable in normal mouse development. Molecular and cellular biology 28:5381-5390.

Zhang H, Dougherty PM (2014) Enhanced excitability of primary sensory neurons and altered gene expression of neuronal ion channels in dorsal root ganglion in paclitaxel-induced peripheral neuropathy. Anesthesiology 120:1463-1475.

Zhang MM, Wilson MJ, Gajewiak J, Rivier JE, Bulaj G, Olivera BM, Yoshikami D (2013) Pharmacological fractionation of tetrodotoxin-sensitive sodium currents in rat dorsal root ganglion neurons by mu-conotoxins. British journal of pharmacology 169:102-114.

Zhang W, Wu J, Ward MD, Yang S, Chuang YA, Xiao M, Li R, Leahy DJ, Worley PF (2015) Structural basis of arc binding to synaptic proteins: implications for cognitive disease. Neuron 86:490-500.

Zhang X, Zhang H, Shao H, Xue Q, Yu B (2014) ERK MAP kinase activation in spinal cord regulates phosphorylation of Cdk5 at serine 159 and contributes to peripheral inflammation induced pain/hypersensitivity. PloS one 9:e87788.

Zhang Z, Majava V, Greffier A, Hayes RL, Kursula P, Wang KK (2009) Collapsin response mediator protein-2 is a calmodulin-binding protein. Cell MolLife Sci 66:526-536.

Zhang Z, Ottens AK, Sadasivan S, Kobeissy FH, Fang T, Hayes RL, Wang KK (2007) Calpain-mediated collapsin response mediator protein-1, -2, and -4 proteolysis after neurotoxic and traumatic brain injury. Journal of neurotrauma 24:460-472.

Zhu J, Zhu S, Guzzo CM, Ellis NA, Sung KS, Choi CY, Matunis MJ (2008) Small ubiquitin-related modifier (SUMO) binding determines substrate recognition and paralog-selective SUMO modification. The Journal of biological chemistry 283:29405-29415.

Zhu LQ, Zheng HY, Peng CX, Liu D, Li HL, Wang Q, Wang JZ (2010) Protein phosphatase 2A facilitates axonogenesis by dephosphorylating CRMP2. J Neurosci 30:3839-3848.

CURRICULUM VITAE

Erik Thomas Dustrude

QUALIFICATIONS

- Training in neuroscience research with emphasis on ion channel regulation.
- Skilled in whole-cell voltage clamp electrophysiology recording and analysis, site-directed mutagenesis, harvest and transfection of primary cell and stable cell line culture, basic biochemistry techniques.
- Outstanding language skills including scientific writing and communication.

EDUCATION

- Ph.D. Medical Neuroscience – Indiana University, Indianapolis, IN (2011-2015)
  Mentor: Dr. Rajesh Khanna, Ph.D.
  All experiments performed for Chapter 4 and some for Chapter 3 were performed in the Khanna laboratory at the University of Arizona.
  Thesis work describes a novel signal transduction pathway wherein multiple post-translational modifications of CRMP2 protein choreograph surface trafficking of neuronal voltage-gated sodium channels.
- B.S. Biology – University of Wisconsin-Eau Claire, Eau Claire, WI (2006-2010)
  Mentor: Dr. Dan Herman
  Student teacher for introductory biology laboratory. Responsibilities included lecture, demonstration, and grading.

AWARDS

Paul and Carole Stark Fellowship in Medical Neuroscience (2012)

PUBLICATIONS

- **Dustrude E.T.,** Moutal A., Yang X.F., Wang Y., Wang Y., Vanderah T.W., Khanna M., Khanna R. Interplay between Cdk5/Fyn phosphorylation and SUMOylation of CRMP2 modulates Nav1.7 channel trafficking via a Numb/Eps15 endocytic pathway. [In progress]
- Torregrosa R., Yang X.F., **Dustrude E.T.**, Cummins T.R., Khanna R., Kohn H. Chimeric Derivatives of Functionalized Amino Acids and α-Aminoamides: Compounds with Anticonvulsant Activity in Seizure Models and Inhibitory Actions on Central, Peripheral, and Cardiac Isoforms of Voltage-gated Sodium Channels. Bioorganic & Medicinal Chemistry. 2015. Apr 11. pii: S0968-0896(15)00311-9. doi: 10.1016/j.bmc.2015.04.014. [Epub ahead of print]
- Park K.D., Yang X.F., **Dustrude E.T.**, Wang Y., Ripsch M.S., White F.A., Khanna R., Kohn. Chimeric Agents Derived from the Functionalized Amino Acid, Lacosamide, and the α-Aminoamide, Safinamide: Evaluation of their Inhibitory Actions on Voltage-gated Sodium Channels, and Antiseizure and Anti-nociception Activities and Comparison with Lacosamide and Safinamide. ACS Chem Neurosci. 2015 Feb 18;6(2):316-30
- Due M.R., Yang X.F., Allette Y.M., Randolph A.L., Ripsch M.S., Wilson S.M., **Dustrude E.T.**, Khanna R., White F.A. Carbamazepine potentiates the

effectiveness of morphine in a rodent model of neuropathic pain. PLoS One. 2014 Sep 15;9(9):e107399

- Lee H., Park K.D., Torregrosa R., **Dustrude E.T.**, Wang Y., Wilson S.M., Barbosa C., Xiao Y., Cummins T.R., Khanna R., Kohn H. Substituted N(biphenyl-4'-yl)methyl (R)-2-acetamido-3-methoxypropionamides: potent anticonvulsants that affect frequency (use) dependence and slow inactivation of sodium channels. J Med Chem. 2014 Jul 24;57(14):6165-82.
- **Dustrude E.T.**, Wilson S.M., Ju W., Xiao Y., Khanna R. CRMP2 Protein SUMOylation Modulates Nav1.7 Channel Trafficking. J Biol Chem. 2013 Aug 23;288(34):24316-31
- Lee H., Park K.D., Yang X.F., **Dustrude E.T.**, Wilson S.M., Khanna R., Kohn H. (Bipehnyl-4-xl)methylammonium Chlorides: Potent Antivonculsants That Modulate Na+ Currents. J Med Chem. 2013 Jul 25;56(14):5931-9
- Park K.D., Yang X.F., Lee, H., **Dustrude E.T.**, Wang Y., Khanna R., Kohn H. Discovery of lacosamide affinity bait agents that exhibit potent voltage-gated sodium channel blocking properties. ACS Chem Neurosci. 2013 Mar 20;4(3):463-74.
- King A.M., Yang X.F., Wang Y., **Dustrude E.T.**, Barbosa C., Due M.R., Piekarz A.D., Wilson S.M., White F.A., Salomé C., Cummins T.R., Khanna R., Kohn H. Identification of the benzyloxyphenyl pharmacophore: a structural unit that promotes sodium channel inactivation. ACS Chem Neurosci. 2012 Dec 19;3(12);1037-49.
- Wilson S.M., Schmutzler B.S., Brittain J.M., **Dustrude E.T.**, Ripsch M.S., Pellman J.J., Yeum T.S., Hurley J.H., Hingtgen C.M., White F.A., Khanna R. Inhibition of transmitter release and attenuation of anti-retroviral-associated and tibial nerve injury-related painful peripheral neuropathy by novel synthetic Ca2+ channel peptides. J Biol Chem. 2012 Oct 12;287(42):35065-77.

PATENTS

- A Non-Narcotic Analgesic Peptide for Chronic pain. University of Arizona Intellectual property ID: UA14-100

PRESENTATIONS AND POSTERS

- Stark Neuroscience Seminar Series. SUMOylation of collapsin response mediator protein 2 alters voltage-gated sodium channel trafficking. (2014)
- Supression of painrelated behavior in two distinct rodent models of peripheral neuropathy by a homopolyarginine-conjugated CRMP2. Neuropathic Pain Special Interest Group (NeuPSIG) Toronto, Canada (2013)